

**TEMPERATURE MEASUREMENT USING RARE
EARTH DOPED FIBRE FLUORESCENCE**

A thesis submitted

by

Scott A. Wade

for the degree of

DOCTOR OF PHILOSOPHY

Optical Technology Research Laboratory,
School of Communications and Informatics,

Victoria University

1999



23125058

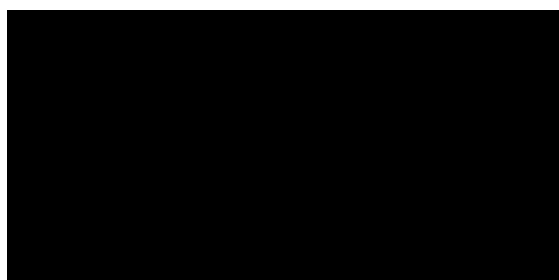
FTS THESIS
536.50287 WAD
30001007295480
Wade, Scott A
Temperature measurement
using rare earth doped fibre
fluorescence

Declaration

I, Scott Andrew Wade, declare that the thesis titled,

“Temperature measurement using rare earth doped fibre fluorescence”

is the result of work performed by the author and has not been submitted previously, in whole or in part, in respect of any other academic award. Sections of the work contained in this thesis, especially in the areas of sensor prototype development and fluorescence lifetime measurements, were performed in collaboration with others, which is acknowledged and referenced where appropriate.



Scott Wade,

dated the 24th day of December, 1999.

Acknowledgements

There are many people I would like to thank for their assistance and support during the time spent working on the PhD studies presented in this thesis.

Firstly I would like to thank all the staff and students (past and present) of the Applied Physics Section at Victoria University. In particular Dr. Gregory Baxter provided invaluable assistance and guidance even when he had thousands of other things to do. Dr. Stephen Collins and Dr. Peter Farrell also provided guidance and both made significant contributions to the work. Additional thanks to Dr. Gregory Baxter and Dr. Stephen Collins for checking through the manuscript. Collaborations were made with and much needed advice was given by Chris Vale, Ian Mitchell, Valentine Bogdanov (who helped with the Eu^{3+} lifetime measurements), Eric Maurice (development of the $\text{Pr}^{3+}:\text{ZBLANP}$ and the initial Yb^{3+} -doped fibre sensors), Jeff Muscat (who helped to develop the Nd^{3+} -doped fibre sensor), Cristina Vegara and Alex Shelamoff – thanks for your help.

During the course of my thesis I was fortunate to spend time studying abroad. My sincere thanks to Prof. K. Grattan, Dr. T. Sun and Dr. J. Milner of the Department of Electrical, Electronic and Information Engineering at City University (England) and Dr. Gérard Monnom and Assist. Prof. M. Sundheimer from the *Laboratoire de Physique de la Matière Condensée* at the *Université de Nice* (France) for their help and hospitality. Additional thanks to Dr. Gérard Monnom and Nice University for providing many of the rare earth doped fibre samples used in this work.

To my “adopted second family” thanks Mary, Eddie and Jim. To my “fireball baby” Catherine, thanks for all the help, love and patience. Lastly, I would like to give my sincerest thanks to my family, especially Janis and Frederick, who provided me with the opportunity to continue my academic studies and have always given me encouragement and support. Thanks for putting up with me all this time!

Abstract

Optical fibre sensors have been developed to measure a wide range of parameters and in many circumstances show significant advantages over conventional measurement techniques. This thesis investigates a relatively new method of measuring temperature using optical fibres, known as the fluorescence intensity ratio technique.

The fluorescence intensity ratio technique uses the thermal coupling of two closely spaced energy levels in an ion. When populated the relative number of ions, and hence the intensity of fluorescence from each of the two closely spaced levels, follow a Boltzmann distribution. Measurements of the fluorescence intensity originating from the two levels can therefore be used to determine temperature.

The fluorescence intensity ratio was studied using six different rare earth ions, doped into a variety of glasses and crystals to investigate the feasibility of developing an accurate, low cost temperature sensor. The work undertaken has improved the understanding of the both the fluorescence intensity ratio technique and the thermalisation process between closely spaced energy levels. Of the materials tested three, namely Pr^{3+} :ZBLANP, Nd^{3+} -doped silica fibre and Yb^{3+} -doped silica fibre, were chosen for further study.

Measurements of the stability of the fluorescence intensity ratio have been made for variations in the excitation power, excitation wavelength, doped fibre length and applied strain. The results obtained indicate that expensive excitation sources required by many other sensor systems should not be needed for appropriate fluorescence intensity ratio based sensors. Measurements also suggest that the fluorescence intensity ratio technique is independent of applied strain eliminating the need for compensation required by many other optical fibre based temperature sensing techniques.

Temperature sensor prototypes were developed using Pr^{3+} :ZBLANP, Nd^{3+} -doped silica fibre and Yb^{3+} -doped silica fibre as the sensing material. The temperatures measured by these materials covered the range of $-50\text{ }^{\circ}\text{C}$ to $610\text{ }^{\circ}\text{C}$, with measurement accuracy better than $1\text{ }^{\circ}\text{C}$. Selected prototypes were subsequently used in measurements of temperature within a new optical fibre cable design during fault current tests and to determine the breakage temperature of window glass during fires.

Table of Contents

DECLARATION.....	i
ACKNOWLEDGMENTS.....	ii
ABSTRACT.....	iii
TABLE OF CONTENTS.....	iv
CHAPTER 1: INTRODUCTION.....	1
1.1 TEMPERATURE MEASUREMENT.....	2
1.2 OPTICAL FIBRE SENSORS.....	2
1.3 OPTICAL FIBRE BASED TEMPERATURE MEASUREMENT.....	3
1.3.1 <i>Blackbody radiation</i>	4
1.3.2 <i>Absorption</i>	4
1.3.3 <i>Intrinsic scattering</i>	5
1.3.4 <i>Interferometry</i>	7
1.3.5 <i>Bragg gratings</i>	7
1.3.6 <i>Fluorescence based optical fibre temperature sensors</i>	8
1.4 CONCLUSION AND SCOPE OF THESIS.....	15
CHAPTER 2: RARE EARTH DOPED OPTICAL MATERIALS.....	17
2.1 THE RARE EARTH ELEMENTS.....	18
2.2 HOST MATERIALS FOR RARE EARTH IONS.....	19
2.3 RARE EARTH DOPED OPTICAL FIBRES.....	21
2.4 THERMAL EFFECTS IN RARE EARTH DOPED MATERIALS.....	24
2.5 SUITABILITY OF HOST MATERIALS FOR USE IN FLUORESCENCE INTENSITY RATIO BASED TEMPERATURE SENSING.....	27
2.6 CONCLUSION.....	28
CHAPTER 3: FLUORESCENCE INTENSITY RATIO THEORY.....	29
3.1 INTRODUCTION.....	30
3.2 THE GENERAL FORM OF THE BOLTZMANN DISTRIBUTION.....	30
3.3 THE BOLTZMANN DISTRIBUTION APPLIED TO FLUORESCENCE INTENSITY RATIO TEMPERATURE SENSING.....	31
3.4 SENSITIVITY OF THE FLUORESCENCE INTENSITY RATIO.....	35
3.5 OPTICAL ARRANGEMENTS FOR MEASURING THE FLUORESCENCE INTENSITY RATIO.....	36
3.6 EFFECT OF THE OPTICAL ARRANGEMENT ON THE MEASURED FLUORESCENCE INTENSITY RATIO AND SENSITIVITY.....	38
3.6.1 <i>Overlap of fluorescence from the thermally coupled levels</i>	39
3.6.2 <i>Stray light</i>	43
3.6.3 <i>Summary</i>	46
3.7 CONCLUSION.....	46
CHAPTER 4: FLUORESCENCE INTENSITY RATIO STUDIES USING RARE EARTH DOPED GLASSES AND CRYSTALS: FEASIBILITY STUDIES FOR USE IN TEMPERATURE SENSING APPLICATIONS.....	48
4.1 INTRODUCTION.....	49
4.2 SEARCH FOR THERMALISING LEVELS IN TRIVALENT RARE EARTH IONS.....	49

Table of Contents cont.

CHAPTER 4: cont.

4.3 EXPERIMENTAL ARRANGEMENTS USED IN FLUORESCENCE INTENSITY RATIO STUDIES	51
4.3.1 Bulk rare earth doped samples.....	54
4.3.2 Rare earth doped optical fibre samples	55
4.4 FLUORESCENCE INTENSITY RATIO VERSUS TEMPERATURE STUDIES.....	57
4.4.1 Praseodymium.....	57
4.4.2 Neodymium.....	66
4.4.3 Samarium	75
4.4.4 Europium.....	77
4.4.5 Dysprosium.....	82
4.4.6 Ytterbium.....	85
4.5 CONCLUSION.....	90

CHAPTER 5: FLUORESCENCE INTENSITY RATIO STABILITY92

5.1 INTRODUCTION.....	93
5.2 EXCITATION SOURCES FOR FLUORESCENCE INTENSITY RATIO TEMPERATURE SENSORS	94
5.3 Pr ³⁺ :ZBLANP	94
5.3.1 Pump wavelength.....	95
5.3.2 Pump power.....	98
5.4 Nd ³⁺ -DOPED SILICA FIBRE.....	100
5.4.1 Pump wavelength.....	100
5.4.2 Pump power.....	101
5.5 Yb ³⁺ -DOPED SILICA FIBRE.....	105
5.5.1 Pump wavelength.....	105
5.5.2 Pump power.....	108
5.5.3 Doped fibre length.....	111
5.5.4 Strain.....	114
5.6 CONCLUSION.....	115

CHAPTER 6: FLUORESCENCE INTENSITY RATIO SENSOR DEVELOPMENT AND APPLICATIONS..... 117

6.1 INTRODUCTION.....	118
6.2 Pr ³⁺ :ZBLANP SENSOR PROTOTYPE.....	118
6.3 Yb ³⁺ -DOPED SILICA FIBRE SENSOR PROTOTYPE.....	122
6.3.1 Sensor development.....	122
6.3.2 Monitoring of optical fibre temperature in OPGW cable during fault current tests.....	126
6.4 Nd ³⁺ -DOPED SILICA FIBRE SENSOR PROTOTYPE.....	130
6.4.1 Sensor development.....	130
6.4.2 Measurement of breakage temperature of window glass during fires.....	134
6.5 CONCLUSION.....	135

CHAPTER 7: FLUORESCENCE LIFETIME STUDIES.....136

7.1 INTRODUCTION.....	137
-----------------------	-----

Table of Contents cont.

CHAPTER 7: cont.

7.2	FLUORESCENCE LIFETIME STUDIES OF Yb ³⁺ -DOPED SILICA FIBRE	137
7.3	FLUORESCENCE LIFETIME STUDIES OF Eu ³⁺ -DOPED SILICA FIBRE	141
7.4	COMPARISON OF THE FLUORESCENCE INTENSITY RATIO AND FLUORESCENCE LIFETIME TECHNIQUES	147
7.5	CONCLUSION	148

CHAPTER 8: DISCUSSION AND CONCLUSION.....149

8.1	INTRODUCTION.....	150
8.2	SUMMARY OF FLUORESCENCE INTENSITY RATIO STUDIES	150
8.3	COMPARISON OF THE FLUORESCENCE INTENSITY RATIO METHOD WITH COMMERCIALY AVAILABLE FIBRE OPTIC TEMPERATURE SENSORS	153
8.4	OTHER RECENT WORK ON FLUORESCENCE INTENSITY BASED TEMPERATURE SENSING.....	154
8.5	FUTURE WORK.....	154
8.6	CONCLUSION	156

REFERENCES157

APPENDIX A: SAMPLE HOLDERS FOR RARE EARTH DOPED MATERIALS.....165

A.1	RARE EARTH DOPED FIBRE HOLDER	166
A.2	Pr ³⁺ :ZBLANP SAMPLE HOLDER	166
A.3	Nd ³⁺ :YAG SAMPLE HOLDER	167
A.4	Nd ³⁺ :YVO ₄ SAMPLE HOLDER	167
A.5	Nd ³⁺ :ZBLANP SAMPLE HOLDER	168

PUBLICATIONS169

Chapter 1: Introduction

- 1.1 TEMPERATURE MEASUREMENT
- 1.2 OPTICAL FIBRE SENSORS
- 1.3 OPTICAL FIBRE BASED TEMPERATURE MEASUREMENT
 - 1.3.1 *Blackbody radiation*
 - 1.3.2 *Absorption*
 - 1.3.3 *Intrinsic scattering*
 - 1.3.4 *Interferometry*
 - 1.3.5 *Bragg gratings*
 - 1.3.6 *Fluorescence based optical fibre temperature sensors*
 - 1.3.6.1 *Fluorescence lifetime based temperature sensors*
 - 1.3.6.2 *Steady state fluorescence based temperature sensors*
- 1.4 CONCLUSION AND SCOPE OF THESIS

Overview of Chapter

Optical fibre based sensing techniques have been developed to measure a wide variety of parameters, including temperature. This chapter presents a summary of the techniques for temperature measurement using optical fibres, together with an overview of the work presented in this thesis.

1.1 TEMPERATURE MEASUREMENT

The accurate and reliable measurement of temperature plays an important role in today's society. Many industrial and scientific processes as well as everyday events, from cooking a cake to the production of complex materials, depend upon temperature. Knowledge of, and hence the ability to control temperature is therefore extremely useful.

Credit for the development of the first device used to measure temperature is usually given to Galileo Galilei [1-3]. The device, known as a thermoscope, consisted of a glass bulb and a long open-ended rod, with the open end of the rod immersed in a liquid. Temperature changes caused the air trapped in the bulb to expand or contract resulting in a rise or a drop in the level of the liquid in the rod. Since this early work many advances have been made in the area of temperature measurement. One of the most significant being the development of temperature scales that allow the comparison of temperatures obtained using different devices, in different locations, or at different times.

Some of the common devices that are presently used for temperature measurement include liquid in glass thermometers, thermoelectric thermometers, resistance thermometers and thermal radiation thermometers [1-2]. However, these and other traditional temperature sensors can suffer from serious performance degradation when operated in harsh environments. For example the electrical interference encountered by metallic based temperature sensors, such as thermocouples, when operated in the presence of strong electromagnetic fields can result in substantial errors in measurement.

The development of new measurement techniques, which demonstrate advantages in either accuracy, stability, measurement range, cost, size or measurement response time while still meeting other performance criterion, is of much interest. One category of sensors that have shown success in several of these areas are temperature sensors using optical fibres.

1.2 OPTICAL FIBRE SENSORS

The first reports of sensors using optical fibres were made nearly 30 years ago. Early forms of these sensors used the light guiding properties of optical fibres in

conjunction with a traditional sensing technique. However, more recent research has expanded this to make use of properties inherent to optical fibres. During the last three decades optical fibre based sensors have been constructed to measure a range of parameters, including temperature, strain, pressure, pH, rotation, current, voltage, and position. In many instances optical fibre sensors now have performance characteristics that are better than non-fibre-based sensors. For more detailed reviews of optical fibre sensing, the reader is referred to references 4 to 8.

The advantages offered by optical fibre based sensors, in comparison to traditional sensors, are well documented [4, 8]. They include, but are not limited to, small size, low weight, electrical insulating properties, and relative immunity to electrical, magnetic and electromagnetic noise. The latter of these advantages, for example, can be used to overcome the problem of electromagnetic interference experienced by metallic based sensors when used to measure temperature in power transformers.

The basic configuration of a typical optical fibre sensor consists of a light source, an optical fibre, a means of measuring the parameter of interest, and a detection system. Sensors which use a change in a material or substance external to the fibre are referred to as extrinsic sensors, while those which use changes in properties of the optical fibre itself to make the measurement are known as intrinsic sensors. Another classification of optical fibre sensors is based on the location of measurement. Sensors which make measurements at a precise location, are known as point sensors, whereas distributed sensors measure continuously over a distance and quasi-distributed sensors make measurements at a number of precise locations.

1.3 OPTICAL FIBRE BASED TEMPERATURE MEASUREMENT

Since the development of the first optical fibre based temperature sensors a variety of measurement techniques have been studied to use the inherent advantages of optical fibres. In the following sections the physical principles and performance characteristics of several of the better known types of optical fibre temperature sensors are reviewed. Special emphasis has been placed on fluorescence based temperature sensors due to their relevance to the present work.

1.3.1 Blackbody radiation

The spectral distribution of thermally generated radiation from a material depends upon the temperature of the body according to Plancks' law [9]:

$$W(\lambda, T) = \frac{C_1}{\lambda^5} \frac{1}{(\exp[C_2/\lambda T] - 1)} \quad (1.1)$$

where W is the radiant power emitted per unit area, C_1 and C_2 are radiation constants, λ is the wavelength of radiation and T is the absolute temperature in kelvin. This phenomenon has been used as a technique for optical fibre temperature sensing by several authors including Dakin and Kahn [10], Gottlieb and Brandt [11], Dils [12] and Morden *et al* [13]. Various sensor configurations have been developed in which the thermal radiation measured is generated either in a blackbody cavity in the tip of the sensing fibre, or by an external body. This technique has shown good accuracy for high temperature measurements, being the physical principle used to define temperatures above 962 °C in the International Temperature Scale of 1990 (ITS-90) [14]. Typically blackbody radiation based sensors have been limited to the measurement of temperatures a few hundred degrees Celsius above room temperature due to the reduced levels of thermal radiation at lower temperatures. Several commercial devices using this technique have been developed, an example of which is the *Accufiber model 100* which has a measurement range of 100 °C to 4000 °C and an accuracy of 0.2% at 1000 °C [15].

1.3.2 Absorption

The variation in the absorption spectrum with temperature of certain materials is another method that has been used for optical fibre temperature sensing. Research in this field has focussed predominantly on the absorption properties of either semiconductor or rare earth doped materials. An example of the former is the work by Kyuma *et al* [16] in which an optical fibre temperature sensor was developed using the shift in the absorption edge of semiconductor materials. In this study an accuracy of ± 1 °C over the -10 °C to +300 °C temperature range was quoted, with a response time of 2 seconds.

Studies of the thermal variation of the absorption spectra of rare earth doped materials, in both bulk and fibre form, have been made by many authors. One example is the use of Nd³⁺-doped silica fibre by Appleyard, Scrivener and Maton [17] to measure temperature with a ± 1 °C accuracy over the 20 °C to 200 °C range. In another example

of this technique, distributed sensing was reported by Farries and colleagues [18] with an optical time domain reflectometer (OTDR) system used in conjunction with Nd³⁺-doped silica fibre. It was found that a maximum accuracy of 2 °C was achievable over the -50 °C to +100 °C temperature range with a spatial resolution of 15 m over a 140 m length of fibre. While the absorption technique has good accuracy and measurement range, the development of an inexpensive technique of referencing to remove induced errors due to changes in the pump source, such as wavelength and power, is yet to be developed.

1.3.3 Intrinsic scattering

The intrinsic scattering category of optical fibre temperature sensors includes sensors that are based on Raman, Rayleigh and Brillouin scattering. These types of scattering are caused by the interaction between light transmitted by the fibre and molecules in the fibre, and have been shown to depend upon temperature. These effects are usually measured using optical time domain reflectometry, which offers the advantage of distributed sensing. Rayleigh scattering, which occurs at the same wavelength as the incident light, has been used to measure temperature by Hartog [19] in conjunction with liquid core optical fibres. The liquid core fibres used in this study provided greater temperature sensitivity than standard silica fibre. In this work it was reported that a measurement accuracy of 1 °C with a spatial resolution of 1 m is obtainable over a fibre length of 100 m.

Both Raman and Brillouin scattering occur at wavelengths slightly shifted from the incident light, with the magnitude of the shift depending on the type of scattering, as shown in figure 1.1. Scattered light is shifted to both longer wavelengths (known as a Stokes shift) and shorter wavelengths (known as an anti-Stokes shift), than the incident light.

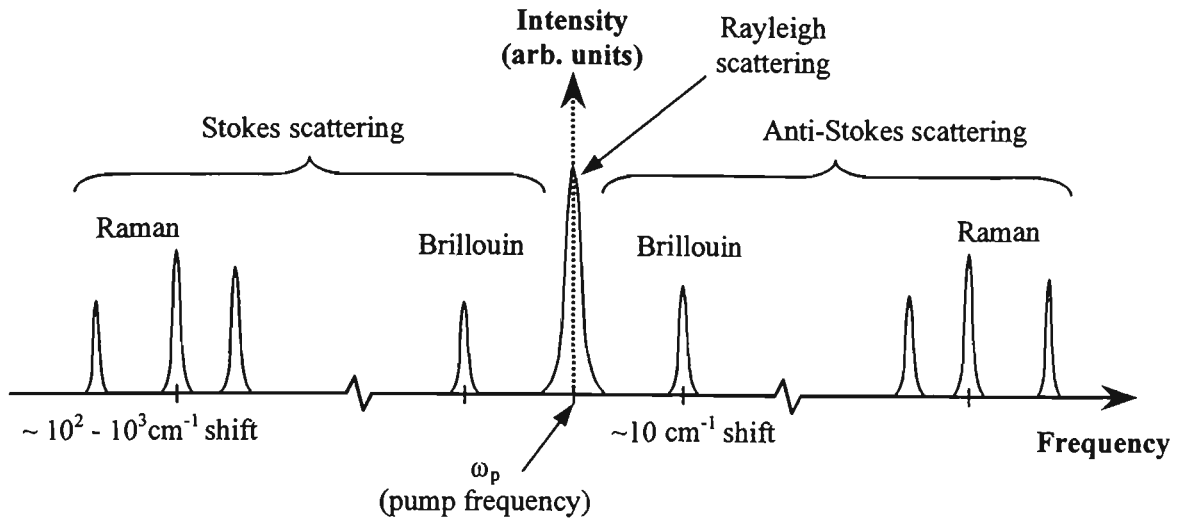


Figure 1.1: Stokes and anti-Stokes shift, Brillouin, Raman and Rayleigh scattering, (after reference 20).

The ratio of Raman anti-Stokes/Stokes backscattered light has been used by Dakin *et al* [21] to produce an optical fibre temperature sensor with an initial temperature and spatial resolution of 10 °C and 3 m respectively. This technique has since been improved and commercialised by *York Sensors* which offer a number of devices with different measurement ranges, resolutions and accuracies. As an example, some of the performance characteristics of the *DTS-800* sensor by *York* are presented in table 1.1 [22].

Sensor	Range	Spatial Resolution	Temperature Resolution/Accuracy	Measurement time
Short Range (SR)	5 km	1 m	1 °C/1 °C	600 sec
Ultra-long Range (ULR)	30 km	8 m	2 °C/2 °C	600 sec

Table 1.1: Performance characteristics of *DST-800* sensor by *York Sensors* (after reference 22).

Recent work in intrinsic scattering based temperature sensing has concentrated on the use of the ratio of Rayleigh and Brillouin backscattered intensities, known as the Landau-Placzek ratio [23]. The advantage of this technique over Raman backscattering is that the intensity of Brillouin backscattered light is approximately an order of magnitude greater than the Raman backscattered intensity. This improves the resolution or response time of the system.

One of the main limitations of optical fibre sensors which use the intrinsic scattering method is their high cost, which is partially due to the signal processing techniques and light sources employed. This limitation, however, is partially offset by

the fact that a single instrument can be used to measure temperatures at a large number of locations, which may provide cost benefits in comparison to purchasing multiple single point sensors.

1.3.4 Interferometry

Optical fibre sensors based on interferometry use the relative shift in phase of light along a fibre which is subjected to the measurand, compared to light in a stabilised reference fibre. In the case of temperature sensing, shifts in phase are due to a change in refractive index of the fibre core or changes in the length of the sensing fibre. Such phase changes are highly sensitive to variations in temperature ($d\phi/dT \sim 100 \text{ rad}/^\circ\text{C}$ per meter of fibre [8]) allowing extremely accurate devices to be constructed. The first report of an optical fibre temperature sensor using this technique was made by Hocker [24] using a Mach-Zehnder interferometer configuration. Following this work several authors have reported the use of a number of different interferometric techniques including the Michelson [25] and Fabry-Perot [26] configurations to either extend the measurable temperature range or improve the accuracy of measurement. The typical measurement resolution which can be achieved using this method of temperature sensing is in the order of $0.01 \rightarrow 0.001 \text{ }^\circ\text{C}$.

One of the main problems highlighted with interferometric based fibre temperature sensors is that the initial relative phase difference between the sensing and reference fibres is not necessarily related to a specific temperature. These devices therefore require calibration with another sensor at start up. Work is currently underway to eliminate this problem using multiple-wavelength or white light interferometric techniques. The ability of these devices to accurately measure the relative change in temperature, however, is quite useful when knowledge of the absolute temperature is not required. Due to the high sensitivity of these devices to changes in other physical quantities, such as strain ($d\phi/d\epsilon \sim 10^7 \text{ rad/m}$ per unit strain[8]) and pressure, care must also be taken to ensure that the measurement is free of influence from such effects.

1.3.5 Bragg gratings

In-fibre Bragg gratings, first discovered by Hill and fellow workers in 1978 [27], are made by inducing a periodic refractive index modulation along an optical fibre. This is usually achieved by exposing the optical fibre to ultraviolet radiation. The induced

variation in refractive index causes the grating to reflect light over a specific wavelength range which depends upon several factors including the spacing between changes in refractive index and the magnitude of refractive index difference of the induced variations compared with the normal fibre refractive index. Variations in temperature affect the centre wavelength and the bandwidth of such reflections via changes in the refractive index and length of the fibre. The sensitivities of in-fibre Bragg gratings to temperature changes have been shown to be in the order of 10 pm/°C [28]. Various sensor configurations that utilise the temperature induced centre wavelength shift have been developed. A recent example of such work was the development of a fibre Bragg grating temperature sensor by Gupta and fellow workers in 1996 for the measurement of temperatures down to 80 K [29]. Sensitivities of 0.04 nm/K at 100 K were obtained for a grating bonded to a poly(methyl methacrylate) substrate. The main problems encountered with in-fibre Bragg grating temperature sensors are due to the sensitivity of the gratings to changes in other parameters such as strain ($d\lambda/d\varepsilon \sim 1 \text{ pm}/\mu\varepsilon$ [28]) and pressure. Precautions, similar to those required for interferometric sensors, must be taken to remove such effects.

1.3.6 Fluorescence based optical fibre temperature sensors

Optical fibre temperature sensors that use changes in the fluorescence properties of certain materials with temperature have received much interest, with several commercial devices based on this technique currently available. Current research with this technique is aimed at improving the measurement range and accuracy. A wide range of temperatures have been measured using such techniques, many of which have the significant advantage of being largely independent of changes in pump intensity, pump wavelength and fibre bend losses. Techniques that display immunity to changes in the excitation source and fibre bend losses are commonly referred to as being self-referenced. A number of different fluorescence properties have been utilised to measure temperature, most of which can be classified in terms of whether time dependent or steady state changes are used, as is outlined below.

1.3.6.1 Fluorescence lifetime based temperature sensors

The fluorescence lifetime of an energy level of a material is a measure of the rate of reduction in the intensity of fluorescence after the source of excitation has been removed. This rate of decay has been shown to depend strongly upon temperature for the energy levels of many materials and therefore can be used as a measure of temperature.

A substantial volume of research on fluorescence based temperature sensing has been undertaken by workers at City University, London. This group has studied the lifetime behavior of many materials including ruby [30], alexandrite [30], Cr^{3+} :YAG [31], Cr^{3+} :LiSAF [30], Pr^{3+} :ZBLAN [32], Er^{3+} -doped silica optical fibre [33], Yb^{3+} -doped silica optical fibre [34] and Nd^{3+} doped in a variety of host materials [35]. An example of this work is the fluorescence lifetime versus temperature characteristics of Cr^{3+} :YAG [36], shown in figure 1.2 for the $-195\text{ }^{\circ}\text{C}$ to $+313\text{ }^{\circ}\text{C}$ temperature range.

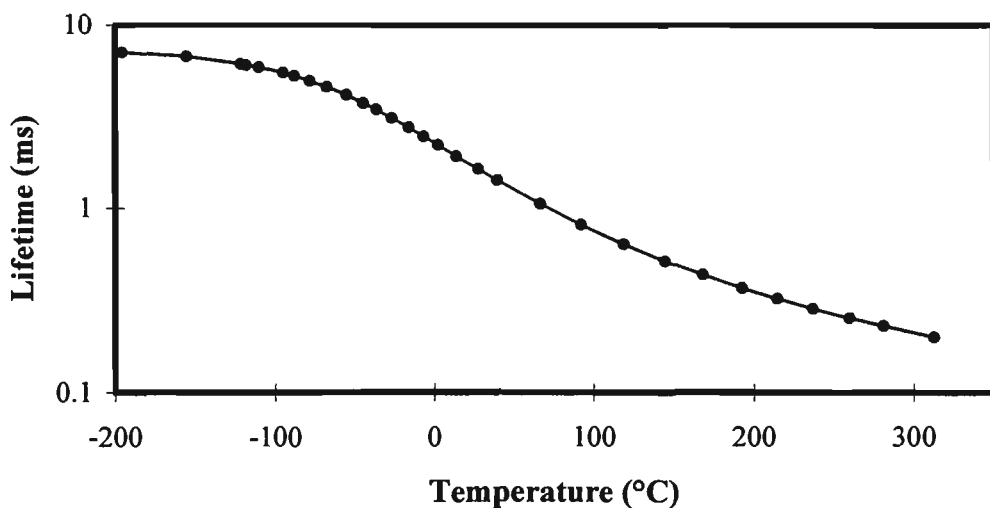


Figure 1.2: Cr^{3+} :YAG fluorescence lifetime versus temperature, data taken from [36].

The temperature range and measurement accuracy of the fluorescence lifetime technique has been found to depend largely upon the sensing material used, several examples of which are provided in table 1.2. Further information regarding the fluorescence lifetime method of temperature sensing can be found in reference 30.

Sensor material	Range	Measurement accuracy	Ref.
Ruby	20→160 °C	0.04 °C ^a	[30]
	20→450 °C	1 °C ^a	[30]
Alexandrite	20→150 °C	0.3 °C ^a	[30]
	20→725 °C	1 °C ^a	[30]
Cr:LiSAF	30→100 °C	0.02 °C ^a	[30]
Nd ³⁺ -doped optical fibre	-190→750 °C	± 3 °C ^b	[35]
Er ³⁺ -doped optical fibre	0→1100 °C	± 5 °C ^b	[33]
Yb ³⁺ -doped optical fibre	20→700 °C	± 5 °C ^b	[34]

Table 1.2: Examples of the temperature range and measurement accuracy obtained using materials studied for fluorescence lifetime based temperature sensing. ^ameasurement deviation, ^bmaximum deviation.

In another example of fluorescence lifetime temperature sensing Wickersheim and Sun [37] of *Luxtron Corp.* reported the use of the decay time of magnesium fluorogermanate for optical fibre temperature sensing. This work has been developed into a range of commercially available devices covering the -195 °C to 450 °C temperature range. The typical accuracy of measurement made by these sensors without in-situ calibration is quoted to be $\leq \pm 2$ °C [38].

One of the main limitations of this technique is the relatively small change in the lifetime at lower temperatures (< 20 °C for many materials) [36]. This usually results in a reduction in the measurement accuracy possible using this technique for such temperatures. Work on improving the temperature range and measurement accuracy of fluorescence lifetime based sensors is currently underway through the investigation of different fluorescence materials.

1.3.6.2 Steady state fluorescence based temperature sensors

In addition to time dependent fluorescence processes several steady state fluorescence processes have been used for temperature sensing. These include changes in the fluorescence intensity, the shift in fluorescence wavelength of materials and changes in the amplified spontaneous emission of materials with temperature. To avoid potential measurement errors due to changes in the excitation source or bend related effects many of these sensors obtain measurements over two different wavelength ranges with a ratio of the two measurements used to determine temperature.

(i) Fluorescence intensity ratio

In the fluorescence intensity ratio technique of temperature sensing the ratio of the fluorescence intensities originating from two different energy levels of a material is used to measure temperature. The physical principle that causes the changes in fluorescence intensity with temperature depends upon the energy levels and the host material used. If the levels of interest are separated by a relatively small energy gap, such that they are in thermal equilibrium, the populations and hence fluorescence intensities of the levels follow a Boltzmann distribution [39, 40] (discussed in detail in chapter 3). If however the energy levels are separated by a large energy gap the relationship between the fluorescence intensity of the levels as a function of temperature depends upon the temperature dependence of the non-radiative rates of the individual levels.

The use of fluorescence intensity ratio techniques for temperature sensing was first discussed by Kusama *et al* in 1976 [41]. The material investigated in this work was $\text{Y}_2\text{O}_2\text{S}:\text{Eu}$ phosphor with the fluorescence intensity ratio measured for both crystal-field split components of energy levels (i.e. Stark sub-levels) and for different $^{2S+1}L_J$ multiplets. Problems including poor sensitivity and the overlap of fluorescence lines were experienced with the energy levels investigated and therefore another technique was chosen for the particular application (see fluorescence line shift below).

The first reports on fluorescence intensity ratio based temperature sensing using optical fibres were made by workers at *Luxtron Corp.* [42, 43] who developed a sensor using fluorescence from europium-doped lanthanum and gadolinium oxysulfide phosphors. From this work a commercial device capable of measuring over the -100 to 290 °C range with a precision of ± 0.1 °C was produced. This device has since been changed by the manufacturer to the fluorescence lifetime based sensor discussed previously.

In 1986 Weinstein [44] reported the use of the ratio of the fluorescence intensity of the ruby R-lines to measure the temperature in a diamond anvil cell. Results were obtained over the 10 to 100 K temperature range and an accuracy of approximately 10% quoted.

A major advance in fluorescence intensity ratio based temperature sensing was the use of rare earth doped optical fibre as the sensing material by Berthou and Jörgensen [45]. As the doped fibre has similar dimensions and can be made of the same

material as the passive light guiding optical fibres used in the sensor, connection problems that exist for other materials can be reduced. The ratio of fluorescence originating from the ${}^2\text{H}_{11/2}$ and ${}^4\text{S}_{3/2}$ energy levels of erbium (Er^{3+}) doped in a fluoride glass was used to measure temperature with an accuracy of 2 K over the 20 to 200 °C temperature range. The main limitation of the sensor reported arises due to the use of fluoride glass as the host material, limiting the maximum operating temperature to approximately 250 °C.

More recently, significant improvements in the fluorescence intensity ratio method were made by Maurice and fellow workers [46-48], who used the aforementioned energy levels of Er^{3+} with a silica fibre host. This host material allows an expanded operating temperature range in comparison to fluoride glass (up to 640 °C measured) and simplifies the joining of the sensing material and the optical fibre used to transmit both the excitation and fluorescence signal. Work was also undertaken which showed that the effect of pump power, pump wavelength and fibre length on the fluorescence intensity ratio is minimal. One of the possible drawbacks of this sensor is that for a practical device to be constructed a high power 800 nm laser diode would be required, increasing the potential cost.

Studies of the fluorescence intensity ratio method of temperature sensing using Er^{3+} have recently been reported for a number of other host materials including fluorindate [49], Ga:La:S:O [50] and Germoniobate [50]. These host materials appear to require lower power excitation sources than those required for a silica fibre host, although they are usually limited to the measurement of temperatures below approximately 250 °C.

(ii) Fluorescence wavelength shift

In many optical materials it has been found that the fluorescence wavelength shifts with temperature, and therefore can be used to measure temperature. This technique was used by Kusama and fellow workers at *Sony Corp.* to measure $\text{Y}_2\text{O}_2\text{S}:\text{Eu}$ phosphor temperature and hence determine the temperature of colour television screens [41]. The technique adopted allowed measurement over the -15 to 75 °C range with an uncertainty of 1 °C. Another report of an optical fibre temperature sensor using the fluorescence wavelength shift technique was made by Ovrén, Adolfsson and Hök in 1984 [51]. In this work the temperature dependent wavelength shift of fluorescence

from a semiconductor crystal was measured over two different wavelength ranges with the ratio used to determine temperature. Results were obtained to an accuracy of 0.5 °C between 0 and 200 °C.

(ii) Amplified spontaneous emission

One of the spin-offs of erbium doped fibre amplifier research has been the development of optical fibre temperature sensors that make use of the wavelength dependent change in the magnitude of amplified spontaneous emission with temperature. This change arises due to the temperature dependent population distribution of the $^4I_{13/2}$ level.

A temperature sensor based on this technique was reported by Imai, Hokazono and Yoshida [52] in 1996. The experimental arrangement used consisted of a 5.9 m length of Er^{3+} -doped fibre, a 1.48 μm laser diode for excitation and an optical spectrum analyser to measure the amplified spontaneous emission spectra. Measurements of the ratio of the peak powers of the 1.552 μm /1.530 μm fluorescence peaks showed a useful change in temperature over the 40 °C to 180 °C temperature range, however no figures of accuracy were reported. Using the same technique Jung and Lee [53] measured temperature with an accuracy of 0.36 °C over the range of 40 °C to 180 °C. The fibre used in the latter work was 7 m in length and was also pumped using a 1.48 μm laser diode.

While this technique shows potential for further development the length of fibre required may present limitations in spatial resolution and sensor dimensions. In addition the amplified spontaneous emission spectrum is strongly dependent on pump power and therefore costly pump stabilisation may be required.

A summary of the optical fibre based techniques developed for temperature measurement is presented in table 1.3.

Measurement technique	Advantages	Disadvantages	Temperature range	Temperature measurement accuracy	Spatial resolution (range)	Ref.
Blackbody radiation*	Good accuracy at higher temperatures	Reduced accuracy at lower temperatures	100→4000 °C	0.2% at 1000 °C		[15]
Absorption	Possible distributed sensing	Requires referencing technique to remove pump fluctuations	-10→300 °C	±1 °C		[16]
Intrinsic scattering*	Allows distributed sensing, standard optical fibres may be used	Complex data analysis, high cost	-50→100 °C	2 °C max.	15 m, (140 m)	[18]
Interferometry	Good accuracy	Cross sensitivity with strain and other parameters, start up problems	-200→1100 °C	1-2 °C	1-8 m, (5-30 km)	[22]
Bragg gratings	Good accuracy	Cross sensitivity with strain and other parameters	not specified	1.4 °C	10 m	[23]
Fluorescence lifetime*	Reasonable accuracy, wide temperature range, self-referenced	Reduced sensitivity at low temperatures	20→67 °C	0.01 °C		[26]
Fluorescence intensity ratio	Reasonable accuracy, wide temperature range, self-referenced, simple data analysis	Er ³⁺ :ZBLAN - limited measurement range, Er ³⁺ :silica - requires high power laser diode	-193→27 °C 45→150 °C	0.5-1 °C 0.7 °C		[29] [54]
Fluorescence wavelength shift	Reasonable accuracy and range		-200→450 °C 20→160 °C 20→725 °C -190→750 °C 0→1100 °C 20→700 °C	±2 °C 0.04 °C 1 °C ±3 °C ±5 °C ±5 °C		[38] [30] [30] [35] [33] [34]
Amplified spontaneous emission	Reasonable accuracy, simple data analysis	Limited spatial resolution, may require pump stabilisation	20→200 °C 20→640 °C -100→290 °C	2 °C 1.1 °C ±0.1 °C		[45] [46] [37]
			0→200 °C	0.5 °C		[51]
			12→80 °C 40→180 °C	not specified 0.36 °C		[52] [53]

Table 1.3: Summary of the characteristics of the various types of optical fibre temperature sensors developed. Measurement techniques that have been commercially developed and are currently available are denoted with an asterix.

1.4 CONCLUSION AND SCOPE OF THESIS

Optical fibre based temperature sensors have been developed using a wide range of measurement techniques, several of which have been made into commercial devices [7]. However, they appear to have only captured small niche markets. This is possibly due to the relatively high cost of the present commercially available sensors, a consequence of the light sources and signal processing techniques employed. Another concern is the cross-sensitivity of several of the techniques to parameters other than temperature, in particular strain. The development of optical fibre based temperature sensors that meet performance and reliability requirements that are low in cost and independent of cross-sensitivity problems are therefore of much interest.

One category of optical fibre based temperature sensors that show good promise in overcoming cost and cross-sensitivity problems are those based on fluorescence. These sensors generally employ relatively simple optical arrangements and signal processing techniques which help to reduce their cost. Many also have the significant advantage of their operation being independent of excitation and bend loss effects.

The majority of research on fluorescence based temperature sensors has focussed on the fluorescence lifetime technique. Results obtained for this method show that good sensitivities can be achieved over a range of temperatures that depend upon the material used. The sensitivity and temperature range required for a particular application would therefore determine which material would be best suited for use with this technique.

In comparison to the fluorescence lifetime method the extent of research undertaken on steady state fluorescence based temperature sensors is relatively small, despite the promising results obtained. The detection schemes required by steady state fluorescence schemes have the potential to be relatively simple and therefore low in cost. Additionally, in a manner similar to the fluorescence lifetime technique, the sensitivity and temperature range measurable with steady state fluorescence based sensing should depend upon the sensor material used. Steady state fluorescence sensors theoretically have the potential for superior sensitivity over certain temperature ranges compared with the fluorescence lifetime technique.

In this thesis a detailed study of the fluorescence intensity ratio technique of temperature sensing based on the population distribution of two close lying excited state levels is presented.

The materials chosen for the sensing element in this work were rare earth ions doped in a variety of glasses and crystals. As outlined in chapter 2 the rare earth ions offer a substantial number of energy levels that may possibly be used in the fluorescence intensity ratio method of temperature sensing. In addition, the optical properties of rare earth doped materials are generally well understood and a range of host materials, including optical fibres doped with these ions, are readily available.

The third chapter of this thesis contains information regarding the theory of the fluorescence intensity ratio technique assuming a Boltzmann population distribution. The effect of stray light and overlap of fluorescence, from the two levels of interest, on the fluorescence intensity ratio is also discussed.

In chapter 4 the results of preliminary fluorescence intensity ratio studies of six different rare earth ions doped in a variety of host materials are presented. These measurements were undertaken to determine the sensitivity of each material at various temperatures and to investigate the feasibility of their use in a practical sensor.

The effect of pump power, pump wavelength, doped fibre length and applied strain on the fluorescence intensity ratio are presented in chapter 5.

The development of prototype fluorescence intensity ratio temperature sensors using the most promising rare earth ions from the preliminary studies, is discussed in chapter 6. This chapter also includes details of the application of prototype sensors in the measurement of temperature in a new optical fibre cable design and for the monitoring of window glass temperature in fire testing.

In chapter 7 the fluorescence lifetime characteristics of Yb^{3+} and Eu^{3+} -doped silica fibre are presented. This includes a comparison between the fluorescence intensity ratio technique and the fluorescence lifetime method of temperature sensing, plus additional information on the thermalisation process.

The final chapter of this thesis (chapter 8) provides a summary of the results presented. These results are then compared with currently available commercial optical fibre based temperature sensors to put the present study in context. Lastly, suggestions for further research on the fluorescence intensity ratio technique of temperature sensing are given.

Chapter 2 - Rare Earth Doped Optical Materials

- 2.1 THE RARE EARTH ELEMENTS
- 2.2 HOST MATERIALS FOR RARE EARTH IONS
- 2.3 RARE EARTH DOPED OPTICAL FIBRES
- 2.4 THERMAL EFFECTS IN RARE EARTH DOPED MATERIALS
- 2.5 SUITABILITY OF HOST MATERIALS FOR USE IN FLUORESCENCE INTENSITY RATIO BASED TEMPERATURE SENSING
- 2.6 CONCLUSION

Overview of Chapter

In this chapter the physical and optical properties of optical materials doped with rare earth ions are discussed in relation to their use in fluorescence intensity ratio based temperature sensing.

2.1 THE RARE EARTH ELEMENTS

One group of elements that have received significant interest in laser research are the rare earth elements. The rare earths consist of two separate groups of 14 elements, known as the lanthanide series and the actinide series (with their position in the periodic table shown in figure 2.1). The majority of laser research has focussed on the lanthanide series of elements and in particular the trivalent (3+) form of these elements. As a result of this work the optical properties of the trivalent rare earth ions are relatively well known and a large number of optical materials doped with these ions are commonly available.

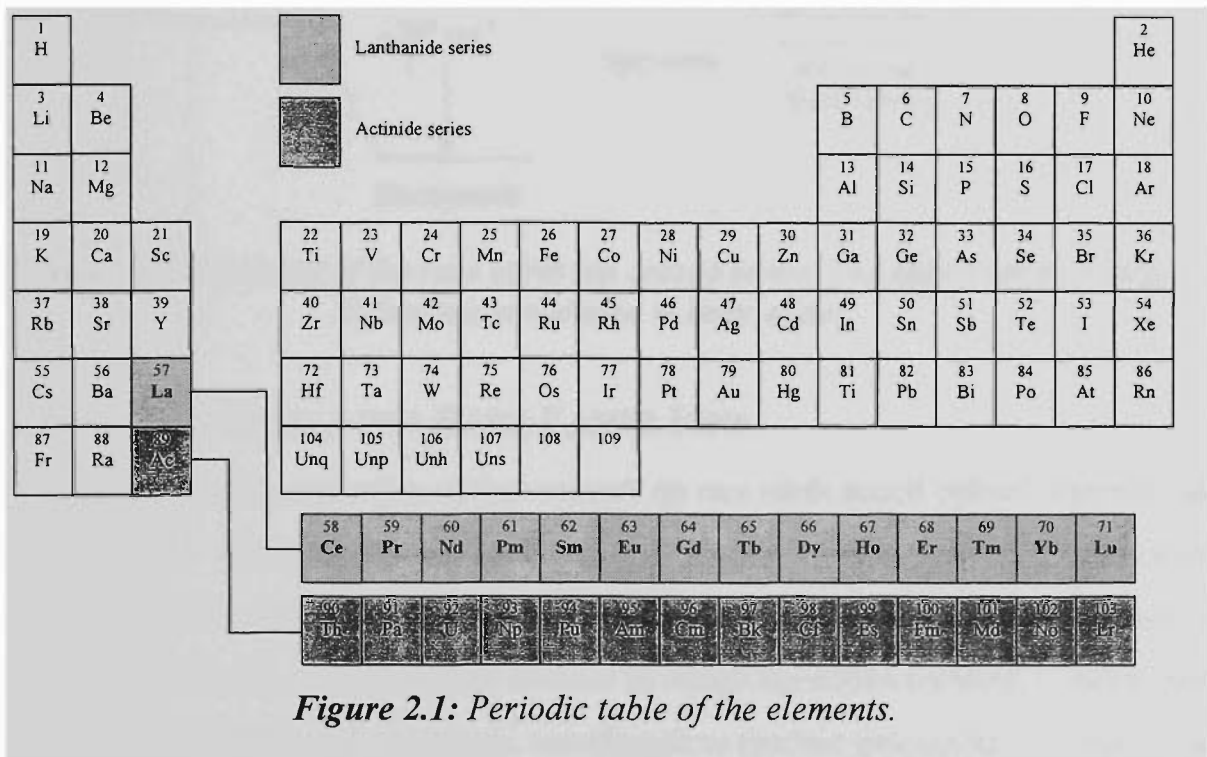


Figure 2.1: Periodic table of the elements.

The basic electronic structure of the lanthanide rare earth elements consists of an outer shell, identical to that of xenon, and a partially filled 4f shell [55]. In the trivalent form of these ions, ionisation usually results in the removal of two 6s and one 4f electron, leaving a partially filled 4f shell shielded by the outer 5s and 5p shells. This shielding results in 4f → 4f optical transitions which are largely unaffected by host fields, unlike many of the optical transitions which take place in transition metals such as Cr³⁺.

The positions of the energy levels of trivalent rare earth ions arise due to electrostatic, spin-orbit and ion-lattice interactions [56, 57], as identified in figure 2.2. Electrostatic interactions have the largest influence on the position of the energy levels,

the ion-lattice interactions have the least. Also shown in figure 2.2 is the spectroscopic notation used to denote individual energy levels. This notation uses the S, L and J quantum numbers that denote the vector sum of the spin and orbital quantum numbers and the total angular momentum respectively. The symbol μ is used to denote the individual energy levels arising due to ion-lattice interactions.

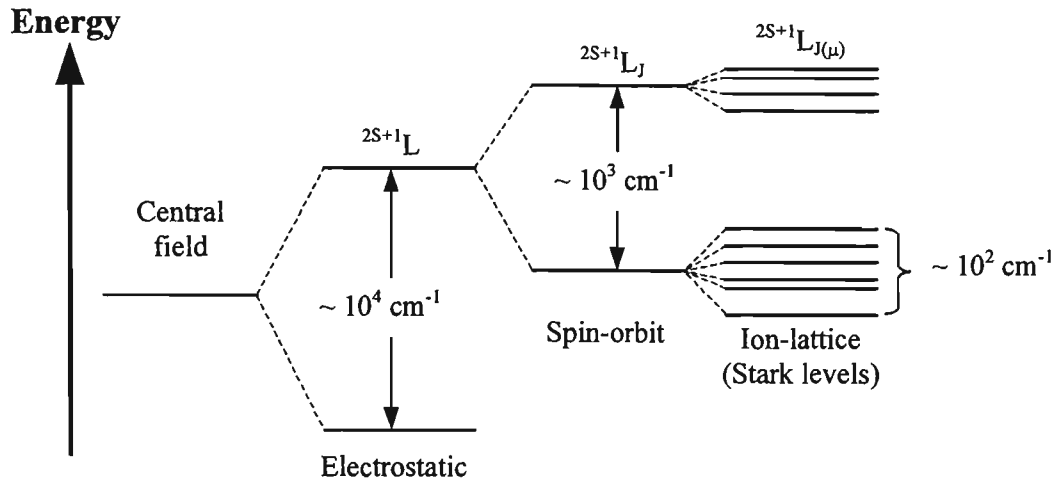


Figure 2.2: Splitting of the rare earth ion energy levels. The approximate energy differences are shown in units of cm^{-1} .

2.2 HOST MATERIALS FOR RARE EARTH IONS

A significant proportion of the research on rare earth doped optical materials has investigated the effect of the host on the optical properties of the dopant. This interest has stemmed from the knowledge that variations in the host material can be used to enhance various properties of optical devices in which the doped material is being used. For example the efficiency, linewidth, wavelength or thermal properties of a laser could be optimised for a particular application through the careful selection of host material.

One of the main contributions to the host dependent effects lies in the structural organisation of the material. In crystal structures for example the ions lie in well defined positions, with the rare earth dopant ions occupying a specific structural site. Glasses on the other hand tend to have disorganised structures which allows the rare earth dopant ions to be positioned in a range of locations in the host material structure. The majority of rare earth ions in crystals are therefore subject to a crystal field of the same magnitude, while in glasses rare earth ions in different structural locations experience different fields from the surrounding ions. This results in the majority of rare earth ions in a crystal host having very similar energy levels, while in glasses the position of the

energy levels (and in particular Stark levels) can vary depending on the local field in which the rare earth ion is located. This tends to broaden the linewidths of transitions of rare earth ions in glass hosts in comparison to crystalline materials [57-59]. An example of the effect of the host composition on the linewidth of fluorescence transitions of a rare earth ion is shown in figure 2.3 for the case of Nd^{3+} doped in glass and YAG host materials.

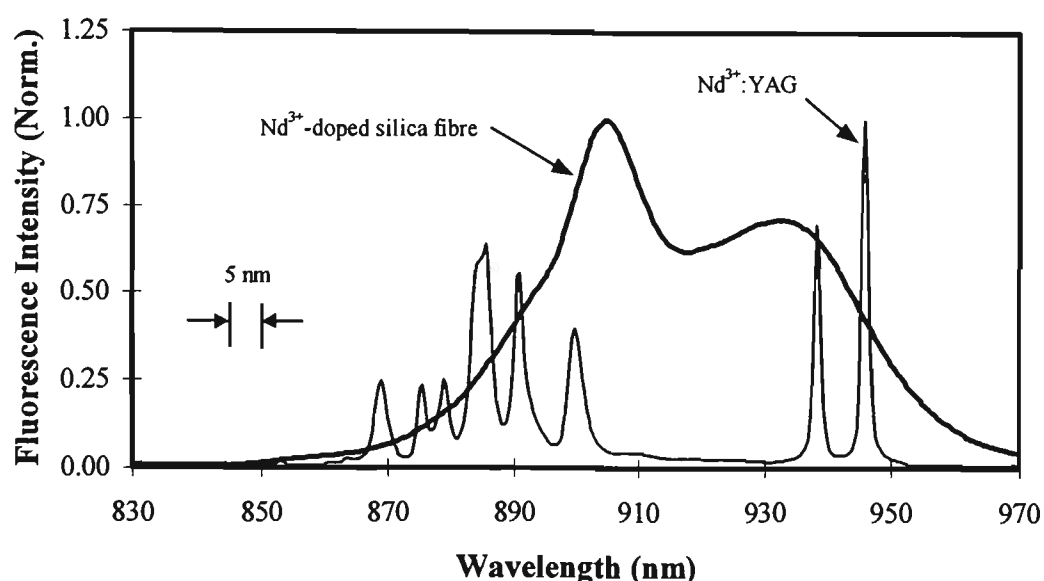


Figure 2.3: Illustration of the effect of host material on the fluorescence linewidth of the Nd^{3+} ion doped in silica fibre (5 nm OSA resolution) and YAG (1 nm OSA resolution).

In addition to varying the linewidth of optical transitions the structural organisation of a rare earth doped material can affect several other of its optical properties. One method of studying this effect is known as site-selective spectroscopy [60, 61], in which changes in the properties of the ions are measured using a narrow band source to excite the material and hence select rare earth ions located in specific sites in the host network. Such studies have shown that the radiative and non-radiative rates, quantum efficiency, branching ratios, intensities and lifetimes can all depend upon the site of the rare earth ion excited.

The composition of rare earth ion host materials has also been found to affect the upper limit of the useful doping concentration of rare earth ions [62]. In many cases the practical dopant concentration limit is determined by reductions in the quantum efficiency or the lifetime of an energy level due to ion-ion interactions such as energy transfer, cross-relaxation and co-operative upconversion. The extent of these interactions depends upon the distance between neighbouring rare earth ions in the host

and increases with reduced average separation. In pure silica for example rare earth ions tend to group together (known as clustering) even at relatively low dopant concentrations. It has been shown however that the addition of modifying materials including Al_2O_3 and P_2O_5 to a silica based host can greatly reduce clustering, allowing higher dopant concentrations to be used [63, 64].

2.3 RARE EARTH DOPED OPTICAL FIBRES

The first rare earth doped optical fibres were reported early in the 1960's, an example of which was the development of a Nd^{3+} -doped fibre amplifier for $1.06 \mu\text{m}$ light by Koester and Snitzer [65] in 1964. At this time however the techniques for producing rare earth doped fibres were still in the early stages of development and the majority of laser research was focussed elsewhere. For the following 20 years only a limited number of reports were made on the use of rare earth doped optical fibres. It wasn't until researchers at the University of Southampton in 1985 altered one of the techniques developed for producing optical fibres for telecommunications to incorporate rare earth ions [66], and the first low loss rare earth doped fibres were produced, that work in this field began in earnest.

The most common host materials currently used for rare earth doped optical fibres are based on either heavy-metal fluorides or oxides. Oxide based rare earth doped fibres were among the first to be developed using manufacturing techniques similar to those used for standard telecommunications fibre, such as chemical vapor deposition CVD. One of the most popular CVD methods is known as modified chemical vapor deposition MCVD [62, 66, 67]. In the MCVD technique, illustrated in figure 2.4, the glass forming materials such as SiCl_4 , GeCl_4 and POCl_3 are heated to produce a vapour. This vapour is then passed through a glass tube that is rotated using a special lathe. As the gas travels through the tube a high temperature torch passes back and forth along the length of the tube causing some of the gas to deposit on the inside walls. After several layers of material have been added to form the cladding of the fibre the gas mixture is altered to produce the core region with a slightly different refractive index. Following the incorporation of the rare earth ions to the core, which can be achieved using a rare earth gas in the mixture or by solution doping, the preform is collapsed using high temperatures, resulting in the finished preform. In the solution doping method of adding

rare earth ions [66] the core deposition stage is controlled so that the core layers are porous. The preform is then soaked in a solution containing the appropriate rare earth ion that permeates the core region. Next the preform is dried by heating with the high temperature torch and finally the preform is collapsed.

Several rare earth doped optical fibres were produced by the author of the thesis using the MCVD technique with solution doping during a research visit to the *Laboratoire de Physique de la Matière Condensée* at the Université de Nice, France. Details of these fibres are given in chapter 4 of this thesis.

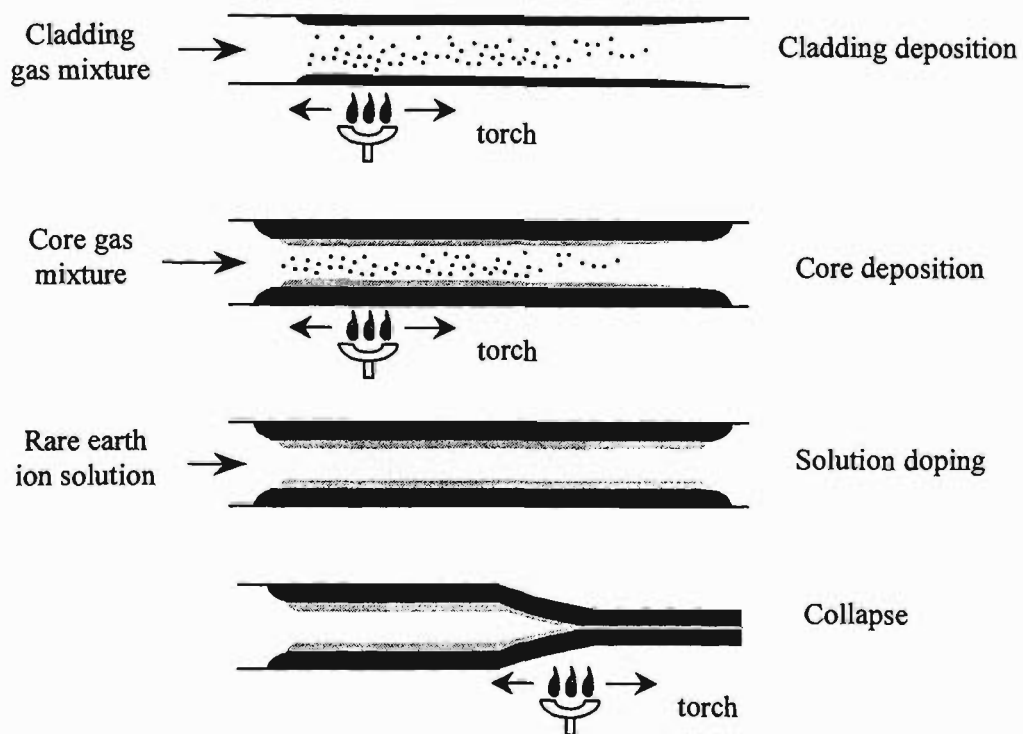


Figure 2.4: Illustration of the MCVD technique with solution doping for the fabrication of rare earth doped silica fibre preforms.

After the preform has been manufactured, optical fibre is fabricated using a drawing tower (see figure 2.5). In this process one end of the preform is heated to melting temperature in high temperature furnace, and the resulting melted section is drawn down at a specific rate to produce fibre with the required dimensions. A jacketing material (typically a polymer) is usually applied in-line to improve the strength of the completed fibre.

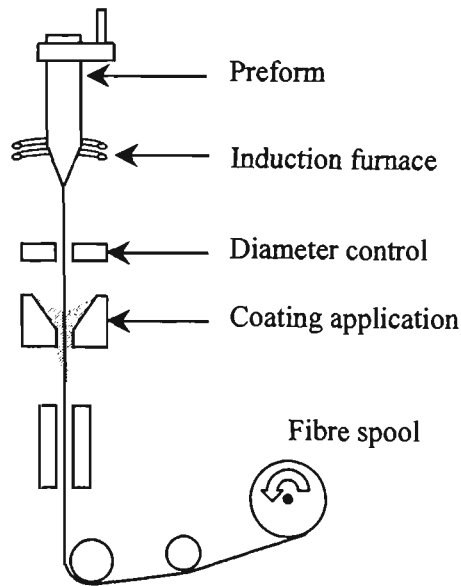


Figure 2.5: Drawing of optical fibre from a preform. *Note:* not to scale.

The techniques used to fabricate heavy metal fluoride optical fibres differ from those used for oxide based fibres mainly because of the tendency of fluoride glasses to crystallise during the manufacturing process [69, 70]. It has been found that the composition of the fluoride glass plays an important role in avoiding crystallisation, with the ZBLAN (ZrF_4 , BaF_2 , LaF_3 , AlF_3 , NaF) composition being amongst the most resilient. The usual methods for producing a heavy metal fluoride glass preform are based on casting, and include built-in casting, rotational casting and suction casting [69, 70]. In the rotational casting technique (see figure 2.6), the melted constituents of the cladding material are poured into a specially designed mold. This mold is then rotated at high speed (typically > 5000 rpm) with the cladding material cooling to produce the cladding tube. Next the melted core material is poured into the centre of the mold and allowed to cool, resulting in the final preform. The method of fibre drawing with heavy metal fluoride glasses is similar to that previously discussed for oxide based fibres except that the drawing temperature is lower and extra care must be taken to ensure that crystallisation does not occur.

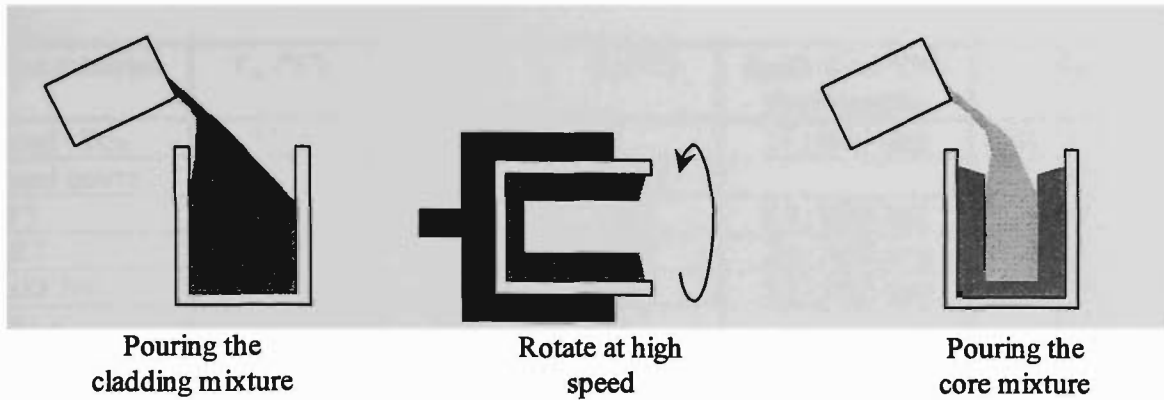


Figure 2.6: Illustration of the production of a rare earth doped fluoride glass preform using the rotational casting technique.

2.4 THERMAL EFFECTS IN RARE EARTH DOPED MATERIALS

Past research has shown that many of the physical and optical properties of optical materials, including glasses and crystals, depend upon the temperature of the material. In this thesis the use of such materials as a host for rare earth ions is investigated for use in temperature sensing. Knowledge of the effects of temperature on these materials is therefore useful in determining which materials will be best suited to this application.

Important changes in the properties of optical materials due to temperature are often defined by what are known as characteristic temperatures [71]. In crystals, for example, the melting temperature (T_m) characterises the point at which a phase transition between a liquid and a solid state occurs. In glasses, however, rather than a pronounced change in state at a particular temperature the structure gradually changes over a wide temperature range. Glasses are therefore characterised by a transformation temperature (T_g), also known as the glass transition temperature, below which the rate of changes in the glass structure decrease and the material approaches a stabilised state. This is usually defined by the temperature at which the viscosity of the glass is approximately 10^{12} Pa · s [72], and has been found to depend upon the rate of cooling. Some of the other characteristic temperatures of glasses are the softening temperature and the annealing temperature. The softening temperature describes the temperature at which glass will deform under its own weight. The annealing temperature defines a temperature that can be used to remove stress introduced into the glass as it is cooled through the transformation temperature. Table 2.1 lists the characteristic temperatures for several well known optical materials.

Host material	T_m (°C)	T_g (°C)	T_a (°C)	dn/dT ($\times 10^{-6}/^\circ\text{C}$) (wavelength)	Ref.
Fused silica	1710	1000, 1075		11 (1064 nm)	[71], [73], [74]
Fused quartz			1050		[70]
LF5		413	411	0.8 (1060 nm)	[75]
BK7		557	557	2.4 (1060 nm)	[76]
LaSF N9		703	694	2.9 (1060 nm)	[76]
ZBLA	513	320			[77]
ZBLAN	455	262		-14.8	[77], [78]
AMTIR 1		362			[74]
IG 1.1		150			[74]
Ruby	2046			13.6 [n_o] 14.7 [n_e] (589 nm)	[73]
Alexandrite	1870				[79]
YAG	1970			7.3 (1064 nm)	[73]
YVO ₄	1810-1940				[73]

Table 2.1: Melting temperature (T_m), glass transition temperature (T_g), annealing temperature (T_a) and the change in refractive index with temperature (dn/dT) of various optical materials.

Aside from the changes defined by characteristic temperatures some of the other important temperature induced variations in the optical and physical properties of optical materials include changes in the refractive index, thermal expansion, changes in the blackbody radiation spectrum of the material and the degradation of materials used to jacket/coat the optical materials.

Refractive Index

Changes in the temperature of an optical material often result in changes in the refractive index of the material. Depending upon the magnitude of the temperature change and the length of time which the material is exposed to the different temperature, the changes in refractive index can be either temporary or permanent [72]. Large variations in the refractive index can result in changes in the guiding and dispersion properties of the material and therefore should be avoided. The variation in the refractive index with temperature (dn/dT) of several well-known optical materials is also listed in table 2.1.

Thermal Expansion

Changes in the temperature of an optical material are usually accompanied by changes in the physical dimensions of the material. This can lead to misalignment between optical components which have different expansion coefficients and in the worst case result in fracture/breakage of optical materials [80, 81].

Blackbody Radiation

The intensity and spectral distribution of blackbody radiation emitted by an optical material depends upon the temperature and composition of the material [82]. In many optical fibre sensor configurations the radiation emitted by sensor components, including optical fibres, may be guided by the transmission fibre to the detection system. If this does occur the transmitted blackbody radiation may interfere with the signal used for temperature measurement and hence introduce measurement errors. Fortunately the intensity of radiation at temperatures near ambient is usually negligible in comparison with the measurement signal. However, as the magnitude of blackbody radiation increases with temperature care must be taken to ensure that the measurement signal is not adversely affected.

Jacketing Material

A jacketing material is normally used on optical fibres to increase the mechanical strength of the fibre and prevent moisture coming into contact with the glass surface. The latter is important as for many glass materials moisture has been found to assist the propagation of surface cracks, especially at raised temperatures, which can lead to fibre breakage. The composition of jacketing material normally used on optical fibres has been found to degrade at temperatures greater than approximately 200 °C, which can cause significant reduction in fibre performance [83]. Practically this problem can be overcome by the use of different jacketing materials, e.g. gold increases the upper temperature limit to approximately 750 °C [84].

Recently the maximum temperature limits of several rare earth doped optical materials have been investigated in relation to their use in fluorescence lifetime based temperature sensing [33-35]. It was discovered that in order to obtain consistent lifetime versus temperature characteristics the rare earth doped sensing material should undergo an annealing process where it is held at an elevated temperature for a specific length of time. In the case of Nd³⁺-doped fibre [35], for example, the fibre was annealed at 750 °C for 100 hours, after which consistent lifetime versus temperature characteristics were observed during temperature cycling between 100 °C and 750 °C.

2.5 SUITABILITY OF HOST MATERIALS FOR USE IN FLUORESCENCE INTENSITY RATIO BASED TEMPERATURE SENSING

In chapter 1 the basic concept of the fluorescence intensity ratio technique for temperature sensing was introduced, in which the fluorescence intensities of two closely spaced energy levels, typically from a rare earth ion, are used to measure temperature. In selecting host materials for use with the fluorescence intensity ratio technique of temperature sensing the following factors should be considered:

(i) Ability to couple with optical fibre

The coupling efficiency between the transmission fibre and the rare earth doped material, and hence the intensity of fluorescence reaching the detection system, largely depends upon the size and shape of the doped material. Host materials with good coupling efficiency may allow reductions in sensor cost through the use of lower power excitation sources and less complicated detection systems. The host materials which best suit this specification are rare earth doped optical fibres and in particular silica based fibres which have well developed, low-loss connection techniques (e.g. fusion splicing).

(ii) Thermal operating range

The host material must be able to withstand a range of temperatures determined by the application in which the sensor is to be used. This thesis is concerned with the measurement of temperature over a wide range from approximately -200 to 600 °C. The most promising host materials for such wide temperature ranges include silica based glasses and crystalline materials.

(iii) Absorption and fluorescence linewidth

Host materials that have relatively large absorption linewidths, such as silica based glasses, increase the range of excitation sources that could be used and therefore can potentially reduce sensor cost. However, if the fluorescence linewidth is large the fluorescence from the two levels of interest may overlap which can reduce the sensitivity of the sensor (this is discussed in further detail in chapter 3). As the absorption and fluorescence linewidths are usually of a similar magnitude in most materials these two factors need to be considered together.

(iv) Fluorescence intensity

The intensity of fluorescence from particular energy levels of a rare earth ion can depend upon the host material in which the ion is doped. Host materials which provide the greatest fluorescence intensity for a given pump power would allow less complex detection systems and/or lower power excitation sources to be employed and hence potentially decrease the sensor cost.

(v) Cost

Finally, one of the aims of the fluorescence intensity ratio technique is to provide an accurate, low cost optical fibre temperature sensor. To help meet the desire for a low cost sensor the rare earth doped material itself should be relatively low in cost.

Ultimately the choice of host material for a particular application is a compromise between each of the above factors. However the materials which appear to best meet the aforementioned conditions are silica based glasses, including optical fibres, and some well known crystalline materials such as YAG and YVO₄.

2.6 CONCLUSION

Rare earth ions can be doped into a wide range of host materials for use in optical applications. The composition of the material into which rare earth ions are doped can have a significant effect on the optical properties of the rare earth ion. In addition, physical properties such as the upper temperature limit are dependent upon the host material. Host materials for rare earth ions that appear to be the best candidates for use with fluorescence intensity ratio based temperature sensing include silica based optical fibres and widely used crystalline host materials such as YAG.

Chapter 3: Fluorescence Intensity Ratio Theory

- 3.1 INTRODUCTION
- 3.2 THE GENERAL FORM OF THE BOLTZMANN DISTRIBUTION
- 3.3 THE BOLTZMANN DISTRIBUTION APPLIED TO FLUORESCENCE INTENSITY RATIO TEMPERATURE SENSING
- 3.4 SENSITIVITY OF THE FLUORESCENCE INTENSITY RATIO
- 3.5 OPTICAL ARRANGEMENTS FOR MEASURING THE FLUORESCENCE INTENSITY RATIO
- 3.6 EFFECT OF THE OPTICAL ARRANGEMENT ON THE MEASURED FLUORESCENCE INTENSITY RATIO AND SENSITIVITY
 - 3.6.1 *Overlap of fluorescence from the thermally coupled levels*
 - 3.6.2 *Stray light*
 - 3.6.3 *Summary*
- 3.7 CONCLUSION

Overview of Chapter

The following chapter presents the theory describing the fluorescence intensity ratio technique. This includes an investigation of how certain aspects of the sensor configuration and sensing material affect both the measured fluorescence intensity ratio and the sensitivity of the fluorescence intensity ratio to changes in temperature.

3.1 INTRODUCTION

In this chapter the theoretical basis of the fluorescence intensity ratio technique of temperature sensing is discussed. Starting with the Boltzmann distribution, the fluorescence intensity ratio from two closely spaced energy levels of an ion is described, together with equations for the individual fluorescence intensity from each of the two levels. Following this, the sensitivity of the fluorescence intensity ratio to changes in temperature is discussed. The later half of the chapter is devoted to developing equations describing how the sensor arrangement and sensing material can affect the measured fluorescence intensity ratio and sensitivity.

3.2 THE GENERAL FORM OF THE BOLTZMANN DISTRIBUTION

When a system consisting of a large number of particles, such as atoms or molecules, is in a state of thermal equilibrium the distribution of particles among the available energy levels is given by the Boltzmann distribution [39, 40]. For a system that has two distinct energy levels, labeled x and y where $E_x > E_y$, the Boltzmann distribution takes the form:

$$\frac{N_x}{N_y} = \exp\left[\frac{-(E_x - E_y)}{kT}\right] \quad (3.1)$$

where N_x and N_y are the relative populations of the levels with energies E_x and E_y respectively, k is the Boltzmann constant (1.38041×10^{-23} J/K) and T is the absolute temperature. Therefore, as the temperature of the system is increased the number of atoms or molecules in the E_x energy level increases relative to the number in the E_y energy level. For simplicity, in this thesis the terms *thermally coupled* and *thermalisation* are used to describe energy levels for which the population distribution amongst the levels is primarily governed by a Boltzmann distribution, over temperature ranges of interest for sensing applications. These terms, in a stricter definition, could be used to describe any group of levels whose relative populations depend upon temperature.

3.3 THE BOLTZMANN DISTRIBUTION APPLIED TO FLUORESCENCE INTENSITY RATIO TEMPERATURE SENSING

In chapter 1 the fluorescence intensity ratio technique of temperature sensing was introduced. The basis of this technique is that the relative populations, and hence fluorescence intensities, of thermally coupled energy levels in rare earth ions follow a Boltzmann distribution. Therefore, temperature can be inferred from measurements of the ratio of the fluorescence intensity (R) from two such energy levels. Referring to the simplified energy level diagram of a rare earth ion shown in figure 3.1 the ratio of the fluorescence intensities from two thermally coupled energy levels, labelled level 2U and level 2L, to a common lower energy level is given by [36]:

$$R(T, \Delta E) = \frac{I_{2Uj}}{I_{2Lj}} = \frac{N_{2U} \sigma_{2Uj} \omega_{2Uj}}{N_{2L} \sigma_{2Lj} \omega_{2Lj}} = \frac{g_{2U} \sigma_{2Uj} \omega_{2Uj}}{g_{2L} \sigma_{2Lj} \omega_{2Lj}} \exp\left[\frac{-\Delta E}{kT}\right] = B \exp\left[\frac{-\Delta E}{kT}\right] \quad (3.2)$$

$$\text{with } B = \frac{g_{2U} \sigma_{2Uj} \omega_{2Uj}}{g_{2L} \sigma_{2Lj} \omega_{2Lj}}$$

where N_i , I_{ij} , g_i , σ_{ij} and ω_{ij} refer to the number of ions, fluorescence intensity, degeneracy, emission cross section and the angular frequency of fluorescence transitions from the upper ($i = 2U$) and lower ($i = 2L$) thermalising energy levels to a terminal level j , and ΔE is the energy gap between the two levels.

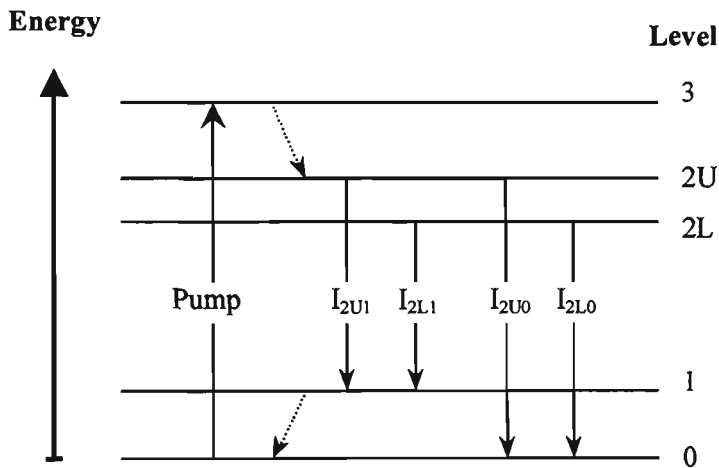


Figure 3.1: Simplified energy level diagram for a generic rare earth ion, where level 3 is the pump level, level 2U and 2L are the thermalising levels, level 1 is one of the possible terminal levels of fluorescence and level 0 is the ground state. Solid lines - radiative transitions, dotted lines - non-radiative transitions.

As shown in figure 3.1 the terminal level of fluorescence can be the ground state or another excited state with energy less than the levels from which fluorescence originates. The upper energy levels used in this work were predominantly two separate J manifolds of a rare earth ion, with an exception being the ${}^2F_{5/2}$ Stark sub-levels of the Yb^{3+} ion doped in a silica host. It is also worth mentioning that the value of the energy gap, ΔE , used when fitting equation 3.2 to experimental data is actually an averaged value that depends upon:

- (a) the population distribution amongst the Stark levels of the J manifolds (if degenerate levels are used),
- (b) the distribution of energy gaps between the two thermally coupled energy levels due to site selective effects.

The physical process responsible for the relative population distribution amongst closely spaced energy levels is the interaction between the rare earth ions and the host lattice. In this process the rare earth ion interacts with vibrational energy from the host lattice and either gives up energy to the lattice, and thus decays to a lower energy level, or receives energy from the lattice and moves to a higher energy level. The quantised lattice vibrational energies are commonly known as phonons. Experiments have shown that for closely spaced energy levels, such as the Stark levels of a J multiplet, the transitions between the energy levels occur on the picosecond to subpicosecond time scale [57].

In figure 3.2 examples of the fluorescence intensity ratio as a function of temperature are plotted for a range of typical energy gaps useful for temperature sensing applications. These have been calculated using equation 3.2 for the cases of $B = 1$ and $B = 10$.

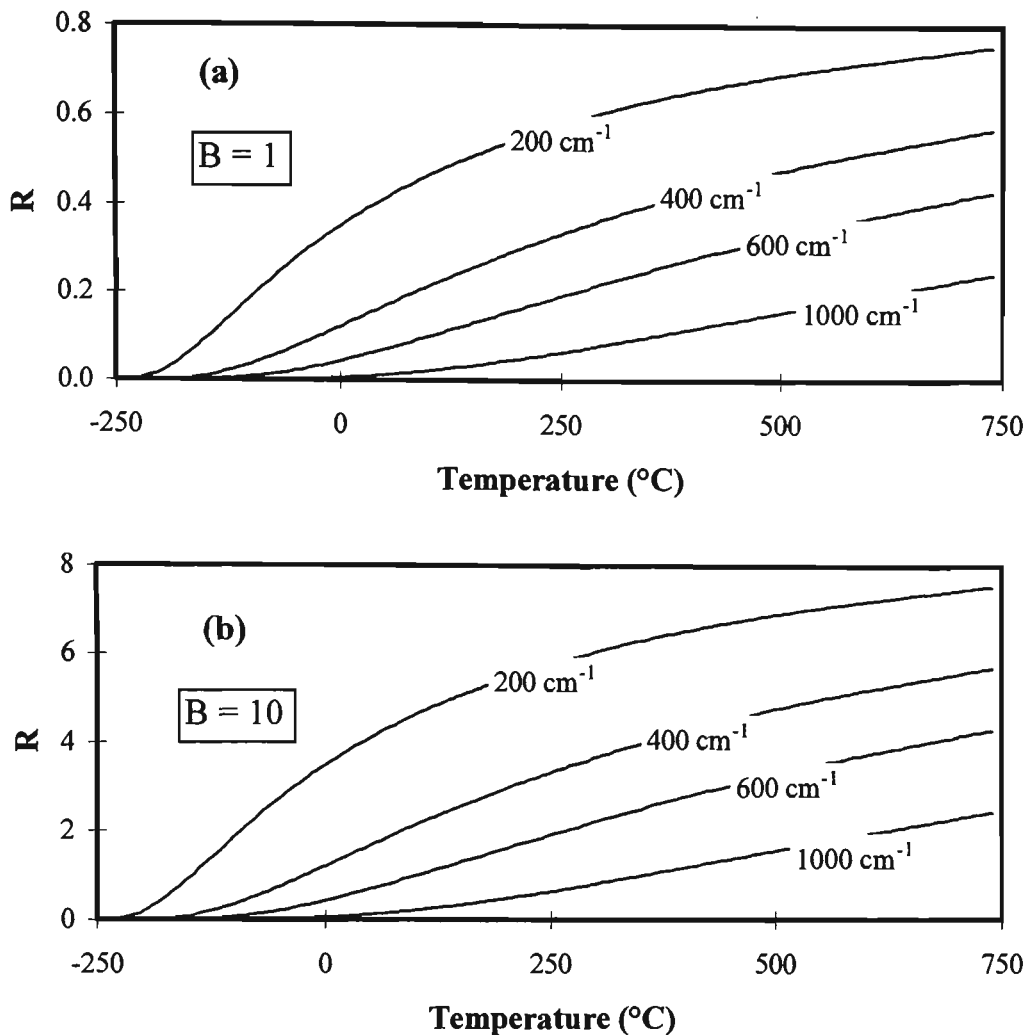


Figure 3.2: Fluorescence intensity ratio versus temperature for energy gaps between 200 cm^{-1} and 1000 cm^{-1} , (a) $B = 1$, (b) $B = 10$.

The individual fluorescence intensity originating from each of the thermalising energy levels, denoted by I_{2L} and I_{2U} , can be calculated for a particular temperature using the total fluorescence intensity from the two levels (I_t), given by:

$$I_t = I_{2U} + I_{2L} \quad (3.3)$$

and the fluorescence intensity ratio, R (equation 3.2). Solving for I_{2L} and I_{2U} we obtain:

$$I_{2U} = \frac{I_t R}{1 + R}, \quad (3.4)$$

$$I_{2L} = \frac{I_t}{1 + R}. \quad (3.5)$$

Two examples of the variation of I_{2L} and I_{2U} with temperature are given in figure 3.3. These figures have been plotted for values of the constant B of 1 and 10 with an energy gap between the thermalising levels of 750 cm^{-1} . The change in the total fluorescence intensity from the two thermally coupled levels with temperature depends upon a

number of factors including the energy levels of interest, the host material and the excitation used. For simplicity, in this chapter the total fluorescence intensity from the two thermally coupled levels is assumed to be constant with temperature.

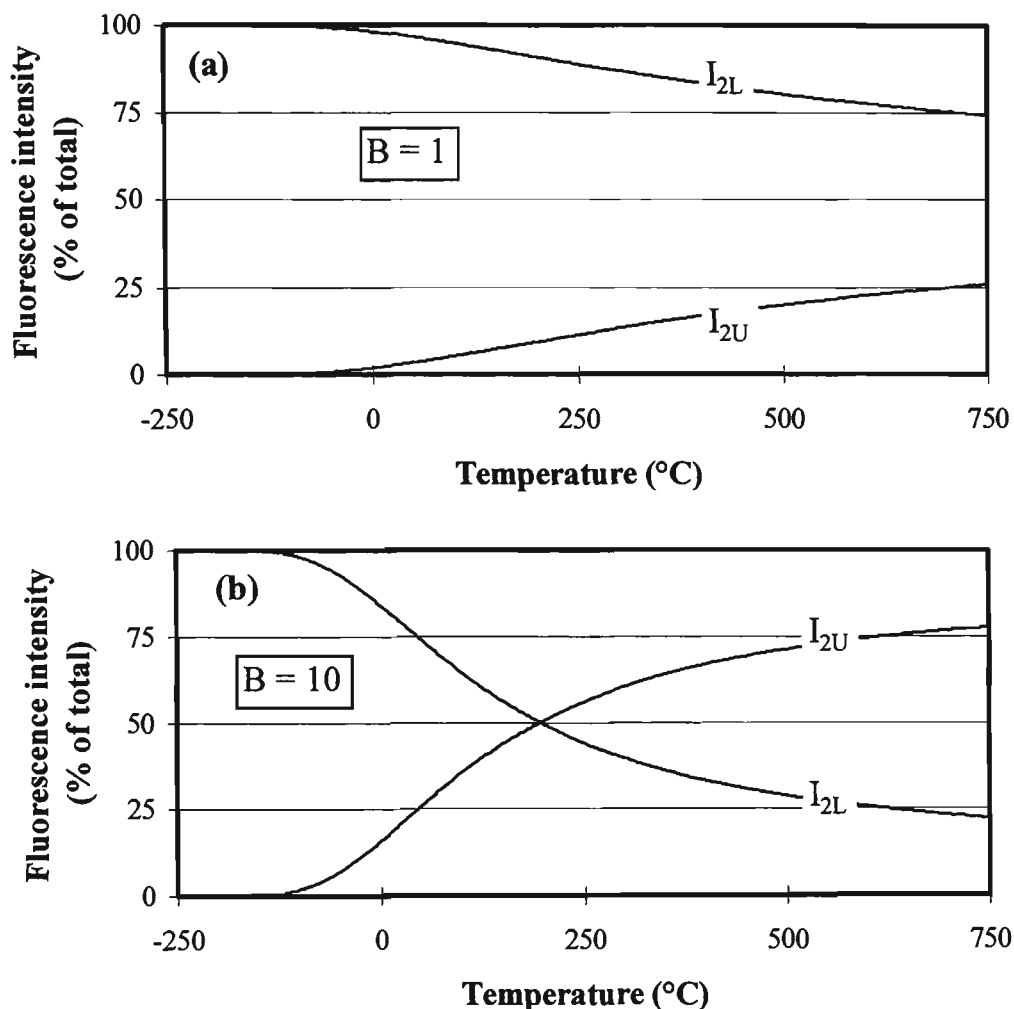


Figure 3.3: Intensity of the upper (I_{2U}) and lower (I_{2L}) thermalising levels as a function of temperature for an energy gap of 750 cm^{-1} , (a) $B = 1$, (b) $B = 10$.

Figure 3.3a illustrates that for the case when $B = 1$ the fluorescence intensity from the upper level (I_{2U}) is small in comparison to that from the lower level (I_{2L}), especially at lower temperatures. One of the problems that this may introduce is the requirement for a more sophisticated detection system to measure the low fluorescence intensity, which has the potential to increase sensor cost. However, as shown in figure 3.3b the fluorescence intensity from the upper level is significantly greater for the same energy gap if the thermally coupled levels have a B factor greater than 1 (i.e. at 20°C and $B = 1$ then $I_{2U} = 2\%$ of total fluorescence intensity, if $B = 10$ then $I_{2U} = 20\%$ of total fluorescence intensity).

3.4 SENSITIVITY OF THE FLUORESCENCE INTENSITY RATIO

The rate of change of the fluorescence intensity ratio with temperature (dR/dT) is commonly referred to as the temperature sensitivity (S) of the fluorescence intensity ratio. To allow easy comparison between the sensitivity values obtained for the fluorescence intensity ratio of different energy level/host material combinations it is usually expressed as a relative value:

$$S = \frac{1}{R} \frac{dR}{dT} = \frac{\Delta E}{kT^2}. \quad (3.6)$$

For simplicity in the remainder of the thesis, unless otherwise stated, any mention of the temperature sensitivity of the fluorescence intensity ratio will be taken to refer to the value expressed by equation 3.6. The importance of this parameter is that it partially determines the limit of the accuracy of measurement (δT) obtainable using the fluorescence intensity ratio technique, which is given by:

$$\delta T = \frac{\Delta R}{S} = \frac{R \sqrt{(\Delta I_{2U}/I_{2U})^2 + (\Delta I_{2L}/I_{2L})^2}}{S} \quad (3.7)$$

where ΔR is the error in the fluorescence intensity ratio measurement, ΔI_{2U} is the error in the upper level fluorescence intensity I_{2U} , ΔI_{2L} is the error in the lower level fluorescence intensity I_{2L} and S is the sensitivity. Figure 3.4 shows the variation in the sensitivity as a function of temperature for some typical values of the energy gap between the two thermalising levels (a log scale has been used to help distinguish the sensitivity values at higher temperatures).

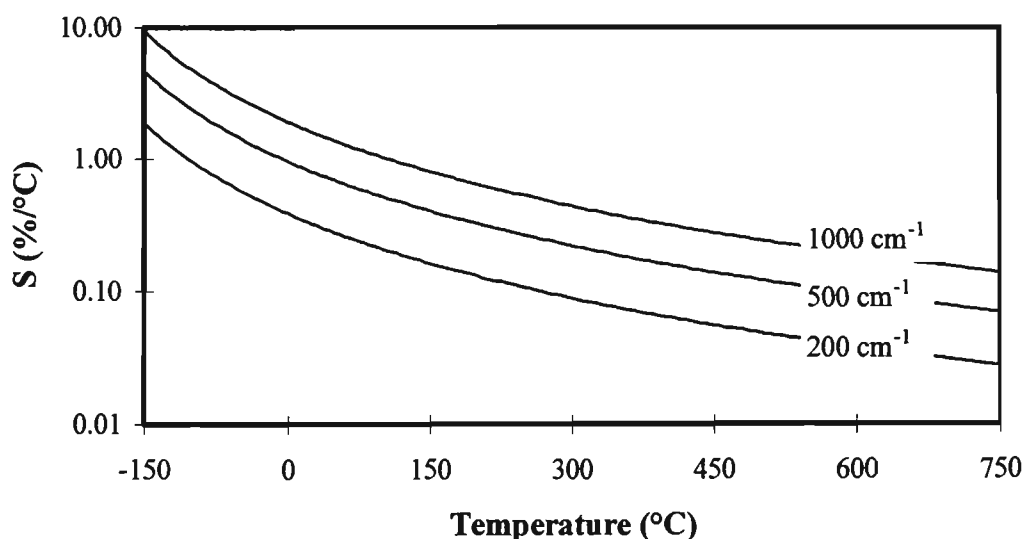


Figure 3.4: Sensitivity versus temperature for energy gap values between 200 cm^{-1} and 1000 cm^{-1} .

The theoretical sensitivity of rare earth ions that have been investigated for fluorescence intensity ratio based sensing (both in this work and by others) are listed in table 3.1

Rare earth ion	ΔE (cm ⁻¹) [Ref.]	Sensitivity (%/°C)		
		@ -100 °C	@ 20 °C	@ 200 °C
Pr ³⁺	580 [85]	2.79	0.97	0.37
Yb ³⁺	680 [86]	3.27	1.14	0.44
Er ³⁺	780 [46]	3.75	1.31	0.50
Nd ³⁺ , Sm ³⁺ , Dy ³⁺	1000 [87]	4.81	1.68	0.64
Eu ³⁺	1750 [87]	8.41	2.93	1.13

Table 3.1: Theoretical sensitivity of rare earth ions used in the fluorescence intensity ratio technique, ΔE is the approximate energy gap between thermally coupled energy levels.

The data shown in figure 3.4 and listed in table 3.1 indicate that the sensitivity of the fluorescence intensity ratio technique is best at lower temperatures and for relatively large energy gaps between the thermalising energy levels.

3.5 OPTICAL ARRANGEMENTS FOR MEASURING THE FLUORESCENCE INTENSITY RATIO

In a practical fluorescence intensity ratio based temperature sensor the fluorescence intensity is usually measured by optically filtering wavelength ranges corresponding to fluorescence from each of the two thermalising energy levels of the rare earth doped sensor material. Three examples of optical arrangements which have been used in fluorescence intensity ratio based temperature sensors are illustrated in figure 3.5 (further information regarding the components and measurements performed using these arrangements is given in chapter 5).

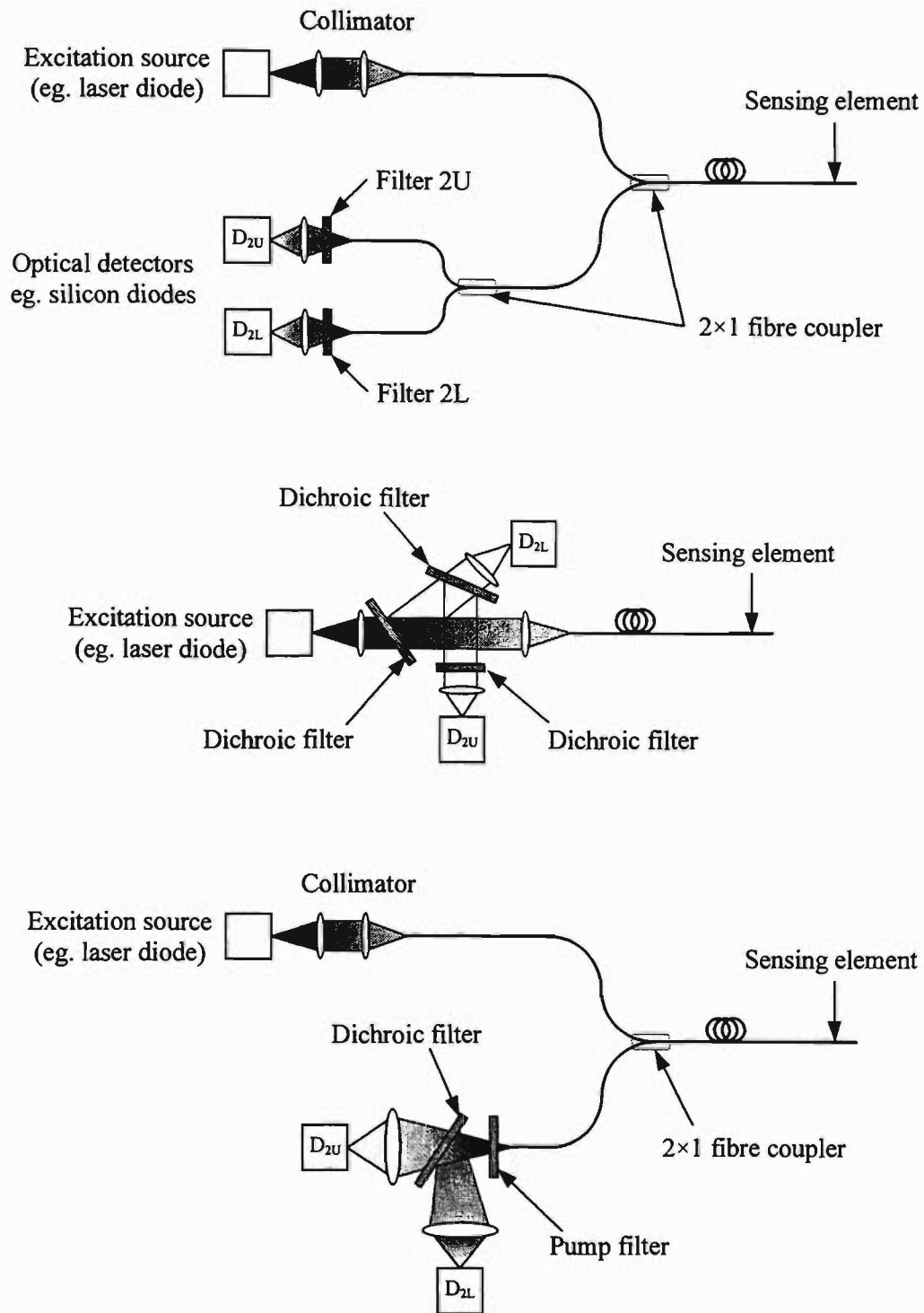


Figure 3.5: Examples of optical arrangements that have been used in a fluorescence intensity ratio based temperature sensor [88-90].

In each of the fluorescence intensity ratio sensor arrangements shown in figure 3.5, the fluorescence intensity ratio is determined by measuring the output voltages, V_{2U} and V_{2L} , of the two detectors D_{2U} and D_{2L} which are assumed to be proportional to the intensity of fluorescence from the upper and lower thermalising energy levels, ie:

$$\frac{V_{2U}}{V_{2L}} \propto \frac{I_{2U}}{I_{2L}} = B \exp\left[\frac{-\Delta E}{kT}\right]. \quad (3.8)$$

Once the sensor has been calibrated over the temperature range required the temperature of the sensing element can be determined from V_{2U}/V_{2L} using either a look-up table or mathematical expression (e.g. polynomial fit) obtained from the calibration data.

3.6 EFFECT OF THE OPTICAL ARRANGEMENT ON THE MEASURED FLUORESCENCE INTENSITY RATIO AND SENSITIVITY

In the previous section several arrangements were displayed for the practical measurement of temperature using the fluorescence intensity ratio technique. One assumption made was that detector voltages are directly proportional to the intensity of fluorescence from the level of interest. In practice however the detector voltage, V , can be calculated from the total intensity, $I(\lambda)$, of the light falling on it and the wavelength response of the detector $\rho(\lambda)$, i.e.:

$$V \propto \int I(\lambda)\rho(\lambda)d\lambda \quad (3.9)$$

and in addition to fluorescence from the level of interest this can consist of light from a number of other sources including fluorescence from other energy levels of the rare earth ion, excitation light (which for example may have been reflected from splices or fibre ends) or stray ambient light. The contribution from each of these sources to the detector output is determined by the filters used and to a lesser extent the wavelength dependence of other optical components in the arrangement (e.g. the splitting ratio of 3 dB couplers is wavelength dependent). If light over the wavelength range $\lambda_a \rightarrow \lambda_b$ is used to measure the fluorescence intensity from the upper energy thermalising level and light over the wavelength range $\lambda_c \rightarrow \lambda_d$ is used to measure the fluorescence intensity from the lower energy thermalising level the voltages measured by the two detectors are given by:

$$V_{2U} \propto \int_{\lambda_b}^{\lambda_a} I(\lambda)\rho(\lambda)d\lambda, \quad (3.10)$$

$$V_{2L} \propto \int_{\lambda_d}^{\lambda_c} I(\lambda)\rho(\lambda)d\lambda, \quad (3.11)$$

where V_{2U} and V_{2L} are the voltages measured by the upper and lower energy thermalising level detectors respectively. In the following sections, equations are developed to describe the effect of light from sources other than the level of interest,

incident upon the detectors, on the fluorescence intensity ratio and sensitivity of the fluorescence intensity ratio to changes in temperature.

3.6.1 Overlap of fluorescence from the thermally coupled levels

The largest possible energy gap between the two thermalising energy levels, ΔE , allowing practical fluorescence intensity ratio based temperature sensing is usually determined by the intensity of fluorescence from the upper energy level. For the majority of materials studied to date the energy levels have been separated by less than approximately 1000 cm^{-1} . For larger energy gaps the upper energy level has a low population of ions for the temperature ranges of interest, and hence the fluorescence intensity, is small. In this case more complicated detection systems may be required, partly negating the potential cost advantages of this technique. The peak wavelengths of fluorescence from the two levels of interest, to a common lower level, can therefore be relatively close (e.g. $\sim 45 \text{ nm}$ for $\Delta E = 750 \text{ cm}^{-1}$ and $\lambda = 800 \text{ nm}$). For many of the glass based rare earth ion host materials the fluorescence linewidths are large enough that a portion of fluorescence from each of the thermally coupled levels will overlap with the other (see figure 3.6). This effect is exacerbated by the Stark splitting of both the initial and terminal levels of fluorescence, which increase the overall width of the fluorescence originating from each of the thermally coupled levels.

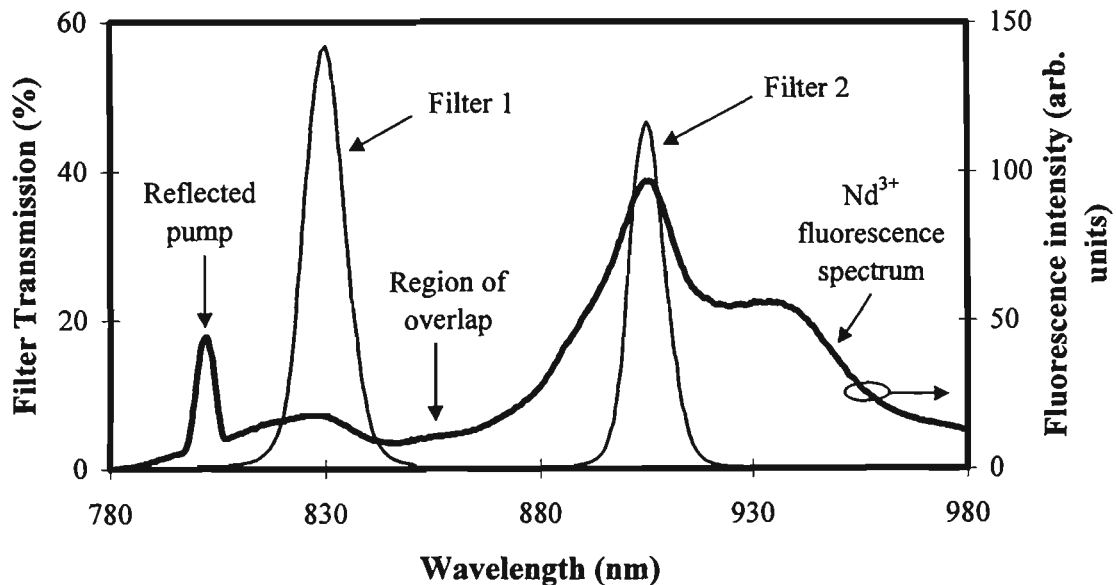


Figure 3.6: Counter-propagating fluorescence spectrum for Nd^{3+} -doped silica fibre containing fluorescence from the levels of interest and reflected pump light. Also shown are examples of the wavelength responses of filters used to measure the fluorescence intensity originating from each of the thermally coupled energy levels.

Fluorescence intensity ratio

For the case where the fluorescence from the two thermalising levels overlap, the intensity of fluorescence over the wavelength ranges measured by each of the detectors will consist of fluorescence originating from the desired level plus fluorescence which originates from the other thermalising energy level, i.e.:

$$I_{\Delta\lambda 2U} = n_{2U}I_{2U} + m_{2L}I_{2L}, \quad (3.12)$$

$$I_{\Delta\lambda 2L} = n_{2L}I_{2L} + m_{2U}I_{2U}, \quad (3.13)$$

where $I_{\Delta\lambda i}$ is the total fluorescence intensity over the wavelength ranges measured by the detectors for the upper energy ($i = 2U$) and lower energy ($i = 2L$) thermalising levels, I_i is the total fluorescence intensity of the transitions used for each of the thermalising energy levels, n_i defines the fraction of the total fluorescence intensity of the transition originating from level i actually measured by the detector for the i level and m_i defines the fraction of the total intensity from level i which is measured by the detector for the other thermalising level. Using these equations and the equations for the individual fluorescence intensity of the two thermalising levels (equations 3.4 and 3.5) the ratio of the fluorescence intensity measured by the two detectors is given by:

$$R = \frac{I_{\Delta\lambda 2U}}{I_{\Delta\lambda 2L}} = \frac{n_{2U}B \exp\left[-\frac{\Delta E}{kT}\right] + m_{2L}}{n_{2L} + m_{2U}B \exp\left[-\frac{\Delta E}{kT}\right]}. \quad (3.14)$$

For the majority of materials investigated in this thesis the fluorescence intensity originating from the upper energy level is relatively small compared to the intensity from the lower energy level, as would be expected from the Boltzmann distribution. In fluorescence spectra this corresponds to a low wavelength peak (originating from the upper energy level) which is small in comparison to a longer wavelength peak (originating from the lower energy level), as shown in figure 3.6 for the case of Nd^{3+} -doped silica fibre. In this case the magnitude of the fluorescence from the upper energy thermalising level which overlaps the fluorescence from the lower energy thermalising level is negligible (i.e. $n_{2L}I_{2L} \gg m_{2U}I_{2U}$) and the fluorescence intensity ratio can be simplified to:

$$R = \frac{I_{\Delta\lambda 2U}}{I_{\Delta\lambda 2L}} = \frac{n_{2U}B \exp\left[-\frac{\Delta E}{kT}\right]}{n_{2L}} + \frac{m_{2L}}{n_{2L}}. \quad (3.15)$$

Therefore for this simplified case the overlap of fluorescence has the effect of adding a constant offset to the equation for the fluorescence intensity ratio.

Examples of the effect of overlap on the fluorescence intensity ratio value as a function of temperature for the simplified case (i.e. equation 3.15) are given in figure 3.7. The curves shown have been plotted using values of overlap roughly corresponding to those observed in measurements of rare earth fluorescence spectra with temperature (see chapter 4). This ranges from the case where the overlap is negligible at 20 °C (i.e. $m_{2L}I_{2L} \sim 0$) to when the contribution from both the upper and lower energy thermalising levels over the upper energy level filter wavelength range are equal at 20 °C (i.e. $n_{2U}I_{2U} = m_{2L}I_{2L}$). The energy gap used in these calculations was 750 cm^{-1} and the value of B was 1. Finally, the fraction of the fluorescence from the lower energy level which overlaps the wavelength range used for the upper energy level (i.e. m_{2L}) was assumed to be constant with temperature.

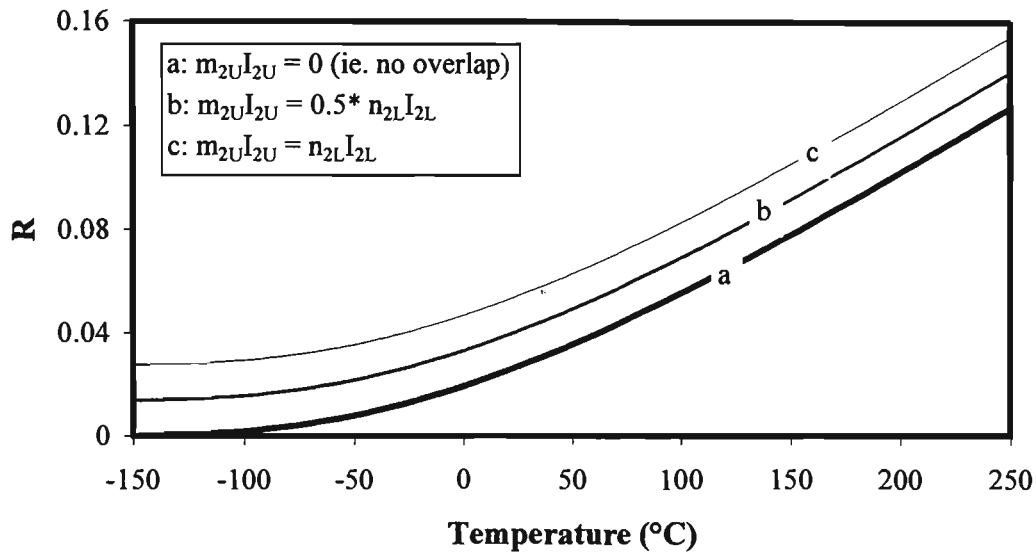


Figure 3.7: The theoretical fluorescence intensity ratio for varying degrees of overlap of the fluorescence from the two thermally coupled levels at 300 K. Calculated using equation 3.15, assuming $B = 1$ and an energy gap of 750 cm^{-1} .

Sensitivity

Using the formula for the fluorescence intensity ratio (equation 3.14), the theoretical sensitivity accounting for overlap between the fluorescence from the two thermally coupled levels is given by:

$$S = \frac{1}{R} \frac{\partial R}{\partial T} = \left(\frac{\Delta E}{kT^2} \right) \left\{ \frac{B \exp[-\Delta E/kT] (n_{2U}n_{2L} - m_{2L}m_{2U})}{(n_{2L} + m_{2U}B \exp[-\Delta E/kT]) (n_{2U}B \exp[-\Delta E/kT] + m_{2L})} \right\}. \quad (3.16)$$

In the simplified case where it is assumed that the effect of overlap is much greater on the upper level fluorescence intensity than for the lower level fluorescence the sensitivity becomes:

$$S = \frac{1}{R} \frac{\partial R}{\partial T} = \left(\frac{\Delta E}{kT^2} \right) \left\{ \frac{n_{2U} B \exp[-\Delta E/kT]}{n_{2U} B \exp[-\Delta E/kT] + m_{2L}} \right\}. \quad (3.17)$$

In figure 3.8 examples of the effect of overlap on the thermal sensitivity of the fluorescence intensity ratio are given. These values have been calculated for the simplified case using equation 3.17, assuming $B = 1$ and an energy gap of 750 cm^{-1} . The data shown have been calculated for the cases when the magnitude of fluorescence from the lower energy thermalising level over the wavelength range used for the upper energy thermalising energy level is equal to 0%, 5%, 25%, or 100% of the fluorescence from the upper energy thermalising energy level at $20 \text{ }^\circ\text{C}$.

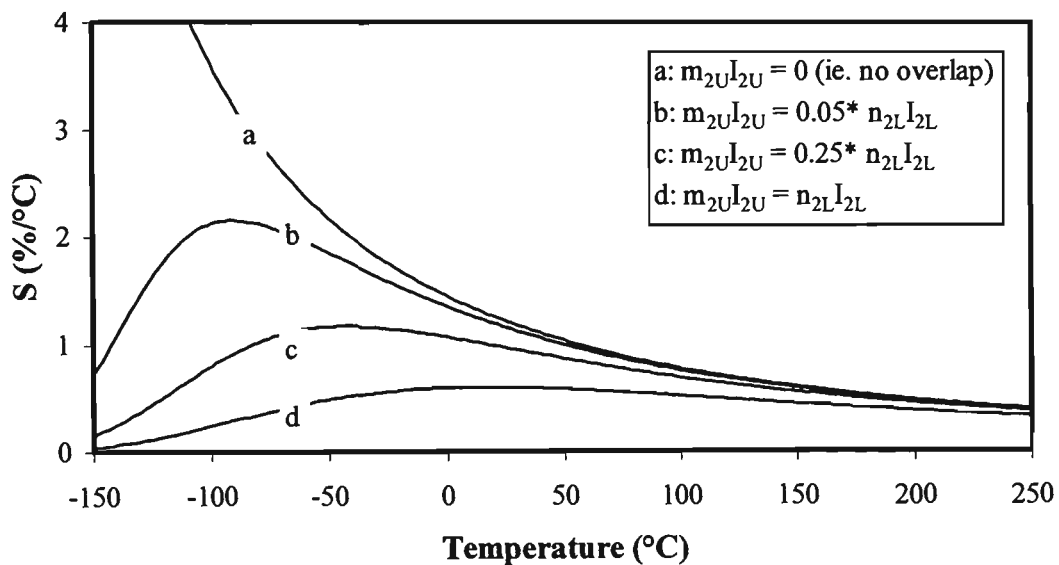


Figure 3.8: Example of the effect of overlap of the fluorescence from the two thermally coupled levels on the thermal sensitivity of the fluorescence intensity ratio for various degrees of overlap, calculated using equation 3.17, assuming $B = 1$ and an energy gap of 750 cm^{-1} .

To avoid the reduction in sensitivity caused by overlap the magnitude of the fluorescence from each of the thermalising energy levels which is present over the wavelength range used to measure the fluorescence from the other thermalising level needs to be minimised. Methods for reducing the overlap include using:

- (a) thermally coupled energy levels with relatively large energy gaps, which increases the separation between the fluorescence wavelengths for the two levels,

- (b) thermally coupled energy levels with $B > 1$, which increases the magnitude of the fluorescence intensity from the upper energy level with respect to the fluorescence intensity from the lower energy energy level,
- (c) host materials which give relatively narrow fluorescence linewidths, and/or,
- (d) filters with narrow transmission ranges or centre wavelengths shifted away from the fluorescence originating from the opposing thermalising energy level.

3.6.2 Stray light

The detection arrangements commonly used to measure the fluorescence intensity from the two thermally coupled levels usually just measure the intensity of light over a relatively narrow wavelength range corresponding to the fluorescence from the energy level of interest. Therefore light originating from sources other than the levels of interest within these wavelength ranges will also be included in the measurement. Examples of such unwanted stray light are fluorescence originating from other energy levels of the rare earth ion and stray excitation light, which may be present due to reflections from splices or other surfaces.

Fluorescence intensity ratio

Assuming that the intensity of the stray light is constant compared to the intensity from the levels of interest the fluorescence intensities measured for the upper ($I_{\Delta\lambda 2U}$) and lower ($I_{\Delta\lambda 2L}$) energy thermalising levels at a given temperature are:

$$I_{\Delta\lambda 2U} = n_{2U}I_{2U} + S_{2U}, \quad (3.18)$$

$$I_{\Delta\lambda 2L} = n_{2L}I_{2L} + S_{2L}, \quad (3.19)$$

where S_{2U} and S_{2L} are the intensity of stray light recorded by the detector used to measure the fluorescence intensity from the upper and lower energy thermalising level respectively and $I_{\Delta\lambda i}$, n_i and I_i are as defined previously. Using equations 3.18, 3.19 and the equations for the individual intensity of each of the thermalising energy levels (equations 3.4 and 3.5) the fluorescence intensity ratio is given by:

$$R = \frac{I_{\Delta\lambda 2U}}{I_{\Delta\lambda 2L}} = \frac{B \exp\left[-\frac{\Delta E}{kT}\right] (n_{2U}I_t + S_{2U}) + S_{2U}}{n_{2L}I_t + S_{2L} + S_{2L} B \exp\left[-\frac{\Delta E}{kT}\right]}. \quad (3.20)$$

One of the most common sources of stray light observed during the work presented in this thesis was reflected excitation light. As the pump wavelength is usually

of shorter wavelength than the fluorescence from the thermally coupled levels, the reflected light has a greater effect on the fluorescence from the upper energy level (see figure 3.6). In addition the fluorescence intensity usually observed from the upper energy level is usually small in comparison to the intensity of the lower energy level. Therefore the stray light has a negligible effect on the fluorescence intensity from the lower energy level in comparison to the effect on the fluorescence from the upper energy level. For this simplified case the fluorescence intensity ratio becomes:

$$R = \left(\frac{n_{2U}I_t + S_{2U}}{n_{2L}I_t} \right) B \exp\left[-\frac{\Delta E}{kT}\right] + \frac{S_{2U}}{n_{2L}I_t}. \quad (3.21)$$

Figure 3.9 shows examples of how stray light can affect the fluorescence intensity ratio for the simplified case (equation 3.21), assuming an energy gap of 750 cm^{-1} and $B = 1$. The magnitude of stray light used in figure 3.9 is equal to 0%, 50% and 100% of the intensity of fluorescence originating from the upper energy thermalising level at $20 \text{ }^\circ\text{C}$. These values were chosen primarily to allow comparison between the effect of fluorescence overlap and stray light.

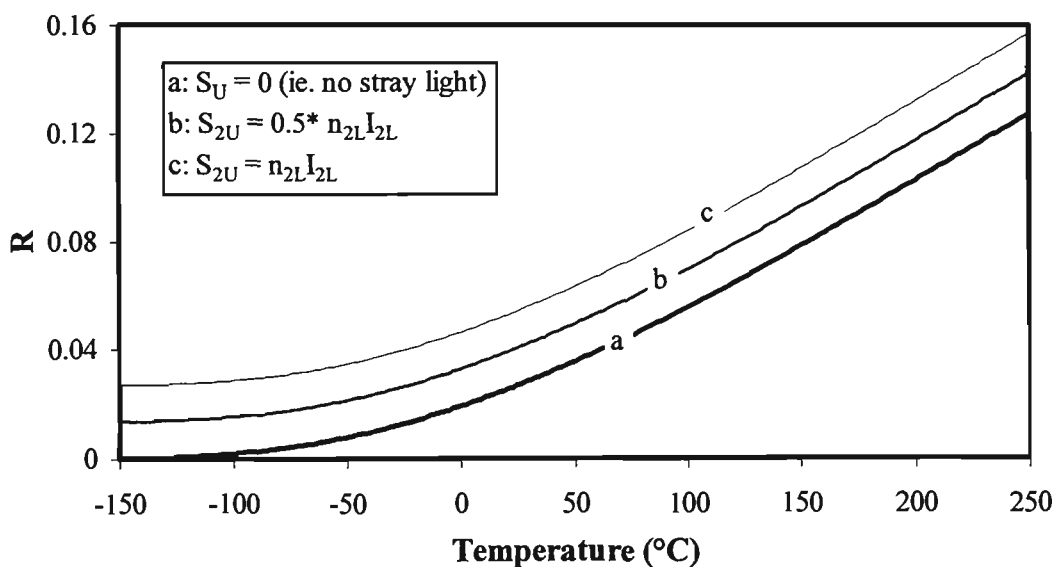


Figure 3.9: Example of how stray light can affect the thermal dependence of the fluorescence intensity ratio. Calculated using equation 3.21 with an energy gap of 750 cm^{-1} and $B = 1$.

Sensitivity

Using equation 3.20 the thermal sensitivity of the fluorescence intensity ratio when stray light is present is given by:

$$S = \left(\frac{\Delta E}{kT^2} \right) \left\{ \frac{I_t B \exp[-\Delta E/kT] (n_{2U} n_{2L} I_t + n_{2U} S_{2L} + n_{2L} S_{2U})}{CD} \right\} \quad (3.22)$$

where:

$$C = n_{2L} I_t + S_{2L} + S_{2L} B \exp[-\Delta E/kT],$$

$$D = n_{2U} I_t B \exp[-\Delta E/kT] + S_{2U} + S_{2U} B \exp[-\Delta E/kT].$$

For the simplified case where the effect of stray light on the upper level fluorescence is much greater than on the lower level fluorescence the sensitivity becomes:

$$S = \frac{1}{R} \frac{\partial R}{\partial T} = \left(\frac{\Delta E}{kT^2} \right) \left\{ \frac{B \exp[-\Delta E/kT] (n_{2U} I_t + S_{2U})}{n_{2U} I_t B \exp[-\Delta E/kT] + S_{2U} + S_{2U} B \exp[-\Delta E/kT]} \right\}. \quad (3.23)$$

An illustration of the effect of stray light on the thermal sensitivity of the fluorescence intensity ratio is given in figure 3.10. The curves were calculated using equation 3.23 with an energy gap of 750 cm^{-1} assuming $B = 1$. Examples are shown for the case when the magnitude of stray light over the wavelength range used for the upper energy thermalising energy level is equal to 0%, 5%, 25% and 100% of the fluorescence from the upper energy thermalising energy level at 20°C .

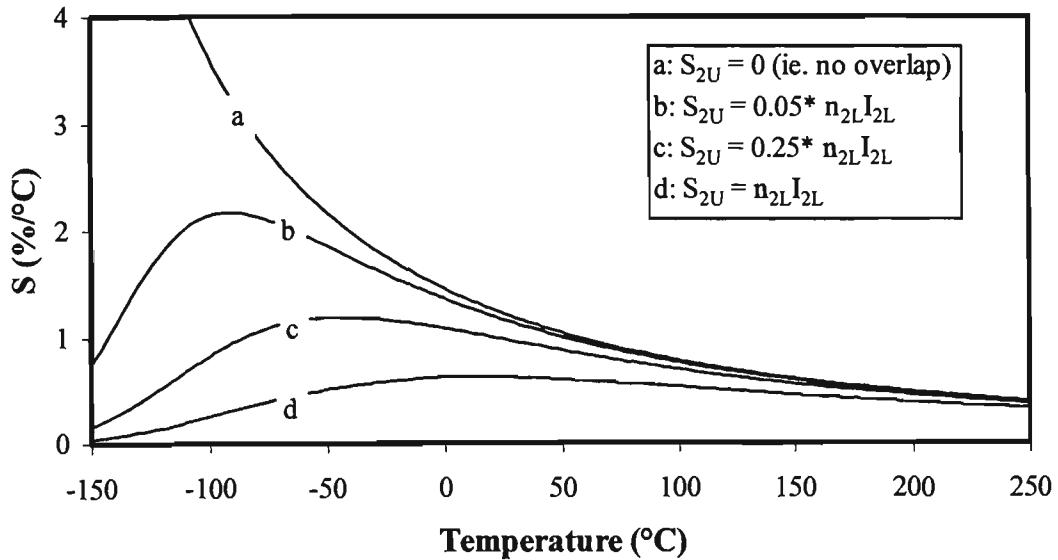


Figure 3.10: Example of the effect of stray light on the thermal sensitivity of the fluorescence intensity ratio.

To reduce the effect of stray light the following precautions should be taken:

- (a) the excitation wavelength should be as far as possible from the fluorescence transitions used to measure the fluorescence intensity ratio,

- (b) the filters should be chosen to reject as much stray light as possible while still measuring sufficient fluorescence intensity from the thermally coupled energy levels, and,
- (c) the configuration of the sensor needs to be designed so that reflections of excitation light are minimised.

3.6.3 Summary

The general form for the fluorescence intensity ratio when the fluorescence peaks overlap or stray light is present is given by:

$$R = C \exp\left[-\frac{\Delta E}{kT}\right] + D, \quad (3.24)$$

for the simplified case when the fluorescence overlap or stray light only affects the fluorescence from the upper energy thermalising level. The values of C and D in equation 3.24 are:

$$C = \frac{n_{2U}}{n_{2L}} \quad \text{and} \quad D = \frac{m_{2L}}{n_{2L}} \quad (\text{for the case of overlap}), \quad (3.25)$$

$$C = \frac{n_{2U}I_t + S_{2U}}{n_{2L}I_t} \quad \text{and} \quad D = \frac{S_{2U}}{n_{2L}I_t} \quad (\text{for the case of stray light}). \quad (3.26)$$

3.7 CONCLUSION

The formulae describing the fluorescence intensity ratio of two closely spaced energy levels and the sensitivity of the fluorescence intensity ratio to changes in temperature have been presented. These formulae suggest thermalising energy levels that are separated by relatively large energy gaps should provide the greatest sensitivity. Care however must be taken to ensure that for such large energy gaps the fluorescence intensity from the upper thermalising energy level is not so small that complex and therefore expensive detectors are required. The choice of energy levels that have a $B > 1$ would be of assistance in this case.

The effects of overlap of fluorescence from the two levels and stray light have also been investigated. Both overlap and stray light were shown to have a detrimental affect on the sensitivity of the fluorescence intensity ratio technique of temperature sensing and therefore should be avoided. To reduce the effect of overlap, thermalising energy levels with a relatively large energy gap (which increases the wavelength

separation of fluorescence from the two levels) and host materials that have relatively narrow linewidths (such as YAG) would be preferable. To reduce the effect of stray light it would be best to use excitation wavelengths which are well separated from the fluorescence transitions of interest and design the sensor arrangement so that reflections of excitation light are minimised. Finally, when choosing filters that select fluorescence from the thermally coupled levels care must be taken to avoid wavelength regions where overlap or stray light exist. Any changes made to avoid the overlap of fluorescence and stray light however need to be balanced with the requirement of adequate fluorescence intensity, which also affects the measurement accuracy.

Chapter 4: Fluorescence Intensity Ratio Studies Using Rare Earth Doped Glasses and Crystals:

Feasibility tests for use in temperature sensing applications.

- 4.1 INTRODUCTION
- 4.2 SEARCH FOR THERMALISING LEVELS IN TRIVALENT RARE EARTH IONS
- 4.3 EXPERIMENTAL ARRANGEMENTS USED IN FLUORESCENCE INTENSITY RATIO STUDIES
 - 4.3.1 *Bulk rare earth doped samples*
 - 4.3.2 *Rare earth doped optical fibre samples*
- 4.4 FLUORESCENCE INTENSITY RATIO VERSUS TEMPERATURE STUDIES
 - 4.4.1 *Praseodymium*
 - 4.4.2 *Neodymium*
 - 4.4.3 *Samarium*
 - 4.4.4 *Europium*
 - 4.4.5 *Dysprosium*
 - 4.4.6 *Ytterbium*
- 4.5 CONCLUSION

Overview of Chapter

In the following chapter the results of fluorescence intensity ratio studies are presented for a range of energy levels in rare earth doped materials.

4.1 INTRODUCTION

The fluorescence intensity ratio technique, utilising the thermal coupling of two closely spaced energy levels of a rare earth ion, has shown promise as a method of fibre optic temperature sensing (as discussed in chapter 1). The development of this technique prior to the work presented in this thesis, however, had mainly been limited to studies of the $^2H_{11/2}$ and $^4S_{3/2}$ levels of the erbium (Er^{3+}) ion doped in a variety of host materials [45-50]. In this chapter results of studies aimed at improving this technique through the use of thermally coupled levels in rare earth ions other than erbium are presented.

The first step of this investigation was to select pairs of closely spaced energy levels that could possibly be used with the fluorescence intensity ratio technique of temperature sensing. Rare earth doped samples containing energy levels chosen for further investigation were obtained and tested to determine if the levels provided sufficient fluorescence upon selective excitation. The fluorescence spectra of rare earth doped materials with adequate fluorescence from the levels of interest were then measured as a function of temperature, from which the variation with temperature of the fluorescence intensity ratio was determined.

4.2 SEARCH FOR THERMALISING LEVELS IN TRIVALENT RARE EARTH IONS

In order to determine which rare earth ions were to be tested for use with the fluorescence intensity ratio technique of temperature sensing a set of criteria that the rare earth ion should meet were developed. These criteria were chosen using knowledge of previous fluorescence intensity ratio studies (i.e. using Er^{3+}), the theory of the fluorescence intensity ratio technique (as discussed in chapter 3) and the well documented fluorescence characteristics of rare earth doped materials.

The first characteristic used to determine if a pair of energy levels were selected for investigation was that the two levels should be thermally coupled (i.e. the number of ions in each of the levels follows a Boltzmann distribution). Secondly, the two levels must provide sufficient fluorescence at wavelengths, which can be detected by commonly available detectors. Finally the fluorescence must be able to be excited by commonly available light sources, such as laser diodes and LED's. To meet the first selection requirement only levels which were separated by an energy gap of less than 2000 cm^{-1} were included in the study as it was believed that for greater energy

separations thermalisation would not be observed for the temperatures of interest. An additional limitation on the energy gap between the levels chosen was that they must be separated by more than 200 cm^{-1} to avoid excessive overlap of fluorescence from the two levels (as discussed in Chapter 3).

Research has found that the energy levels of rare earth ions need to be separated by a minimum amount of energy from the next lower energy level in order to be sufficiently stable to exhibit fluorescence [56]. For levels that are separated by energy gaps smaller than this amount non-radiative processes (e.g. multiphonon decay) dominate the decay process rather than the emission of photons (i.e. fluorescence). This minimum energy gap to the next lower energy level depends upon a number of factors including the host material and the energy levels involved. For example in the case of the LaCl_3 host material the energy gap to the next lower energy level should be at least 1000 cm^{-1} [56]. In silica hosts fluorescence is normally observed for energy levels with energy gaps to the next lower level greater than 3000 cm^{-1} [91]. As the major host material investigated in this work was silica it was decided that the thermally linked levels should have an energy gap of more than 3000 cm^{-1} to the next lower energy level, in order to ensure sufficient fluorescence intensity.

Finally, as a restriction of the excitation and detection wavelengths involved, only levels that had energies between 6000 cm^{-1} and 25000 cm^{-1} were selected for investigation. A literature search was carried out using the above criteria, the results of which are given in table 4.1.

Rare Earth	Energy Levels	ΔE_1 (cm ⁻¹)	ΔE_2 (cm ⁻¹)	Host [Ref.]
Pr ³⁺	³ P ₀ & ³ P ₁	592	3847	LaCl ₃ [92]
		582	3841	ZBLANPb [85]
Nd ³⁺	⁴ F _{3/2} & ⁴ F _{5/2}	1035	5554	LaCl ₃ [87]
		1030	5710	ZBLANPb [85]
		1187	N/A	Barium crown glass [93]
Pm ³⁺	⁵ F ₂ & ⁵ F ₁	424	5809	LaCl ₃ [87]
		420	N/A	YAG [94]
Sm ³⁺	⁴ G _{5/2} & ⁴ F _{3/2}	1008	7400	LaCl ₃ [87]
Eu ³⁺	⁵ D ₀ & ⁵ D ₁	1758	12360	LaCl ₃ [87]
		1745	12475	ZBLA [95]
Dy ³⁺	⁴ F _{9/2} & ⁴ I _{15/2}	991	7849	LaCl ₃ [87]
		~1070	7850	ZBLA [96]
Er ³⁺	⁴ S _{3/2} & ² H _{11/2}	748	3135	LaCl ₃ [87]
		740	3170	ZBLANPb [85]
Yb ³⁺	² F _{5/2} Stark levels	300	10250	ZBLAN [97]
		680	10240	silica [86]

Table 4.1: Details of energy levels highlighted in thermalising levels search, where ΔE_1 is the energy gap between the thermalising energy levels and ΔE_2 is the gap between the thermalising levels and the next lower energy level. N/A – not available.

4.3 EXPERIMENTAL ARRANGEMENTS USED IN FLUORESCENCE INTENSITY RATIO STUDIES

During the course of fluorescence intensity ratio measurements a number of standard experimental arrangements were developed for use with rare earth doped bulk and fibre samples. These general arrangements consisted of an excitation source, a guide for excitation and fluorescence light, the doped material under investigation and a detection system to monitor the fluorescence signal. Details of the components of these experimental arrangements are provided below, followed by the generic arrangements used for rare earth doped bulk and optical fibre samples.

Excitation Sources

The two methods of excitation employed were direct pumping of one of the energy levels suspected of being thermally coupled, and excitation of a higher energy level with population of the thermally coupled levels occurring via rapid non-radiative decay, as shown in figure 4.1. The technique used for each rare earth ion was determined by the energy of the levels under investigation, the absorption properties of the ion (both the wavelength ranges and the absorption strength) and the excitation sources available.

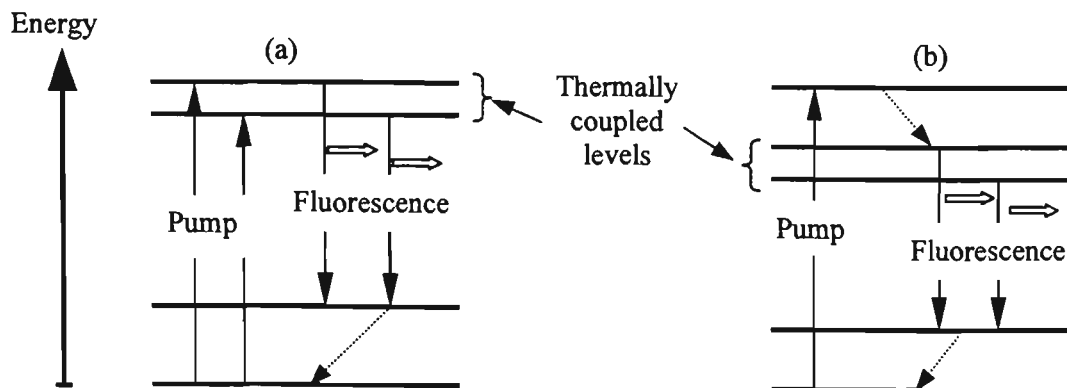


Figure 4.1: Excitation methods (a) direct excitation (b) excitation of higher lying level followed by rapid non-radiative decay.
(Note: dashed lines indicate non-radiative decay.)

The two main pump sources utilised were an argon ion laser, initially a Spectra Physics model 2025-5 which was later replaced by a Spectra Physics Stabilite 2017, and a Spectra Physics Model 3900S Ti:sapphire laser. These sources provided a wide coverage of wavelength ranges and relatively high pump powers. The argon ion lasers produced a number of individual output wavelengths between 456.9 nm and 514.6 nm with single line output powers up to approximately 1 W, while the Ti:sapphire laser could be tuned between approximately 650 nm and 1050 nm with a maximum output power of 1 W. Other excitation sources used during preliminary fluorescence intensity ratio tests were a pair of laser diodes, one with a temperature tunable centre wavelength between 802 nm and 811 nm (maximum output power of ~ 400 mW) and the second a fibre coupled laser diode with a centre wavelength of 845 nm (maximum output power ~ 2.5 mW in fibre with a core diameter of $5 \mu\text{m}$).

Rare Earth Doped Samples

The rare earth doped materials tested in the preliminary fluorescence intensity ratio studies are listed in table 4.2. Each of the rare earth ions were obtained doped in silica fibre, while for Pr^{3+} and Nd^{3+} samples were also obtained in a number of other host materials, allowing a comparison of the suitability of certain host materials to be made. The promethium (Pm^{3+}) ion, highlighted in the energy level search, was not tested, as it is radioactive [69].

Rare-earth ion	Host materials
Pr ³⁺	Silica fibre
	Aluminosilica fibre
	ZBLANP
Nd ³⁺	Silica fibre
	ZBLANP
	YVO ₄
	YAG
Sm ³⁺	Silica fibre
Eu ³⁺	Silica fibre
Dy ³⁺	Silica fibre
Yb ³⁺	Silica fibre

Table 4.2: Rare earth ion/host material combinations studied.

Detection Systems

The fluorescence spectra of rare earth doped samples were recorded by coupling a portion of the fluorescence from the sample into an ANDO AQ-6310B optical spectrum analyser (OSA). The OSA settings, including wavelength range, resolution, sensitivity and averaging, were varied between individual tests depending upon the intensity of fluorescence from the test material and the stability of the spectra with time. In general these settings were chosen to record the fluorescence spectra in a short measurement time, to reduce possible problems introduced by drift in the sample temperature and intensity fluctuations due to external factors such as changes in pump power, during the scan. The time taken to record an individual OSA trace varied from less than one minute, for strong fluorescence signals (with peak powers in the 10's of nanowatts range), to more than 10 minutes for weak signals (with peak powers in the 10's of picowatts range). To avoid noise dominating the fluorescence signal the minimum peak intensity measured was approximately 20 pW. The peak input power for the OSA was kept below 1 mW, the maximum for the device, through the use of a number of techniques including optical filters. Spectra recorded on the OSA were transferred to computer for further analysis.

Heating and Cooling

Heating of the rare earth doped samples was achieved by placing the sample holders (details of which are provided in Appendix A), containing the rare earth doped material, on an IEC 2090.001 hot plate or in a model K4 Tetlow oven. The hot plate was used for temperatures up to approximately 300 °C while the oven was used for temperatures up to 500 °C. Samples were cooled by introducing either liquid nitrogen,

ice or dry ice into the sample holder. The lowest temperatures achievable with liquid nitrogen, dry ice and ice water were approximately $-196\text{ }^{\circ}\text{C}$, $-80\text{ }^{\circ}\text{C}$ and $0\text{ }^{\circ}\text{C}$ respectively.

For temperatures below ambient, measurements were generally taken as the sample slowly warmed up after being cooled to the minimum temperature with the occasional addition of a small amount of coolant, such as liquid nitrogen, as required to stabilise the temperature. In tests that involved measurements at temperatures both below and above ambient the rare earth doped samples were first cooled to a minimum temperature and then spectra were recorded as the sample gradually warmed. After the sample reached ambient temperature spectra were taken during heating, allowing a continuous set of readings to be taken from minimum to maximum temperature.

The temperature of rare earth doped samples were measured during tests by a Fluke 52 K/J K-type thermocouple, located in-situ with the sample. The measurement accuracy of such thermocouples depends upon the temperature range measured, the thermocouple probe used and the experimental arrangement. The accuracy of the Fluke 52 K/J thermocouple is quoted as $\pm[0.1\% + 0.7\text{ }^{\circ}\text{C}]$ [98]. The range of temperatures measured in this work were a minimum of approximately $-200\text{ }^{\circ}\text{C}$ and a maximum of approximately $+600\text{ }^{\circ}\text{C}$. Therefore the thermocouple measurement accuracy was approximately $\pm 0.9\text{ }^{\circ}\text{C}$ at $-200\text{ }^{\circ}\text{C}$, $\pm 0.72\text{ }^{\circ}\text{C}$ at $20\text{ }^{\circ}\text{C}$ and $\pm 1.3\text{ }^{\circ}\text{C}$ at $600\text{ }^{\circ}\text{C}$. The stability of a sample's temperature during tests was determined by the rate at which the sample was heated or cooled and the time taken to record the fluorescence spectra, the latter of which varied substantially from test to test as previously mentioned. During tests the heating and cooling rates were controlled such that the sample temperature did not vary substantially from the desired measurement temperature. In general the average stability of rare earth doped sample temperature during tests was approximately $\pm 4\text{ }^{\circ}\text{C}$.

4.3.1 Bulk Rare Earth Doped Samples

The general arrangement used for recording the fluorescence spectra of rare earth doped bulk samples is illustrated in figure 4.2.

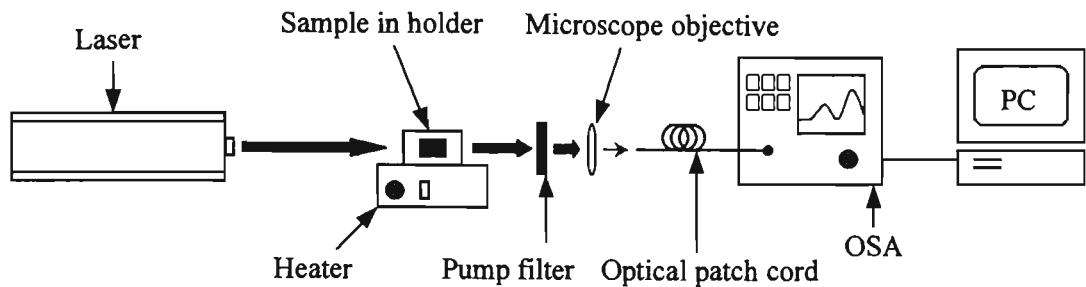


Figure 4.2: Side view of bulk sample test arrangement for fluorescence intensity ratio measurements.

In this arrangement the doped samples, mounted in a holder on top of the hotplate, were excited directly by the laser output. A portion of the fluorescence from the sample was focussed by a microscope objective into a optical fibre patch cord connected to the OSA. To reduce the amount of pump light entering the OSA the microscope objective was positioned at a slight angle to the pump beam path and if required a pump filter was also placed in the path of the measured fluorescence light.

4.3.2 Rare Earth Doped Optical Fibre Samples

For rare earth doped fibre samples two techniques were developed to measure fluorescence spectra, with the choice of technique determined predominantly by the pump wavelength used to excite the sample. In both techniques counter-propagating fluorescence was measured to help reduce the amount of pump light in the recorded fluorescence spectra.

The first technique described is illustrated in figure 4.3 and was used with Pr^{3+} , Sm^{3+} , Eu^{3+} and Dy^{3+} doped fibres. With these ions the excitation and fluorescence wavelengths involved were usually shorter than available with commonly available optical fibre couplers and therefore a technique incorporating a cubic beamsplitter was developed.

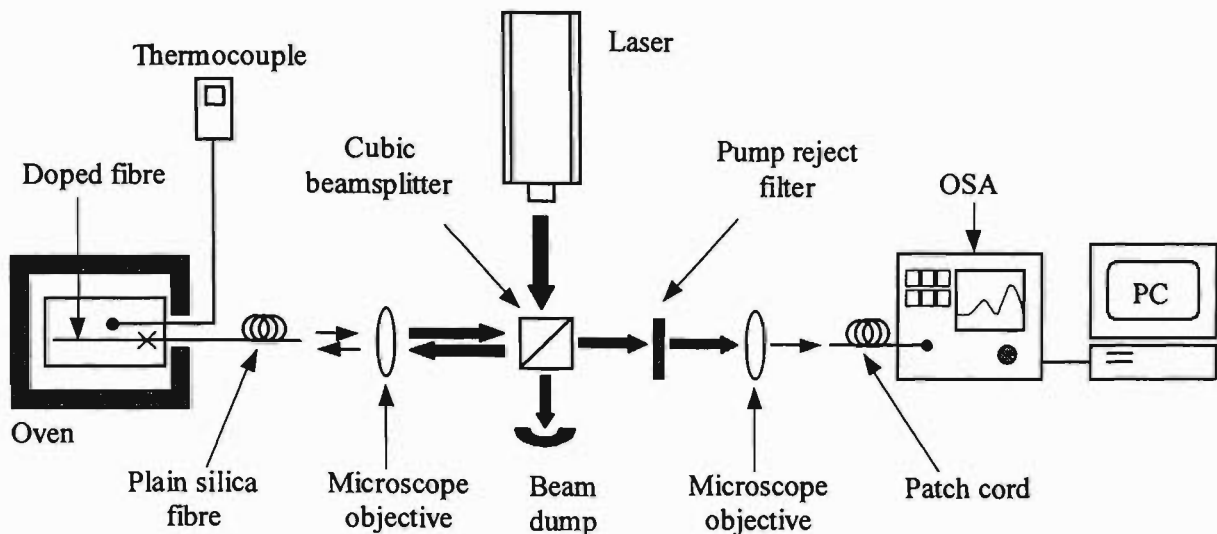


Figure 4.3: *Experimental arrangement for rare earth doped fibre fluorescence measurements using a cubic beamsplitter.*

In the arrangement shown in figure 4.3, a 45° angle cubic beamsplitter was placed in the beam path of the excitation laser with approximately half of the pump light reflected at 45° towards a microscope objective. The reflected light was then coupled by the objective into a length of non-doped silica fibre, which was spliced to the doped fibre under investigation. This allowed the complete length of doped fibre to be heated and/or cooled and for this to take place away from the optical arrangement. Counter-propagating fluorescence from the doped fibre passing back through the beamsplitter was then filtered to reduce the intensity of reflected excitation light, using a coloured glass filter, and coupled into a patch cord by another microscope objective. This patch cord was attached to the optical spectrum analyser mentioned earlier in section 4.3.

The second of the experimental arrangements used to measure fluorescence spectra of rare earth doped fibre is shown in figure 4.4 and was used for Nd³⁺ and Yb³⁺ doped fibre. In this arrangement light from the pump laser was focussed into port 1 of a 3 dB optical fibre coupler, using a microscope objective, with a length of the doped fibre under investigation spliced onto port 3 of the coupler. The counter-propagating fluorescence from the fibre was measured by connecting the second input port of the coupler to an optical spectrum analyser. Again for temperature related studies the doped fibre was placed in a holder together with a thermocouple and heated or cooled using previously discussed methods. To reduce the amount of pump light from fibre end reflections entering the OSA, port 4 of the coupler was placed in index matching fluid.

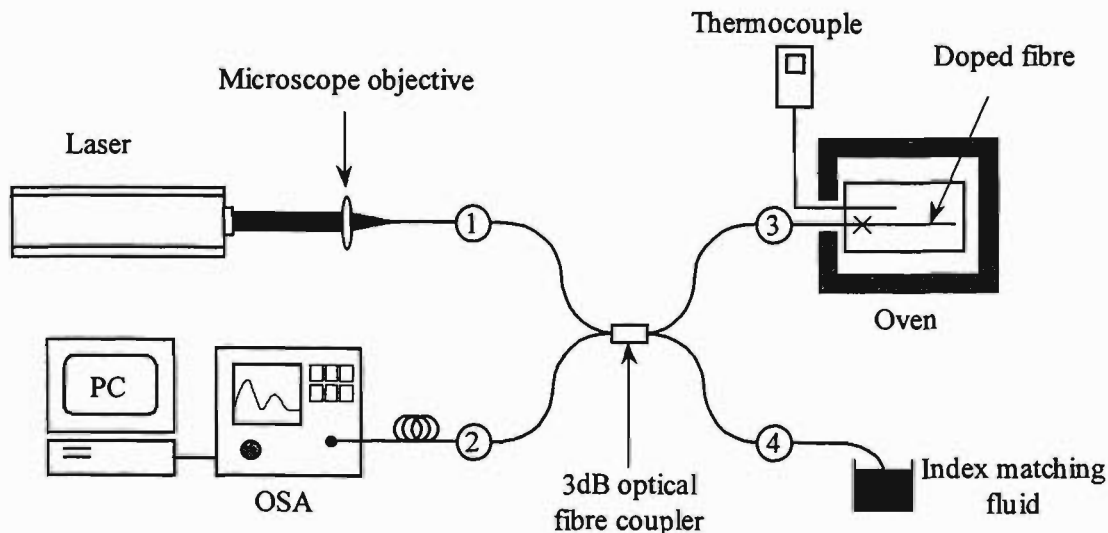


Figure 4.4: Experimental arrangement for rare earth doped fibre fluorescence measurements using a fibre coupler.

4.4 FLUORESCENCE INTENSITY RATIO VERSUS TEMPERATURE STUDIES

These “initial” tests consisted of measuring the fluorescence spectra of rare earth doped samples as a function of temperature. Using the results it was possible to determine if the intensity from the two levels of interest varied as was expected from theory and decide, in conjunction with other data, if the sample would be suitable for sensor development.

4.4.1 Praseodymium

The energy levels identified as being of interest in the praseodymium (Pr^{3+}) ion were the $^3\text{P}_0$ and $^3\text{P}_1+^1\text{I}_6$ levels, shown in figure 4.5. These levels are separated by approximately 580 cm^{-1} in a fluoride host [85] and have received interest recently in amplification [99] and laser [100, 101] studies. A number of different samples of Pr^{3+} -doped materials were tested including bulk $\text{Pr}^{3+}:\text{ZBLANP}$, silica fibre and aluminosilica fibre.

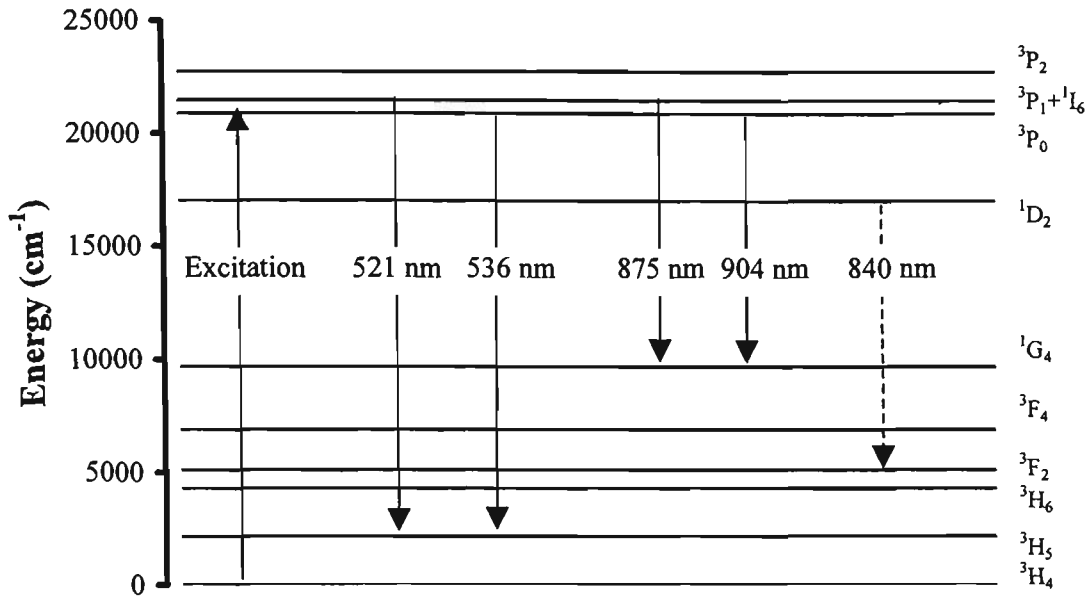


Figure 4.5: Partial energy level diagram of Pr³⁺:ZBLANPb, including the transitions of interest and the approximate wavelengths of these transitions [85].

Pr³⁺:ZBLANP

The bulk sample experimental arrangement (as described in section 4.3.1) was used to measure the fluorescence spectra of the Pr³⁺:ZBLANP sample with an argon ion laser as the excitation source. The sample used in this investigation was a rod (8 mm diameter, 40 mm length) of Pr³⁺-doped ZBLANP, with an approximate doping concentration of 2000 ppm. Measurements of the fluorescence spectra for transitions originating from the levels of interest (i.e. ³P₀ and ³P₁+¹I₆) terminating at the ¹G₄ and ³H₅ energy levels were performed with excitation at 476.5 nm and 465.8 nm. For the 476.5 nm excitation, fluorescence spectra were obtained at sample temperatures between 24 °C and 200 °C while spectra were recorded for temperatures between 20 °C and 145 °C with the 465.8 nm pump wavelength. Fluorescence spectra for the 476.5 nm pump wavelength at various temperatures are given in figure 4.6. Results for the 465.8 nm excitation have not been shown as they are virtually identical to the spectra shown in figure 4.6.

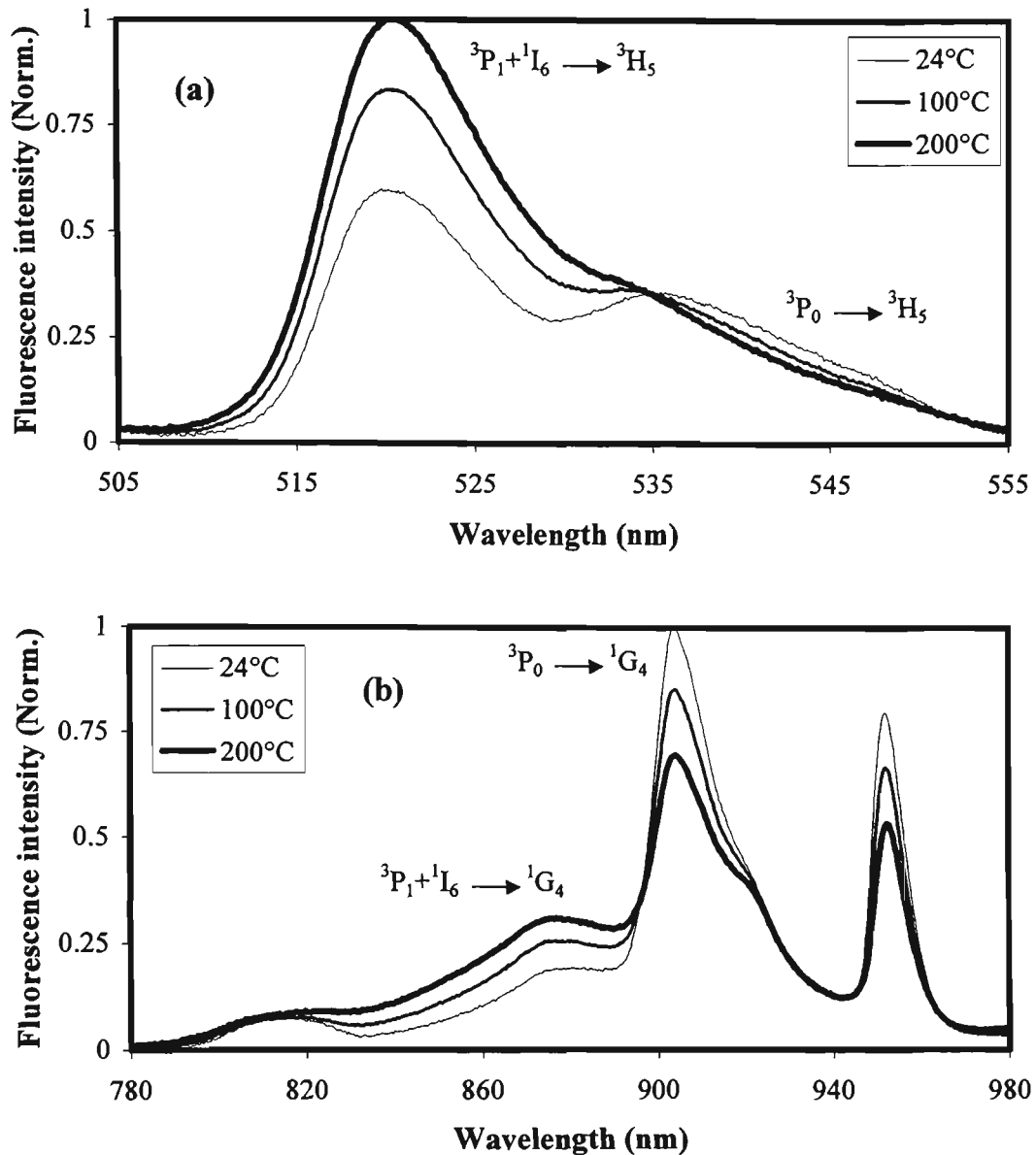


Figure 4.6: Fluorescence spectra of $\text{Pr}^{3+}:\text{ZBLANP}$ at various temperatures using 476.5 nm pump wavelength (2 nm OSA resolution), (a) ${}^3P_0, {}^3P_1+{}^1I_6 \rightarrow {}^3H_5$ transition, and, (b) ${}^3P_0, {}^3P_1+{}^1I_6 \rightarrow {}^1G_4$ transition.

Pr^{3+} -doped silica fibre and Pr^{3+} -doped aluminosilica fibre

The experimental arrangement used for the Pr^{3+} -doped silica and Pr^{3+} -doped aluminosilica fibre samples was the counter-propagating set-up using the cubic beamsplitter (see section 4.3.2) with excitation from the 488 nm line of an argon ion laser. Both of the Pr^{3+} -doped fibre samples were manufactured at the *Laboratoire de Physique de la Matière Condensée, Université de Nice*. The Pr^{3+} -doped silica fibre had a core diameter and doping concentration of approximately 6 μm and 1000 ppm respectively while the Pr^{3+} -doped aluminosilica fibre had a 6 μm core diameter and praseodymium/aluminium doping concentrations of 1000/4000 ppm respectively. The latter of these two fibres was fabricated by the author of this thesis. The length of Pr^{3+} -

doped fibre used in these tests was 1 m. For each of the doped fibre samples temperature dependent measurements of fluorescence spectra were recorded for transitions from the 3P_0 and $^3P_1+^1I_6$ levels to the 1G_4 energy level. The fluorescence spectra of the Pr^{3+} -doped silica fibre were recorded at temperatures between 21.8 °C and 250 °C (see figure 4.7) while for the Pr^{3+} -doped aluminosilica fibre measurements were made over the -186 °C to +257 °C temperature range (see figure 4.8).

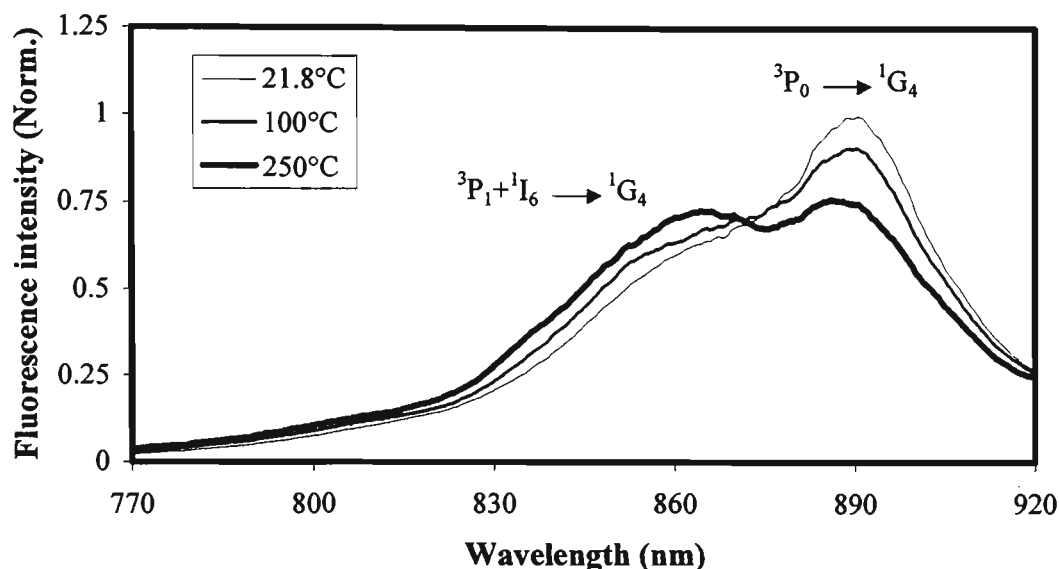


Figure 4.7: Counter-propagating fluorescence spectra of 1 m length of Pr^{3+} -doped silica fibre at various temperatures (10 nm OSA resolution).

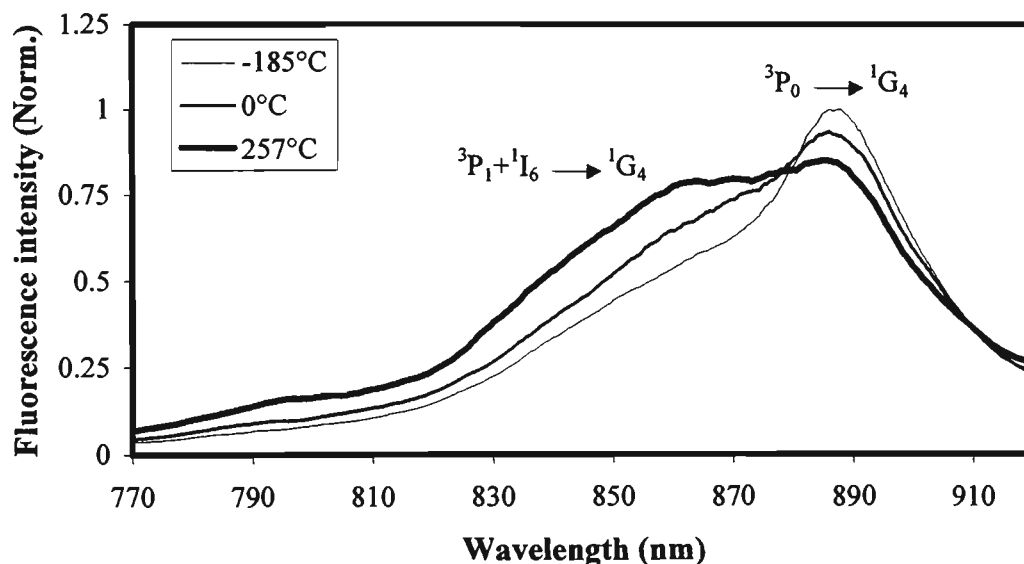


Figure 4.8: Counter-propagating fluorescence spectra of 1 m length of Pr^{3+} -doped aluminosilica fibre at various temperatures (5 nm OSA resolution).

As expected from theory (discussed in chapter 3) the recorded Pr^{3+} fluorescence spectra for all samples exhibited increased fluorescence from transitions originating from the higher energy ${}^3\text{P}_1+{}^1\text{I}_6$ levels and a reduction in the fluorescence from the lower energy ${}^3\text{P}_0$ level with increasing temperature.

Using the fluorescence spectra data at various temperatures, values of the fluorescence intensity originating from the levels of interest were calculated using areas beneath the fluorescence curves. The wavelength ranges over which fluorescence intensity was calculated were chosen to select fluorescence from the thermalising level of interest while avoiding the region of overlap between the two peaks (which has been shown in chapter 3 to reduce sensitivity). Table 4.3 lists the wavelength ranges chosen for each of the Pr^{3+} -doped materials studied. Fluorescence intensity ratio values were subsequently calculated by dividing the fluorescence intensity originating from the upper ${}^3\text{P}_1+{}^1\text{I}_6$ levels by the fluorescence intensity from the lower energy ${}^3\text{P}_0$ level. Graphs of the fluorescence intensity ratio versus temperature for the Pr^{3+} -doped samples tested are given in figure 4.9. To aid in comparison fluorescence intensity ratio values were normalised at ambient temperature by dividing the fluorescence intensity ratio value at each temperature by the room temperature value.

Rare earth sample	Transition	Wavelength range	
		${}^3\text{P}_0$	${}^3\text{P}_1+{}^1\text{I}_6$
Pr^{3+} :ZBLANP	${}^3\text{P}_0, {}^3\text{P}_1 \rightarrow {}^3\text{H}_5$	541-551 nm	515-525nm
	${}^3\text{P}_0, {}^3\text{P}_1 \rightarrow {}^1\text{G}_4$	900-910 nm	830-870 nm
Pr^{3+} silica fibre	${}^3\text{P}_0, {}^3\text{P}_1 \rightarrow {}^1\text{G}_4$	890-900 nm	820-850 nm
Pr^{3+} aluminosilica fibre	${}^3\text{P}_0, {}^3\text{P}_1 \rightarrow {}^1\text{G}_4$	890-900 nm	820-850 nm

Table 4.3: Wavelength ranges used in fluorescence intensity ratio calculations for Pr^{3+} -doped samples.

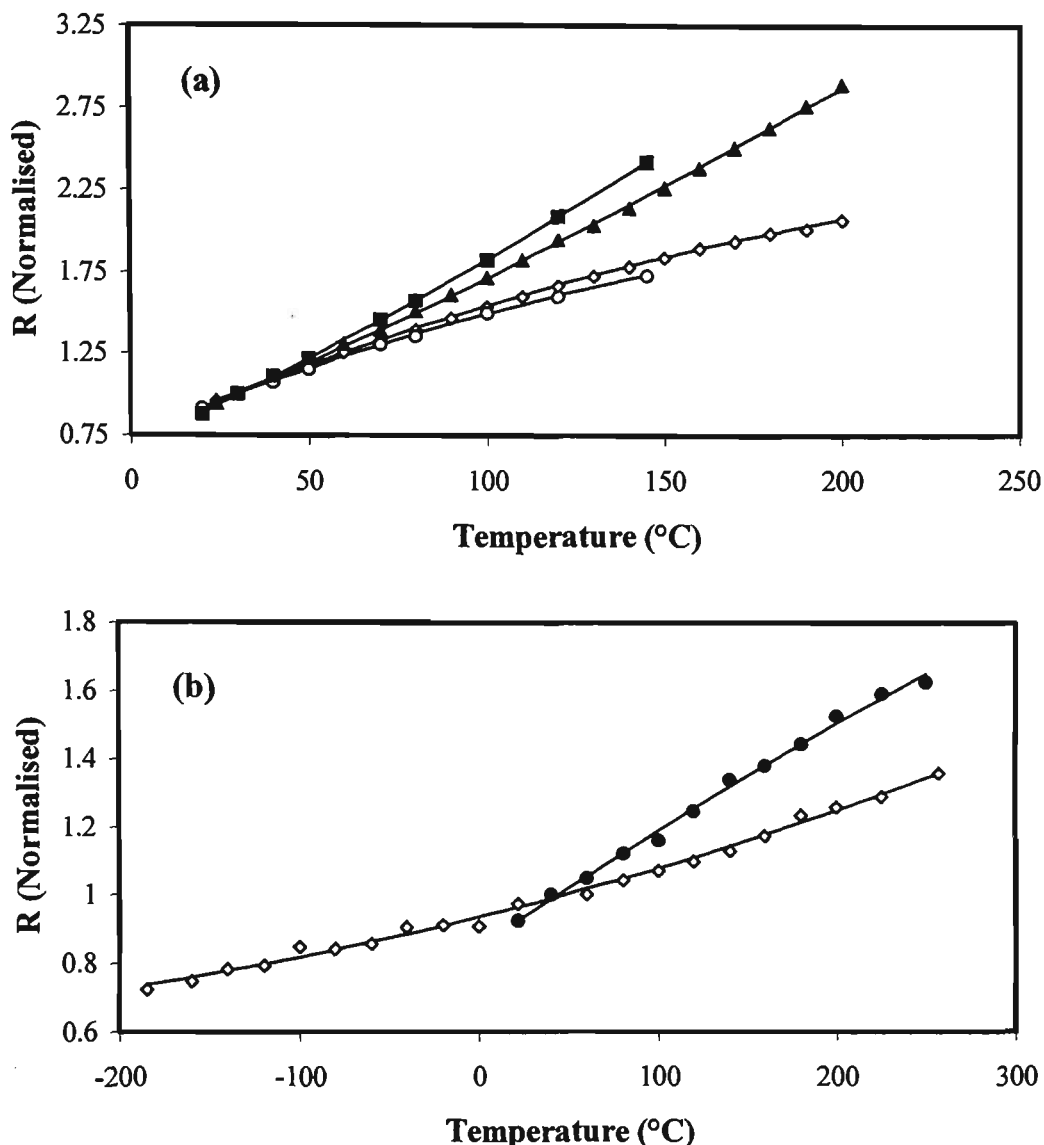


Figure 4.9: (a) Normalised fluorescence intensity ratio versus temperature for bulk ZBLANP, $^3P_0, ^3P_1 + ^1I_6 \rightarrow ^3H_5$ transition, 466 nm excitation (o), 477 nm excitation (\diamond), $^3P_0, ^3P_1 + ^1I_6 \rightarrow ^1G_4$ transition, 466 nm excitation (\blacksquare), 477 nm excitation (\blacktriangle), (b) Normalised fluorescence intensity ratio versus temperature for silica fibre (\bullet) and aluminosilica fibre hosts (\diamond). The solid lines in both graphs are fits to the data, see table 4.4.

The data in figure 4.9 were fitted using a Boltzmann distribution of the form:

$$R = A + B \exp\left[\frac{-\Delta E}{kT}\right]$$

where ΔE is the energy gap between the thermally coupled levels, k is the Boltzmann constant, T is the absolute temperature. The values A and B allow both overlapping of the fluorescence from the thermally coupled levels and stray light to be taken into account as discussed in chapter 3. Details of fits to the fluorescence intensity ratio versus temperature data are given in table 4.4 together with the errors in the fits, to indicate the accuracy the fits. The fit errors were calculated as the standard deviation of

the difference between the measurement temperature, as recorded by the thermocouple, and the temperature implied from the fluorescence intensity ratio data using the fit as a look-up table. It is important to note that the error in the fit to the fluorescence intensity ratio will depend upon the temperature range over which the fluorescence intensity ratio has been measured. This should be taken into account during any comparison between individual fit errors.

Host	Transition (pump wavelength)	FiR fit equation	Fit error (°C)
ZBLANP	${}^3P_0, {}^3P_1+{}^1I_6 \rightarrow {}^1G_4$ (466 nm)	$7.990 \exp[-682.18/kT]$	0.55
	${}^3P_0, {}^3P_1+{}^1I_6 \rightarrow {}^3H_5$ (466 nm)	$-10.412 + 0.0631T - 5.586 \times 10^{-5}T^2$ $1.090 + 26.959 \exp[-564.0/kT]$ *	0.71 4.43
	${}^3P_0, {}^3P_1+{}^1I_6 \rightarrow {}^1G_4$ (477 nm)	$0.0663 + 7.791 \exp[-697.07/kT]$	0.94
	${}^3P_0, {}^3P_1+{}^1I_6 \rightarrow {}^3H_5$ (477 nm)	$-7.734 + 0.0459T - 3.669 \times 10^{-5}T^2$ $1.137 + 36.295 \exp[-564.0/kT]$ *	1.11 6.31
Silica fibre	${}^3P_0, {}^3P_1+{}^1I_6 \rightarrow {}^1G_4$ (488 nm)	$0.460 + 3.924 \exp[-451.8/kT]$	4.89
Aluminosilica fibre	${}^3P_0, {}^3P_1+{}^1I_6 \rightarrow {}^1G_4$ (488 nm)	$0.956 + 8.002 \times 10^{-4}T + 1.882 \times 10^{-6}T^2$ $1.085 + 3.058 \exp[-498.5/kT]$ *	10.82 14.52

Table 4.4: Fits to Pr^{3+} fluorescence intensity ratio data.

(Note: fits denoted with asterix have not been plotted and are for comparison only)

When examining the accuracy of the Boltzmann distribution fits to the Pr^{3+} fluorescence intensity ratio data it was observed that the fit errors were comparatively large for the short wavelength (i.e. ${}^3P_0, {}^3P_1+{}^1I_6 \rightarrow {}^3H_5$) Pr^{3+} :ZBLANP data and the Pr^{3+} -doped fibre data. In the case of the short wavelength Pr^{3+} :ZBLANP data the results obtained for both excitation wavelengths appear to follow a non-Boltzmann distribution temperature dependence suggesting that the deviation from the expected trend is not limited to a specific pump wavelength. In addition reasonable low fit errors were achieved when 2nd order polynomials were used to fit the data suggesting that the poor Boltzmann distribution fits are not due to random fluctuations in the fluorescence intensity ratio during the test. To further investigate the cause of the departure from the anticipated behaviour, the intensity of the ${}^3P_0 \rightarrow {}^3H_5$ and the ${}^3P_1+{}^1I_6 \rightarrow {}^3H_5$ transitions were fitted as a function of temperature using the theory outlined in chapter 3 (equations 3.4 and 3.5). The resulting fits are plotted in figure 4.10. These graphs show that although the ${}^3P_1+{}^1I_6 \rightarrow {}^3H_5$ intensity follows the trend expected from Boltzmann theory the ${}^3P_0 \rightarrow {}^3H_5$ does not. One of the possible causes for the deviation in the data is that the rates which control the population distribution amongst the thermally coupled

energy levels, i.e. ${}^3P_1+{}^1I_6 \rightarrow {}^3P_0$ and ${}^3P_0 \rightarrow {}^3P_1+{}^1I_6$, are slow compared to other radiative and non-radiative rates for these levels. However this can be ruled out, as if this were the cause, the transitions to the 1G_4 level would be affected in the same way (which they are not). Another possible cause is the non-uniform transmission of the pump filter (used to reduce the intensity of reflected excitation light) over the wavelength ranges corresponding to the fluorescence originating from the 3P_0 and ${}^3P_1+{}^1I_6$ terminating at the 3H_5 energy level.

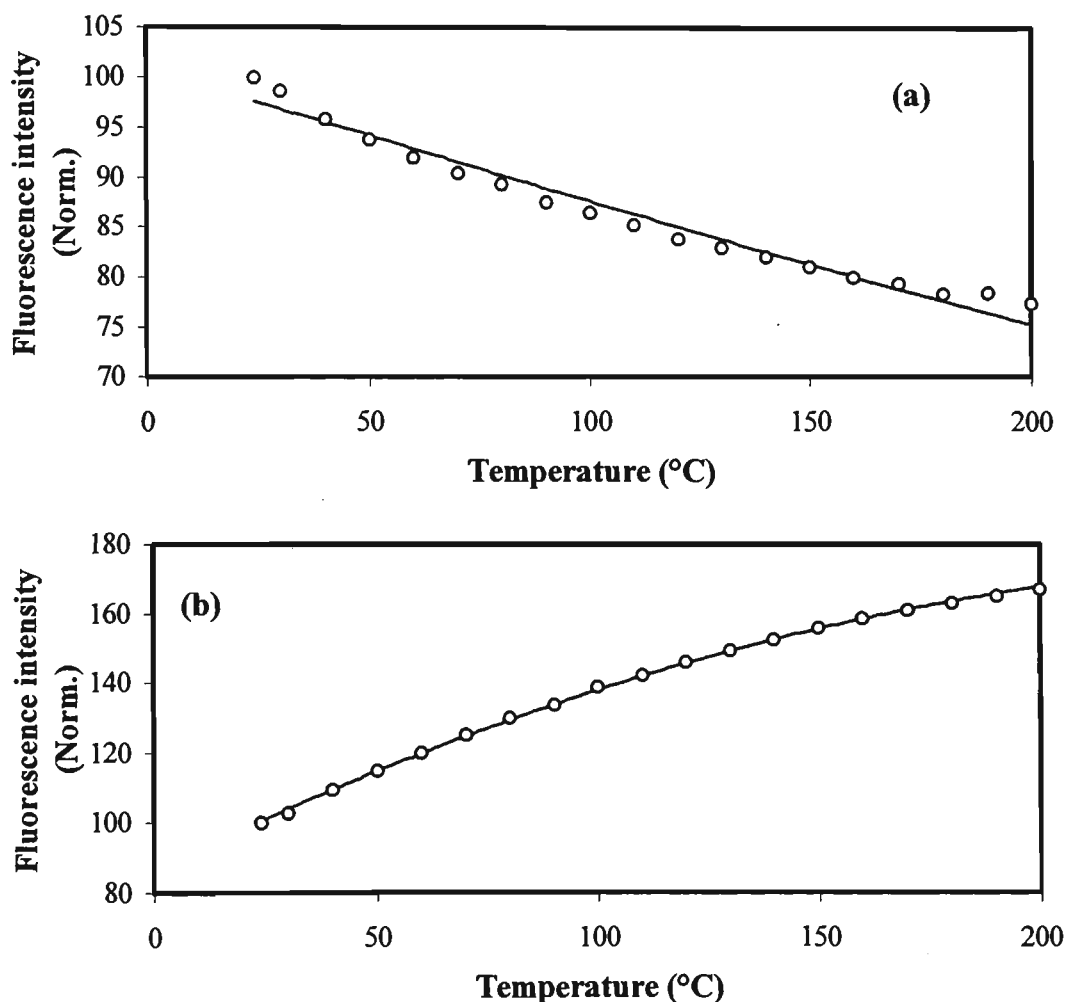


Figure 4.10: Fluorescence intensity versus temperature for the (a) ${}^3P_0 \rightarrow {}^3H_5$ and the (b) ${}^3P_1+{}^1I_6 \rightarrow {}^3H_5$ transitions of $\text{Pr}^{3+}:\text{ZBLANP}$. Open circles - experimental data, Solid lines - theoretical fits.

Unlike the $\text{Pr}^{3+}:\text{ZBLANP}$ case the relatively large errors in Boltzmann distribution fits to Pr^{3+} -doped silica and aluminosilica fibre appear to be caused by random fluctuations in the fluorescence intensity from the mean value at individual test temperatures. To further investigate this a series of tests were performed to determine the stability of the fluorescence intensity ratio from both of the Pr^{3+} -doped fibre samples at room temperature. The standard deviation of the fluorescence intensity ratio was

found to be approximately 1.5% for the silica fibre host and 3% for the aluminosilica fibre host. Using the formula for measurement accuracy given in chapter 3 (equation 3.7) with these values and the values of sensitivity for these fibres (table 4.5) gives a measurement error of roughly 4 °C for the silica fibre host and roughly 21 °C for the aluminosilica fibre host which agree well with the data given in table 4.4. The source of these errors is believed to be random fluctuations in the intensity of light transferred to the Pr³⁺-doped fibre (core diameters ~ 6 µm) from the non-doped silica fibre (used to allow all of the doped fibre to be heated and/or cooled, core diameter ~ 8 µm) and in the opposite direction back to the OSA. These fluctuations could be caused by modal noise [102] as several modes should propagate in the Pr³⁺-doped optical fibres and the in the non-doped fibres at the excitation and fluorescence wavelengths.

The sensitivity of the fluorescence intensity ratio values (i.e. the rate of change of the fluorescence intensity ratio with temperature) for each of the Pr³⁺-doped samples were determined at both 20 °C and 100 °C, using fluorescence intensity ratio fit data, and are listed in table 4.5. Included in the table for comparison is the theoretical sensitivity for an energy gap of 580 cm⁻¹.

Sample	Transition (pump wavelength)	Sensitivity (%/°C)		
		@ -100°C	@ 20 °C	@ 100 °C
Pr ³⁺ :ZBLANP	³ P ₀ , ³ P ₁ + ¹ I ₆ → ¹ G ₄ (466 nm)		0.94	0.65
	³ P ₀ , ³ P ₁ + ¹ I ₆ → ³ H ₅ (466 nm)		0.94	0.40
	³ P ₀ , ³ P ₁ + ¹ I ₆ → ¹ G ₄ (477 nm)		1.15	0.71
	³ P ₀ , ³ P ₁ + ¹ I ₆ → ³ H ₅ (477 nm)		0.96	0.44
Pr ³⁺ silica fibre	³ P ₀ , ³ P ₁ + ¹ I ₆ → ¹ G ₄ (488 nm)		0.39	0.28
Pr ³⁺ aluminosilica fibre	³ P ₀ , ³ P ₁ + ¹ I ₆ → ¹ G ₄ (488 nm)	0.13	0.14	0.15
Theory (580 cm ⁻¹)		2.79	0.97	0.60

Table 4.5: Sensitivity values for Pr³⁺-doped samples.

From table 4.5 we can see that the sensitivity values obtained for the Pr³⁺:ZBLANP sample are significantly higher than those from the Pr³⁺-doped silica and aluminosilica fibre samples. There are several possible explanations for the reduced sensitivity of the Pr³⁺-doped fibre results including:

- (a) increased overlap of fluorescence from the thermally coupled levels,
- (b) a smaller energy gap between the thermally coupled levels than for the ZBLANP host, and,

(c) the overlap of fluorescence originating from the 1D_2 energy level which may occur at similar wavelengths to those used to measure the fluorescence intensity ratio.

Some of the work presented here relating to the fluorescence intensity ratio of Pr^{3+} :ZBLANP has been published in reference 103.

4.4.2 Neodymium

The energy levels of interest for the neodymium (Nd^{3+}) ion were the $^4F_{3/2}$ and $^4F_{5/2}$ levels which are separated by approximately 1000 cm^{-1} . These levels are shown in figure 4.11 for a YAG host [92] together with other energy levels of interest to this study. This rare earth ion is commonly available in a range of host materials, due to its widespread use in solid state lasers, allowing a study of the host material dependence for the fluorescence intensity ratio technique of temperature sensing. The study of this ion included an examination of the fluorescence intensity ratio versus temperature characteristics of Nd^{3+} -doped in silica fibre, YAG, YVO_4 and ZBLANP.

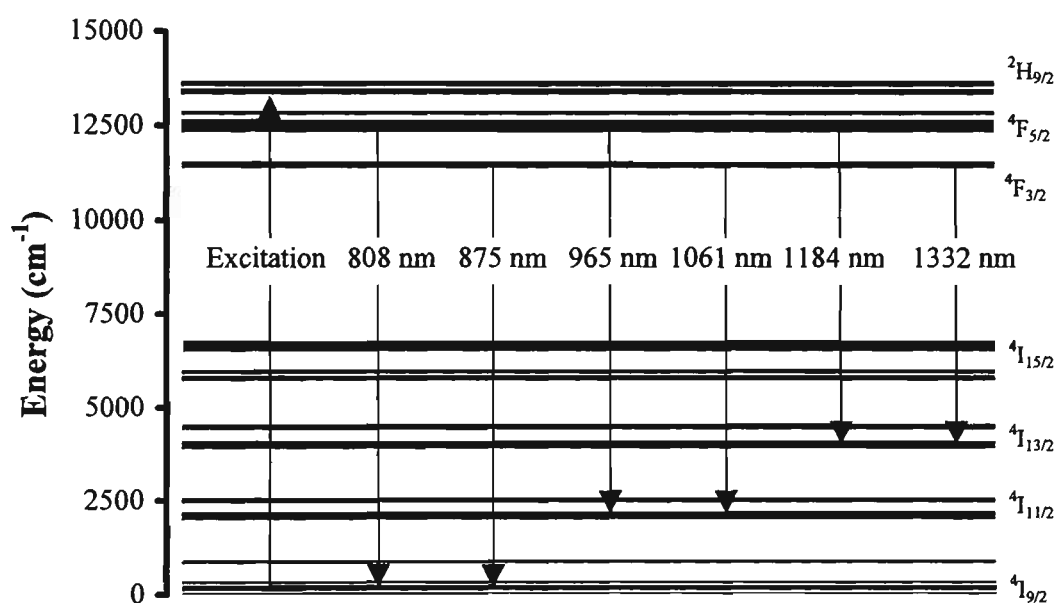


Figure 4.11: Partial energy level diagram of Nd:YAG, including the transitions of interest and the approximate wavelengths of these transitions [92].

Nd:YAG, Nd:YVO₄ and Nd:ZBLANP

The fluorescence spectra of the Nd^{3+} -doped bulk samples (i.e. Nd:YAG, Nd:YVO₄ and Nd:ZBLANP) were measured as a function of temperature using the bulk sample test arrangement (see section 4.3.1) with a Ti:sapphire laser as the excitation source. Table 4.6 provides the temperature ranges over which each of the samples were

tested as well as the pump wavelength, and energy gap between the ${}^4F_{3/2}$ and ${}^4F_{5/2}$ levels. The fluorescence spectra of the Nd^{3+} -doped samples at various temperatures are given in figures 4.12, 4.13 and 4.14 for transitions from the levels of interest to the ${}^4I_{9/2}$, ${}^4I_{11/2}$ and ${}^4I_{13/2}$ terminal levels.

Host	Doping concentration	Sample size	Temperature range (°C)	Pump wavelength	Energy gap [ref.]
YAG	1%	6×8 mm ^a	26 → 260	748 nm	943 cm ⁻¹ [92]
YVO ₄	1%	3×3×0.5 mm ^b	23.2 → 260	757 nm	1000 cm ⁻¹ [92]
ZBLANP	1%	13×4 mm ^c	22.6 → 200	790 nm	1030 cm ⁻¹ [85]

Table 4.6: Details of bulk Nd^{3+} -doped samples tested in this study, ^arod (diameter, length), ^brectangular prism (height, width, thickness), ^cbutton (diameter, width).

Nd^{3+} Silica Fibre

Measurements of the fluorescence spectra of Nd^{3+} -doped silica fibre were made using the 3 dB fibre coupler counter-propagating fluorescence arrangement (see section 4.3.2) using an 802 nm laser diode for excitation. The doped fibre used in the study was 25 cm in length, had a core diameter of 5 μm and a doping concentration of approximately 500 ppm. Fluorescence spectra were recorded at temperatures between $-62\text{ }^\circ\text{C}$ and $500\text{ }^\circ\text{C}$, examples of which are shown in figure 4.15. Below room temperature readings were obtained by introducing liquid nitrogen into the thermal chamber containing the doped fibre while an oven was used to heat the fibre up to $500\text{ }^\circ\text{C}$.

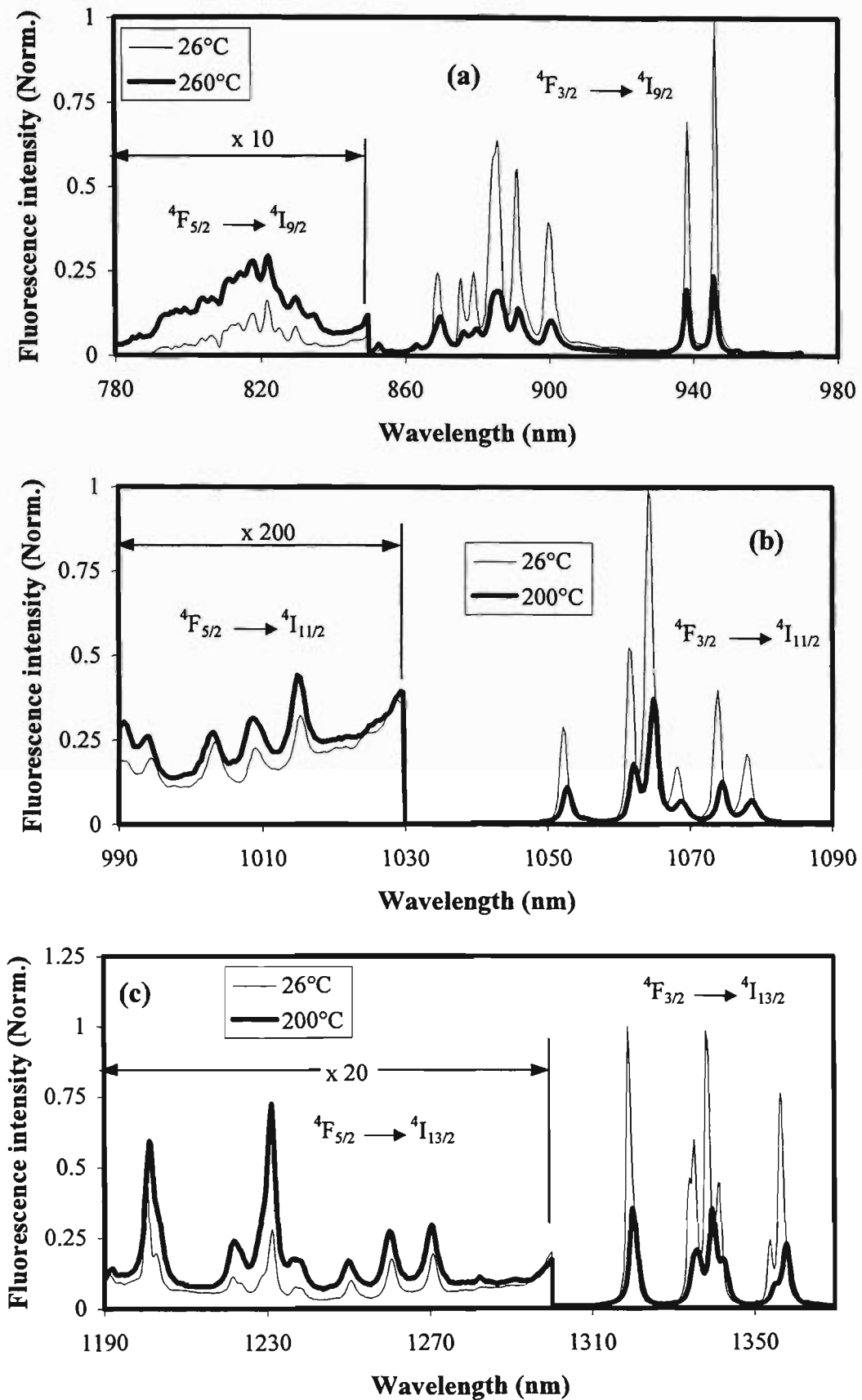


Figure 4.12: Fluorescence spectra of Nd:YAG at various temperatures (1 nm OSA resolution), (a) ${}^4F_{3/2}$, ${}^4F_{5/2} \rightarrow {}^4I_{9/2}$, (b) ${}^4F_{3/2}$, ${}^4F_{5/2} \rightarrow {}^4I_{11/2}$ and (c) ${}^4F_{3/2}$, ${}^4F_{5/2} \rightarrow {}^4I_{13/2}$.

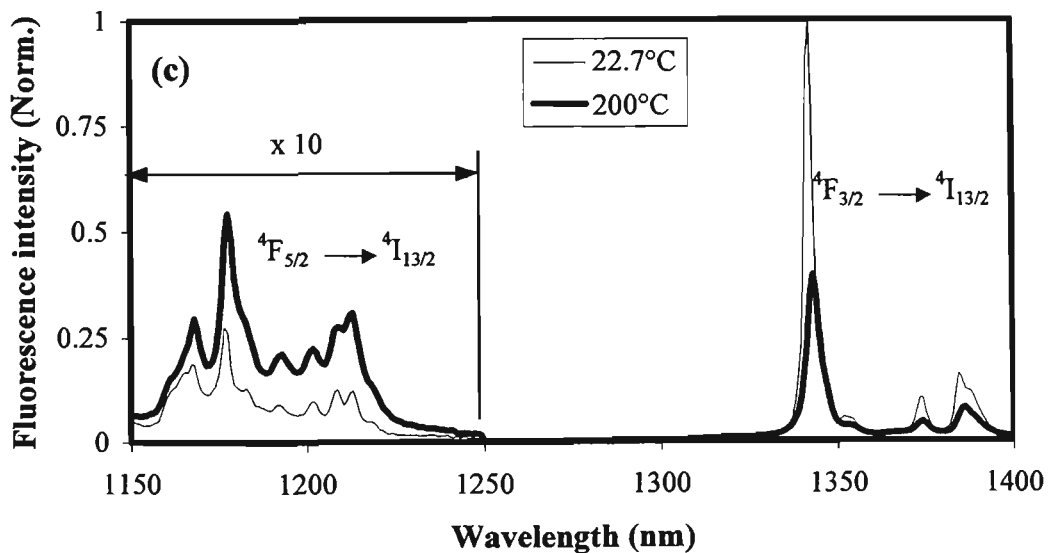
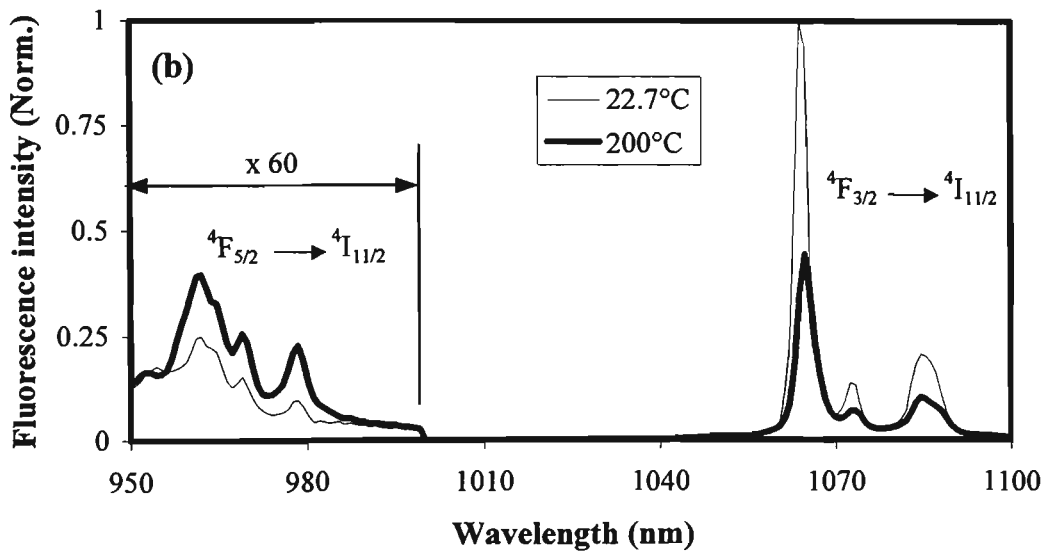
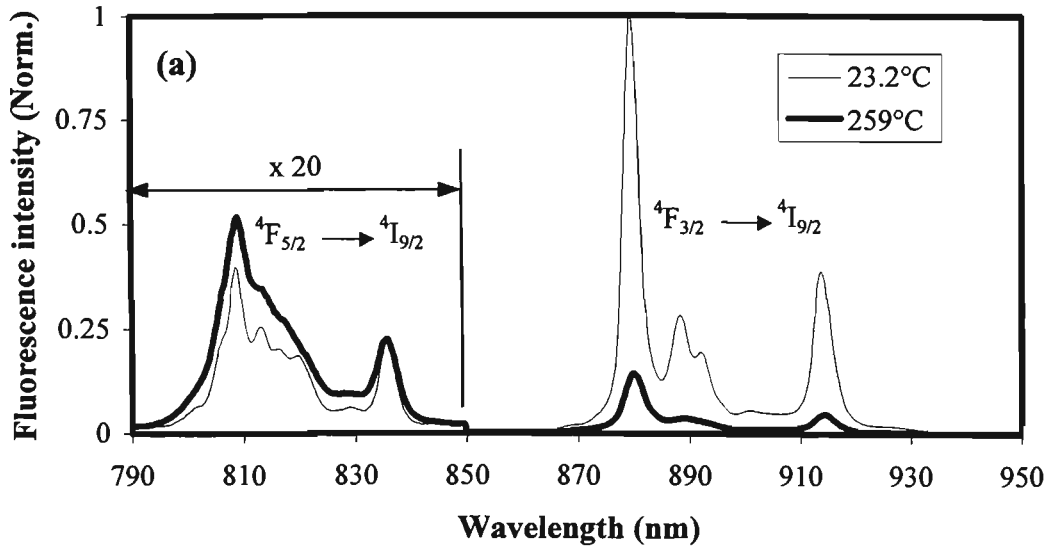


Figure 4.13: Fluorescence spectra of Nd:YVO₄ at various temperatures (2 nm resolution), (a) $^4F_{3/2}, ^4F_{5/2} \rightarrow ^4I_{9/2}$, (b) $^4F_{3/2}, ^4F_{5/2} \rightarrow ^4I_{11/2}$ and (c) $^4F_{3/2}, ^4F_{5/2} \rightarrow ^4I_{13/2}$.

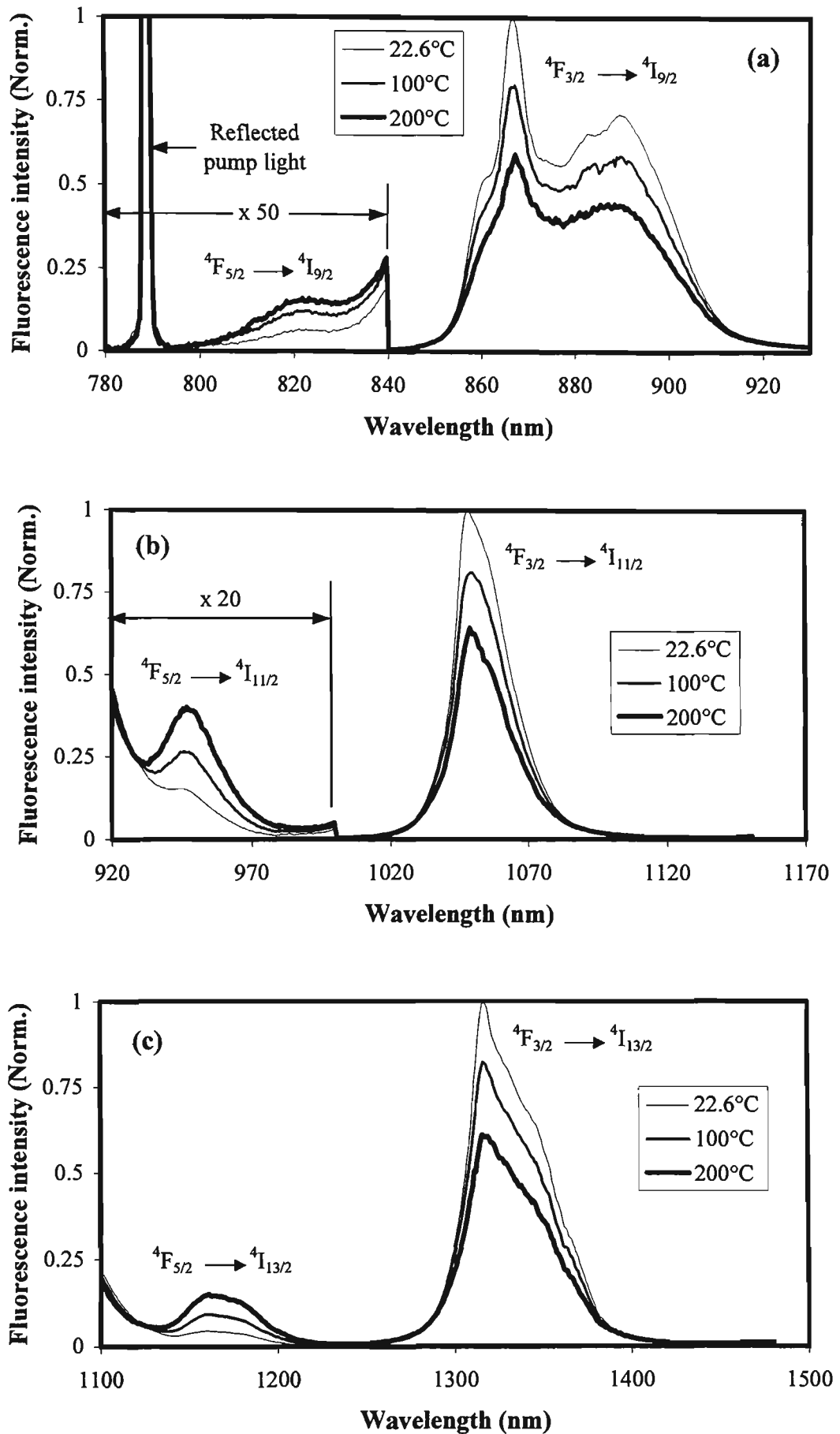


Figure 4.14: Fluorescence spectra of Nd:ZBLANP at various temperatures (2 nm OSA resolution), (a) ${}^4F_{3/2}, {}^4F_{5/2} \rightarrow {}^4I_{9/2}$, (b) ${}^4F_{3/2}, {}^4F_{5/2} \rightarrow {}^4I_{11/2}$ and (c) ${}^4F_{3/2}, {}^4F_{5/2} \rightarrow {}^4I_{13/2}$.

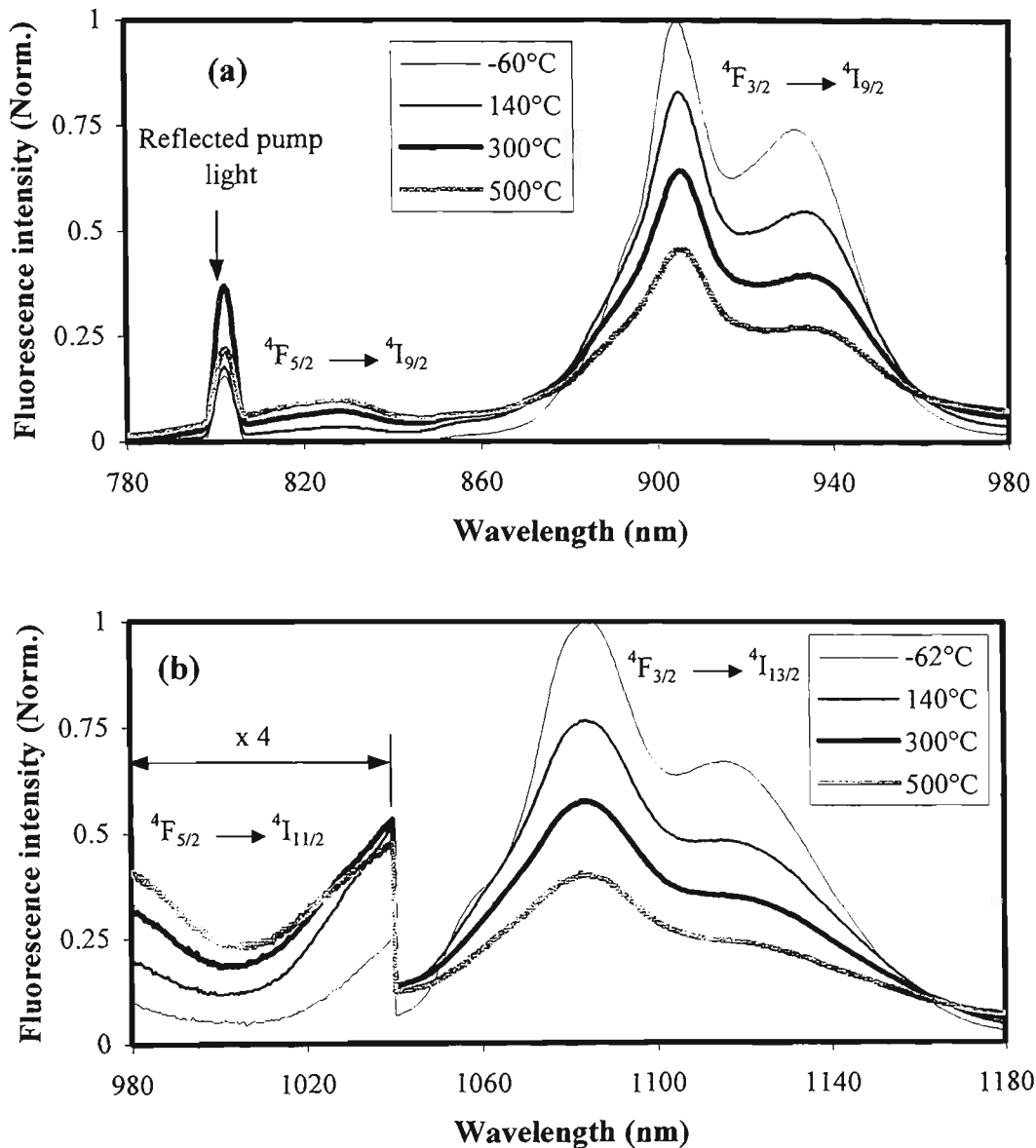


Figure 4.15: Counter-propagating fluorescence spectra of 25 cm length of Nd^{3+} -doped silica fibre at various temperatures (5 nm OSA resolution), (a) ${}^4F_{3/2}$, ${}^4F_{5/2} \rightarrow {}^4I_{9/2}$ and (b) ${}^4F_{3/2}$, ${}^4F_{5/2} \rightarrow {}^4I_{11/2}$.

The temperature dependent fluorescence spectra for each of the Nd^{3+} -doped materials tested suggest that the ${}^4F_{3/2}$ and ${}^4F_{5/2}$ energy levels are thermally coupled, with the ${}^4F_{3/2}$ fluorescence intensity decreasing and the ${}^4F_{5/2}$ intensity increasing with increasing temperature, following the Boltzmann theory.

Values of the fluorescence intensity ratio were calculated using the method discussed previously in the Pr^{3+} section, using the wavelength ranges shown in table 4.7. These wavelength ranges were chosen to correspond to commercially available optical bandpass filters [104-107] in an attempt to approximate the results that would be obtained by a prototype sensor. Again filters were chosen to maximise the measured

fluorescence intensity while avoiding overlap from other fluorescence peaks. A top hat response has been assumed for all the filters used for reasons of simplicity.

Graphs 4.16 to 4.18 show the calculated fluorescence intensity ratio versus temperature results obtained for Nd:YAG, Nd:YVO₄, Nd:ZBLANP and Nd³⁺-doped silica fibre with fluorescence intensity ratio values normalised at room temperature (approximately 20 °C) to assist comparison.

Host	Transition	⁴ F _{5/2} wavelength range	⁴ F _{3/2} wavelength range
YAG	⁴ F _{3/2} , ⁴ F _{5/2} → ⁴ I _{9/2}	810-830 nm	866-894 nm
	⁴ F _{3/2} , ⁴ F _{5/2} → ⁴ I _{11/2}	995-1005 nm	1059-1069 nm
	⁴ F _{3/2} , ⁴ F _{5/2} → ⁴ I _{13/2}	1190-1270 nm	1310-1360 nm
YVO ₄	⁴ F _{3/2} , ⁴ F _{5/2} → ⁴ I _{9/2}	800-820 nm	866-894 nm
	⁴ F _{3/2} , ⁴ F _{5/2} → ⁴ I _{11/2}	970-980 nm	1051.5-1076.5 nm
	⁴ F _{3/2} , ⁴ F _{5/2} → ⁴ I _{13/2}	1175-1225 nm	1300-1400 nm
ZBLANP	⁴ F _{3/2} , ⁴ F _{5/2} → ⁴ I _{9/2}	810-830 nm	866-894 nm
	⁴ F _{3/2} , ⁴ F _{5/2} → ⁴ I _{11/2}	945-955 nm	1045-1055 nm
	⁴ F _{3/2} , ⁴ F _{5/2} → ⁴ I _{13/2}	1160-1190 nm	1310-1380 nm
Silica fibre	⁴ F _{3/2} , ⁴ F _{5/2} → ⁴ I _{9/2}	820-840 nm	880-930 nm
	⁴ F _{3/2} , ⁴ F _{5/2} → ⁴ I _{11/2}	995-1005 nm	1095-1105 nm

Table 4.7: Wavelength ranges used to calculate fluorescence intensity ratio values for Nd³⁺-doped samples tested in this study.

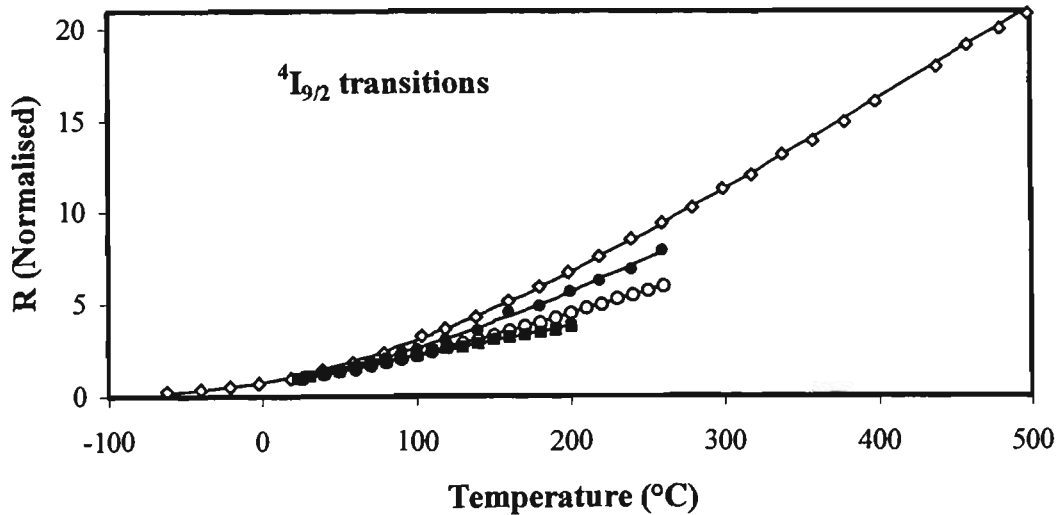


Figure 4.16: Fluorescence intensity ratio versus temperature for the ⁴F_{3/2}, ⁴F_{5/2} → ⁴I_{9/2} transitions of Nd³⁺ in silica fibre (◇), YAG (○), YVO₄ (●) and ZBLANP (■) hosts.

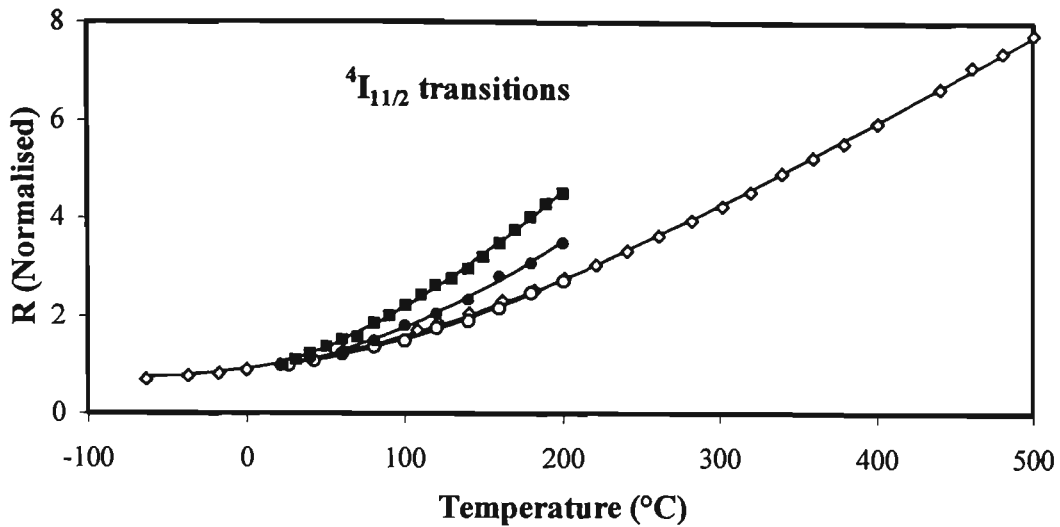


Figure 4.17: Fluorescence intensity ratio versus temperature for the $^4F_{3/2}, ^4F_{5/2} \rightarrow ^4I_{11/2}$ transitions of Nd^{3+} in silica fibre (\diamond), YAG (\circ), YVO_4 (\bullet) and ZBLANP (\blacksquare) hosts.

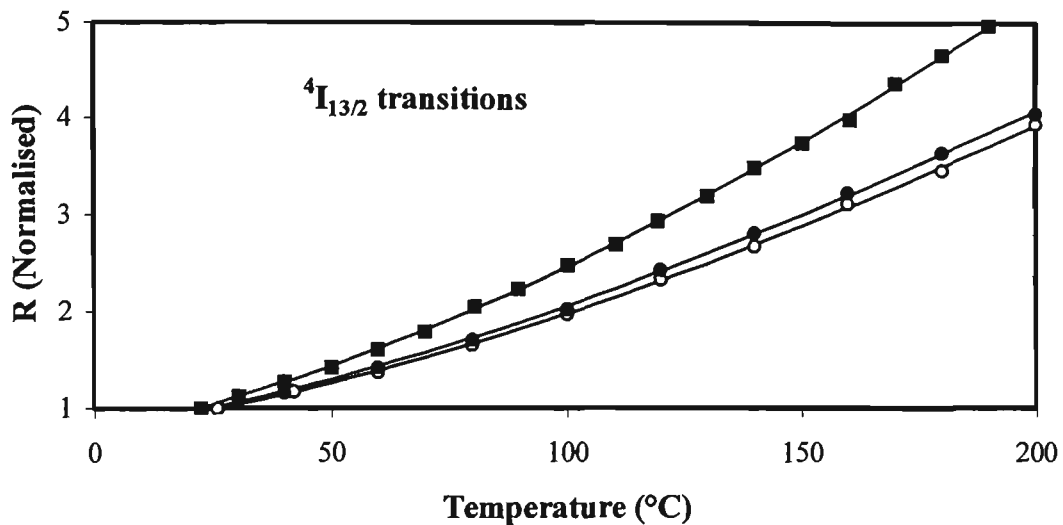


Figure 4.18: Fluorescence intensity ratio versus temperature for the $^4F_{3/2}, ^4F_{5/2} \rightarrow ^4I_{13/2}$ transitions of Nd^{3+} in YAG (\circ), YVO_4 (\bullet) and ZBLANP (\blacksquare) hosts.

The fluorescence intensity ratio versus temperature data presented in figures 4.16 to 4.18 have been fitted using Boltzmann distributions (as previously discussed for the Pr^{3+} -doped samples), details of which are given in table 4.8. Also listed in table 4.8 are the fit errors calculated as the standard deviation of the difference between the thermocouple temperature and the temperature implied from the fit.

Sample	Transition	FIR fit equation	Fit error (°C)
Nd ³⁺ :YAG	⁴ F _{3/2} , ⁴ F _{5/2} → ⁴ I _{9/2}	8.07×10 ⁻⁴ + 1.7716exp[-856.6/kT]	1.12
	⁴ F _{3/2} , ⁴ F _{5/2} → ⁴ I _{11/2}	2.292×10 ⁻³ + 0.2024exp[-1150.8/kT]	2.55
	⁴ F _{3/2} , ⁴ F _{5/2} → ⁴ I _{13/2}	0.0145 + 2.8480exp[-971.3/kT]	1.06
Nd ³⁺ :YVO ₄	⁴ F _{3/2} , ⁴ F _{5/2} → ⁴ I _{9/2}	1.299×10 ⁻³ + 3.4609exp[-967.0/kT]	2.85
	⁴ F _{3/2} , ⁴ F _{5/2} → ⁴ I _{11/2}	2.1605×10 ⁻³ + 0.3201exp[-1102.2/kT]	3.86
	⁴ F _{3/2} , ⁴ F _{5/2} → ⁴ I _{13/2}	0.0133 + 3.0334exp[-941.2/kT]	1.42
Nd ³⁺ :ZBLANP	⁴ F _{3/2} , ⁴ F _{5/2} → ⁴ I _{9/2}	0.0349exp[-682.5/kT]	4.25
	⁴ F _{3/2} , ⁴ F _{5/2} → ⁴ I _{11/2}	2.288×10 ⁻³ + 0.6043exp[-994.5/kT]	2.09
	⁴ F _{3/2} , ⁴ F _{5/2} → ⁴ I _{13/2}	4.7204×10 ⁻³ + 2.9297exp[-990.9/kT]	0.99
Nd ³⁺ silica fibre	⁴ F _{3/2} , ⁴ F _{5/2} → ⁴ I _{9/2}	0.7335exp[-980/kT]	3.92
	⁴ F _{3/2} , ⁴ F _{5/2} → ⁴ I _{11/2}	0.0197 + 1.3373exp[-1042.9/kT]	4.65

Table 4.8: Fits to Nd³⁺ fluorescence intensity ratio data.

The sensitivities of the Nd³⁺ transitions investigated were calculated using data obtained in fluorescence intensity ratio versus temperature fits. These values are presented in table 4.9 together with the theoretical sensitivity for an energy gap of 1000 cm⁻¹ between the two thermalising levels. In general the sensitivities of the ⁴F_{3/2}, ⁴F_{5/2} → ⁴I_{9/2} transitions agreed well with the theoretical predictions. Poorer agreement was observed for the ⁴F_{3/2}, ⁴F_{5/2} → ⁴I_{11/2} and ⁴F_{3/2}, ⁴F_{5/2} → ⁴I_{13/2} transitions. This is believed to be due to overlapping of fluorescence from the ⁴F_{5/2} level by fluorescence from the ⁴F_{3/2} level that reduces the change in the ⁴F_{5/2} intensity with temperature, especially at lower temperatures.

Sample	Transition	Sensitivity (%/°C)			
		@ -62 °C	@ 20 °C	@ 100°C	@ 500°C
Nd ³⁺ :YAG	⁴ F _{3/2} , ⁴ F _{5/2} → ⁴ I _{9/2}		1.41	0.87	
	⁴ F _{3/2} , ⁴ F _{5/2} → ⁴ I _{11/2}		0.46	0.61	
	⁴ F _{3/2} , ⁴ F _{5/2} → ⁴ I _{13/2}		1.02	0.83	
Nd ³⁺ :YVO ₄	⁴ F _{3/2} , ⁴ F _{5/2} → ⁴ I _{9/2}		1.55	0.99	
	⁴ F _{3/2} , ⁴ F _{5/2} → ⁴ I _{11/2}		0.74	0.77	
	⁴ F _{3/2} , ⁴ F _{5/2} → ⁴ I _{13/2}		1.09	0.84	
Nd ³⁺ :ZBLANP	⁴ F _{3/2} , ⁴ F _{5/2} → ⁴ I _{9/2}		1.14	0.71	
	⁴ F _{3/2} , ⁴ F _{5/2} → ⁴ I _{11/2}		1.11	0.88	
	⁴ F _{3/2} , ⁴ F _{5/2} → ⁴ I _{13/2}		1.38	0.96	
Nd ³⁺ silica fibre	⁴ F _{3/2} , ⁴ F _{5/2} → ⁴ I _{9/2}	3.17	1.64	1.01	0.24
	⁴ F _{3/2} , ⁴ F _{5/2} → ⁴ I _{11/2}	0.18	0.50	0.59	0.23
Theory (1000 cm ⁻¹)		3.23	1.68	1.03	0.24

Table 4.9: Sensitivity values for Nd³⁺ transitions investigated.

Each of the Nd³⁺-doped samples tested showed useful changes in the fluorescence intensity ratio with temperature. The most favourable of the transitions

studied appears to be the transitions that terminate at the $^4I_{9/2}$ ground state which suffer less from the problem of overlap with fluorescence from other transitions.

Some of the data presented here for Nd^{3+} -doped samples has been published in references 108 and 109.

4.4.3 Samarium

The energy levels selected for study in the samarium (Sm^{3+}) ion were the $^4F_{3/2}$ and $^4G_{5/2}$ levels which are separated by approximately 1000 cm^{-1} in LaCl_3 [87] as shown in figure 4.19.

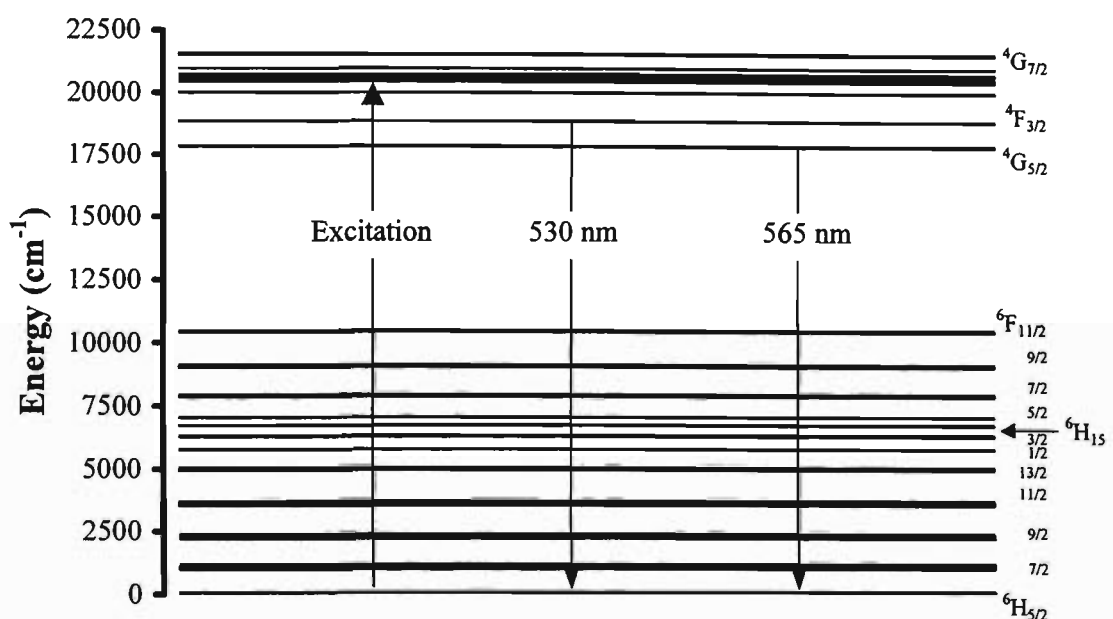


Figure 4.19: Partial energy level diagram of Sm^{3+} in LaCl_3 , including the transitions of interest and the approximate wavelengths of these transitions [87].

In this study the thermal coupling of these levels were investigated using a 30 cm length of Sm^{3+} -doped silica fibre with a doping concentration of approximately 3000 ppm and a $4.5 \mu\text{m}$ core diameter. Excitation was provided by the 476.5 nm line of an argon ion laser using the counter-propagating arrangement incorporating a cubic beamsplitter (see 4.3.2). The fluorescence spectra of the Sm^{3+} -doped fibre were recorded for temperatures between $22.3 \text{ }^\circ\text{C}$ and $475 \text{ }^\circ\text{C}$, several examples of which are shown in figure 4.20.

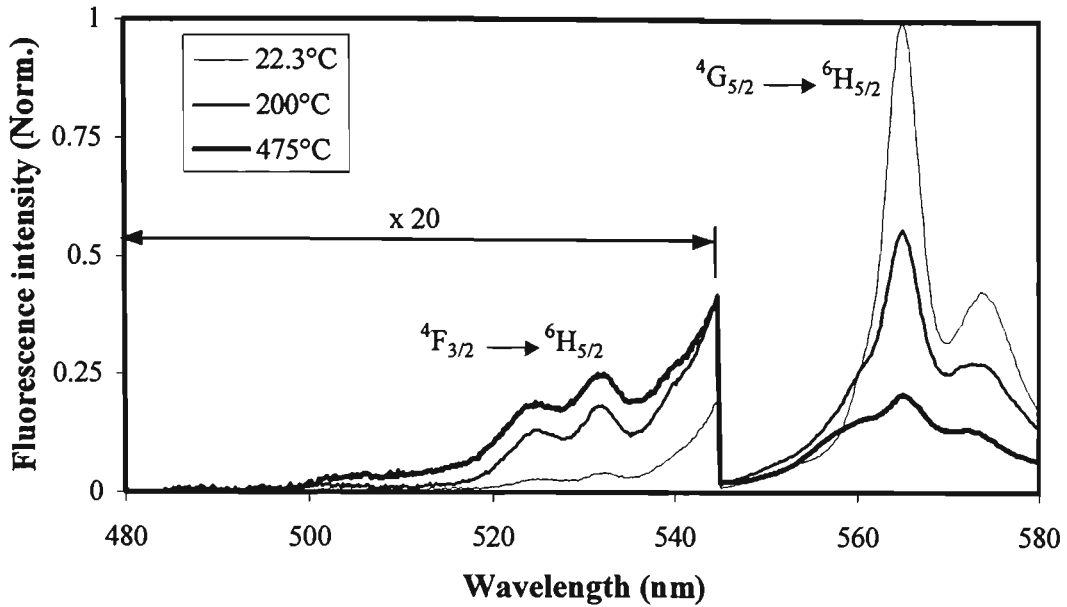


Figure 4.20: Fluorescence spectra of Sm^{3+} -doped silica fibre at various temperatures (2 nm OSA resolution).

The variation of the fluorescence intensity ratio with temperature was calculated using the 520 nm to 535 nm wavelength range for the ${}^4\text{F}_{3/2}$ level and 564 nm to 574 nm wavelength range for the ${}^4\text{G}_{5/2}$ level. These wavelength ranges were chosen to reduce the effect of the overlap of fluorescence from the two levels on the fluorescence intensity ratio while maintaining sufficient fluorescence signal to minimise noise problems. Figure 4.21 shows the measured values of the fluorescence intensity ratio as a function of temperature (points) fitted with a Boltzmann distribution (solid line) of the form:

$$FIR = 0.7577 \exp\left[-1099.3/kT\right]$$

The error in the Boltzmann distribution fit, calculated as the standard deviation of the difference between the thermocouple temperature and the temperature implied from the fit, was 3.8 °C.

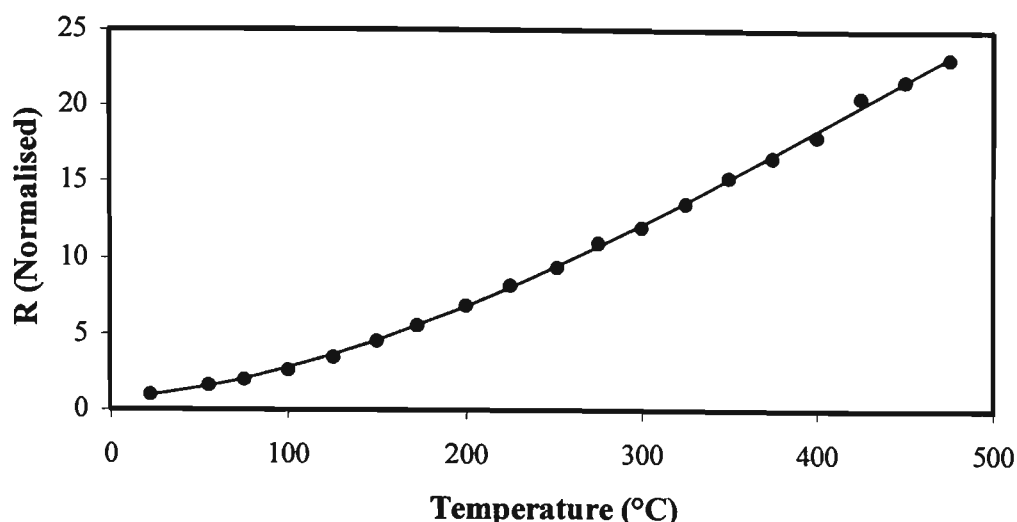


Figure 4.21: Fluorescence intensity ratio versus temperature for Sm^{3+} -doped silica fibre. Closed circles - experimental data, solid line - theoretical fit.

The sensitivity of the Sm^{3+} fluorescence intensity ratio was calculated at various temperatures using fluorescence intensity ratio fit data and is given in table 4.10 together with theoretical values of the sensitivity calculated for an energy gap of 1099.3 cm^{-1} (determined from the Boltzmann fit to the fluorescence intensity ratio data).

	Sensitivity (%/°C)		
	@ 20 °C	@ 100 °C	@ 475 °C
Experimental	1.85	1.14	0.28
Theory (1099.3 cm^{-1})	1.84	1.14	0.28

Table 4.10: Comparison of theoretical and experimental sensitivity values for Sm^{3+} -doped silica fibre.

The results presented in table 4.10 show the good agreement between theoretical and experimentally determined sensitivity values for Sm^{3+} -doped fibre.

4.4.4 Europium

The energy levels selected for study in the europium (Eu^{3+}) ion were the $^5\text{D}_0$ and $^5\text{D}_1$ levels, which are separated by approximately 1750 cm^{-1} [87, 95]. This is the largest energy gap investigated in this study. These levels are shown in figure 4.22 together with other energy levels of interest to this study.

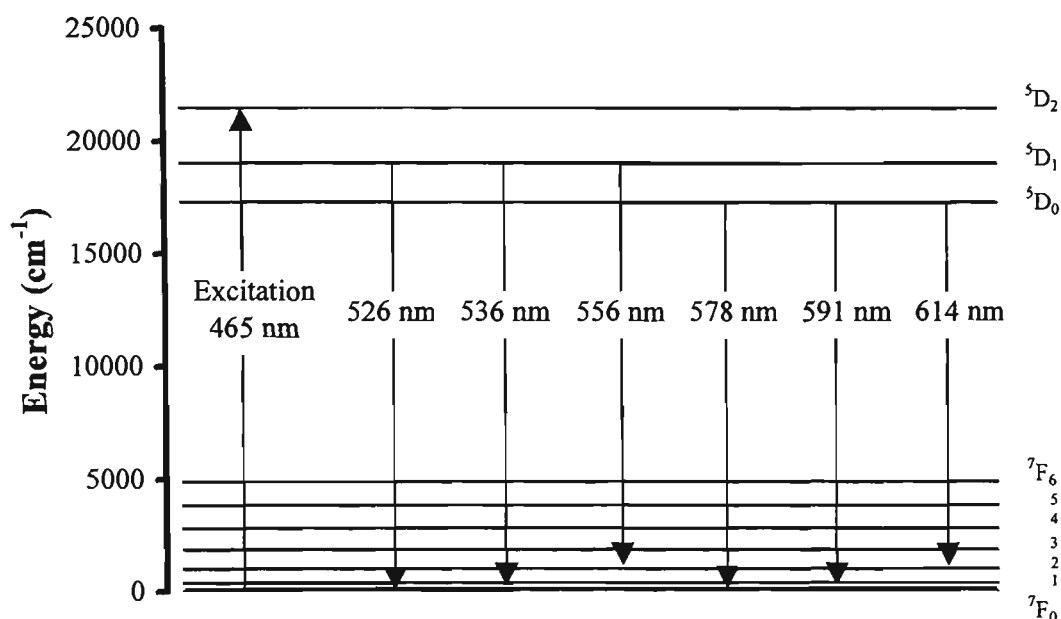


Figure 4.22: Partial energy level diagram of Eu^{3+} in ZBLA, including the transitions of interest and the approximate wavelengths of these transitions [95].

The Eu^{3+} -doped material used in this work was a 1.84 m length of Eu^{3+} -doped silica fibre (doping concentration ~ 450 ppm, core diameter $4.5 \mu\text{m}$), manufactured at the *Laboratoire de Physique de la Matière Condensée, Université de Nice*. A counter-propagating experimental arrangement incorporating a cubic beamsplitter (see section 4.3.2) was used with excitation at 465 nm from an argon ion laser. Fluorescence spectra of the doped fibre were recorded over the -172 °C to $+400$ °C temperature range using a Tetlow oven to heat the fibre above room temperature, while cooling was achieved by introducing liquid nitrogen into the doped fibre holder. Examples of the Eu^{3+} -silica fibre fluorescence spectra at various temperatures are given in figure 4.23.

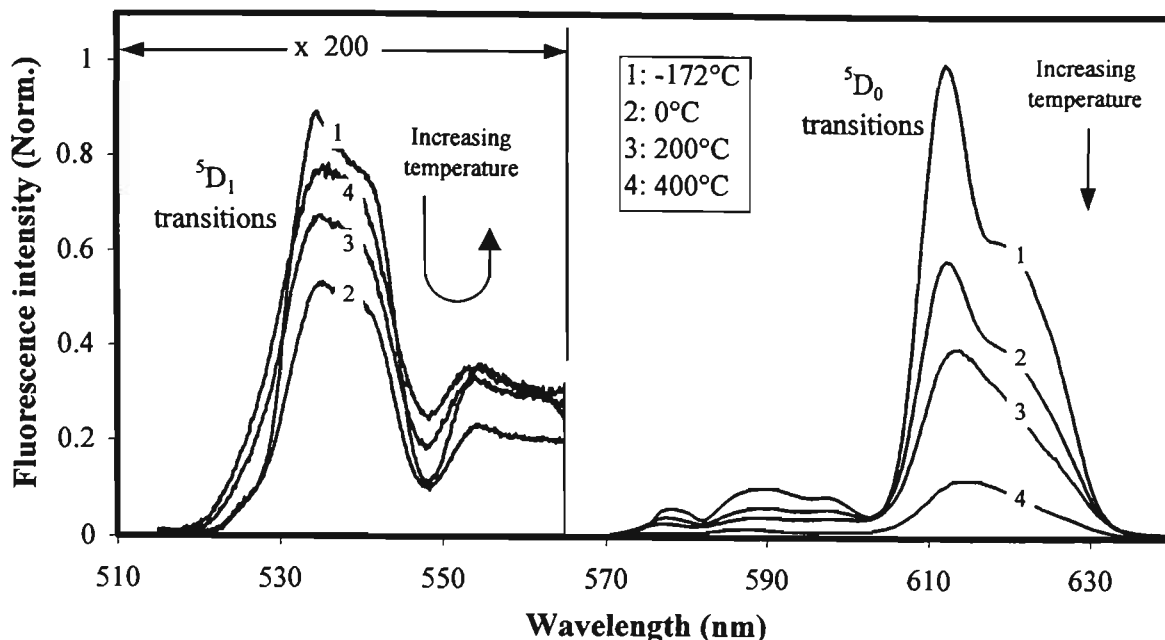


Figure 4.23: Counter-propagating fluorescence spectra of 1.84 m length of Eu^{3+} -doped silica fibre at various temperatures (5 nm OSA resolution).

Figure 4.23 shows that the fluorescence intensity originating from the ${}^5\text{D}_0$ level decreases with increasing temperature, as is expected by Boltzmann distribution theory. The intensity of transitions originating from the ${}^5\text{D}_1$ level, however, appear to initially decrease with temperature before increasing with temperature at approximately 80 °C. Theory however predicts that if the populations are governed by a Boltzmann distribution the intensity from the upper level should always increase as the temperature is raised. To further investigate this point the measured intensities of the ${}^5\text{D}_0$, ${}^5\text{D}_1 \rightarrow {}^7\text{F}_1$ fluorescence transitions were plotted as a function of temperature (figure 4.24). Also shown in figure 4.24 are theoretical fits, using equations 3.4 and 3.5, to the fluorescence intensities assuming a Boltzmann distribution for the population of the ${}^5\text{D}_0$ and ${}^5\text{D}_1$ levels. Figure 4.24b shows that the ${}^5\text{D}_1 \rightarrow {}^7\text{F}_1$ intensity at low temperatures decreases as the temperature is raised until approximately 80 °C when it starts to follow the trend expected from theory. The cause for this variation is believed to be the reduction in thermalising rates from the ${}^5\text{D}_0$ level to the ${}^5\text{D}_1$ level at low temperatures due to the large energy gap between the two levels. As a result other radiative and non-radiative rates dominate this thermalising rate at low temperatures such that the two levels act as though they are not fully thermally coupled as predicted by the Boltzmann distribution. The ${}^5\text{D}_0 \rightarrow {}^7\text{F}_1$ intensity on the other hand appears to follow the predicted theory well over the complete temperature range tested. It is important to note that the drop in the

$^5D_1 \rightarrow ^7F_1$ fluorescence intensity at 400 °C is believed to be due to changes in the pump intensity rather than any other effect such as population re-distribution between the 5D_0 and 5D_1 levels. Further investigation of this variation from theory was undertaken through measurements of the fluorescence lifetime of the 5D_0 and 5D_1 energy levels as a function of temperature. The results of the fluorescence lifetime studies are presented in chapter 7.

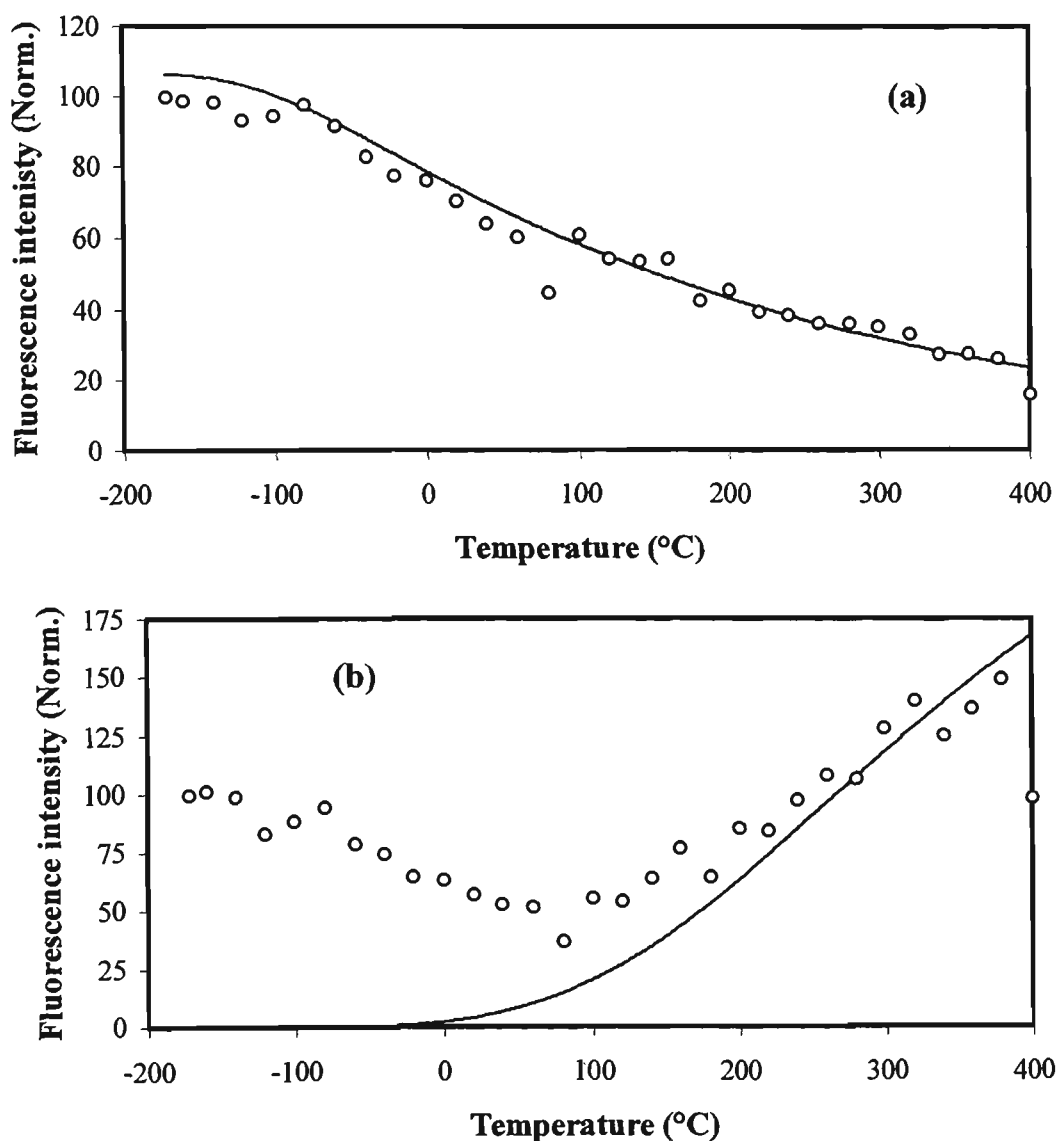


Figure 4.24: Intensity of (a) $^5D_0 \rightarrow ^7F_1$ and (b) $^5D_1 \rightarrow ^7F_1$ fluorescence transitions versus temperature for Eu^{3+} -doped fibre. Open circles – experimental data, solid lines - theoretical fits.

The variation in the fluorescence intensity ratio with temperature for the Eu^{3+} -doped fibre is plotted for a number of wavelength ranges in figure 4.25. The wavelength ranges used, which are given in table 4.11, correspond to transitions from the 5D_0 and 5D_1 levels to the 7F_1 , 7F_2 and the combination of the $^7F_{0 \rightarrow 3}$ levels. Again the fluorescence

intensity ratio data has been normalised by dividing each fluorescence intensity ratio value by the room temperature fluorescence intensity ratio for that particular transition to aid in comparison.

Transition	Wavelength ranges	
	5D_1	5D_0
$^5D_0, ^5D_1 \rightarrow ^7F_1$	525-545 nm	585-595 nm
$^5D_0, ^5D_1 \rightarrow ^7F_2$	552-560 nm	607-630 nm
$^5D_0, ^5D_1 \rightarrow ^7F_{0 \rightarrow 3}$	515-560 nm	575-665 nm

Table 4.11: Wavelength ranges used to calculate fluorescence intensity ratio values for Eu^{3+} transitions tested in this study.

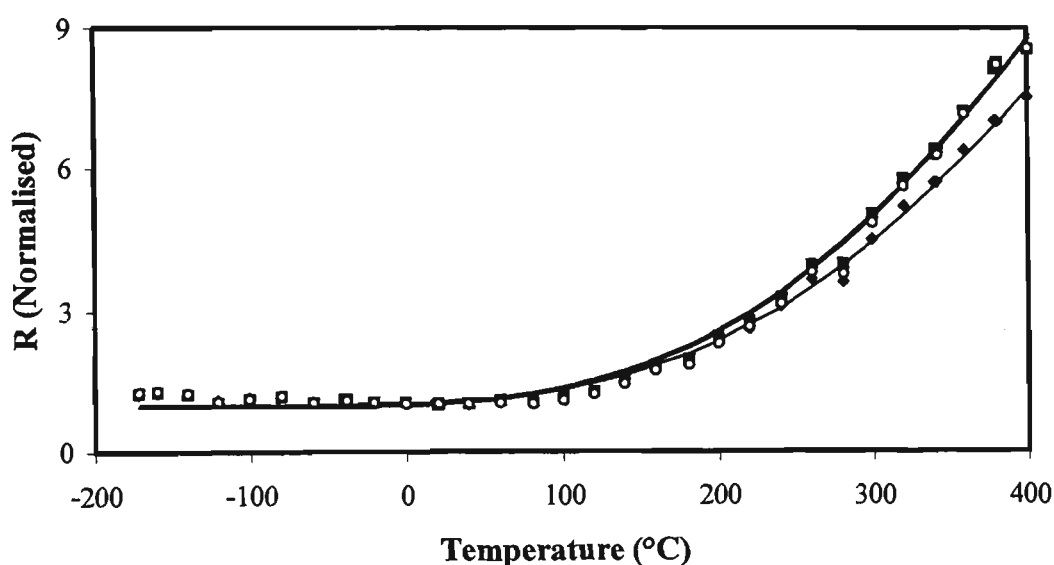


Figure 4.25: Fluorescence intensity ratio versus temperature for Eu^{3+} -doped silica fibre, $^5D_0, ^5D_1 \rightarrow ^7F_1$ (\blacklozenge), $^5D_0, ^5D_1 \rightarrow ^7F_2$ (\blacksquare) and $^5D_0, ^5D_1 \rightarrow ^7F_{0 \rightarrow 3}$ (\circ). Solid lines are Boltzmann distribution fits to the data.

The fluorescence intensity ratio data shown in figure 4.25 have been fitted by Boltzmann distributions with a fixed energy gap of 1760 cm^{-1} . Details of the fits used for each of the transitions are given in table 4.12. The fit errors given correspond to the errors over the $220 \text{ }^\circ\text{C}$ to $400 \text{ }^\circ\text{C}$ temperature range since for lower temperatures the errors are quite large due to the sensitivity approaching $0\%/^\circ\text{C}$.

Transition	FIR fit equation	Fit error ($^\circ\text{C}$)
$^5D_0, ^5D_1 \rightarrow ^7F_1$	$0.0537 + 14.981 \exp[-1750/kT]$	6.55
$^5D_0, ^5D_1 \rightarrow ^7F_2$	$8.671 \times 10^{-4} + 0.289 \exp[-1750/kT]$	7.12
$^5D_0, ^5D_1 \rightarrow ^7F_{0 \rightarrow 3}$	$3.669 \times 10^{-3} + 1.276 \exp[-1750/kT]$	9.69

Table 4.12: Details of the fits to fluorescence intensity ratio versus temperature data obtained for Eu^{3+} -doped silica fibre.

The sensitivity of the Eu^{3+} fluorescence intensity ratios to changes in temperature were calculated using the Boltzmann distribution fit data and are presented in table 4.13 together with the theoretical sensitivity for an energy gap of 1750 cm^{-1} .

Transition	Sensitivity (%/°C)			
	@ -100 °C	@ 20 °C	@ 100 °C	@ 400 °C
${}^5\text{D}_0, {}^5\text{D}_1 \rightarrow {}^7\text{F}_1$	0.0013	0.144	0.445	0.482
${}^5\text{D}_0, {}^5\text{D}_1 \rightarrow {}^7\text{F}_2$	0.0017	0.171	0.506	0.492
${}^5\text{D}_0, {}^5\text{D}_1 \rightarrow {}^7\text{F}_{0 \rightarrow 3}$	0.0019	0.178	0.522	0.494
Theory (1750 cm^{-1})	8.413	2.933	1.809	0.556

Table 4.13: Comparison of theoretical and experimental sensitivity values for Eu^{3+} -doped silica fibre.

The data presented in table 4.13 shows that the measured sensitivity of the fluorescence intensity ratio for Eu^{3+} -doped fibre is significantly lower than the theoretical values, especially at lower temperatures. This is believed to arise from the initial drop in the fluorescence intensity of the ${}^5\text{D}_1$ level at low temperatures, as previously mentioned. This result highlights that care must be taken when assuming that high sensitivity values can be obtained by simply using energy levels separated by a large energy gap.

The results of fluorescence intensity ratio versus temperature studies for Eu^{3+} -doped silica fibre have been reported in reference 110.

4.4.5 Dysprosium

The energy levels of the trivalent dysprosium (Dy^{3+}) ion investigated for possible use in fluorescence intensity ratio based temperature sensing were the ${}^4\text{F}_{9/2}$ and ${}^4\text{I}_{15/2}$ levels. These levels, illustrated in figure 4.26, are separated by approximately 1000 cm^{-1} [96].

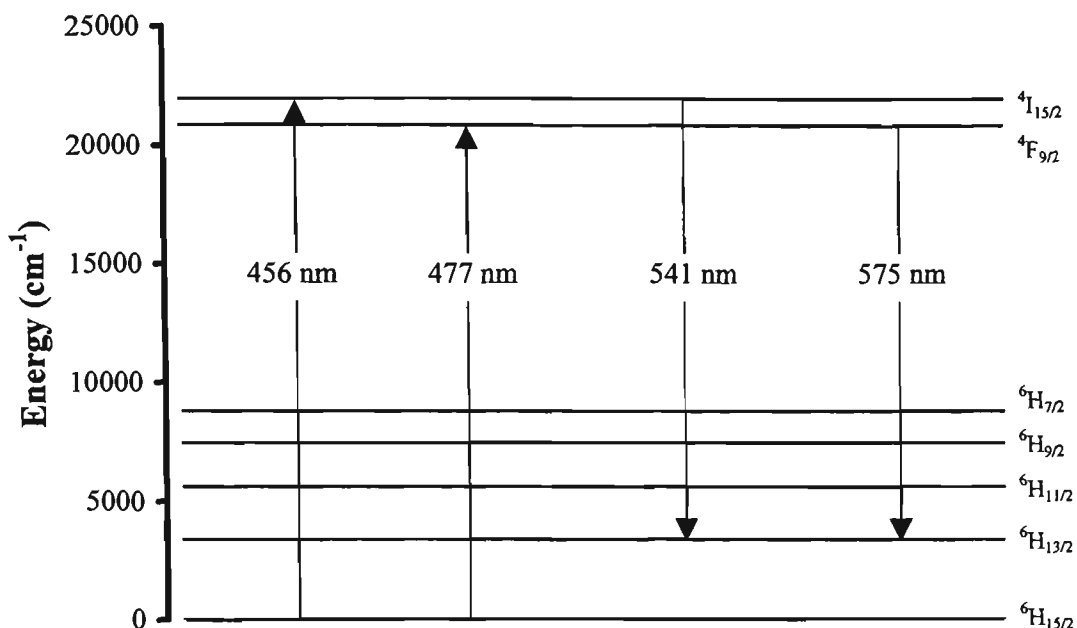


Figure 4.26: Partial energy level diagram of Dy^{3+} in fluorozirconate glass, including the transitions of interest and the approximate wavelengths of these transitions [96].

A 1.28 m length of Dy^{3+} -doped silica fibre, with a doping concentration of approximately 1000 ppm and a core diameter of approximately $9 \mu\text{m}$, was used in this study. An argon ion laser was used for excitation in the counter-propagating experimental arrangement incorporating a cubic beamsplitter (see 4.3.2). Measurements of the Dy^{3+} fluorescence spectra were recorded at temperatures between 21.5°C and 250°C for excitation at 457.9 nm and 476.5 nm , examples of which are shown in figure 4.27. These pump wavelengths were chosen to allow a comparison of the change in the fluorescence intensity ratio with temperature for selective excitation of each of the thermally coupled levels, i.e. the ${}^4\text{I}_{15/2}$ and ${}^4\text{F}_{9/2}$ levels. The data shown in figure 4.27 reveal that the fluorescence originating from both the upper and lower thermalising energy levels increase with temperature. The fluorescence intensity ratio theory however predicts that only the fluorescence from the upper energy thermalising level should increase with temperature. One possible explanation for this is that for the pump wavelength used increases in temperature resulted in increased pump absorption and hence increased the overall fluorescence intensity. Another possible explanation is that increases in temperature resulted in a reduction in the fluorescence re-absorbed by the fibre.

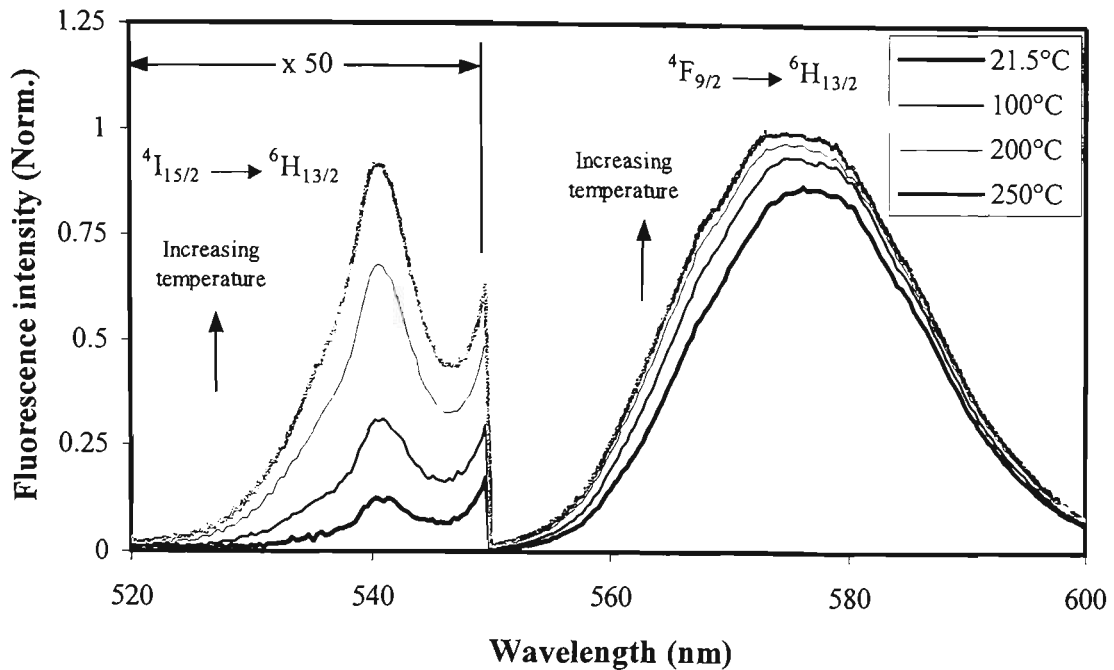


Figure 4.27: Counter-propagating fluorescence spectra of 1.28 m length of Dy^{3+} -doped silica fibre at various temperatures for a pump wavelength of 456 nm (2 nm OSA resolution).

Figure 4.28 shows the fluorescence intensity ratio values versus temperature calculated using the 530 nm to 542.5 nm wavelength range for fluorescence originating from the $^4\text{I}_{15/2}$ level and 560 nm to 590 nm range for the $^4\text{F}_{9/2}$ fluorescence. These wavelength ranges were chosen to select fluorescence from the thermalising level of interest while avoiding the region of overlap between the two peaks.

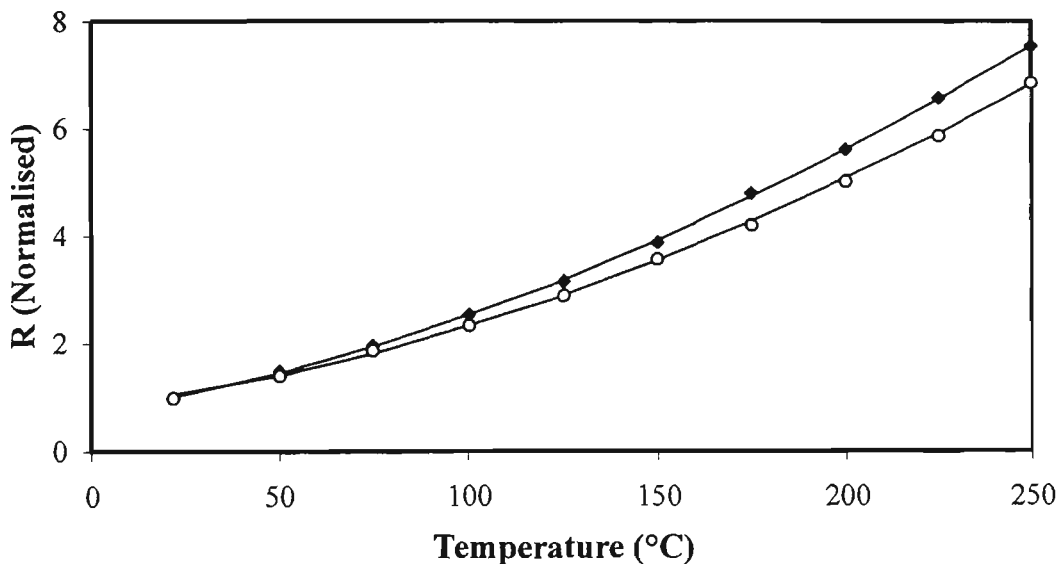


Figure 4.28: Fluorescence intensity ratio versus temperature for Dy^{3+} -doped silica fibre, 456 nm pump (◆) and 477 nm pump (○). The solid lines are Boltzmann distribution fits with offsets (see table 4.14).

Pump wavelength	FIR fit equation	Fit error (°C)
456 nm	$2.11 \times 10^{-4} + 0.105 \exp[-1067.2/kT]$	1.16
	$0.086 \exp[-984.1/kT]$	2.58
477 nm	$3.71 \times 10^{-4} + 0.112 \exp[-1112.8/kT]$	1.83
	$0.077 \exp[-955.6/kT]$	4.03

Table 4.14: Fits to Dy^{3+} fluorescence intensity ratio data and fit errors.

The data shown in figure 4.28 and the Boltzmann distribution fits to these data, given in table 4.14, indicate that there is good agreement between fluorescence intensity ratio data obtained for direct excitation of each of the $^4F_{9/2}$ and $^4I_{15/2}$ levels. This suggests that the thermalisation rates between the two levels, i.e. $^4F_{9/2} \rightarrow ^4I_{15/2}$ and $^4I_{15/2} \rightarrow ^4F_{9/2}$, are much faster than the radiative rates for these levels. The sensitivity values for the fits given in table 4.14 are provided in table 4.15 together with the theoretical sensitivity for an energy gap of 1000 cm^{-1} . Good agreement between the theoretical (1000 cm^{-1}) and experimental sensitivity values was obtained for the Boltzmann distribution fits. For the Boltzmann distribution fits with an offset, which provided more accurate fits than the simple Boltzmann distributions, the sensitivity values were lower than predicted. A slight discrepancy between the sensitivity values obtained for each of the pump wavelengths is believed to be due to site selective effects, as discussed in chapter 2.

Pump wavelength	Fit	Sensitivity (%/°C)	
		@ 20 °C	@ 100 °C
456 nm	Boltzmann + offset	1.30	0.98
	Boltzmann	1.65	1.02
477 nm	Boltzmann + offset	1.05	0.93
	Boltzmann	1.61	0.99
Theory (1000 cm^{-1})		1.68	1.03

Table 4.15: Sensitivity values for Dy^{3+} -doped silica fibre.

The results of this work were presented in reference 111.

4.4.6 Ytterbium

The energy levels selected for study in the ytterbium (Yb^{3+}) ion were the $^2F_{5/2(a)}$ and $^2F_{5/2(b)}$ Stark sub-levels, which are separated by approximately 680 cm^{-1} in silica fibre [86]. Figure 4.29 illustrates the energy level diagram for Yb^{3+} -doped silica fibre using the energy values given in reference 86.

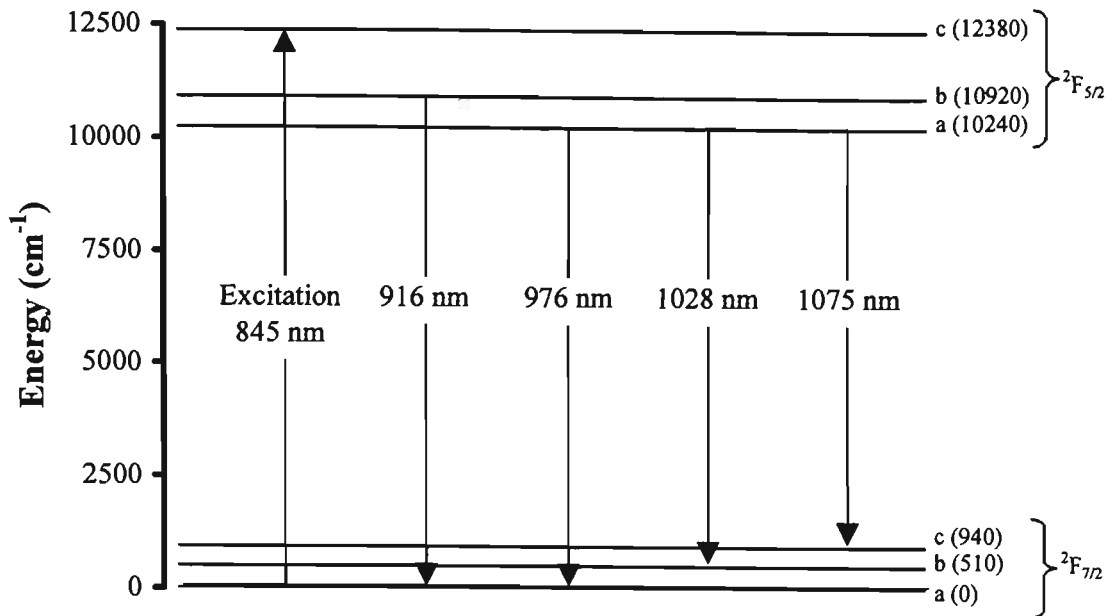


Figure 4.29: Partial energy level diagram of Yb^{3+} doped in silica fibre, including the transitions of interest and the approximate wavelengths of these transitions [86].

The results of fluorescence intensity ratio studies of two Yb^{3+} -doped silica fibre samples, with different doping concentrations, are presented here. Details of the doping concentrations and dimensions of each of the fibre samples are given in table 4.16. Measurements of the fluorescence spectra of both samples were obtained using the 3 dB coupler doped fibre test arrangement (discussed in section 4.3.2). The Yb^{3+} fibre with lower doping concentration (YbL) was excited by approximately 2.5 mW of light from a pigtailed laser diode with an 845 nm centre wavelength, while the fibre with higher Yb^{3+} doping concentration (YbH) was excited using approximately 13 mW of light at 830 nm from a Ti:sapphire laser. Measurements of the fluorescence spectra were obtained between 24 °C and 500 °C for the lower dopant concentration fibre and between 22 °C and 160 °C for the higher dopant concentration fibre. Several examples of fluorescence spectra from each of the Yb^{3+} -doped fibre samples are presented in figures 4.30 and 4.31. Both fibre samples were manufactured at the *Laboratoire de Physique de la Matière Condensée, Université de Nice*.

Code	Doping concentration	Core/Cladding diameter (μm)	Length (cm)
YbL	700 ppm	13/130	52
YbH	2500 ppm	5.2/116	30.5

Table 4.16: Composition and dimensions of Yb^{3+} -doped silica fibre used in fluorescence intensity ratio tests.

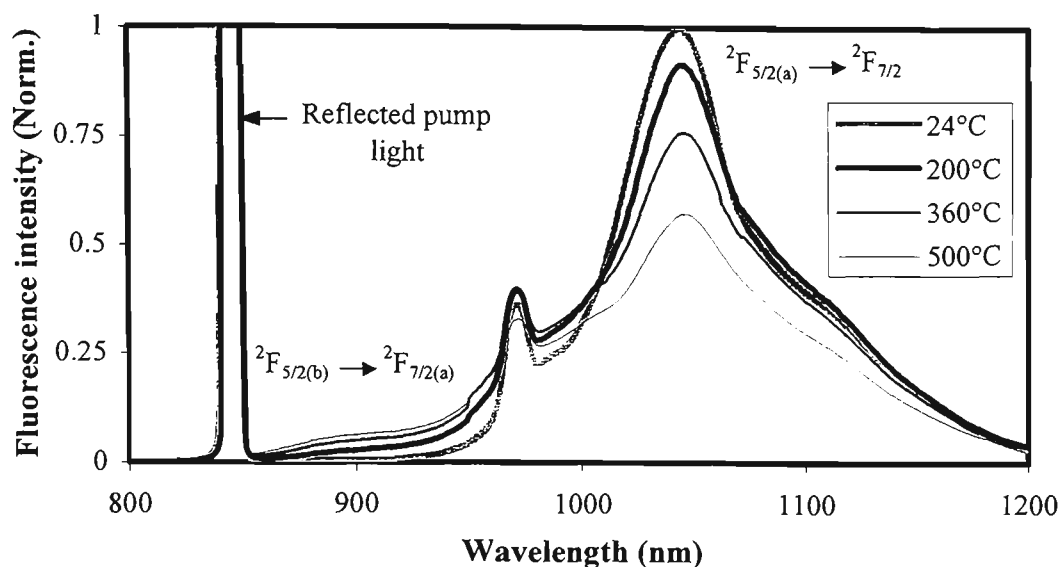


Figure 4.30: Fluorescence spectra of a 52 cm length of 700 ppm Yb^{3+} -doped silica fibre at various temperatures (10 nm OSA resolution).

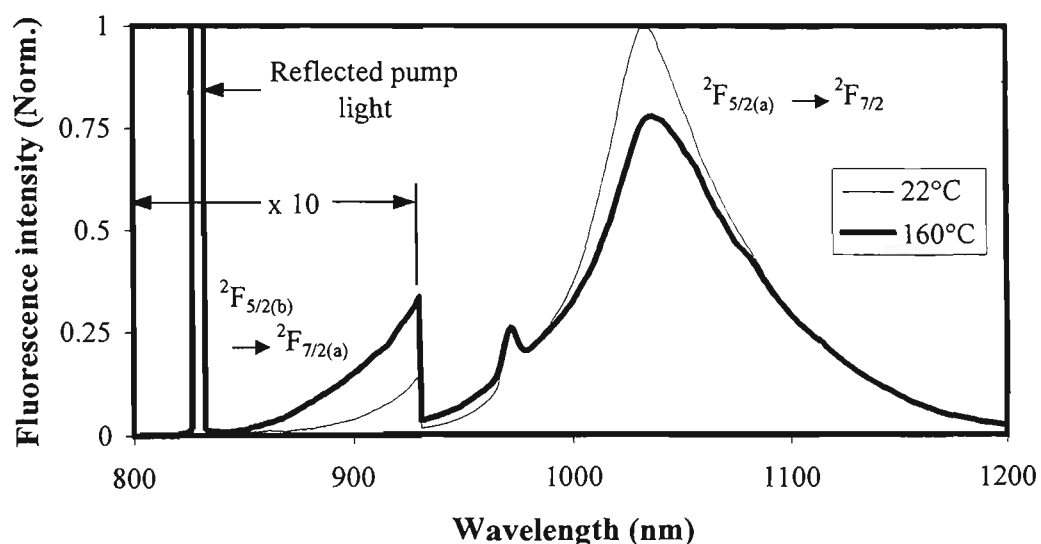


Figure 4.31: Fluorescence spectra of a 30.5 cm length of 2500 ppm Yb^{3+} -doped silica fibre at various temperatures (5 nm OSA resolution).

From the fluorescence spectra values of the fluorescence intensity ratio versus temperature were calculated for a number of different wavelength ranges, for each of the doping concentrations tested (figures 4.32 and 4.33). The wavelength ranges used for the fluorescence from the ${}^2\text{F}_{5/2(a)}$ and ${}^2\text{F}_{5/2(b)}$ levels are listed in table 4.17 and were all chosen to correspond to commercially available optical bandpass filters.

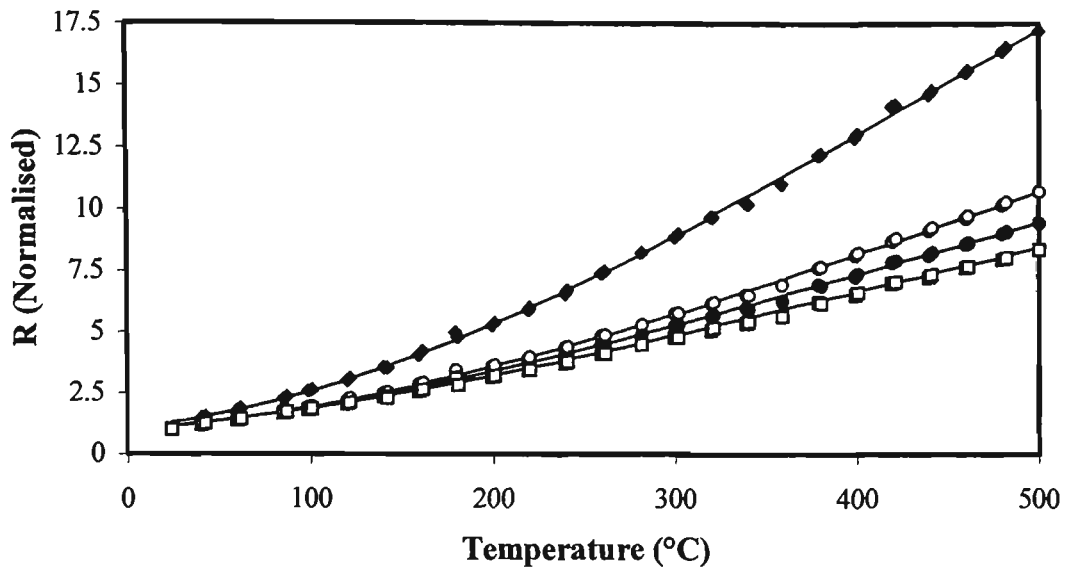


Figure 4.32: Fluorescence intensity ratio versus temperature for 700 ppm Yb^{3+} -doped silica fibre, ratio a (\blacklozenge), ratio b (\bullet), ratio c (\circ) and ratio d (\square). Solid lines are Boltzmann distribution fits (see table 4.17).

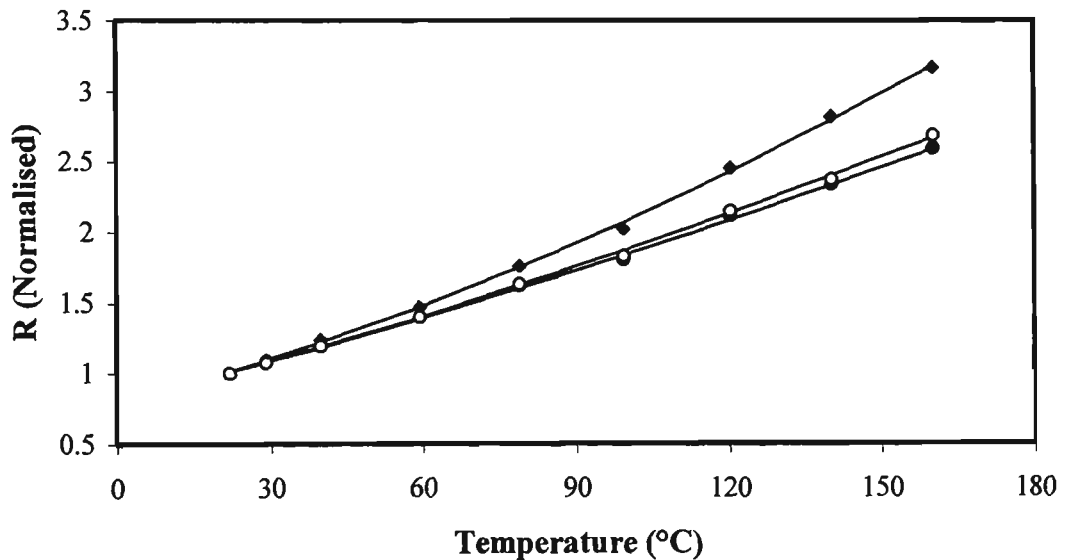


Figure 4.33: Fluorescence intensity ratio versus temperature for 2500 ppm Yb^{3+} -doped silica fibre, ratio a (\blacklozenge), ratio b (\bullet) and ratio c (\circ). Solid lines are Boltzmann distribution fits (see table 4.17).

Ratio	Wavelength ranges		FIR fit equation
	${}^2F_{5/2(a)}$	${}^2F_{5/2(b)}$	
a (YbL) (YbH)	900-910 nm	1051.5-1076.5 nm	$1.98 \times 10^{-3} + 0.411 \exp[-1064.6/kT]$
			$1.2 \times 10^{-3} + 0.228 \exp[-896.2/kT]$
b (YbL) (YbH)	920-930 nm	1051.5-1076.5 nm	$4.95 \times 10^{-3} + 0.406 \exp[-987.5/kT]$
			$1.63 \times 10^{-3} + 0.197 \exp[-696.1/kT]$
c (YbL) (YbH)	920-930 nm	1045-1055 nm	$9.09 \times 10^{-3} + 0.902 \exp[-1054.4/kT]$
			$3.99 \times 10^{-3} + 0.447 \exp[-751.9/kT]$
d (YbL)	920-930 nm	1095-1105 nm	$2.16 \times 10^{-2} + 1.380 \exp[-948.2/kT]$

Table 4.17: Wavelength ranges used to calculate fluorescence intensity ratio values for Yb^{3+} transitions tested in this study and formulae used to fit fluorescence intensity ratio data.

The fluorescence intensity ratio versus temperature data shown in figure 4.32 and figure 4.33 have been fitted using Boltzmann distributions, details of which are given in table 4.17. For all of the wavelength ranges tested the value of the energy gap used in the fit was larger than the predicted value of 680 cm^{-1} . This is believed to be the result of temperature dependent changes in re-absorption of the fluorescence from the ${}^2F_{5/2(a)}$ and ${}^2F_{5/2(b)}$ levels due to changes in the population distribution of the ${}^2F_{7/2}$ ground state and the fact that the measured fluorescence transitions from these levels terminate at different ground state Stark levels. Measurements of the changes in the absorption spectra of Yb^{3+} -doped silica fibre with temperature [86] show that re-absorption of ${}^2F_{5/2(b)}$ fluorescence decreases as the fibre temperature is raised which would result in the ${}^2F_{5/2(b)}$ fluorescence appearing to increase faster with temperature than predicted by the Boltzmann population distribution of the ${}^2F_{5/2(a)}$ and ${}^2F_{5/2(b)}$ levels. Conversely the re-absorption of the ${}^2F_{5/2(a)}$ fluorescence transition increases with temperature causing the ${}^2F_{5/2(a)}$ fluorescence to appear to decrease faster with increasing temperature than predicted.

The sensitivity values for each of the wavelength ranges tested, calculated from the Boltzmann distribution fits, are given in table 4.18 together with theoretical values calculated using equation 3.6. Also shown in table 4.18 are the errors in the Boltzmann distribution fits to the fluorescence intensity ratio versus temperature data, calculated as the standard deviation between the measurement temperature and the temperature predicted by the fluorescence intensity ratio fit. The best sensitivity data were obtained when the 900-910 nm/1051.5-1076.5 nm wavelength ranges were used to obtain the fluorescence intensity ratio. This may be due to less overlap of the ${}^2F_{5/2(b)}$ fluorescence with the ${}^2F_{5/2(a)}$ fluorescence at 976 nm.

	Ratio	Sensitivity (%/°C)			Fit error (°C)
		@ 20 °C	@ 100 °C	@ 500 °C	
Experimental	a (YbL)	0.94	0.85	0.25	3.06
	(YbH)	1.06	0.80		1.50
	b (YbL)	0.65	0.66	0.22	3.60
	(YbH)	0.93	0.64		1.40
	c (YbL)	0.63	0.69	0.24	3.62
	(YbH)	0.93	0.67		1.54
	d (YbL)	0.60	0.62	0.21	3.79
	Theory (680 cm ⁻¹)		1.14	0.70	0.16

Table 4.18: Sensitivity values for Yb³⁺-doped fibre.

4.5 CONCLUSION

The fluorescence intensity ratio versus temperature characteristics of closely spaced excited state energy levels of six different rare earth ions doped in a variety of host materials have been presented. For each of the fluorescence transitions studied in these rare earth doped samples the fluorescence intensity ratio was found to increase as the temperature of the sample was raised, generally following the trend predicted by Boltzmann theory. One important example which differed from the predicted trend was the fluorescence transitions of the ⁵D₀ and ⁵D₁ levels of Eu³⁺-doped silica fibre. For these levels, separated by approximately 1760 cm⁻¹, the upper ⁵D₁ level fluorescence intensity was found to decrease with increasing temperature for temperatures below approximately 80 °C before increasing with temperature. It is believed that, because of the large gap between these levels, other radiative and non-radiative rates dominate the thermalising rate at low temperatures. As a result the thermal coupling of the two levels does not appear to follow the Boltzmann distribution

Using the fits to the fluorescence intensity ratio data the sensitivity of the fluorescence intensity ratio to changes in temperature was calculated for each of the transitions investigated. Aside from the Eu³⁺ data, the results showed that the sensitivity increased with the energy gap between the thermalising levels as expected from theory. It was also found that overlap of the fluorescence peaks can result in reduced sensitivity. To aid comparison the sensitivity values of all the transitions studied are provided in table 4.19.

Rare earth	Host	Transition (excitation)	Sensitivity (%/°C)	
			@20 °C	@100 °C
Pr ³⁺	ZBLANP	³ P ₀ , ³ P ₁ → ¹ G ₄ (465.8 nm)	0.94	0.65
		³ P ₀ , ³ P ₁ → ³ H ₅ (465.8 nm)	0.94	0.40
		³ P ₀ , ³ P ₁ → ¹ G ₄ (476.5 nm)	1.15	0.71
		³ P ₀ , ³ P ₁ → ³ H ₅ (476.5 nm)	0.96	0.44
	silica fibre	³ P ₀ , ³ P ₁ → ¹ G ₄	0.40	0.28
	aluminosilica fibre	³ P ₀ , ³ P ₁ → ¹ G ₄	0.14	0.15
Nd ³⁺	YAG	⁴ F _{3/2} , ⁴ F _{5/2} → ⁴ I _{9/2}	1.41	0.87
		⁴ F _{3/2} , ⁴ F _{5/2} → ⁴ I _{11/2}	0.46	0.61
		⁴ F _{3/2} , ⁴ F _{5/2} → ⁴ I _{13/2}	1.02	0.83
	YVO ₄	⁴ F _{3/2} , ⁴ F _{5/2} → ⁴ I _{9/2}	1.55	0.99
		⁴ F _{3/2} , ⁴ F _{5/2} → ⁴ I _{11/2}	0.74	0.77
		⁴ F _{3/2} , ⁴ F _{5/2} → ⁴ I _{13/2}	1.09	0.84
	ZBLANP	⁴ F _{3/2} , ⁴ F _{5/2} → ⁴ I _{9/2}	1.14	0.72
		⁴ F _{3/2} , ⁴ F _{5/2} → ⁴ I _{11/2}	1.11	0.88
		⁴ F _{3/2} , ⁴ F _{5/2} → ⁴ I _{13/2}	1.38	0.96
	silica fibre	⁴ F _{3/2} , ⁴ F _{5/2} → ⁴ I _{9/2}	1.64	1.01
	⁴ F _{3/2} , ⁴ F _{5/2} → ⁴ I _{11/2}	0.50	0.59	
Sm ³⁺	silica fibre	⁴ G _{5/2} , ⁴ F _{3/2} → ⁶ H _{5/2}	1.85	1.14
Eu ³⁺	silica fibre	⁵ D ₀ , ⁵ D ₁ → ⁷ F ₁	0.14	0.45
		⁵ D ₀ , ⁵ D ₁ → ⁷ F ₂	0.17	0.51
		⁵ D ₀ , ⁵ D ₁ → ⁷ F _{0, 1, 2, 3}	0.188	0.52
Dy ³⁺	silica fibre	⁴ F _{9/2} , ⁴ I _{15/2} → (456 nm)	1.22	0.95
		⁴ F _{9/2} , ⁴ I _{15/2} → (477 nm)	0.99	0.90
Yb ³⁺	silica fibre (YbL)	² F _{5/2a} , ² F _{5/2b} → ² F _{7/2}	0.94	0.85
	silica fibre (YbH)	² F _{5/2a} , ² F _{5/2b} → ² F _{7/2}	1.06	0.80

Table 4.19: Sensitivity of fluorescence intensity ratio for the rare earth doped materials tested at various temperatures [112].

The next step in the development of fluorescence intensity ratio based temperature sensors was to determine which rare earth ions should be selected for further sensor development. Some of the factors that determine the suitability of a rare earth ion for use in a practical sensor are:

- the ability to excite the fluorescence using cheap, commonly available light sources,
- the ability to detect the fluorescence within suitable signal to noise requirements,
- the sensitivity to temperature variation,
- the temperature range measurable.

The most promising candidates at present are the Nd³⁺ and Yb³⁺ rare earth ions, each of which can be excited using commonly available laser diodes. The development of new laser sources such as blue laser diodes should however improve the suitability of many of the other rare earth ions to fluorescence intensity ratio based temperature sensing.

Chapter 5: Fluorescence Intensity Ratio Stability

- 5.1 INTRODUCTION
- 5.2 EXCITATION SOURCES FOR FLUORESCENCE INTENSITY RATIO TEMPERATURE SENSORS
- 5.3 Pr^{3+} :ZBLANP
 - 5.3.1 *Pump wavelength*
 - 5.3.2 *Pump power*
- 5.4 Nd^{3+} -DOPED SILICA FIBRE
 - 5.4.1 *Pump wavelength*
 - 5.4.2 *Pump power*
- 5.5 Yb^{3+} -DOPED SILICA FIBRE
 - 5.5.1 *Pump wavelength*
 - 5.5.2 *Pump power*
 - 5.5.3 *Doped fibre length*
 - 5.5.4 *Strain*
- 5.6 CONCLUSION

Overview of Chapter

In this chapter the results of tests to determine the stability of the fluorescence intensity ratio with changes in the power and wavelength of excitation, the length of doped fibre and applied strain are presented.

5.1 INTRODUCTION

Prior to the development of a temperature sensor based on the fluorescence intensity ratio it is important to have knowledge of the stability of the fluorescence intensity ratio under normal operating conditions. This knowledge and an understanding of the causes of non-temperature induced fluctuations are vital for improvement in the accuracy of fluorescence intensity ratio based temperature sensors. The measurements presented in this chapter indicate the accuracy of the fluorescence intensity ratio technique of temperature measurement with changes in excitation power, excitation wavelength, doped fibre length and applied strain.

In the initial stages of the development of the fluorescence intensity ratio method of temperature sensing it was speculated that the technique would be largely independent of changes in excitation parameters, giving the technique a significant advantage over several other methods of temperature sensing. Work by Maurice and co-workers [46-48], however, found that there was a slight dependence of the fluorescence intensity ratio from erbium-doped silica fibre on factors such as pump power, pump wavelength and doped fibre length, which if present in a practical device could lead to induced temperature errors. A summary of the pump wavelength and pump power dependence of the fluorescence intensity ratio for Er^{3+} -doped silica fibre is given in table 5.1.

Fluorescence Transitions	λ_p (nm)	ΔT for a 1 nm change in λ_p ($^{\circ}\text{C}/\text{nm}$)	P_p (mW)	ΔT for a 1% change in P_p ($^{\circ}\text{C}$)	Ref.
$^4\text{S}_{3/2}, ^2\text{H}_{11/2} \rightarrow ^4\text{I}_{15/2}$	785-830	< 1.3	15-250	0.07	[46]
$^4\text{S}_{3/2}, ^2\text{H}_{11/2} \rightarrow ^4\text{I}_{11/2}$	790-820	< 0.14	15-250	0.06	[47]

Table 5.1: Stability of the fluorescence intensity ratio with changes in pump wavelength (λ_p) and pump power (P_p) for Er^{3+} -doped fibre. ΔT is the induced temperature error.

In this chapter an analysis of the stability of the fluorescence intensity ratio with changes in the pump power, pump wavelength, doped fibre length and applied strain are presented. These measurements have been undertaken using $\text{Pr}^{3+}:\text{ZBLANP}$, Nd^{3+} -doped silica fibre and Yb^{3+} -doped silica fibre. Also presented in this chapter is information on the effect of pump power, pump wavelength and doped fibre length on the intensity of fluorescence from the doped fibre samples. The later information is useful in determining the appropriate excitation source and detection systems to be used with a particular rare earth doped material.

5.2 EXCITATION SOURCES FOR FLUORESCENCE INTENSITY RATIO

TEMPERATURE SENSORS

The requirements for an excitation source which is to be used with the fluorescence intensity ratio technique are that it should,

- (a) have emission wavelengths which excite the thermally coupled levels,
- (b) be compatible with efficient coupling into optical fibre,
- (c) have output powers on the order of 10's of milliwatts, and,
- (d) be relatively low in cost and small in size.

The light source which best meets these requirements is the laser diode.

The stability of the output power of laser diodes depends upon a number of factors including the drive current, temperature and unwanted optical feedback [113, 114]. A number of techniques have been developed to control the output power of laser diodes, which usually rely on some form of feedback. From personal experience basic, low cost, driver circuits generally allow the output power to be controlled to approximately 1%. If greater stability of the output power is required greater control of both the drive current and temperature of the laser diode are needed, which usually involves increased cost. In the case of drive current, several manufacturers market laser diode drivers with current control in the order of 10 ppm full scale [e.g. ref. 115]. To control the temperature of a laser diode, which also affects the emission wavelength of the diode, with typical variations of approximately 0.3 nm/°C [114], again a number of devices are commercially available. If precise control of emission wavelength is required temperature controllers are available with long term (24 hr) stabilities in the range of 0.001 °C [116], which corresponds to a wavelength change of approximately 0.0003 nm.

5.3 Pr³⁺:ZBLANP

The stability of the fluorescence intensity ratio of Pr³⁺:ZBLANP was measured as a function of pump wavelength and pump power for fluorescence transitions originating from the ³P₀ and ³P₁+¹L₆ energy levels terminating at both the ¹G₄ and ³H₅ levels. The Pr³⁺:ZBLANP sample used in these tests was a rod (8 mm diameter, 40 mm length) with a dopant concentration of approximately 2000 ppm, which was also used in the temperature dependent studies discussed in section 4.4.1. A bulk sample

experimental arrangement (see section 4.3.1) was used in each of these experiments and all measurements were made with the Pr^{3+} -doped sample at ambient temperature.

5.3.1 Pump Wavelength

The fluorescence spectra of Pr^{3+} :ZBLANP were measured for the 457.9 nm, 465.8 nm, 472.7 nm and 476.5 nm pump wavelengths using the single line output of an argon ion laser for excitation (linewidth ~ 4 GHz). The pump power was set to 200 mW at each excitation wavelength. Figure 5.1 shows the pump wavelengths tested relative to the absorption spectrum for the Pr^{3+} :ZBLANP sample.

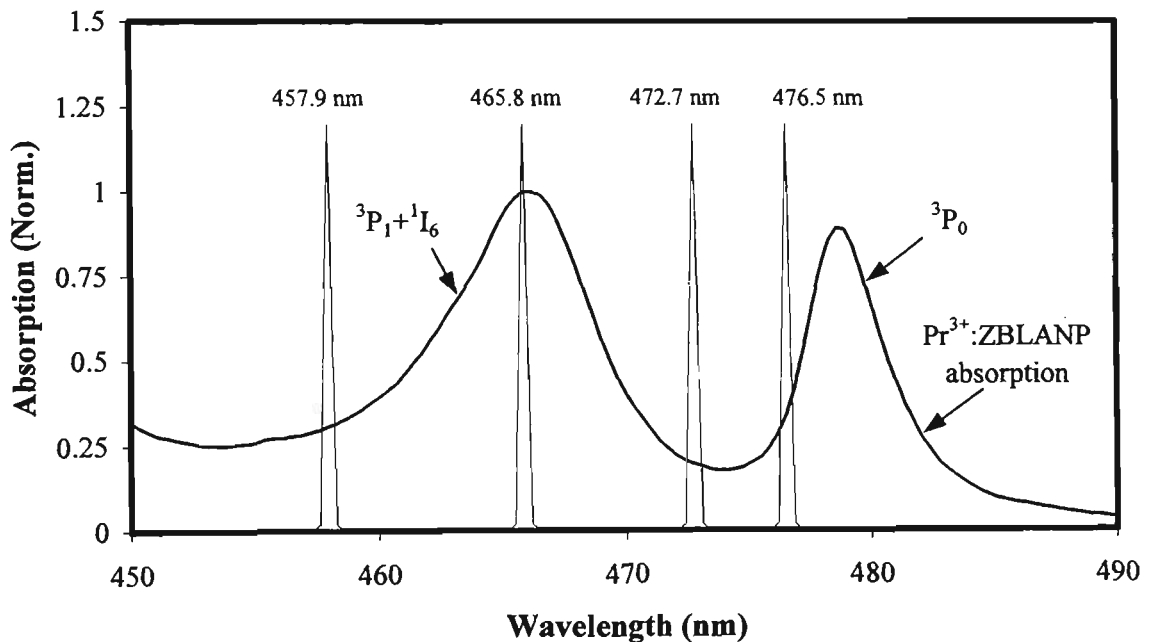


Figure 5.1: Absorption spectrum of Pr^{3+} :ZBLANP sample and pump wavelengths used in fluorescence intensity ratio stability tests (2 nm OSA resolution). The width of the pump spectra are not to scale.

The largest changes in the fluorescence spectra of the Pr^{3+} :ZBLANP sample were obtained for the 465.8 nm and 476.5 nm excitation wavelengths, which are shown in figure 5.2 for transitions terminating at both the $^1\text{G}_4$ and $^3\text{H}_5$ levels. The spectra shown have been normalised to the peak fluorescence intensity over the wavelength ranges displayed to aid in comparison and reveal that the width of the fluorescence peaks vary for the pump wavelengths tested. The fluorescence spectra for the 457.9 nm and 472.7 nm pump wavelengths lie in-between the spectra shown in figures 5.2a and 5.2b and have not been plotted for reasons of clarity. The change in the width of the fluorescence spectra do not appear to depend upon absorbed pump power and instead

are believed to be due to site-selective effects which have been discussed previously in chapter 2.

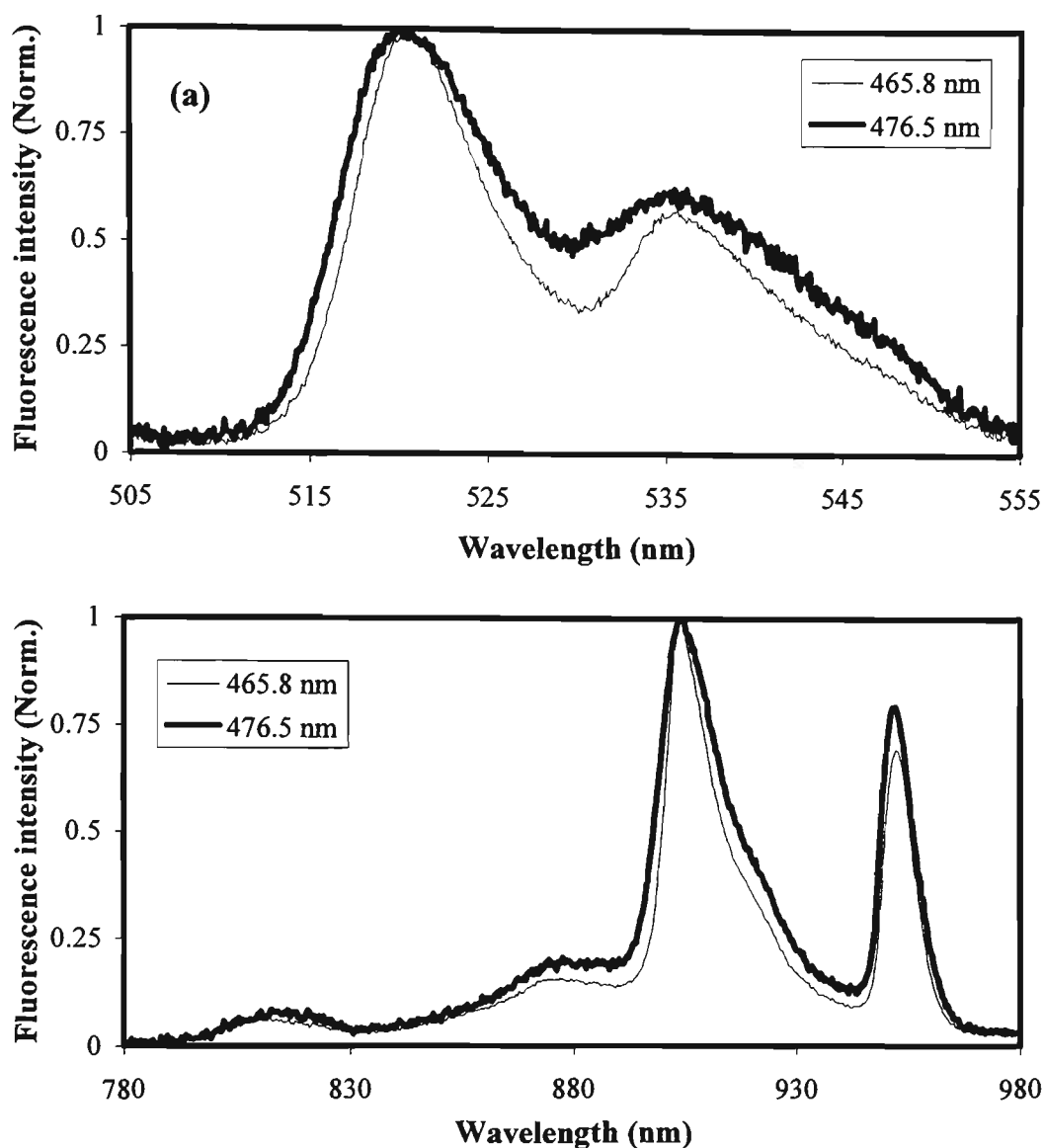


Figure 5.2: Pr^{3+} :ZBLANP fluorescence spectra at pump wavelengths of 465.8 nm and 476.5 nm (2 nm OSA resolution), (a) ${}^3P_0, {}^3P_1 + {}^1I_6 \rightarrow {}^3H_5$ transition, and, (b) ${}^3P_0, {}^3P_1 + {}^1I_6 \rightarrow {}^1G_4$ transition.

The fluorescence intensity ratio of the Pr^{3+} :ZBLANP transitions investigated were calculated as a function of pump wavelength using the technique discussed earlier for temperature dependent changes (chapter 4), the results of which are shown in figure 5.3. The wavelength ranges used for the 3H_5 transitions were 515-525 nm and 541-551 nm, while for the 1G_4 transitions the 830-870 nm and 900-910 nm wavelength ranges were used. These are the same wavelength ranges as were used to calculate fluorescence intensity ratio values in temperature dependent tests. The fluorescence intensity ratio values shown in figure 5.3 have been normalised, by dividing each value

by the average fluorescence intensity ratio, to assist comparison with the results obtained for other rare earth ions.

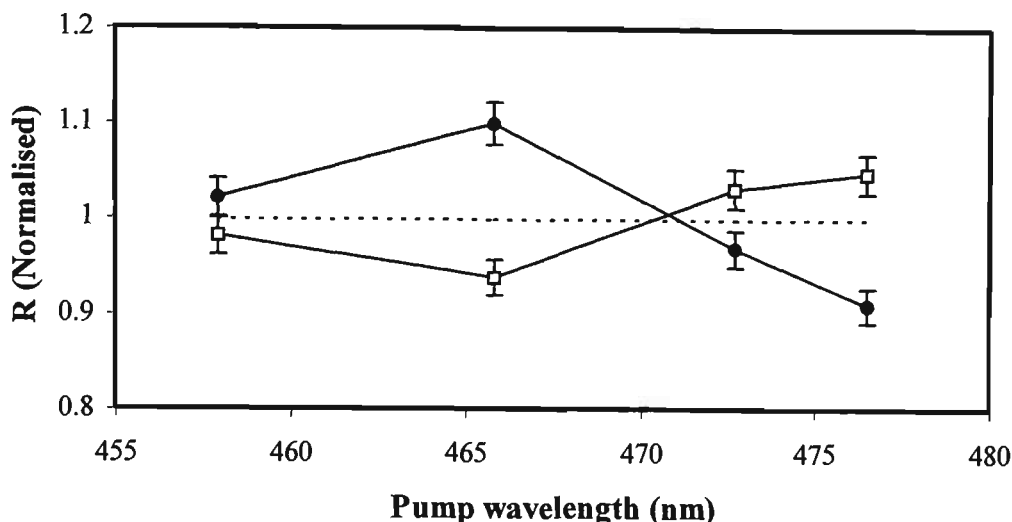


Figure 5.3: Fluorescence intensity ratio versus pump wavelength for Pr^{3+} :ZBLANP, 3H_5 transitions (●), 1G_4 transitions (□). Solid lines used as a guide to the eye.

Unfortunately only a limited number of pump wavelengths were available from the argon ion laser over the desired wavelength range. While this makes it difficult to obtain an accurate analysis of the effect of changes in the pump wavelength on the fluorescence intensity ratio for Pr^{3+} :ZBLANP, the results should at least give a feel for the variation in the fluorescence intensity ratio for different pump wavelengths.

An estimate of the induced temperature error due to changes in the pump wavelength was obtained by calculating the change in the fluorescence intensity ratio between subsequent pump wavelengths. The apparent temperature change that would be induced due to such shifts in pump wavelength were then calculated using look-up tables of temperature versus fluorescence intensity ratio (determined from tests discussed in section 4.4.1). The results, given in table 5.2, suggest that the induced temperature error for a 1 nm shift in pump wavelength should be in the order of 1 °C.

Pump wavelengths	$\Delta\lambda$ (nm)	Induced temperature error (°C)	
		${}^3P_0, {}^3P_1+{}^1I_6 \rightarrow {}^3H_5$	${}^3P_0, {}^3P_1+{}^1I_6 \rightarrow {}^1G_4$
457.9 → 465.8 nm	7.9	8 ± 5	5 ± 4
465.8 → 472.7 nm	6.9	12 ± 4	10 ± 5
472.7 → 476.5 nm	3.8	7 ± 4	2 ± 4

Table 5.2: Approximate temperature errors induced by changes in pump wavelength for Pr^{3+} :ZBLANP. $\Delta\lambda$ – wavelength difference between adjacent pump wavelengths.

5.3.2 Pump Power

The effect of changes in the pump power on the fluorescence spectra of $\text{Pr}^{3+}:\text{ZBLANP}$ were measured for launched pump powers between 220 mW and 850 mW using the 476.5 nm line of an argon ion laser. Figure 5.4 shows the fluorescence spectra, normalised to the peak fluorescence power, recorded for a pump power of 850 mW. Unlike the pump wavelength spectra no obvious change in the $\text{Pr}^{3+}:\text{ZBLANP}$ fluorescence spectra was observed over the range of pump powers tested.

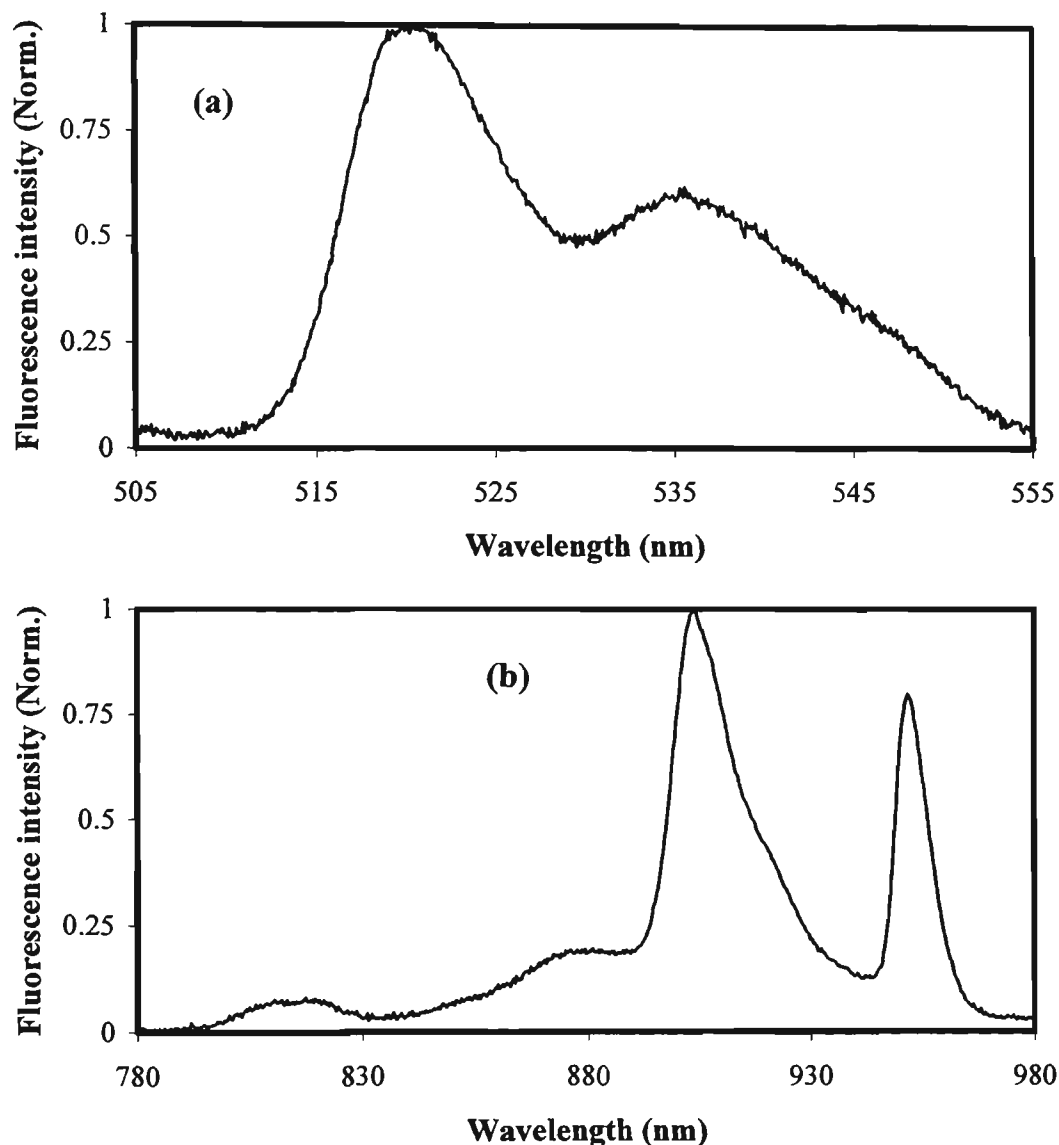


Figure 5.4 $\text{Pr}^{3+}:\text{ZBLANP}$ fluorescence spectra for 850 mW pump power using 476.5 nm pump wavelength (2 nm OSA resolution), (a) ${}^3P_0, {}^3P_1+{}^1I_6 \rightarrow {}^3H_5$ transition (b) ${}^3P_0, {}^3P_1+{}^1I_6 \rightarrow {}^1G_4$ transition.

The fluorescence intensity ratio versus pump power, calculated from the fluorescence spectra using the wavelength ranges mentioned in the pump wavelength section, are illustrated in figure 5.5 for both the ${}^3P_0, {}^3P_1+{}^1I_6 \rightarrow {}^3H_5$ and ${}^3P_0, {}^3P_1+{}^1I_6 \rightarrow {}^1G_4$ transitions.

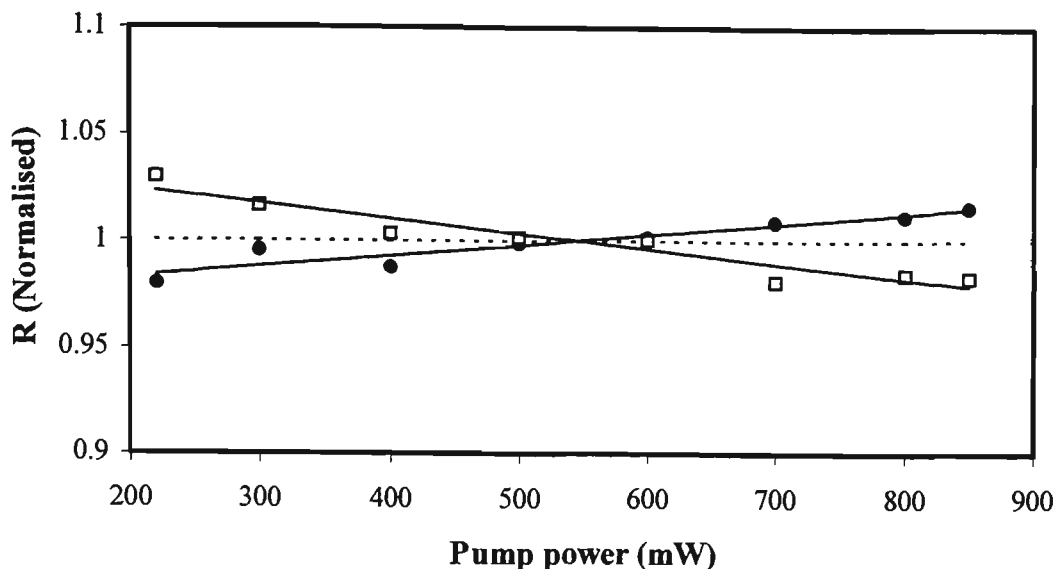


Figure 5.5: Fluorescence intensity ratio versus pump power for Pr^{3+} :ZBLANP using the 476.5 nm pump wavelength, 3H_5 transitions (●), 1G_4 transitions (□). The solid lines are straight line fits to the data.

The induced temperature errors for changes in the pump power were calculated by fitting a straight line to the fluorescence intensity ratio data. The gradient of the fit was then divided by the sensitivity of the fluorescence intensity ratio for Pr^{3+} :ZBLANP at room temperature (determined from tests discussed in section 4.4.1) to ascertain the induced temperature errors for each of the transitions. For the 3H_5 transition this value was found to be approximately $5.2 \times 10^{-5} \text{ }^\circ\text{C/mW}$, while for the 1G_4 transition a value of $-6.1 \times 10^{-5} \text{ }^\circ\text{C/mW}$ was calculated. Therefore induced temperature errors due to a one percent pump power variation should be less than $0.1 \text{ }^\circ\text{C}$ for both the $^3P_0, ^3P_1 + ^1I_6 \rightarrow ^3H_5$ transitions and $^3P_0, ^3P_1 + ^1I_6 \rightarrow ^1G_4$ transitions of Pr^{3+} :ZBLANP over the pump power range tested.

It should be noted that although the pump powers used in this test would be impractical for a sensor prototype it is actually the energy density of the pump radiation, i.e. pump intensity, rather than the power which is the cause for many of the potential changes in the fluorescence spectra. The beam diameter of the argon ion laser used in these tests was approximately 1 mm. In a practical sensor however the sensor material would either be doped in or excited by an optical fibre with core diameters in the order of 10's to 100's of micrometres. For these smaller pump diameters the pump powers tested are equivalent to pump powers of less than 0.1 mW, which are indeed more practical.

5.4 Nd³⁺-DOPED SILICA FIBRE

The stability of the fluorescence intensity ratio from Nd³⁺-doped fibre was measured for changes in pump wavelength and pump power using the ${}^4F_{3/2}, {}^4F_{5/2} \rightarrow {}^4I_{9/2}$ transitions. A 25 cm length of Nd³⁺-doped fibre (core size 5 μm , doping concentration ~ 500 ppm) was tested in a 3 dB-coupler experimental arrangement (see section 4.3.2). Excitation was provided by a Ti:sapphire laser (linewidth ~ 40 GHz) and in all measurements the doped fibre sample was at ambient temperature.

5.4.1 Pump Wavelength

Fluorescence spectra of the Nd³⁺-doped fibre were measured at intervals of 2 nm for pump wavelengths between 780 nm and 810 nm. The pump power (coupled in-fibre) for these wavelengths varied from a minimum of approximately 35 mW at 780 nm to approximately 50 mW at 810 nm due to changes in the Ti:sapphire output power with wavelength. Data presented have not been corrected for these variations. Examples of the fluorescence spectra, normalised to the peak intensity to aid in comparison, are given in figure 5.6. The main change in the spectra is the intensity of the long wavelength peak of the ${}^4F_{3/2} \rightarrow {}^4I_{9/2}$ transition at approximately 940 nm, which initially decreases as the pump wavelength gets longer before increasing at longer pump wavelengths, i.e. near 810 nm. Similar changes in the fluorescence spectrum of Nd³⁺-doped silica fibre with pump wavelength have been observed by others [117-119] and are usually attributed to site-selective effects, as discussed in chapter 2.

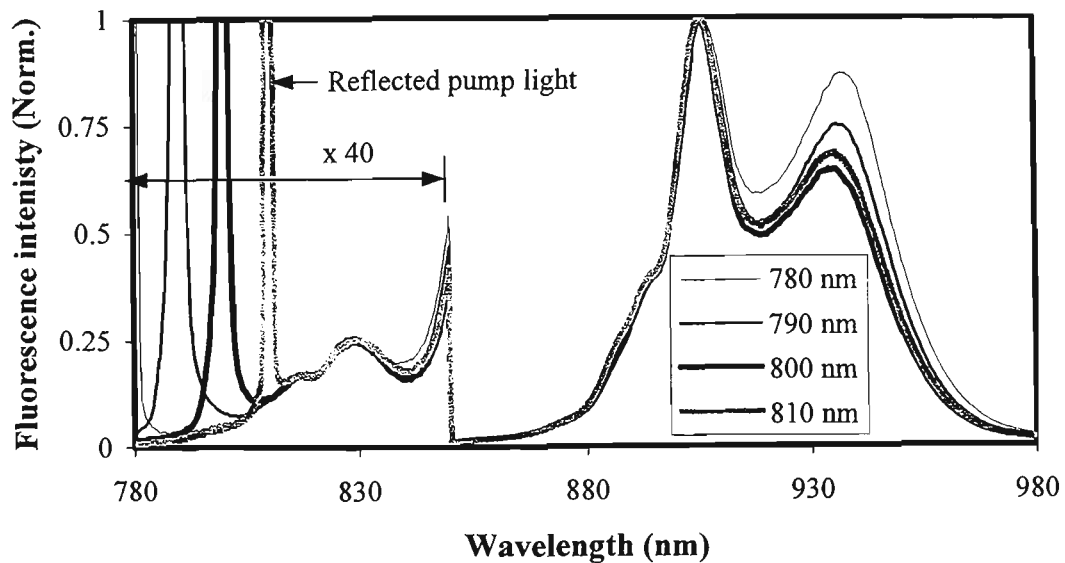


Figure 5.6: Nd³⁺-doped silica fibre fluorescence spectra for various pump wavelengths (2 nm OSA resolution).

The fluorescence intensity ratio was calculated as a function of pump wavelength using the 820 nm to 840 nm wavelength range for the ${}^4F_{3/2} \rightarrow {}^4I_{9/2}$ transition and 880 nm to 930 nm for the ${}^4F_{5/2} \rightarrow {}^4I_{9/2}$ transition (figure 5.7). These wavelength ranges were the same as those used previously in temperature dependent tests and were chosen to correspond to commercially available optical band pass filters. In addition the choice of wavelength range for the ${}^4F_{5/2} \rightarrow {}^4I_{9/2}$ transition should reduce the effect of changes in the fluorescence intensity near 940 nm on the fluorescence intensity ratio.

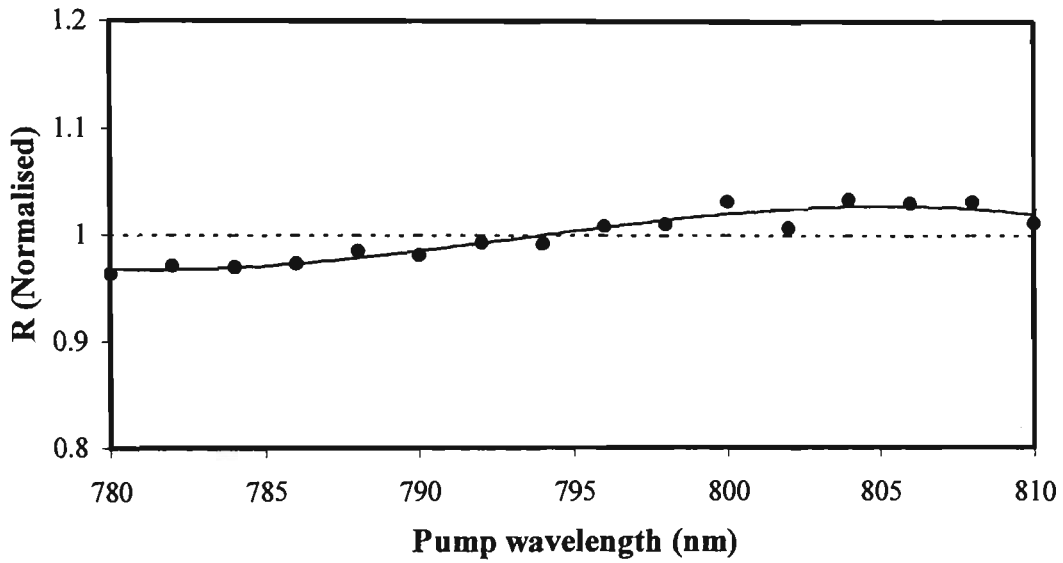


Figure 5.7: Fluorescence intensity ratio versus pump wavelength for Nd^{3+} -doped silica fibre. The solid line is a 3rd order polynomial fit to the data.

Figure 5.7 indicates that the fluorescence intensity ratio is less influenced by changes in pump wavelength for a pump wavelength of approximately 805 nm. The induced temperature error due to shifts in the pump wavelength from the most stable value (table 5.3) indicate that the error can be kept to less than 0.1 °C provided the pump wavelength is within 2 nm of the most stable pump wavelength (e.g. 805.2 nm).

Induced temperature error (°C)			Most stable pump wavelength (nm)
1 nm shift	2 nm shift	5 nm shift	
0.02	0.08	0.48	805.2

Table 5.3: Induced temperature error due to 1 nm, 2 nm and 5 nm shifts from the most stable pump wavelength for Nd^{3+} -doped fibre.

5.4.2 Pump Power

The fluorescence spectra of the Nd^{3+} -doped fibre sample was measured for pump powers between 1.19 mW and 13.96 mW (coupled in-fibre) using a pump

wavelength of 802 nm. Pump powers were varied by placing neutral density filters between the Ti:sapphire laser output and the microscope objective used to couple pump light into the 3 dB-coupler. Examples of the Nd^{3+} -doped fibre fluorescence spectra at various pump powers are given in figure 5.8. Compared to the pump wavelength data shown previously (figure 5.6) there is less change in the long wavelength ${}^4\text{F}_{3/2} \rightarrow {}^4\text{I}_{9/2}$ peak at approximately 930 nm for the pump powers tested. The intensity of the ${}^4\text{F}_{5/2}$ fluorescence, however, appears to decrease as the pump power is raised compared to the ${}^4\text{F}_{3/2}$ peak at 905 nm. This may possibly be due to wavelength selective amplification of spontaneous emission favouring the 905 nm peak as the pump power is raised. Similar wavelength dependent changes in the fluorescence spectrum with pump power have been observed for Er^{3+} -doped fibre [120] and are discussed in detail in reference 118.

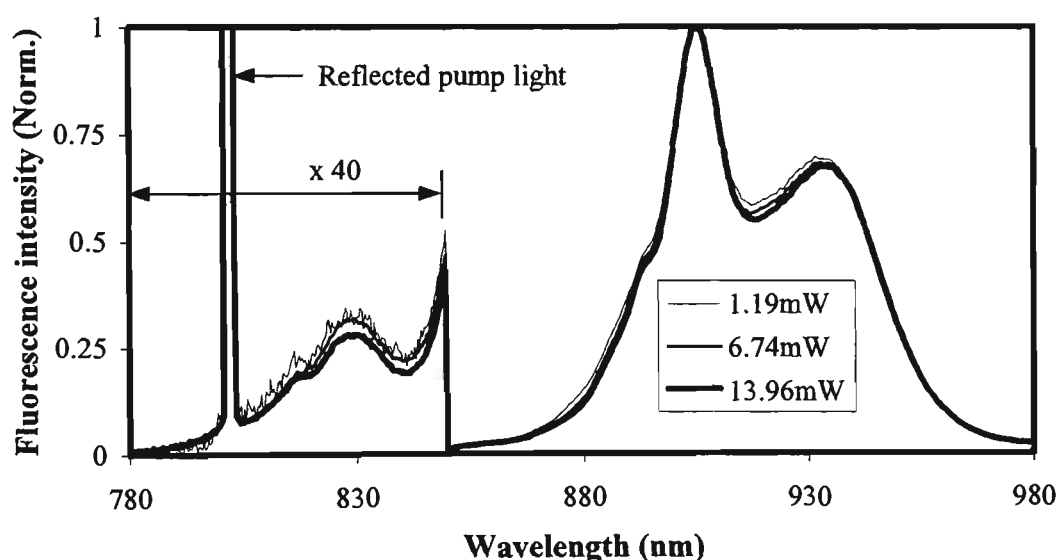


Figure 5.8: Fluorescence spectra of Nd^{3+} -doped fibre for pump powers between 1.19 mW and 13.96 mW (2 nm OSA resolution).

Using the fluorescence spectra obtained the fluorescence intensity ratio was calculated as a function of pump power for the same wavelength ranges as used in the pump wavelength calculations. The fluorescence intensity ratio versus pump power graph, shown in figure 5.9, is reasonably stable at lower pump powers, however at higher pump powers the fluorescence intensity ratio decreases as the pump power is raised.

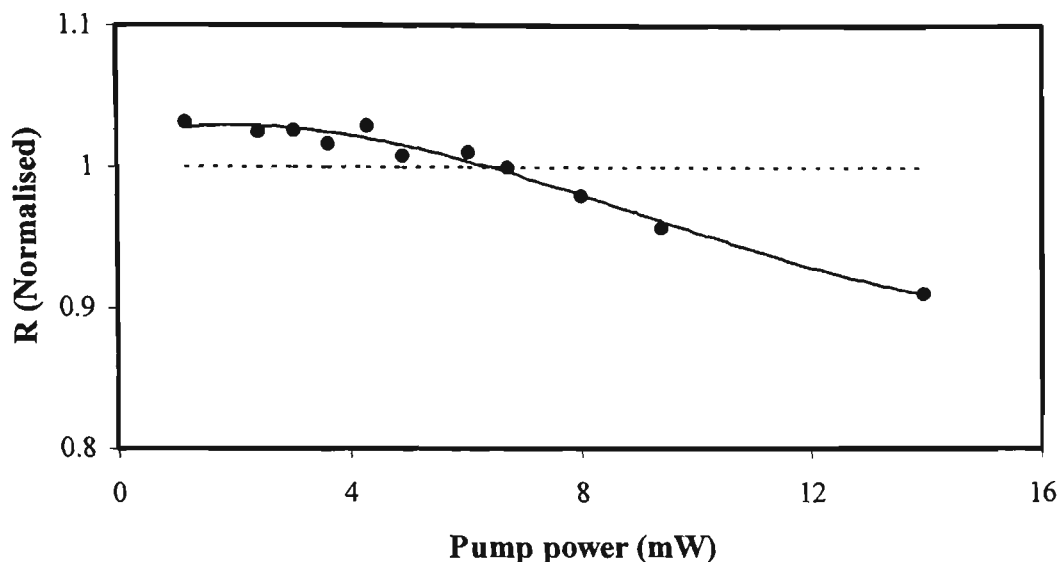


Figure 5.9: Fluorescence intensity ratio versus pump power for Nd^{3+} -doped fibre. The solid line is a 3rd order polynomial fit to the data.

The induced temperature errors calculated for a range of pump powers, given in table 5.4, suggest that induced temperature errors due to a one percent change in pump power should be less than 0.1 °C for the pump power range investigated.

Pump power (mW)	Induced error (°C)
4	0.016
8	0.066
12	0.090
14	0.069

Table 5.4: Induced temperature errors for a one percent change in pump power for Nd^{3+} -doped fibre.

In figure 5.10 the individual intensity of the ${}^4\text{F}_{3/2} \rightarrow {}^4\text{I}_{9/2}$ and ${}^4\text{F}_{5/2} \rightarrow {}^4\text{I}_{9/2}$ fluorescence transitions, measured over the wavelength ranges of 820-840 nm and 880-930 nm, are plotted as a function of pump power. These values were measured by the OSA at the second input arm of the 3dB-coupler.

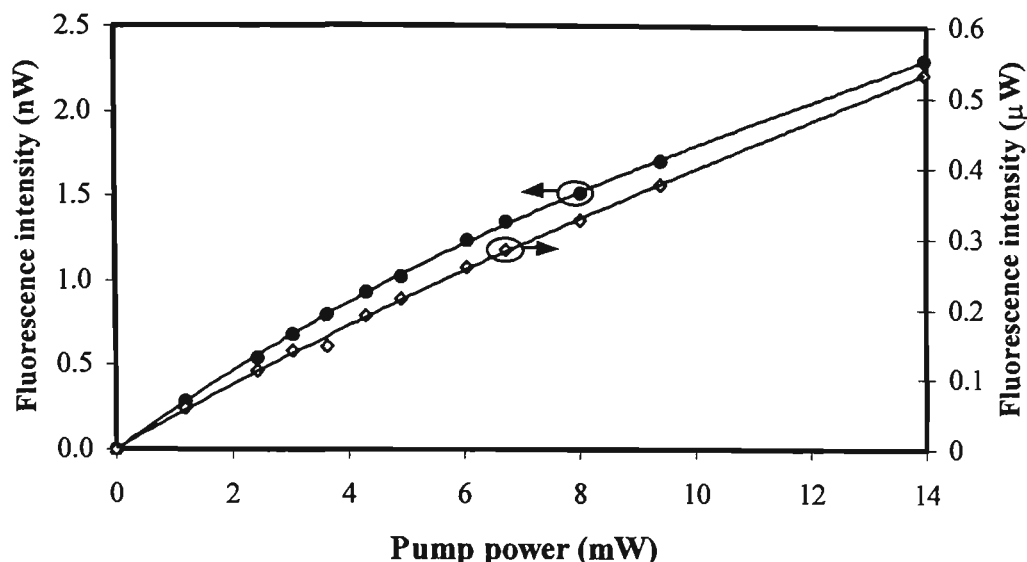


Figure 5.10: Intensity of the ${}^4F_{3/2} \rightarrow {}^4I_{9/2}$ (\diamond) and ${}^4F_{5/2} \rightarrow {}^4I_{9/2}$ (\bullet) fluorescence transitions for a 25 cm length of Nd^{3+} -doped silica fibre terminating at the ${}^4I_{9/2}$ level versus pump power with an 802 nm pump wavelength. Solid lines used as guide to the eye only.

The total fluorescence intensity of the ${}^4F_{3/2} \rightarrow {}^4I_{9/2}$ and ${}^4F_{5/2} \rightarrow {}^4I_{9/2}$ transitions, using the 805 nm to 980 nm wavelength range, is shown in figure 5.11 for the range of pump powers tested.

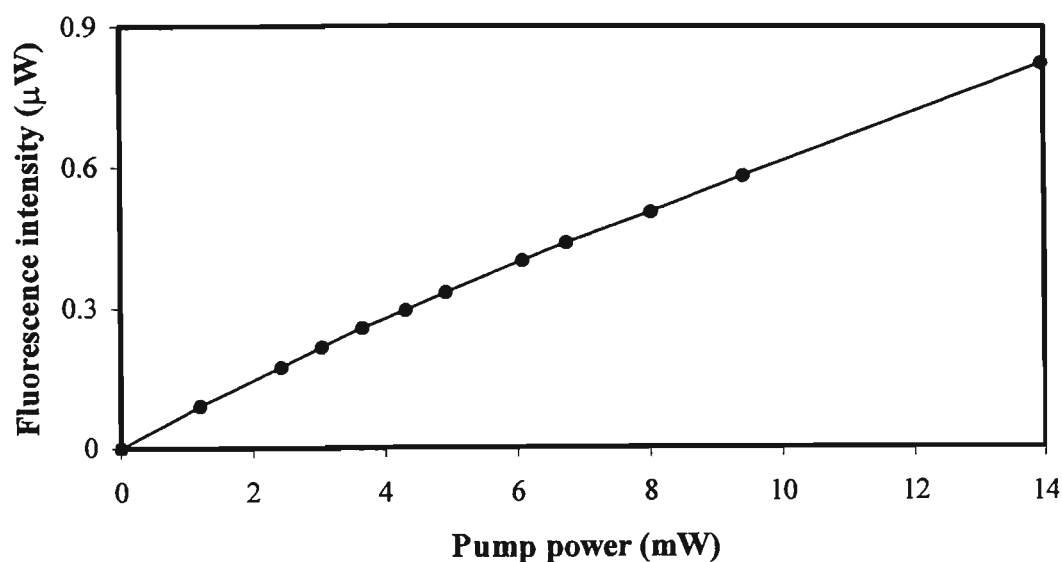


Figure 5.11: Total intensity of ${}^4F_{3/2}$ and ${}^4F_{5/2}$ fluorescence transitions for a 25 cm length of Nd^{3+} -doped silica fibre terminating at the ${}^4I_{9/2}$ level versus pump power using an 802 nm pump wavelength. Solid line used as guide to the eye only.

Figures 5.10 and 5.11 indicate that bleaching of the relevant transitions is not a problem for the range of pump powers tested and that if required further increases in the fluorescence intensity of the transitions investigated could be obtained by simply increasing the pump power.

5.5 Yb³⁺-DOPED SILICA FIBRE

The stability of the fluorescence intensity ratio of a sample of Yb³⁺-doped silica fibre was measured for changes in pump wavelength, pump power, doped fibre length and applied strain. The Yb³⁺-doped fibre sample used in these tests was excited using a Ti:sapphire laser in the 3dB-coupler experimental arrangement. The core/cladding diameters of the fibre were 5.2/116 μm and the doping concentration was approximately 2500 ppm. All measurements were made with the doped fibre at ambient temperature.

5.5.1 Pump Wavelength

Measurements of the fluorescence spectra of Yb³⁺-doped fibre were recorded for excitation wavelengths between 800 nm and 850 nm using a 2.6 m length of doped fibre. The excitation power during tests was approximately 25 mW (coupled in-fibre). Examples of the Yb³⁺-doped fibre fluorescence spectra at various pump wavelengths, normalised to aid in comparison, are given in figure 5.12. These spectra show that the width of the $^2F_{5/2(a)}$ to $^2F_{7/2}$ fluorescence peak at approximately 1045 nm decreases with increased pump power and also shifts slightly to lower wavelengths. It is believed that these effects are due to increased amplified spontaneous emission resulting from increased absorbed pump power as the pump wavelength is raised. This behaviour has been observed previously in work on superfluorescent fibre sources using Yb³⁺-doped silica fibre [121]. To illustrate how the absorbed pump power increases as the pump wavelength is raised from 800 nm to 850 nm the absorption spectrum of the Yb³⁺-doped fibre used in these tests is provided in figure 5.13.

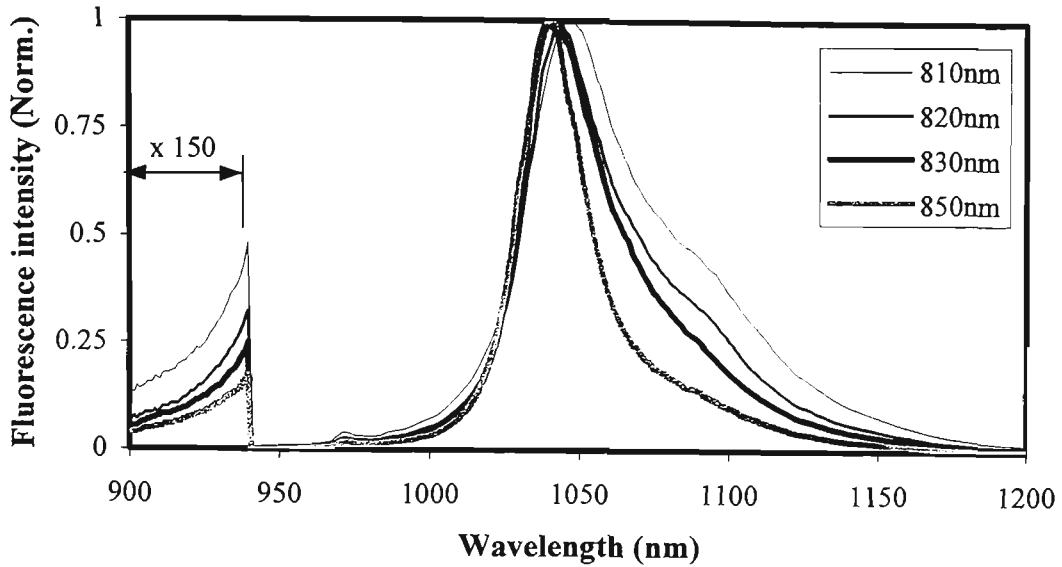


Figure 5.12: Fluorescence spectra of Yb^{3+} -doped silica fibre for various pump wavelengths (1 nm OSA resolution).

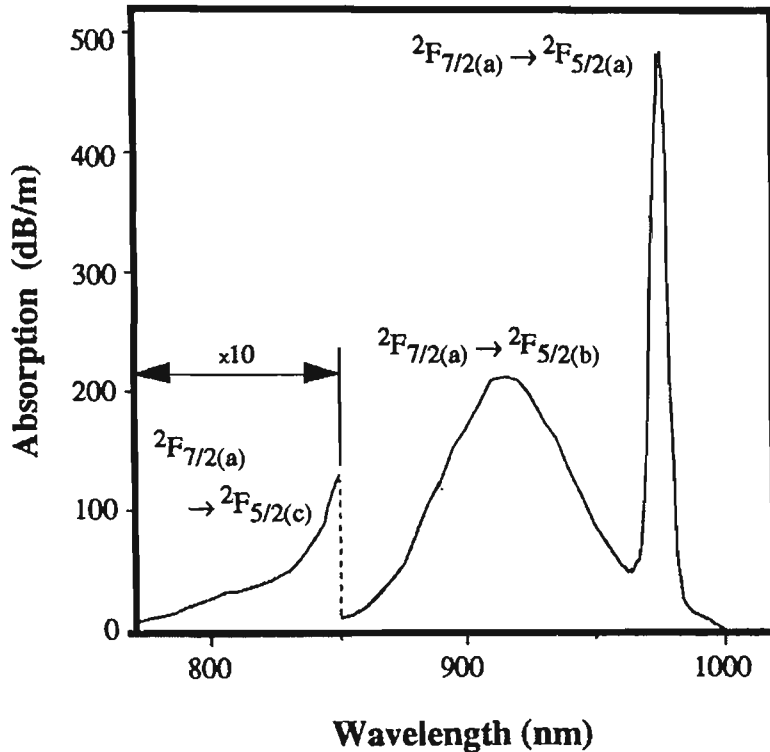


Figure 5.13: Yb^{3+} -doped fibre absorption spectrum (2500 ppm doping concentration).

The change in the fluorescence intensity ratio of Yb^{3+} -doped silica fibre with pump wavelength was calculated using a number of different fluorescence wavelength ranges for each of the ${}^2\text{F}_{5/2(a)}$ and ${}^2\text{F}_{5/2(b)}$ levels. These wavelength ranges, given in table 5.5, were chosen to correspond to commercially available optical band pass filters.

Ratio	Wavelength ranges	
	${}^2F_{5/2(a)}$	${}^2F_{5/2(b)}$
a	900-910 nm	1051.5-1076.5 nm
b	920-930 nm	1051.5-1076.5 nm
c	920-930 nm	1045-1055 nm
d	920-930 nm	1095-1105 nm

Table 5.5: Wavelength ranges used to calculate fluorescence intensity values for Yb^{3+} transitions tested in this study.

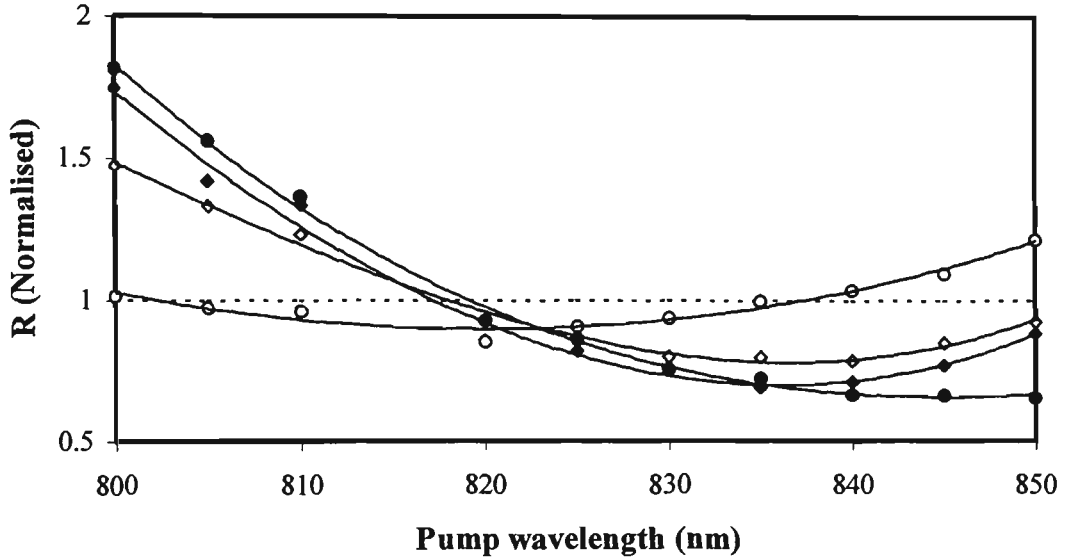


Figure 5.14: Fluorescence intensity ratio versus pump wavelength for Yb^{3+} -doped silica fibre using the wavelength ranges given in table 5.5. Ratio a (\blacklozenge), ratio b (\circ), ratio c (\bullet), ratio d (\circ) (see table 5.5). The solid lines are 3rd order polynomial fits to the data.

The fluorescence intensity ratio versus pump wavelength graphs (figure 5.14) show that the wavelength ranges used to measure the fluorescence intensity of the ${}^2F_{5/2(a)}$ and ${}^2F_{5/2(b)}$ levels strongly influences the stability of the fluorescence intensity ratio with pump wavelength variations. These graphs also indicate that the pump wavelength at which the fluorescence intensity ratio is most stable can shift with the filter wavelength ranges used. For example the fluorescence intensity ratio is most stable at 845.1 nm for the 920-930 nm/1045-1055 nm filter ranges and at 820 nm for the 920-930 nm/1095-1105 nm filter ranges.

The induced temperature errors due to shifts of 1 nm, 2nm and 5 nm from the most stable pump wavelength for the filter ranges investigated are given in table 5.6. The lowest induced temperature errors were found to occur for the 920-930 nm/1095-1105 nm ratio. This appears to be due to the reduced effect of amplified spontaneous emission for this ${}^2F_{5/2(a)}$ filter wavelength range in comparison to the other ${}^2F_{5/2(a)}$ filter ranges used. The data for the Yb^{3+} -doped fibre tested indicate that in order to obtain

errors of less than 0.2 °C the pump wavelength should be less than 1 nm from the most stable pump wavelength.

Ratio	Induced temperature error (°C)			Most stable pump wavelength (nm)
	1 nm shift	2 nm shift	5 nm shift	
a	0.15	0.60	3.70	836.1
b	0.13	0.51	3.18	836.5
c	0.08	0.34	2.09	845.1
d	0.05	0.20	1.24	820.0

Table 5.6: Induced temperature errors due to shifts in pump wavelength for Yb³⁺-doped fibre.

5.5.2 Pump Power

The stability of the fluorescence intensity ratio of a 2.6 m length of Yb³⁺-doped silica fibre was measured for pump powers between 3.2 mW and 38.5 mW (coupled in-fibre) using a pump wavelength of 845 nm. Examples of the fluorescence spectra at various pump powers, normalised to the peak intensity near 1045 nm, are given in figure 5.15. These spectra show similar changes in the width of the ²F_{5/2(a)} fluorescence peak at approximately 1045 nm as were observed in Yb³⁺ pump wavelength tests discussed previously. It is believed that increased amplified spontaneous emission of the 1045 nm fluorescence is also the cause for the change in the fluorescence spectra with increased pump power.

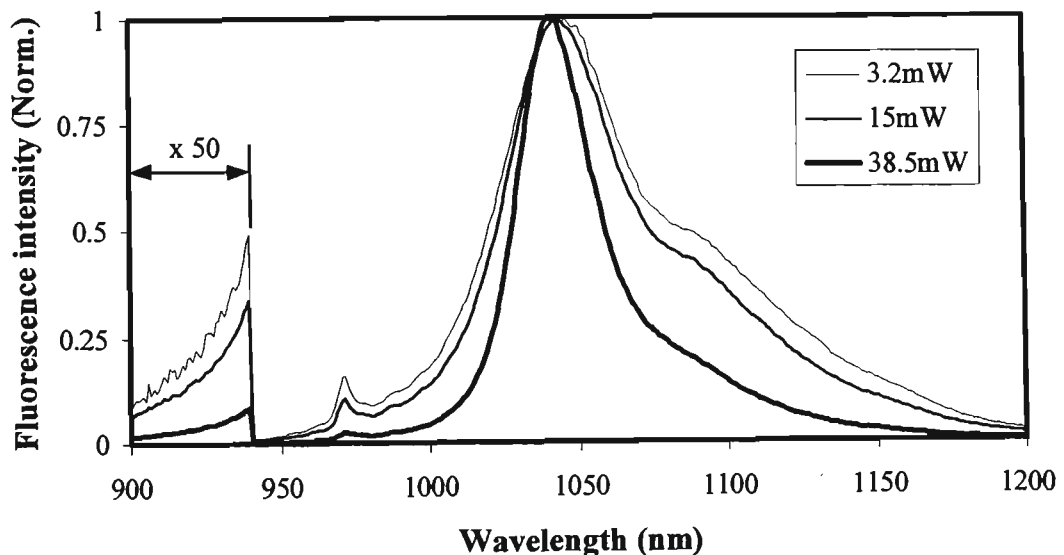


Figure 5.15: Fluorescence spectra of Yb³⁺-doped silica fibre for pump powers between 3.2 mW and 38.5 mW (1 nm OSA resolution).

Using the fluorescence spectra obtained the fluorescence intensity ratios were calculated as a function of pump power using the wavelength ranges given in table 5.5. The results, shown in figure 5.16, indicate that the fluorescence intensity ratio drops as the pump power is increased for all the wavelength ranges tested.

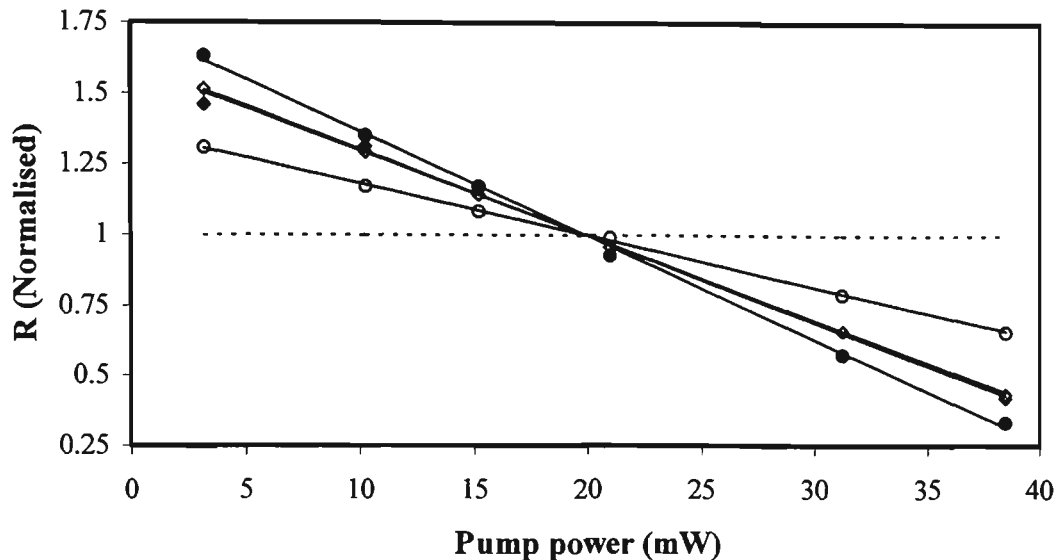


Figure 5.16: Fluorescence intensity ratio versus pump power for Yb^{3+} -doped silica fibre. Ratio a (\blacklozenge), ratio b (\diamond), ratio c (\bullet), ratio d (\circ) (see table 5.5). The solid lines are straight line fits to the data.

The stability of the fluorescence intensity ratio with changes in pump power, given in table 5.7, show that the induced temperature error increases with pump power for all the fluorescence wavelength ranges investigated. The most stable fluorescence intensity ratio was achieved when the 920-930 nm/1095-1105 nm filter wavelength ranges were used. Similarly to the Yb^{3+} pump wavelength data mentioned previously, this can be explained by the fact that the longer wavelength filter is on the wing of the ${}^2\text{F}_{5/2(a)}$ fluorescence where the effects of amplified spontaneous emission are reduced. It appears that with the fibre used in this study the pump power must be kept to less than approximately 4 mW in order to obtain temperature errors of less than 0.1 °C for 1% fluctuations in pump power.

Ratio	Induced temperature error (°C)			
	@ 4 mW	@ 14 mW	@ 24 mW	@ 35 mW
a	0.10	0.42	0.97	2.28
b	0.11	0.48	1.11	2.65
c	0.12	0.55	1.36	3.82
d	0.04	0.31	0.64	1.20

Table 5.7: Induced temperature errors for a one percent change in pump power for a number of wavelength ranges used to calculate the fluorescence intensity ratio.

The intensity of the fluorescence originating from the ${}^2F_{5/2(a)}$ and ${}^2F_{5/2(b)}$ levels is shown in figure 5.17, calculated using fluorescence over the 920-930 nm and 1051.5-1076.5 nm wavelength ranges.

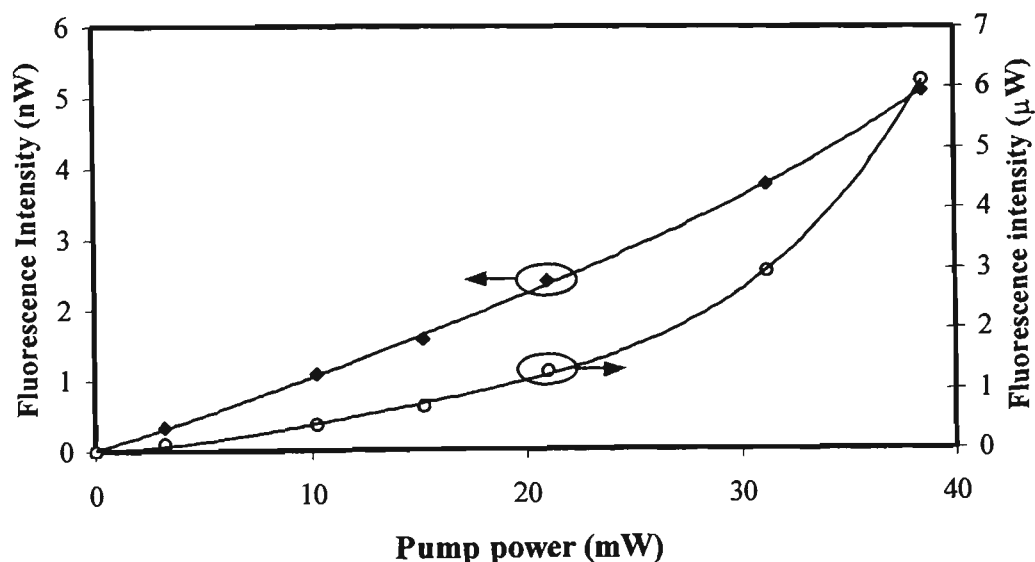


Figure 5.17: Fluorescence intensity of the ${}^2F_{5/2(a)}$ and ${}^2F_{5/2(b)}$ levels for a 2.6 m length of Yb^{3+} -doped silica fibre (2500 ppm) versus pump power for the 920-930 nm (\blacklozenge) and 1051.5-1076.5 nm (\circ) wavelength ranges. Solid lines used as guide to the eye only.

The total fluorescence intensity of the Yb^{3+} -doped fibre, measured using the 900 nm to 1200 nm wavelength ranges, as a function of pump power is shown in figure 5.17.

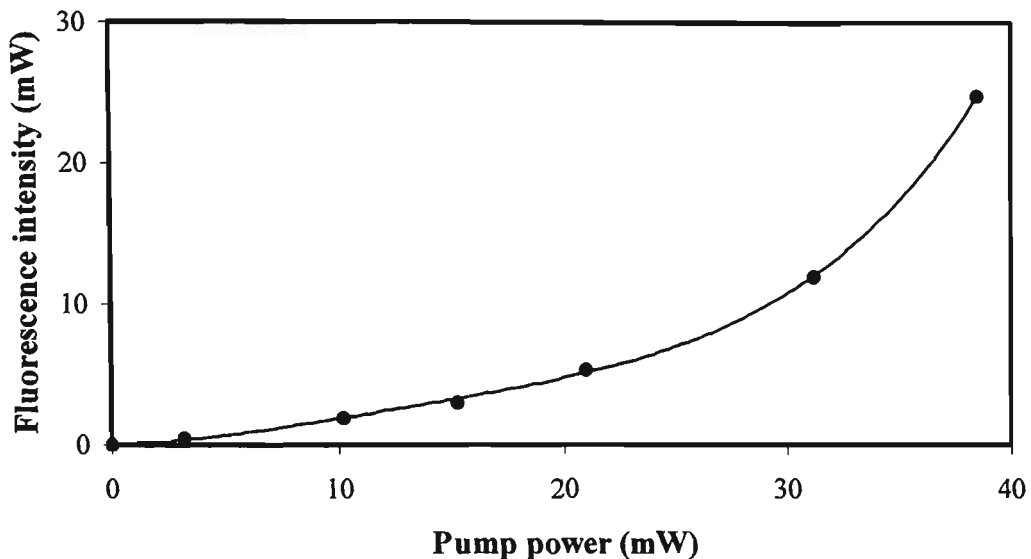


Figure 5.18: Total fluorescence intensity of the ${}^2F_{5/2(a)}$ and ${}^2F_{5/2(b)}$ levels for a 2.6 m length of Yb^{3+} -doped silica fibre (2500 ppm) versus pump power. Solid line used as guide to the eye only.

The data in figures 5.17 and 5.18 indicate that if required further increases in the fluorescence intensity from the Yb^{3+} -doped fibre tested could be achieved by increasing the pump power.

5.5.3 Doped Fibre Length

The effect of changes in the length of Yb^{3+} -doped fibre on the fluorescence intensity ratio were measured for doped fibre lengths between 0.05 m and 2.22 m. Fluorescence spectra were recorded with the doped fibre pumped by approximately 28 mW of light (coupled in-fibre) at 845 nm. Examples of the fluorescence spectra for various doped fibre lengths are given in figure 5.19. These spectra show that the ${}^2F_{5/2(a)} \rightarrow {}^2F_{7/2(b)}$ peak near 1040 nm shifts to longer wavelengths and increases in intensity compared to both the 976 nm and the ${}^2F_{5/2(b)}$ fluorescence as the length of the doped fibre is increased. This is believed to be due to the reduced re-absorption for fluorescence at wavelengths greater than approximately 1000 nm in comparison to those at shorter wavelengths, as can be seen from the absorption spectrum (figure 5.13).

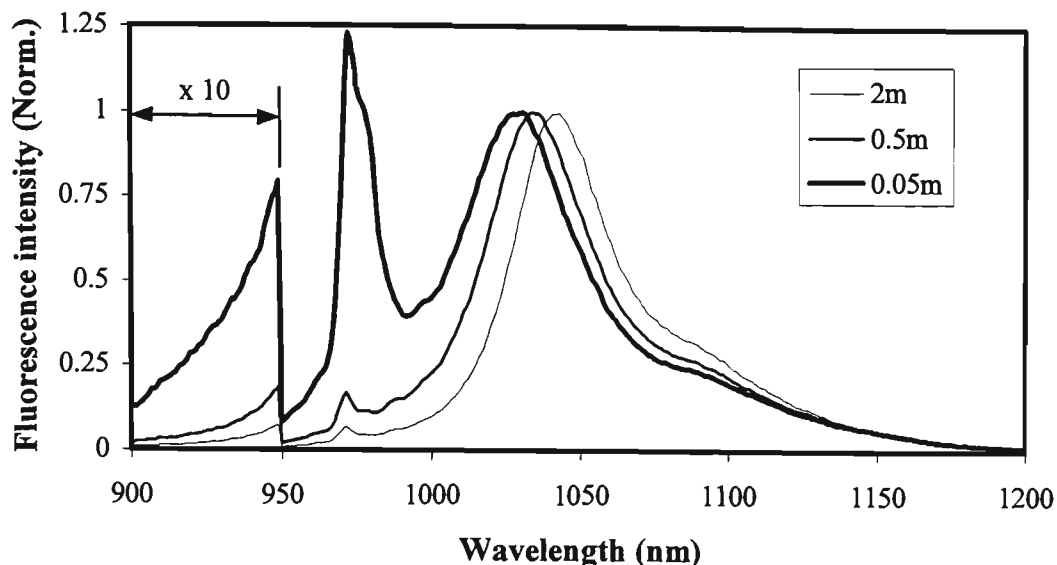


Figure 5.19: Fluorescence spectra versus doped fibre length for Yb^{3+} -doped silica fibre (1 nm OSA resolution). Note: spectra normalised to the 1040 nm peak intensity.

The fluorescence intensity ratio versus doped fibre length is given in figure 5.20 for the 920-930 nm/1051.5-1076.5 nm wavelength ranges. This graph shows that there is a sharp drop in the ratio at short fibre lengths before the ratio approaches a constant value.

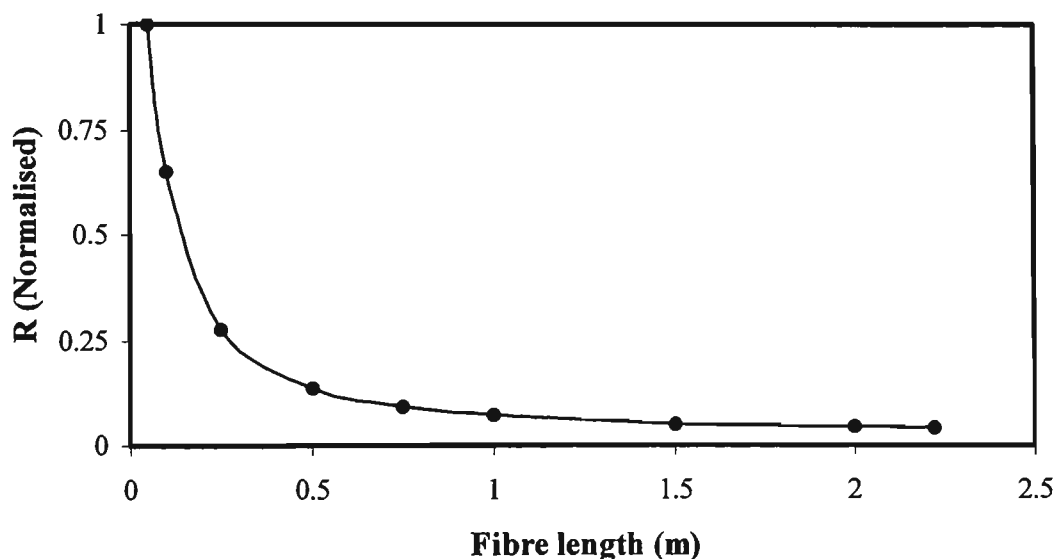


Figure 5.20: Fluorescence intensity ratio (ratio *b*) versus doped fibre length for Yb^{3+} -doped silica fibre (2500 ppm). Solid line used as guide to the eye only.

The induced temperature errors due to a 2.5 cm increase in the length of the Yb^{3+} -doped fibre were calculated using double exponential fits to the fluorescence intensity ratio versus doped fibre length data and fluorescence intensity ratio versus temperature look-up tables. Table 5.8 lists the results of these calculations and shows

that the error due to such a slight increase in doped fibre length can be quite large when the length of the doped fibre is short.

Ratio	Induced temperature error (°C)			
	@ 0.05 m	@ 0.5 m	@ 1 m	@ 2 m
a	2.64	0.56	0.29	0.04
b	3.03	0.63	0.33	0.04
c	2.93	0.63	0.31	0.04
d	3.02	0.60	0.31	0.04

Table 5.8: Induced temperature errors due to a 0.25 cm increase in doped fibre length for Yb^{3+} -doped silica fibre (2500 ppm).

The fluorescence intensity originating from the ${}^2F_{5/2(a)}$ and ${}^2F_{5/2(b)}$ levels are given in figure 5.21 as a function of doped fibre length for the 920-930 nm and 1051.5-1076.5 nm filter ranges. From this graph the fluorescence intensity of the ${}^2F_{5/2(a)}$ and ${}^2F_{5/2(b)}$ levels was determined to be 3.2 nW and 1.2 μW respectively for a doped fibre length of 1 m and a pump power of 28 mW. The data in figure 5.21 also graphically demonstrate the effect of re-absorption on the intensity of fluorescence originating from the ${}^2F_{5/2(b)}$ level. For this particular sample of Yb^{3+} -doped fibre the length need not be greater than 30 cm to obtain the maximum fluorescence from the ${}^2F_{5/2(b)}$ level.

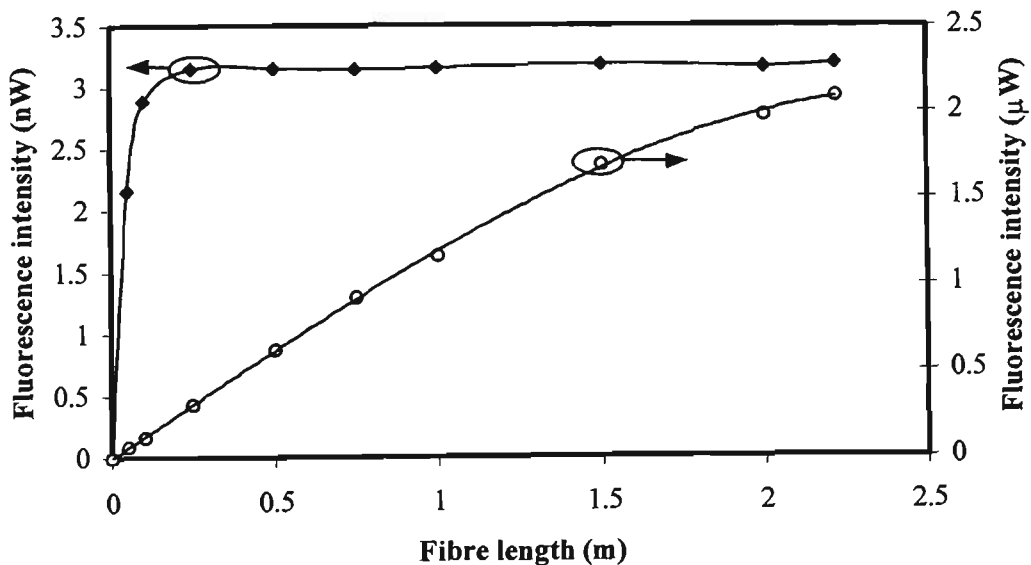


Figure 5.21: Fluorescence intensity of the ${}^2F_{5/2(a)}$ and ${}^2F_{5/2(b)}$ levels of Yb^{3+} -doped silica fibre (2500 ppm) versus doped fibre length; 920-930 nm (\blacklozenge) and 1051.5-1076.5 nm (\circ) wavelength ranges. Solid lines provided as a guide for the eye only.

5.5.4 Strain

The effect of applied strain on the fluorescence intensity ratio from Yb^{3+} -doped silica fibre was measured using a 30.5 cm length of doped fibre in the arrangement shown in figure 5.22 [122, 123]. Strain was applied to the doped fibre section by attaching weights to a section of un-doped fibre which was spliced to the end of the Yb^{3+} fibre. The doped fibre was excited by approximately 13 mW of light at 830 nm from a Ti:sapphire laser and an OSA was used to record fluorescence spectra.

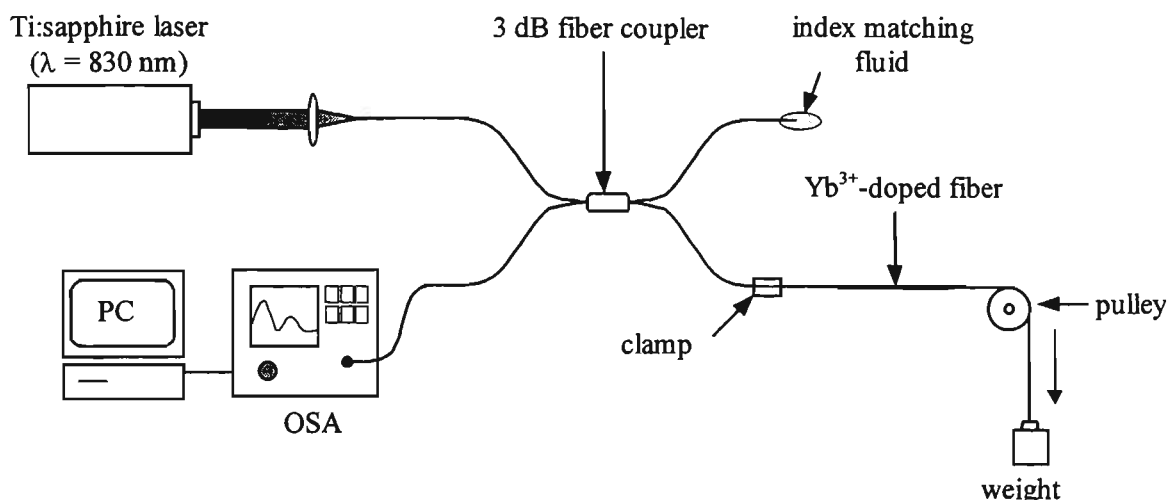


Figure 5.22: Experimental arrangement used in strain tests on Yb^{3+} -doped silica fibre.

Measurements of the fluorescence spectra were made for attached weights between 4 g and 176 g, which for the doped fibre used correspond to strain values of approximately $52 \mu\epsilon \rightarrow 2200 \mu\epsilon$. No obvious changes in the fluorescence spectra were observed over the range of strain values tested. The fluorescence intensity ratio was calculated as a function of applied strain using the recorded fluorescence spectra with the 900-910 nm and 1051.5-1076.5 nm wavelength ranges (figure 5.23).

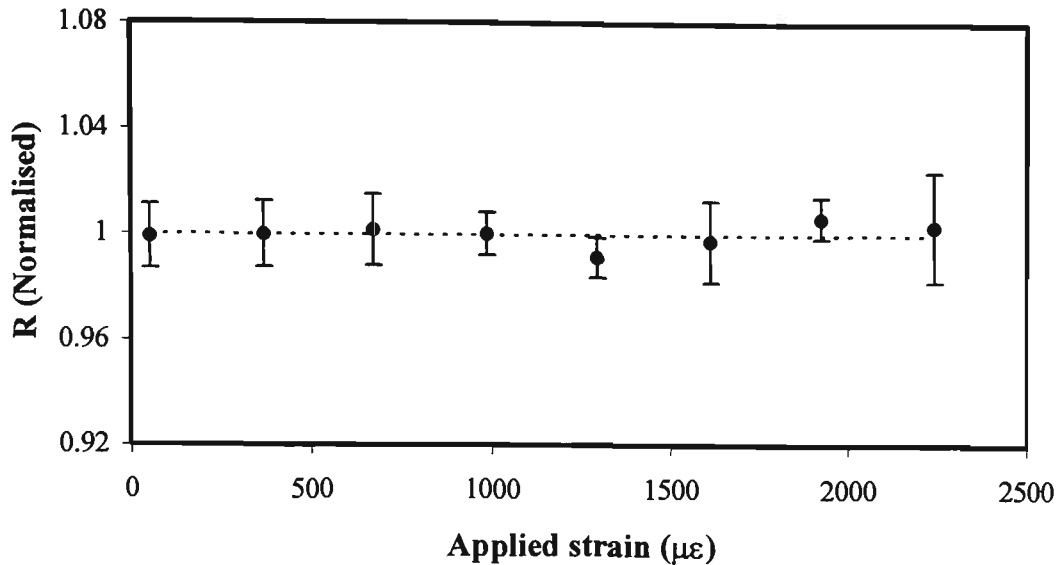


Figure 5.23: Fluorescence intensity ratio versus applied strain for Yb^{3+} -doped silica fibre.

Using a straight line fit to the data in figure 5.23 the strain sensitivity of the fluorescence intensity ratio for the Yb^{3+} -doped fibre tested was found to be $(2\pm 3)\times 10^{-4} \text{ \%}/^\circ\text{C}$. This implies a temperature to strain cross-sensitivity of $(2\pm 3)\times 10^{-4} \text{ }^\circ\text{C}/\mu\epsilon$, suggesting that the fluorescence intensity ratio technique of temperature sensing is independent of applied strain. This value is significantly smaller than the *fundamental* strain-temperature cross-sensitivities experienced in many other common optical fibre temperature sensing techniques (see table 5.9).

Technique	$dT/d\epsilon$ ($^\circ\text{C}/\mu\epsilon$)	Ref.
Fluorescence intensity ratio	$(2\pm 3)\times 10^{-4}$	This work
Fluorescence lifetime	$(7\pm 1)\times 10^{-3}$	[124]
Bragg-gratings	1×10^{-1}	calculated using data from [28]

Table 5.9: Strain-temperature cross sensitivities of optical fibre based temperature sensing techniques.

5.6 CONCLUSION

The stability of the fluorescence intensity ratio technique of temperature sensing with changes in pump wavelength, pump power, doped fibre length and applied strain have been investigated using Pr^{3+} :ZBLANP, Nd^{3+} -doped silica fibre and Yb^{3+} -doped silica fibre samples. As a result of these tests the processes which cause changes in the fluorescence intensity ratio and hence measured temperature have been identified.

For the Pr^{3+} :ZBLANP sample changes in the pump wavelength appear to have a reasonable effect on the fluorescence spectra and hence fluorescence intensity ratio via

site-selective affects. On the other hand changes in the pump power appear to have an almost negligible affect on the fluorescence intensity ratio. Therefore to ensure that pump induced errors are minimal with this sample the output wavelength of the excitation source should be stabilised. Alternatively the use of a broadband excitation source such as a LED should avoid site-selective affects.

The effect of changes in pump wavelength and power on the Nd³⁺-doped silica fibre sample were minimal, with induced temperature errors of less than 0.1 °C for the ranges tested. The small changes observed in the fluorescence spectra appear to be due to site-selective affects and amplified spontaneous emission. If required, a reduction in site-selective effects should be possible by slightly altering the host material e.g. the addition of P₂O₅ to the host material has been found to reduce changes in the fluorescence spectrum on Nd³⁺-doped silica due to changes in pump wavelength. Amplified spontaneous emission effects on the other hand may be reduced by lowering the gain of the doped fibre through changes in fibre dimensions and doping concentration. Further tests that could be performed on Nd³⁺-doped silica fibre include examining the effect of doped fibre length and doping concentration on the fluorescence intensity ratio.

The main cause of changes in the fluorescence intensity ratio of Yb³⁺-doped silica fibre with pump power and pump wavelength variations appears to be amplified spontaneous emission. While the induced errors due to changes in pump wavelength are negligible over the range tested the errors due to variations in pump power become significant as the pump power is increased, e.g. the induced temperature error for a 1% change in pump power at 24 mW is approximately 1 °C. Reductions in this effect should be achieved by lowering the fibre gain as previously discussed. Measurements of the effect of changes in the doped fibre length on the fluorescence intensity ratio indicate that for the fibre tested wavelength dependent re-absorption is a potential source of errors. This however could be avoided by individually calibrating sensors. Lastly, measurements indicate that the fluorescence intensity ratio technique has negligible strain-temperature cross sensitivity which would be a significant advantage for this method compared with many other fibre optic temperature sensors.

Chapter 6: Fluorescence Intensity Ratio Sensor Development and Applications

- 6.1 INTRODUCTION
- 6.2 Pr³⁺:ZBLANP SENSOR PROTOTYPE
- 6.3 Yb³⁺-DOPED FIBRE PROTOTYPE SENSOR
 - 6.3.1 *Sensor development*
 - 6.3.2 *Monitoring of optical fibre temperature in OPGW cable during fault current tests*
- 6.4 Nd³⁺-DOPED FIBRE PROTOTYPE SENSOR
 - 6.4.1 *Sensor development*
 - 6.4.2 *Measurement of breakage temperature of window glass during fires*
- 6.5 CONCLUSION

Overview of Chapter

In the following chapter the development of fluorescence intensity ratio sensor prototypes is presented together with examples of their use in applications in environments which present difficulties for conventional sensing techniques.

6.1 INTRODUCTION

The previous chapter reported the results of experiments performed to show the feasibility of the fluorescence intensity ratio technique for temperature measurement and to determine which rare earth doped materials were suitable for use with this technique. Often in these tests bulky laboratory based excitation and detection systems were used which would not be suitable for use in non-laboratory based experiments. The next stage in the development of fluorescence intensity ratio based sensors therefore involved building prototype sensors using more compact, low cost excitation and detection schemes. In this chapter details of prototype sensors utilising the three rare earth doped materials selected for further investigation, namely Pr^{3+} :ZBLANP, Nd^{3+} -doped silica fibre and Yb^{3+} -doped silica fibre are presented. This includes results of the use of these sensors prototypes in applications including:

- (a) the measurement of optical fibre temperature in a new optical fibre cable design during fault current tests, and,
- (b) monitoring of window breakage temperature during fires.

The majority of this work was performed in collaboration with co-workers at the Optical Technology Research Laboratory of Victoria University, who are referenced where appropriate.

6.2 Pr^{3+} :ZBLANP SENSOR PROTOTYPE

Development of a Pr^{3+} :ZBLANP based fluorescence intensity ratio prototype sensor was undertaken by Eric Maurice, the author of this thesis and other collaborators [89], following preliminary work which highlighted the promise of this material (see chapter 4). The sensing element used in the prototype sensor was a rod (8 mm diameter, 40 mm length) of Pr^{3+} :ZBLANP with a doping concentration of 1%. In earlier tests with this material, reported in chapter 4, the Pr^{3+} sample was excited using an argon ion laser, which would be unsuitable in a practical sensor due to size and cost. Instead a blue LED, with an output power of approximately 2 mW and a centre wavelength of 450 nm (FWHM 60 nm), was incorporated into the prototype sensor. As shown in figure 6.1 the output of the LED was collimated and coupled into a 600 μm core diameter silica-silicone fibre the other end of which was fixed to the Pr^{3+} :ZBLANP sensing material. To maximise the thermal stability of the Pr^{3+} sample it was placed in an aluminium holder

together with a thermocouple to monitor its temperature. The pump power launched was approximately $100 \mu\text{W}$. Counter-propagating fluorescence from the sensing material was guided to a dichroic mirror M_1 ($T = 60\%$ at $450 \pm 30 \text{ nm}$, $R = 90\%$ at $900 \pm 50 \text{ nm}$) which reflected the fluorescence light to a dichroic absorber filter M_2 ($T = 80\%$ at 910 nm , $T < 1\%$ at 870 nm , $T = 0\%$ at 450 nm , $R = 85\%$ at 870 nm). This filter passed light from the 3P_0 level, which was then focussed onto a silicon detector D_1 , and reflected light from the ${}^3P_1+{}^1I_6$ levels towards another dichroic filter M_3 ($T = 40\%$ at 870 nm , $T < 1\%$ at 910 nm , $T = 0\%$ at 450 nm). Fluorescence from the ${}^3P_1+{}^1I_6$ levels which passed through M_3 was then focussed onto another silicon detector D_2 . Due to the low light levels measured by the silicon detectors the excitation light was chopped at 270 Hz with a reference signal sent to the lock-in amplifiers (Princeton model 128A and Stanford SR530) used to measure the detector outputs. The wavelength ranges measured by each of the silicon detectors is shown in figure 6.2.

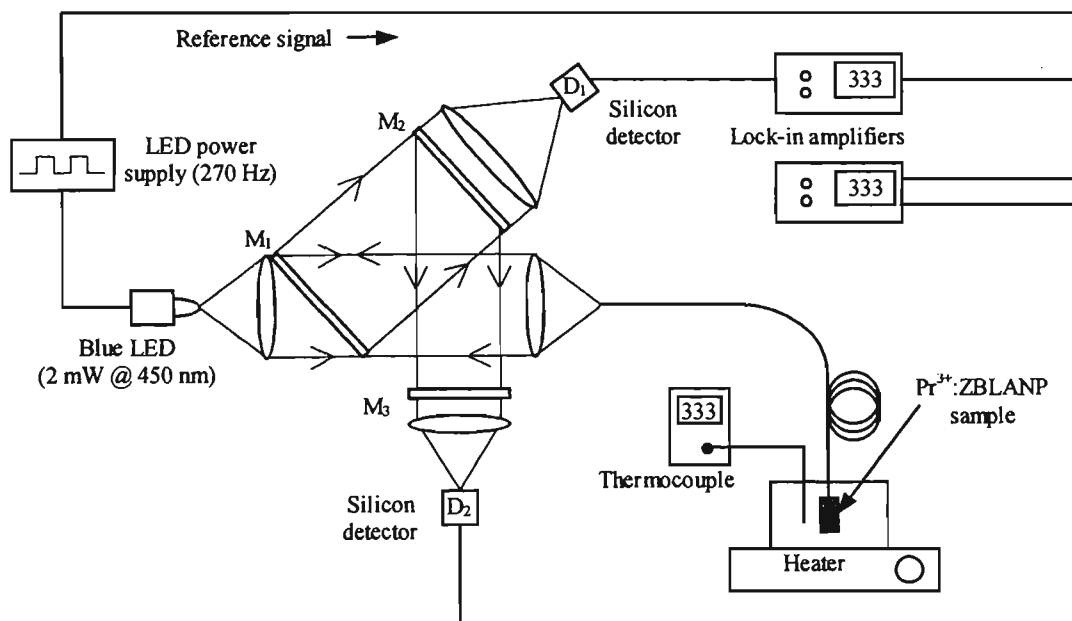


Figure 6.1: Experimental set up for $\text{Pr}^{3+}:\text{ZBLANP}$ sensor prototype.

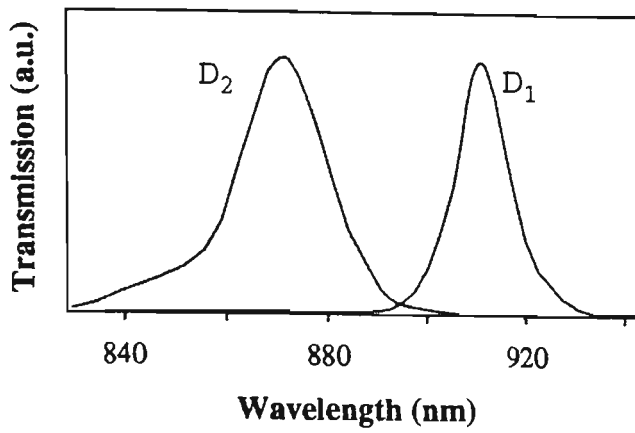


Figure 6.2: Wavelength ranges measured by the D_1 and D_2 silicon detectors.

The $\text{Pr}^{3+}:\text{ZBLANP}$ prototype sensor was calibrated against a K-type thermocouple over the $-45\text{ }^\circ\text{C}$ to $+255\text{ }^\circ\text{C}$ temperature range, the results of which are displayed in figure 6.3 (where $\text{FIR} = D_2 \text{ detector voltage}/D_1 \text{ detector voltage}$), together with a 3rd order polynomial fit. In order to determine the quality of the fit compared to the K-type calibration thermocouple the data shown in figure 6.1 were used to create look-up tables, with 3rd \rightarrow 6th order polynomial fits. Temperature errors were then calculated as the difference between the thermocouple values and the temperatures obtained from the measured fluorescence intensity ratio values and the look-up tables (figure 6.3b). Table 6.1 lists the standard deviations and maximum errors for each of the fits. The technique of generating look-up tables was chosen as it is often used with thermocouples as a method of determining temperature from the measured thermocouple voltages. A K-type thermocouple for example uses a 10th order polynomial for the $-270\text{ }^\circ\text{C}$ to $0\text{ }^\circ\text{C}$ temperature range and a 9th order polynomial plus an exponential for the $0\text{ }^\circ\text{C}$ to $1372\text{ }^\circ\text{C}$ range [125]. In this work a 6th order polynomial was the maximum order reported as it was found that only minimal improvements were obtained from higher order polynomials.

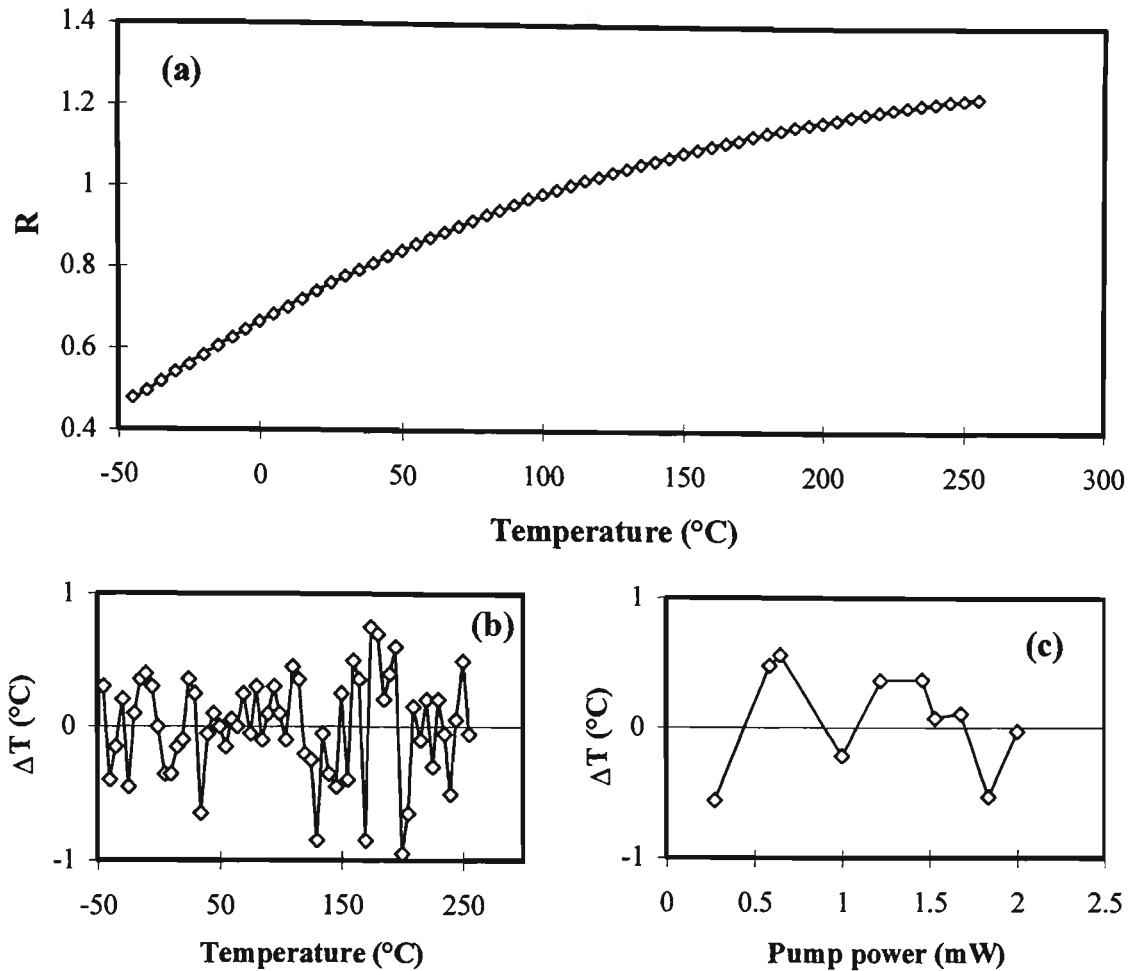


Figure 6.3: (a) Variation of the fluorescence intensity ratio of the $\text{Pr}^{3+}:\text{ZBLANP}$ sensor prototype over the $-45\text{ }^{\circ}\text{C}$ to $+255\text{ }^{\circ}\text{C}$ temperature range. (b) Temperature errors for a 6th order polynomial fit. (c) Induced temperature error due to changes in the pump power.

The sensitivity of the fluorescence intensity ratio was found to be approximately $0.51\%/^{\circ}\text{C}$ at $20\text{ }^{\circ}\text{C}$ which is lower than the value of $0.97\%/^{\circ}\text{C}$ predicted from theory (equation 3.6), using an energy gap of 580 cm^{-1} . This reduction in sensitivity may be due to a combination of the strong overlap between the fluorescence peaks corresponding to the two levels of interest and the filtering arrangement used.

Polynomial fit	σ_T ($^{\circ}\text{C}$)	ΔT_{max} ($^{\circ}\text{C}$)
3 rd order	0.54	1.40
4 th order	0.65	2.40
5 th order	0.38	0.95
6 th order	0.38	0.95

Table 6.1: Standard deviation (σ_T) and maximum deviation (ΔT_{max}) for 3rd \rightarrow 6th order polynomial fits to $\text{Pr}^{3+}:\text{ZBLANP}$ sensor prototype fluorescence intensity ratio data.

In addition to the thermal calibration the change in the fluorescence intensity ratio with pump power was investigated for the $\text{Pr}^{3+}:\text{ZBLANP}$ sensor prototype. It was

found that the fluorescence intensity ratio varied by less than 0.4% when the pump power was reduced by nearly an order of magnitude from 2 mW to 0.3 mW. Using a look-up table created with a 6th order polynomial this change corresponds to a maximum induced temperature error of less than ± 0.6 °C (figure 6.3c).

6.3 Yb³⁺-DOPED SILICA FIBRE SENSOR PROTOTYPE

The development of a Yb³⁺-doped fibre fluorescence intensity ratio prototype sensor was first reported by Eric Maurice, the author of this thesis and other collaborators [90] in 1997. Following this work the sensor was modified by the author of this thesis for use in the testing of a new optical fibre cable manufactured by Olex Cables (now Belden Australia Pty. Ltd.) [126, 127]. In this section the configuration of the Yb³⁺-doped fibre sensor prototype used in the aforementioned work is described, the results of calibrations are presented and the application of the sensor in cable tests is discussed.

6.3.1 Sensor development

Figure 6.4 shows the basic sensor configuration used in both the initial and modified sensor prototypes. The Yb³⁺-doped fibre, spliced to an output arm of a 3 dB coupler, was excited by the output of a laser diode via one of the input arms of the coupler. Counter-propagating fluorescence emitted from the second input arm of the 3 dB coupler was guided to a Schott glasss RG850 absorbent filter to remove pump light reflected from the splice and the doped fibre end. Next a dichroic mirror (transmission spectrum given in figure 6.5) was used to separate the remaining fluorescence into the components originating from the ²F_{5/2(a)} and ²F_{5/2(b)} levels, which were then focussed onto silicon detectors. The intensity of the fluorescence from the ²F_{5/2(a)} and ²F_{5/2(b)} levels were measured by multimeters connected to the output of the silicon detectors. Details of the components specific to each of the sensor prototypes (e.g. laser diode) are given in table 6.2.

Sensor prototype	Yb ³⁺ -doped fibre	Laser diode	3 dB coupler
Initial	large core, 40 μm	Sony SLD303, 810 nm, 30 mW	50 μm core diameter
Modified	small core, < 10 μm	Mitsubishi ML2701, 843 nm, 2.5 mW	10 μm core diameter

Table 6.2: Details of components used in the initial and modified Yb^{3+} -doped fibre sensor prototypes.

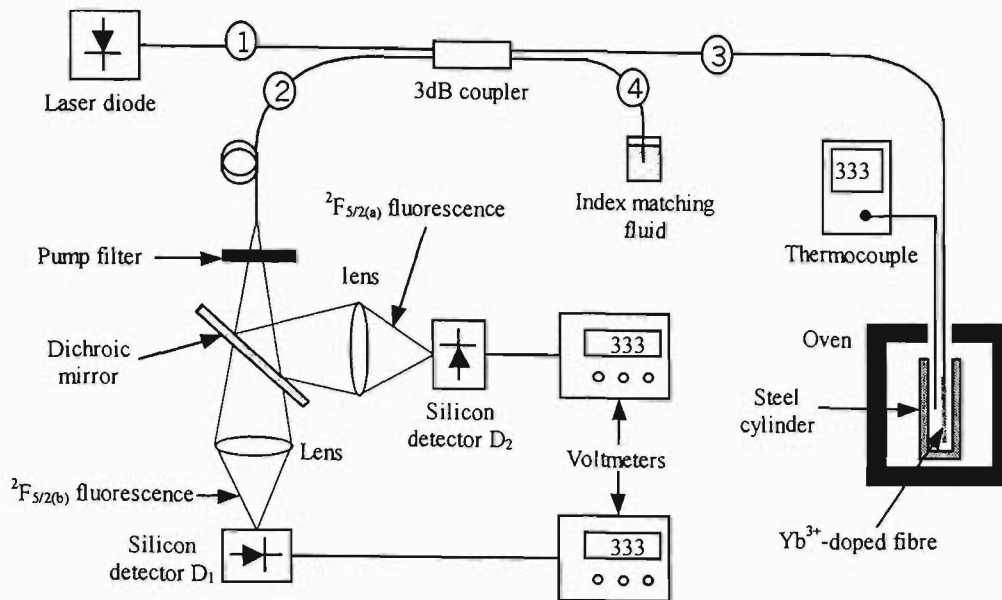


Figure 6.4: Basic configuration for Yb^{3+} -doped fibre sensor prototype.

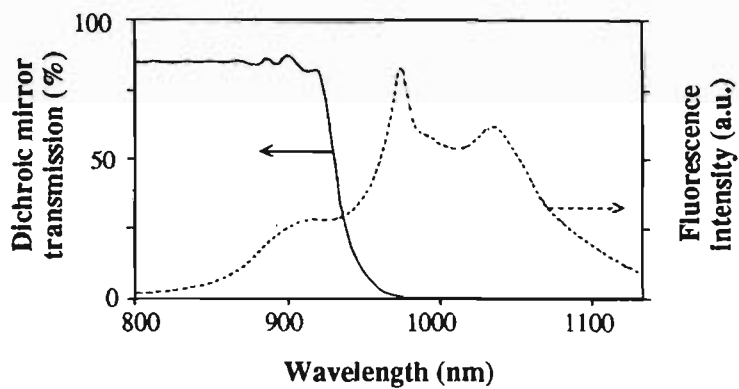


Figure 6.5: Transmission spectrum of Schott glass RG850 dichroic mirror together with Yb^{3+} -doped silica fibre fluorescence spectrum at 500 °C for comparison.

The fluorescence intensity ratio, calculated by dividing the D_1 detector output by the D_2 detector output, was measured as a function of temperature for the two sensor prototypes, the results of which are shown in figure 6.6 together with 4th order polynomial fits. The Yb^{3+} -doped fibre used in the calibration of the initial sensor configuration was 14 cm in length and had a doping concentration of 2500 ppm and a core diameter of 40 μm . The results for the modified configuration were obtained with a 25 cm length of Yb^{3+} -doped fibre with a doping concentration of 2500 ppm and a core diameter of 5.2 μm . In each of the calibrations the doped fibre was placed in a steel cylinder and heated to the maximum test temperature by an oven with data being recorded during the cooling process. A K-type thermocouple co-located with the doped fibre was used to monitor the doped fibre temperature.

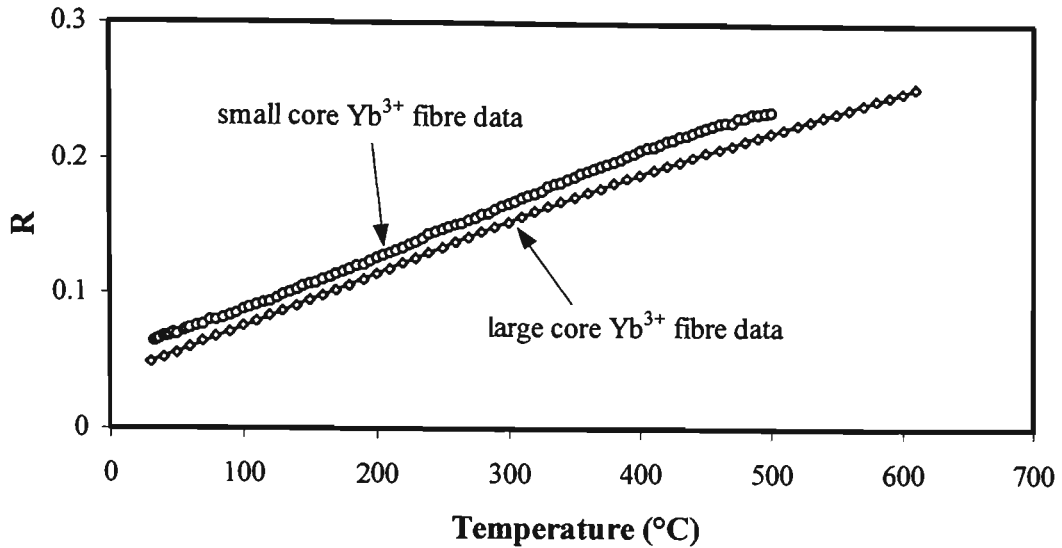


Figure 6.6: Fluorescence intensity ratio versus temperature data obtained for the two Yb^{3+} -doped fibre sensor prototypes discussed.

To estimate the quality of the fit in comparison to the K-type calibration thermocouple for each of the sensor configurations the data shown in figure 6.6 were used to create look-up tables with polynomial fits. The temperature errors, calculated as the difference between the look-up table fit values and the thermocouple data, are listed in table 6.3. Figures 6.7a and 6.7b show the temperature differences for these fits over the measured temperature ranges.

Sensor configuration	Polynomial fit	σ_T (°C)	ΔT_{\max} (°C)
Initial	3 rd order	1.95	6.10
	4 th order	0.78	1.65
	5 th order	0.66	1.70
	6 th order	0.44	1.10
Modified	5 th order	1.36	4.65
	6 th order	1.39	5.00
	7 th order	1.30	5.00

Table 6.3: Standard deviation (σ_T) and maximum deviation (ΔT_{\max}) for Yb^{3+} -doped fibre prototype sensor data using polynomial fit look-up tables.

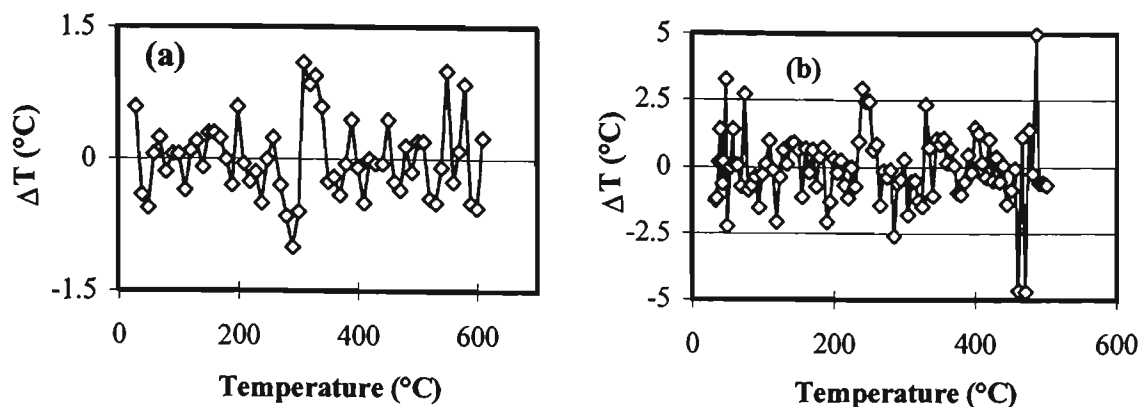


Figure 6.7: Temperature difference between 6th order polynomial fits and recorded fluorescence intensity ratio values for the (a) initial and (b) modified Yb³⁺-doped fibre sensor prototypes.

The sensitivity of the initial sensor configuration at 30 °C was approximately 0.83%/°C, while the modified configuration had a sensitivity of approximately 0.5%/°C at the same temperature. It is believed that the reduced sensitivity of the modified configuration was due to a change in the angle of the dichroic mirror, which occurred during the re-configuration process and affected the wavelength ranges analysed by each of the silicon detectors. The theoretical sensitivity value at 30 °C for an energy gap of 680 cm⁻¹, corresponding to the ²F_{5/2(a)} and ²F_{5/2(b)} levels, is 1.07%/°C.

The stability of the fluorescence intensity ratio with changes in the pump wavelength, pump power and bending loss in the transmission fibre was measured for the initial sensor configuration (figures 6.8a-c). To measure the effect of pump wavelength on the fluorescence intensity ratio the laser diode output was scanned from 802.5 nm to 811 nm. The resulting change in the fluorescence intensity ratio was approximately ±0.3% which corresponds to temperature errors of less than 0.4 °C at 30 °C. The fluorescence intensity ratio was monitored as the pump power was reduced from 30 mW down to 5 mW. For this large variation in the pump power the fluorescence intensity ratio changed by less than ±0.4% corresponding to an induced temperature error of less than ±0.5 °C. Finally the effect of induced bend loss on the fluorescence intensity ratio was investigated by winding a section of the fibre on the output arm of the 3 dB coupler around a cylinder while applying a tension of 50 g. Measurements of the fluorescence intensity ratio were recorded for a bend radius of 11 mm down to 1.8 mm. As figure 6.8c shows despite a drop of 64% in the fluorescence intensity from the doped fibre the change in the fluorescence intensity ratio would cause temperature errors of less than ±2 °C. These results show that a fluorescence intensity

ratio based temperature sensor using Yb^{3+} -doped fibre should have excellent stability under normal operating conditions.

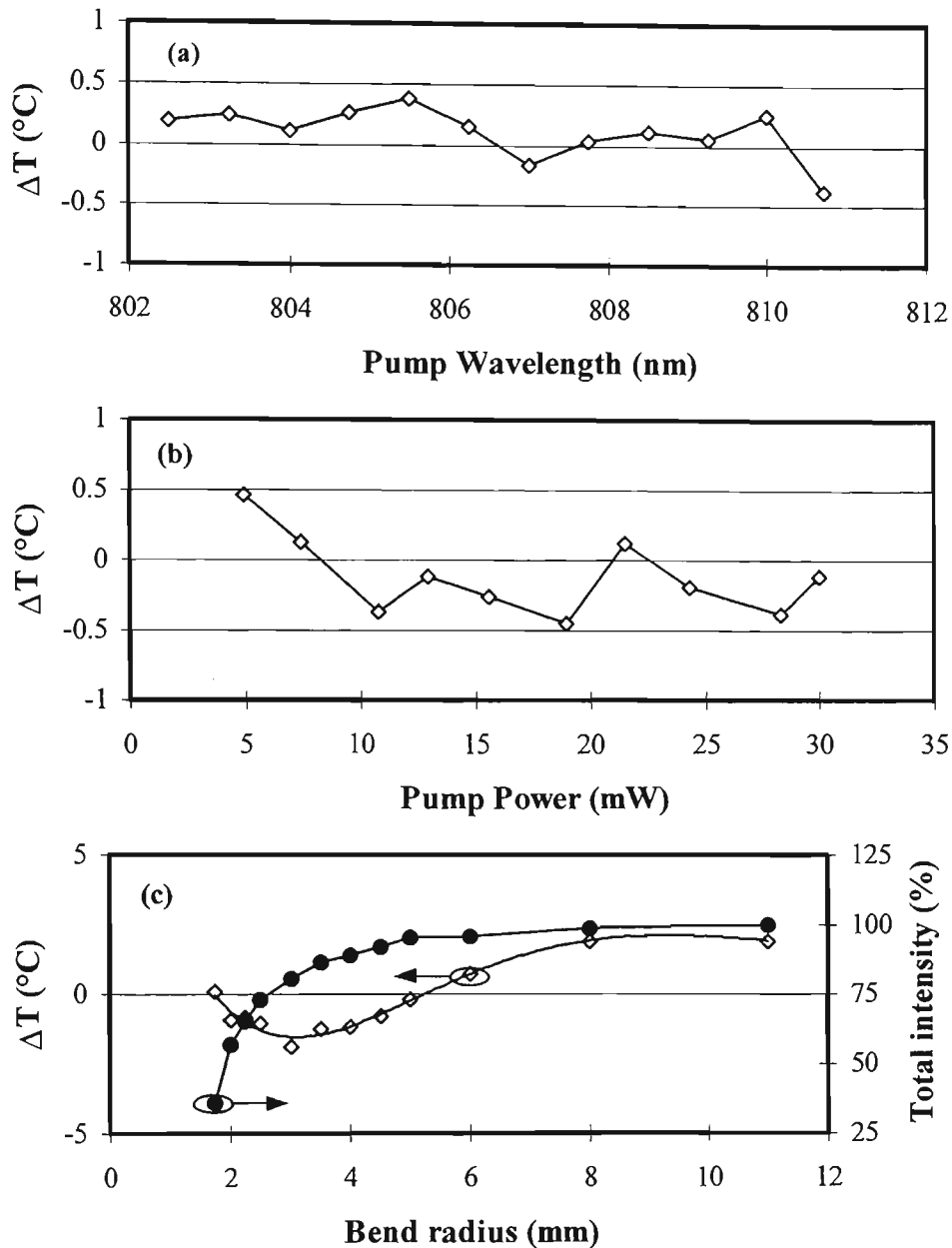


Figure 6.8: Induced temperature errors due to changes in (a) pump wavelength, (b) pump power and (c) bend loss for the initial Yb^{3+} -doped fibre sensor configuration. Solid lines used as a guide to the eye only.

6.3.2 Monitoring of optical fibre temperature in OPGW cable during fault current tests

In 1996 the Optical Technology Research Laboratory at Victoria University was approached by Olex Cables (Tottenham, Victoria - now Belden Australia Pty. Ltd.) for assistance in the measurement of temperature in a new design optical power ground wire (OPGW) cable, during fault current testing. OPGW cables are used as a protective

ground wire for high voltage transmission circuits and also provide telecommunications links via the incorporation of optical fibres (see figure 6.9). These cables are expected to withstand high current pulses, such as lightning strikes, during their normal course of operation. New cable designs (or modifications of existing designs) therefore undergo fault current testing in which a high current pulse (in this case approximately 20 kA) is sent down a test section of the cable. During these tests the temperature of the cable can rise significantly and to make sure that this does not cause damage to cable components, or affect the cable performance, the thermal response of various sections of the cable are monitored. While thermocouples can be used to measure the temperature of the outer metallic jacket, substantial difficulties arise when attempting to insert these devices in the loose tubes so that the temperature of the optical fibres in the core of the cable can be monitored. To overcome this problem it was proposed that the fluorescence intensity ratio temperature sensing technique with Yb^{3+} -doped optical fibre be used to monitor optical fibre temperature in the core of the cable. This method has the significant advantage that the sensing element could be incorporated with little difficulty into the OPGW cable during the normal tubing stage of manufacture.

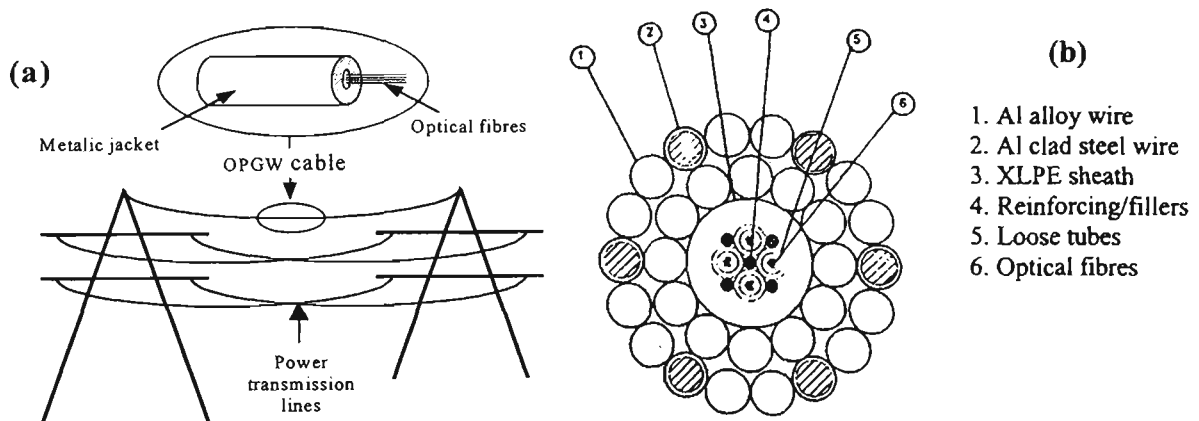


Figure 6.9: (a) Example of OPGW use on high voltage transmission lines, (b) cross section of new OPGW design.

The monitoring of optical fibre temperature in an OPGW cable during fault current tests was performed using the “modified” Yb^{3+} -doped fibre sensor prototype (i.e. 843 nm laser diode) discussed in the previous section. This sensor was modified from the original arrangement to:

- (a) improve the coupling stability of the excitation light (important as the sensor had to be transported a considerable distance, from Melbourne to Sydney, for the tests),
- and,

(b) incorporate Yb^{3+} -doped fibre with dimensions and physical properties which could be placed in the OPGW cable with minimum difficulty.

To meet the first of these requirements the 810 nm laser diode, which required manual coupling adjustments, was replaced by an 843 nm pigtailed laser diode. The longer wavelength was chosen to reduce the drop in the fluorescence intensity caused by the reduction in pump power, as the absorbed pump power increases by a factor of approximately 3 for the longer wavelength. A smaller diameter Yb^{3+} -doped fibre was used in the modified arrangement as the 40 μm core doped fibre had a cladding diameter of approximately 800 μm which would have presented major problems in terms of both size and flexibility during the incorporation into the OPGW cable. The Yb^{3+} -doped fibre used in the fault current tests was 95 cm in length with a doping concentration and core size of 350 ppm and 11 μm respectively.

Figure 6.10 shows the arrangement for the fault current tests which were performed at the National Measurement Laboratory of CSIRO (Commonwealth Scientific and Industrial Research Organisation) in Sydney, Australia. The fault current simulations involved exposing the cable to a current pulse of 20 kA rms (50 Hz) for 0.45 seconds. Cable behaviour during fault current tests was observed by recording optical attenuation of fibres in the OPGW core, temperatures in various sections of the cable, cable tension and cable sag.

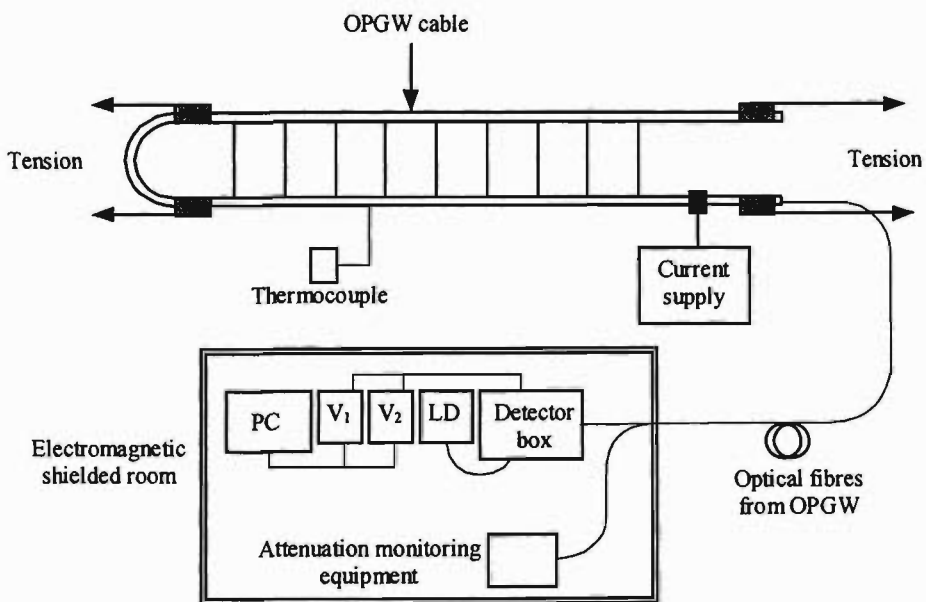


Figure 6.10: Layout of fault current tests performed at the National Measurement Laboratory of CSIRO in Sydney.

Prior to fault current testing the fluorescence intensity ratio of a section of Yb^{3+} -doped fibre (with the same properties as the doped fibre in the OPGW cable) was calibrated against a K-type thermocouple for temperatures between 18 °C and 210 °C. A 4th order polynomial fit to this data demonstrated a standard deviation of 0.45 °C, with a maximum deviation of 1.7 °C.

Optical fibre temperatures during fault current tests were obtained by inserting the fluorescence intensity ratio, calculated as the division of the ${}^2F_{5/2(b)}$ fluorescence detector reading by the ${}^2F_{5/2(a)}$ reading, into a 4th order polynomial from the calibration data. A typical result of the optical fibre temperature during a fault current test (fault current applied at time = 0 seconds) is shown in figure 6.11. Also shown in figure 6.11 is the temperature of the outer metallic jacket of the OPGW cable (solid line) measured by a thermocouple which shows an almost instantaneous rise in temperature after the fault current was applied. As the heat flows inwards the temperature of the optical fibres in the core of the cable, indicated by the open circles in figure 6.11, gradually heat up. This behaviour agrees well with a computer model developed to predict the temperature of various cable layers during fault current tests [126].

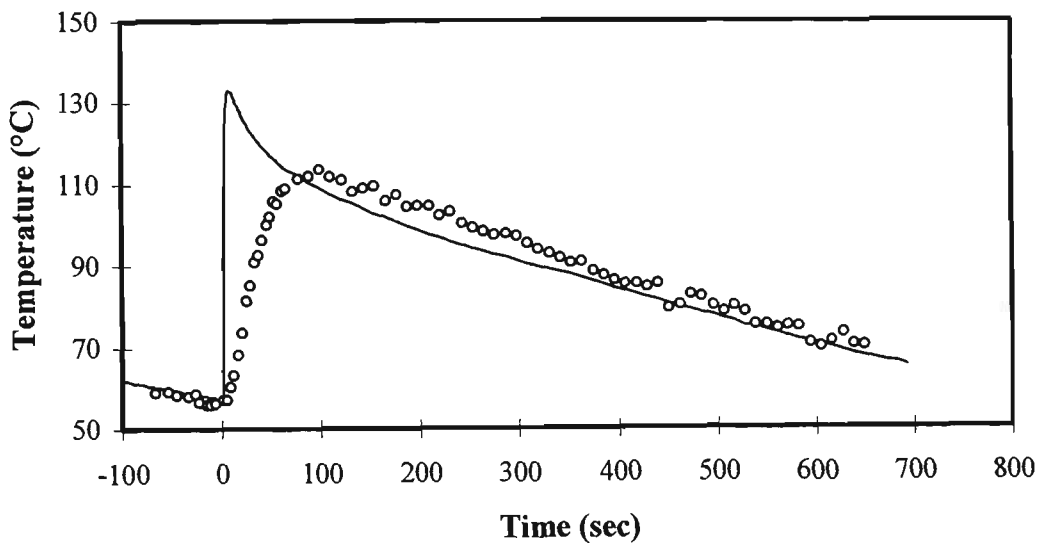


Figure 6.11: Optical fibre temperature in OPGW cable core during a fault current test, OPGW jacket temperature measured by a thermocouple (straight line), optical fibre temperature measured by the fluorescence intensity ratio sensor (o).

For the data shown in figure 6.11 the optical fibre temperature in the OPGW cable core reached a maximum temperature of 114 °C approximately 100 seconds after the fault current was applied. An estimation of the accuracy of temperature measurement during

these tests was calculated from the difference between the experimental data and an exponential fit applied to the cooling slope, which gave a standard and maximum deviation of 0.8 °C and 4 °C respectively for the example shown. Further information on these tests can be found in references 126 and 127.

6.4 Nd³⁺-DOPED SILICA FIBRE PROTOTYPE SENSOR

6.4.1 Sensor development

The latest fluorescence intensity ratio based prototype temperature sensor to be reported uses the thermalisation of the $^4F_{3/2}$ and $^4F_{5/2}$ levels in Nd³⁺-ion [88, 128]. A schematic of the prototype sensor is shown in figure 6.12. The sensing material used in this case was Nd³⁺-doped silica fibre with a dopant concentration of 500 ppm and a core size of 5 µm, which is spliced onto one of the output arms of coupler A. Excitation of the doped fibre was provided by an Sharp LM017 808 nm laser diode (chopped at 270 Hz) with a peak power of approximately 13 mW. To increase the mechanical stability of the sensor the bulk optical filtering arrangement used in previous sensor prototypes (i.e. Pr³⁺:ZBLANP and Yb³⁺-doped fibre) was replaced by a dual 3 dB fibre coupler arrangement. In this arrangement fluorescence from the two levels of interest (i.e. $^4F_{3/2}$ and $^4F_{5/2}$) was selected by filtering the light exiting the two output arms of the second 3 dB coupler using dichroic band pass filters. The fluorescence transmitted by each of the filters was then focussed onto silicon detectors, with voltmeters connected to record the signal intensities. The wavelength ranges of these filters are given in figure 6.13 together with the Nd³⁺ fluorescence spectrum at 500 °C for comparison. A phase sensitive detection system, similar to the system reported in reference 129, was used to reduce noise in the measured signals.

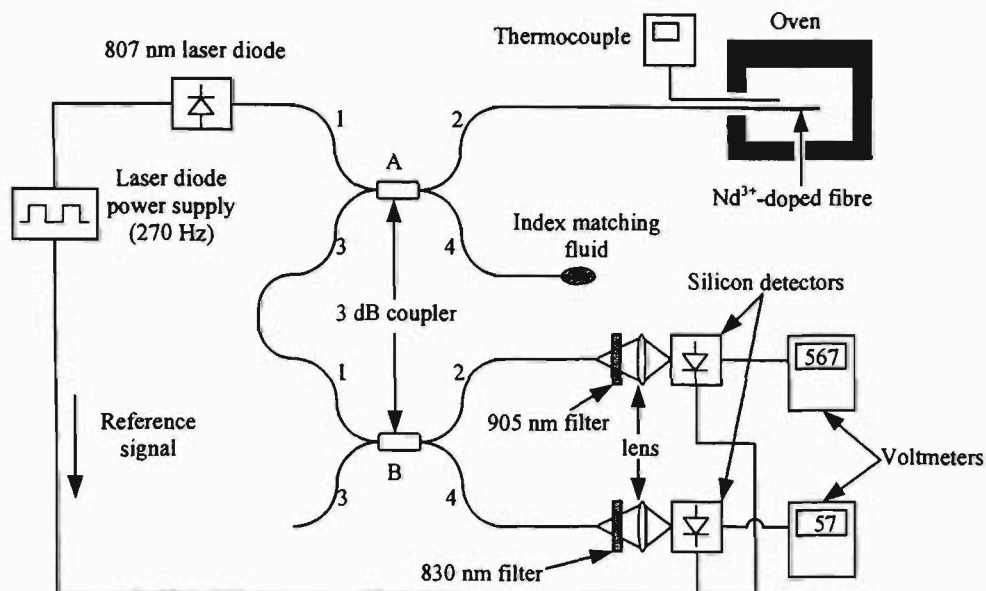


Figure 6.12: Experimental arrangement for Nd^{3+} -doped fibre sensor prototype.

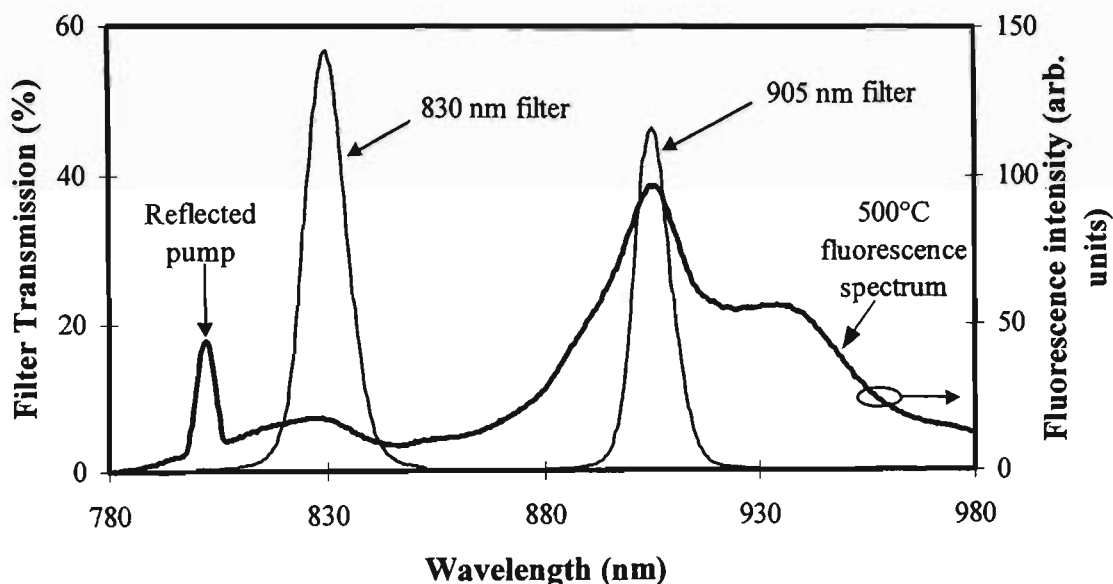


Figure 6.13: Wavelength response of bandpass filters used to select fluorescence from the ${}^4F_{3/2}$ and ${}^4F_{5/2}$ levels and the fluorescence spectrum of Nd^{3+} -doped fibre at 500 °C.

The Nd^{3+} -doped fibre prototype sensor was calibrated against a K-type thermocouple over the $-50\text{ }^\circ\text{C} \rightarrow +500\text{ }^\circ\text{C}$ temperature range. Figure 6.14a shows the results of the initial calibration obtained using a 59 cm length of Nd^{3+} -doped fibre (500 ppm doping concentration) as the sensing element. During the calibration the Nd^{3+} -doped fibre and thermocouple were placed in an aluminium holder which was cooled below ambient temperature using dry ice and heated by placing the holder in an oven.

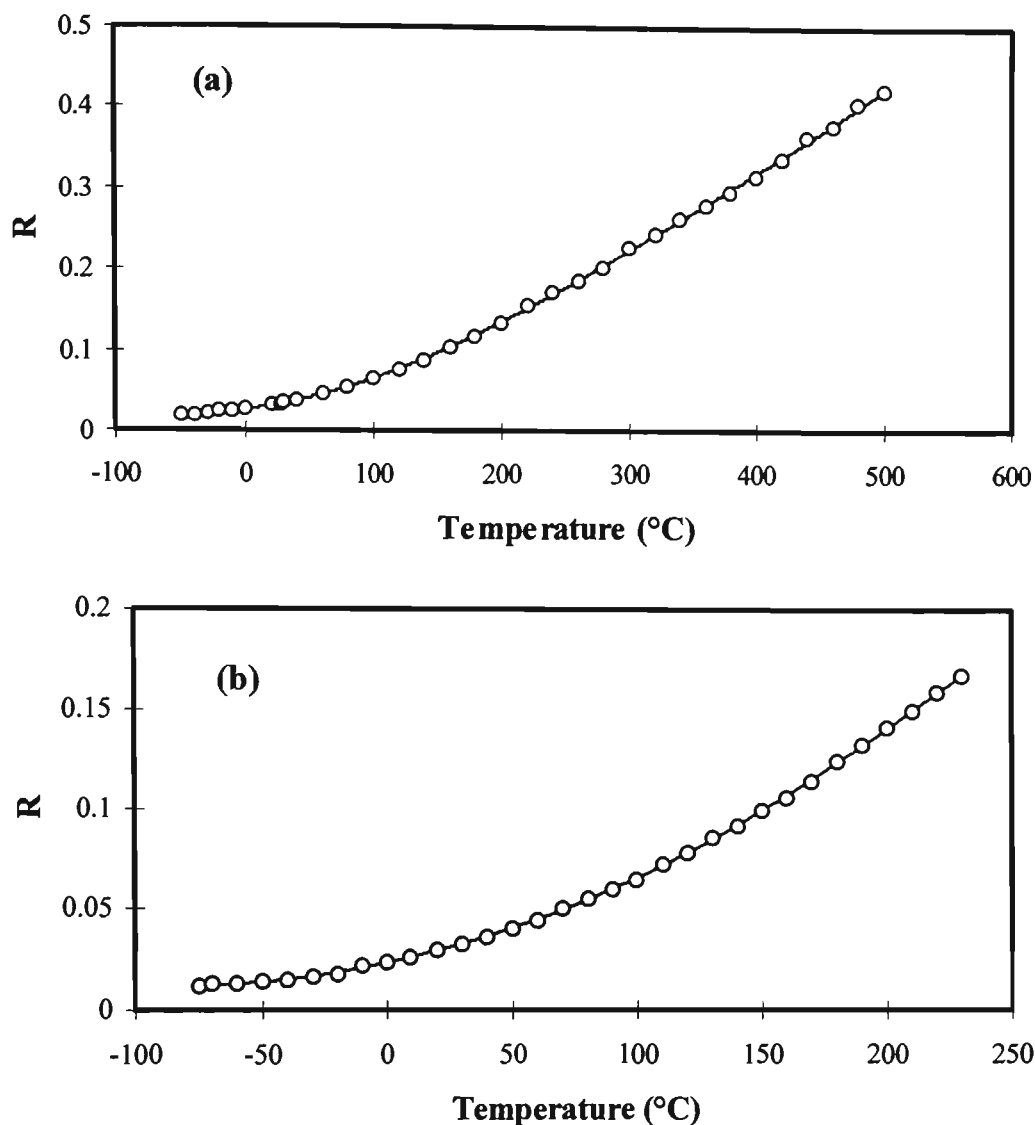


Figure 6.14: Calibration of Na^{3+} prototype sensor using (a) a 59 cm and (b) a 2 m length of Na^{3+} -doped fibre as the sensing element. The straight lines are 5th order polynomial fits to the experimental data.

The accuracy of the temperature measurement with the sensor prototype was determined using look-up tables created with polynomial fits to the calibration data. Temperature errors, calculated as the difference between the values determined from look-up tables and the thermocouple readings are shown for 6th order polynomial fits in figure 6.15. Table 6.4 lists a summary of the measurement accuracy for 3rd \rightarrow 6th order polynomial fits.

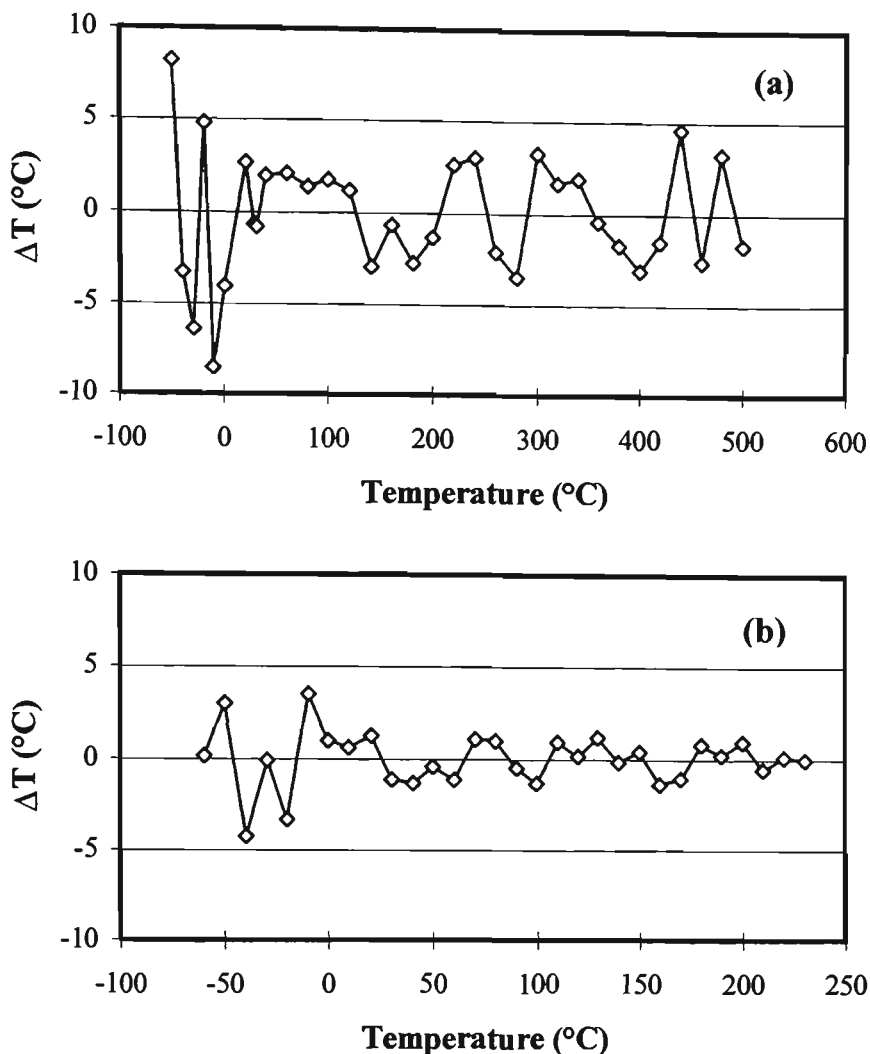


Figure 6.15: Temperature difference between thermocouple readings and look-up table values created using 6th order polynomial fits for the Nd^{3+} sensor using (a) a 59 cm length of sensing fibre and (b) a 2 m length of sensing fibre.

Polynomial fit	-50 °C → +500 °C		0 °C → +500 °C	
	σ_T (°C)	ΔT_{\max} (°C)	σ_T (°C)	ΔT_{\max} (°C)
3 rd order	3.7	10.9	2.9	5.1
4 th order	4.2	12.4	2.5	4.8
5 th order	3.5	10.1	2.6	5.8
6 th order	3.4	8.5	2.3	4.3

Table 6.4: Standard deviation (σ_T) and maximum deviation (ΔT_{\max}) for Nd^{3+} -doped fibre prototype sensor data, 59 cm sensor length, using polynomial fit look-up tables.

The sensitivity of the sensor at 20 °C was calculated to be 1.02%/°C which is lower than the predicted value of 1.67%/°C, for a energy gap of 1000 cm^{-1} . This drop is believed to be a result of the pump light reflections entering the 830 nm detector. This reflected pump light is also believed to be the cause of the large deviations between the measured and fitted data at low temperatures where changes in the index matching of the end of the doped fibre, caused by condensation, resulted in fluctuations in the

830 nm detector readings. As the data in table 6.4 shows a substantial improvement in the temperature difference between thermocouple and look-up table values is obtained for readings above 0 °C.

To check the accuracy of the prototype sensor without the effect of pump reflections from the end of the doped fibre a second calibration was undertaken, this time using a 2 m length of doped fibre. For this length of Nd³⁺ fibre it was expected that the intensity of pump light at the doped fibre end, and hence reflected pump power, would be substantially less than the for the shorter length. The calibration was performed between -60 °C and +230 °C using a similar arrangement to that mentioned previously (figure 6.14b). For this calibration the standard deviation between the thermocouple readings and the values calculated using a 5th order polynomial look-up table dropped to 1.36 °C with a maximum error of 4.7 °C.

Currently work is underway to improve the accuracy of the sensor by increasing the signal to noise ratio of the detectors and through reductions of the effect of pump reflections. The first may be achieved by increasing the Nd³⁺ fluorescence intensity via a combination of increased pump power, using Nd³⁺ fiber with a higher doping concentration or reducing detector noise. The effect of reflected pump power can be reduced by either improved pump filtering or using a pump wavelength which is further removed from the ⁴F_{5/2} fluorescence, such as 780 nm which are readily available at low cost.

6.4.2 Measurement of breakage temperature of window glass during fires

The latest application of the fluorescence intensity ratio technique of temperature measurement is in the area of fire safety. In this work a Nd³⁺ fluorescence intensity ratio sensor is being used to measure the temperature of window glass in fire simulations [130, 131]. Knowledge of the temperature at which window glass breaks during a fire is important as the break creates an opening for the entry of fresh air and the exit of hot fire gases. The resulting change in the ventilation affects the growth and spread of the fire. Previously thermocouples have been used to measure window glass temperature in fire simulations. However it has been found that the differing thermal properties of glass and the thermocouple materials can affect the tests results [132]. The fluorescence intensity ratio technique has the significant advantage that the material used to measure

temperature (i.e. the doped fibre sensing element) is essentially the same material as the window and therefore will have similar thermal properties.

6.5 CONCLUSION

Fluorescence intensity ratio prototype temperature sensors have been developed using Pr^{3+} :ZBLANP, Yb^{3+} -doped silica fibre and Nd^{3+} -doped silica fibre as sensing materials. The combination of these sensors covers the $-50\text{ }^{\circ}\text{C}$ to $610\text{ }^{\circ}\text{C}$ temperature range with a measurement accuracy of approximately $1\text{ }^{\circ}\text{C}$. The application of these prototypes in the measurement of temperature in environments unsuitable for conventional temperature sensors has also been demonstrated.

Chapter 7: Fluorescence Lifetime Studies

- 7.1 INTRODUCTION
- 7.2 FLUORESCENCE LIFETIME STUDIES OF Yb^{3+} -DOPED SILICA FIBRE
- 7.3 FLUORESCENCE LIFETIME STUDIES OF Eu^{3+} -DOPED SILICA FIBRE
- 7.4 COMPARISON OF THE FLUORESCENCE INTENSITY RATIO AND FLUORESCENCE LIFETIME TECHNIQUES
- 7.5 CONCLUSION

Overview of Chapter

In the following chapter results of fluorescence lifetime measurements of Yb^{3+} and Eu^{3+} doped silica fibre are presented. This chapter also contains a comparison between the fluorescence intensity ratio and fluorescence lifetime techniques for temperature sensing.

7.1 INTRODUCTION

One of the most well known and researched optical fibre temperature sensing techniques is the fluorescence lifetime method, introduced in chapter 1. This technique uses the same physical principle (i.e. the thermalisation of closely spaced energy levels) and often the same materials as have been investigated with the fluorescence intensity ratio method of temperature sensing. In this chapter the results of fluorescence lifetime studies of Yb^{3+} and Eu^{3+} -doped silica fibre, which have also been used in fluorescence intensity ratio studies (chapter 4), are presented. This allows a direct comparison between the fluorescence intensity ratio technique and another well known and established method of temperature sensing using optical fibres.

7.2 FLUORESCENCE LIFETIME STUDIES OF Yb^{3+} -DOPED SILICA FIBRE

The ytterbium (Yb^{3+}) ion doped in a silica fibre has recently been shown to be a promising candidate for both fluorescence lifetime [34] and fluorescence intensity ratio (see chapters 4 - 6) based temperature sensing. In the work reported here the temperature dependence of the fluorescence lifetime of Yb^{3+} -doped silica fibre previously used in fluorescence intensity ratio studies (see chapters 4 - 6) is presented. The data allow a comparison between the fluorescence intensity ratio and fluorescence lifetime temperature sensing techniques using Yb^{3+} -doped fibre and the fluorescence lifetime behaviour observed with different fibre compositions.

The experimental arrangement used to study the fluorescence lifetime of the Yb^{3+} -doped fibre is shown in figure 7.1. In this arrangement the doped fibre under investigation was spliced to a length of plain telecommunications fibre which was spliced to the sensor arm of a 2×1 coupler. Ytterbium-doped fibres with doping concentrations of 700 ppm (YbL) and 2500 ppm (YbH), the same as those used in fluorescence intensity ratio studies, were tested in this investigation. The doped fibre was excited by the square wave modulated output of a 980 nm laser diode connected to one of the input arms of the coupler. An InGaAs photodetector was used to measure the counter-propagating fluorescence from the doped fibre. The fluorescence signal was converted into a lifetime value by a phase-locked detection (PLD) method [30], and recorded on a desktop computer. Heating of the doped fibre was achieved by placing the

doped fibre into a quartz sheath, which was inserted into a thermostatically controlled calibration oven (CARBOLITE type: MTF 12/38/400).

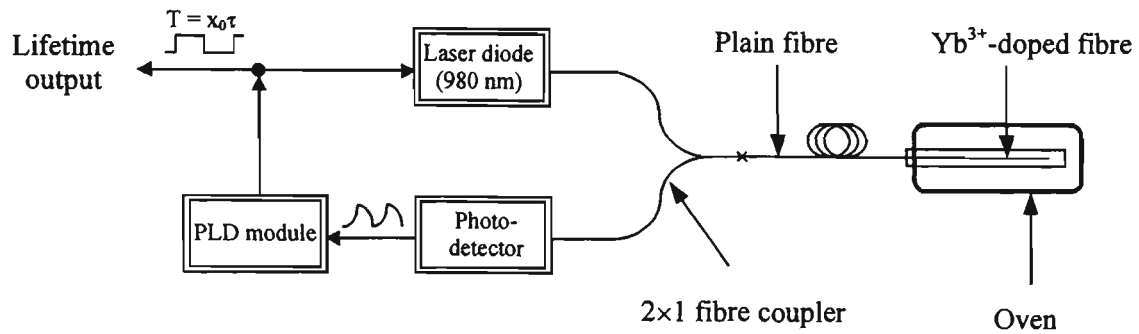


Figure 7.1: Experimental arrangement used for fluorescence lifetime studies of Yb^{3+} -doped silica fibre.

In previous fluorescence lifetime studies it was found that in order to obtain reliable and repeatable data, the rare earth doped fibre must undergo an annealing process [33-35]. This involves heating the doped fibre at an elevated temperature for a number of hours to remove metastable conditions that may have been caused during fusion splicing [35] or the fibre drawing process. The temperature and duration of the annealing process has been found to depend upon the dopant rare earth ion and should also depend upon the host composition. Similar annealing processes are used in glass production to remove residual stress in the glass brought about by the manufacturing process [134, 135].

The effect of annealing was examined for both the YbL and YbH fibres using annealing temperatures near 700 °C. This temperature was used in previous annealing tests on Yb^{3+} -doped fibre [34]. For the YbL fibre a stable fluorescence lifetime was achieved after annealing for approximately 35 hours at 720 °C. During this time the fluorescence lifetime increased by $\sim 49 \mu\text{sec}$ from the initial lifetime to a stable value of $\sim 718 \mu\text{sec}$, which corresponds to an equivalent temperature change of $\sim 200 \text{ }^\circ\text{C}$. After the lifetime reached a stabilised value the standard deviation was measured to be $\sim 1.4 \mu\text{sec}$ over a 14 hour period, which corresponds to a temperature change of $\sim 5.6 \text{ }^\circ\text{C}$. To illustrate the effect of annealing on the lifetime of the YbL fibre the lifetime is plotted as a function of temperature in figure 7.2 for readings taken before and after the annealing process.

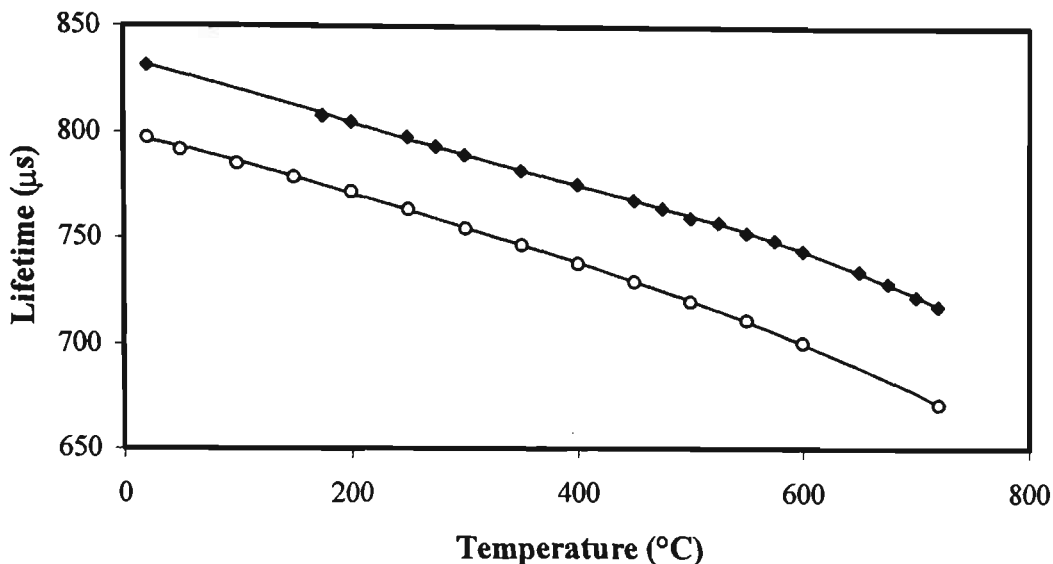


Figure 7.2: Fluorescence lifetime versus temperature before (o) and after (◆) annealing for YbL (700 ppm) fibre. The solid lines are theoretical fits (see table 7.1).

The repeatability of the fluorescence lifetime characteristics of the YbL fibre after annealing were measured by temperature cycling the fibre between 200 °C and 700 °C, recording lifetime values every 100 °C. The differences between the individual and average lifetime values at each temperature over 6 cycles, corresponded to a standard deviation of 3.8 °C. This is within the ± 5 °C accuracy of the oven used.

Annealing of the YbH fibre was performed at 700 °C for more than 90 hours. However, unlike the YbL fibre, the lifetime of the YbH fibre did not reach a steady value in this time. Additional tests at higher temperatures of 800 °C and 950 °C also did not result in stable fluorescence lifetimes. It is unclear why it was not possible to achieve a stabilised lifetime through annealing of this fibre. One potential cause is a small amount of Er^{3+} in the fibre present from contamination in the manufacturing process. In previous studies Er^{3+} was shown to have an annealing temperature of approximately 1100 °C [33].

The fluorescence lifetime versus temperature characteristics of the YbL (after annealing) and YbH (no annealing) fibres are shown in figure 7.3. Also shown in figure 7.3 for comparison are the fluorescence lifetime data obtained by workers at City University for two other Yb^{3+} -doped fibres. These fibres labeled here as YbCL and YbCH, with doping concentrations of 550 ppm and 2500 ppm respectively, were manufactured by INO, Canada. The fluorescence lifetime data have been fitted using a configurational coordinate model [30, 34] where the fluorescence lifetime, τ , is given by:

$$\tau = \frac{1 + \exp[-\Delta E/kT]}{\tau_1^{-1} + \tau_2^{-1} \exp[-\Delta E/kT] + \tau_q^{-1} \exp[-(\Delta E + \Delta E_q)/kT]} \quad (7.1)$$

where τ_1 and τ_2 are the intrinsic lifetimes of the lower and upper energy thermally coupled levels (i.e. ${}^2F_{5/2(a)}$ and ${}^2F_{5/2(b)}$ in this case), ΔE is the energy gap between these levels, τ_q and ΔE_q are the lifetime and energy gap due to thermal quenching, k is the Boltzmann constant and T is the absolute temperature. The values obtained for the fits are provided in table 7.1.

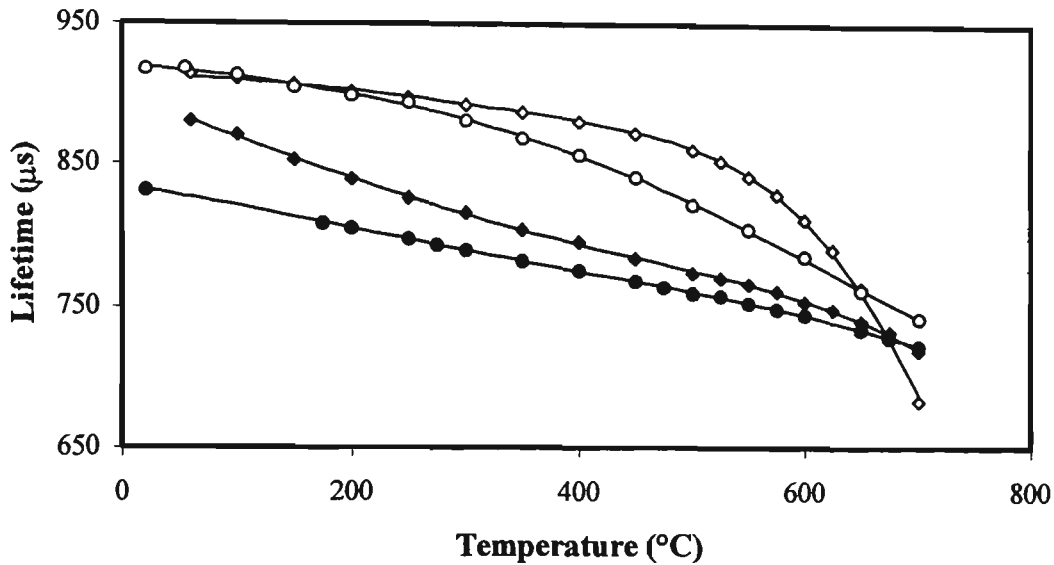


Figure 7.3: Lifetime versus temperature characteristics of Yb^{3+} -doped fibres, YbL (●), YbH (○), YbCL (◆) and YbCH (◇). The solid lines are theoretical fits (see table 7.1).

Fibre	τ_1 (μs)	τ_2 (μs)	τ_q (μs)	ΔE (cm^{-1})	ΔE_q (cm^{-1})	σ_n (%)
YbL (ba)	804	508	36	840	3863	0.083
(aa)	840	545	5	804	5528	0.048
YbH (ba)	923	699	80	843	2674	0.147
YbCL (aa)	916	504	0.069	687	7558	-
YbCH (aa)	914	548	0.0039	1301	7973	-

Table 7.1: Fitting parameters for Yb^{3+} -doped silica fibre lifetime versus temperature using configurational coordinate model, ba – before annealing, aa – after annealing. Data for YbCL and YbCH obtained from reference 34.

The sensitivity of the fluorescence lifetime to changes in temperature were calculated using the configurational coordinate fits to the experimental data and are presented in table 7.2.

Fibre	Sensitivity (%/°C)			
	@ 20 °C	@ 100 °C	@ 300 °C	@ 700 °C
YbL (ba)	0.01	0.02	0.02	0.04
(aa)	0.01	0.02	0.02	0.04
YbH (ba)	0.01	0.01	0.02	0.06
YbCL (aa)	0.03	0.03	0.03	0.06
YbCH (aa)	0.002	0.01	0.01	0.27
FIR (YbL)	0.94	0.86	0.44	0.16

Table 7.2: Sensitivity of the fluorescence lifetime of Yb³⁺-doped fibres at various temperatures. Also given for comparison is the sensitivity of the fluorescence intensity ratio for the YbL fibre determined in the tests presented in chapter 4.

A number of conclusions can be drawn from the work presented here in conjunction with the work reported in reference 34. Firstly, the annealing process has been found to produce stable and repeatable lifetime characteristics for several fibre samples using annealing temperatures close to 700 °C; however the data for the YbH fibre require further investigation. The results also indicate that both the fluorescence intensity ratio and the fluorescence lifetime of Yb³⁺ doped in silica fibre have significant and useful variations with temperature over the ranges investigated. At lower temperatures the fluorescence intensity ratio has a superior sensitivity in comparison to that of the fluorescence lifetime; however at higher temperatures the two techniques show similar sensitivities. Finally the composition of Yb³⁺-doped fibres, including the rare earth ion doping concentration, have a significant effect on the lifetime characteristics and therefore could be used to optimise sensor performance.

This work has been published in reference 136.

7.3 FLUORESCENCE LIFETIME STUDIES OF Eu³⁺-DOPED SILICA FIBRE

The second rare earth ion to be used in fluorescence lifetime studies was europium (Eu³⁺). This ion has been widely used as an activator in phosphor based fluorescence lifetime studies [131]. However, to the author's knowledge, the Eu³⁺ ion has not yet been studied for use in fluorescence lifetime based temperature sensing in an optical fibre host. In addition to the possible use in temperature sensing, it was hoped that studies of the fluorescence lifetime of Eu³⁺-doped silica fibre may provide further information on the "non-thermalisation" of the ⁵D₀ and ⁵D₁ energy levels observed at low temperatures in fluorescence intensity ratio studies (see chapter 4).

In these experiments a tunable Spectra-Physics MOPO, pumped by a frequency doubled Nd:YAG laser and with a repetition rate of 10 Hz, was used to populate the levels of interest. As illustrated in figure 7.4, the pump light at 463 nm was coupled into a length of undoped fibre using a microscope objective. Neutral density filters were used to avoid potential damage to the end of the transmission fibre caused by the high optical densities of the focussed MOPO output. The Eu^{3+} -doped silica fibre under investigation (dopant concentration ~ 450 ppm, core diameter $4.5 \mu\text{m}$) was spliced between two lengths of undoped fibre that allowed remote heating and cooling of the Eu^{3+} fibre. Co-propagating fluorescence was focussed onto the input slit of a 0.275 m f/3.8 Jarrell-Ash monochromator, with a resolution of 3 nm, after passing through suitable colour glass pump rejection filters. The fluorescence intensity of the $^5\text{D}_0$ and $^5\text{D}_1$ energy levels (at 600 nm and 535 nm respectively) versus time were measured by a Hamamatsu R928 photomultiplier tube connected to the output slit of the monochromator. The response time of the photomultiplier tube, which depended upon the load resistor used (e.g. <10 ns with 50Ω), was much faster than any of the lifetimes measured. A Tektronics model TDS 320C CRO connected to a PC was used to record the data. Heating of the doped fibre was achieved by placing the doped fibre contained in a thermal chamber in either an oven or on a hotplate depending on the temperatures required. Liquid nitrogen was introduced into the thermal chamber for cooling below ambient temperature. A K-type thermocouple, co-located with the doped fibre, was used to record the temperature of the Eu^{3+} -doped fibre.

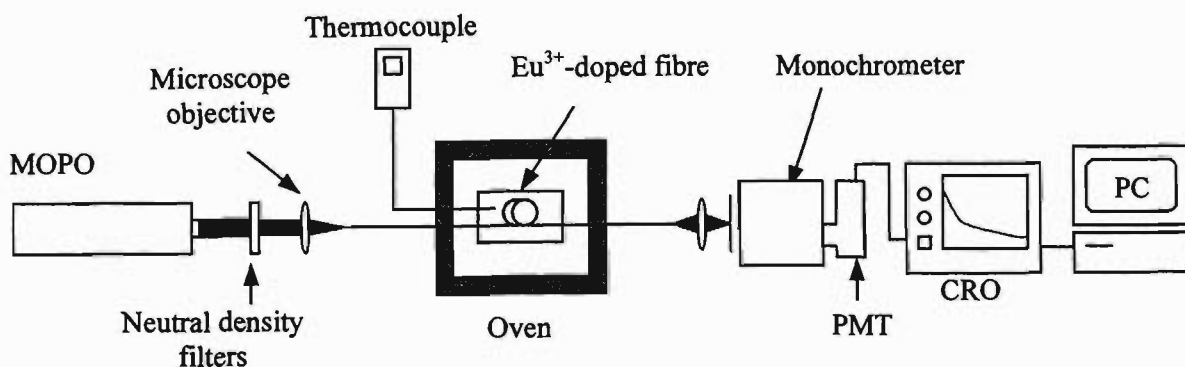


Figure 7.4: Experimental arrangement used in Eu^{3+} -doped fibre fluorescence lifetime tests.

The decay in the fluorescence intensity from the $^5\text{D}_1$ energy level was measured using a 0.75 m length of Eu^{3+} -doped fibre for temperatures between 21.2°C and 500°C .

During these measurements it was observed that the fluorescence decay from this level contained both a slow (~ 1 ms) and fast (~ 4 μ s) component. As shown in figure 7.5 the magnitude of the slow decay component increased with respect to the fast decay component as the temperature was raised. Similar dual decay behavior has been observed for the higher energy level of several other closely spaced energy levels in rare earth doped materials [138-140]. The fast initial decay has been related to the relaxation from the higher energy level to the next lower level, which is followed by a longer decay due to thermalisation.

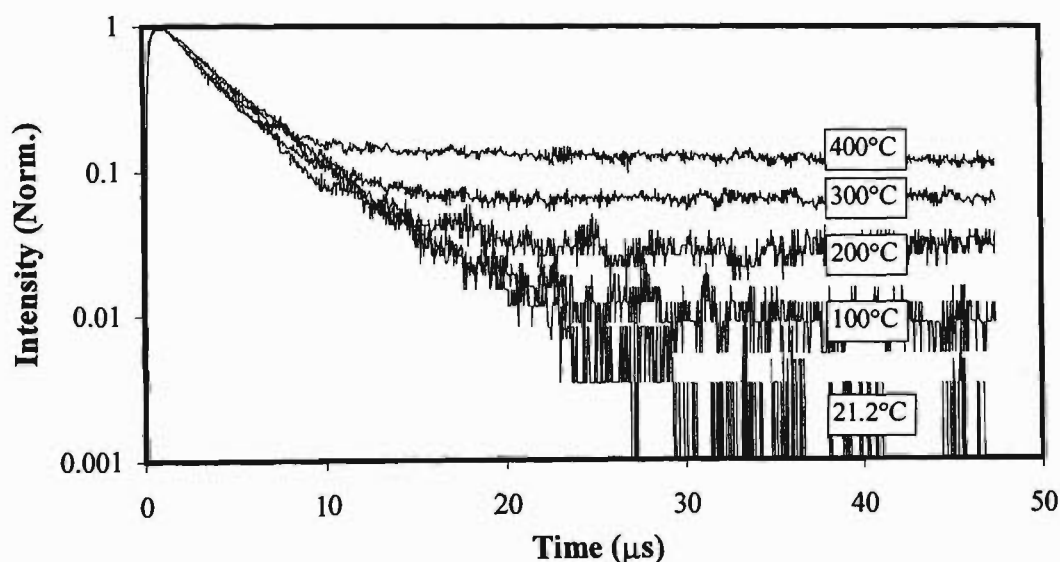


Figure 7.5: Fluorescence decay of 5D_1 level of Eu^{3+} -doped silica fibre at 535 nm for temperatures between 21.2 °C and 400 °C, showing fast and slow decay components.

The decay constants (also commonly known as the lifetimes) of the slow and fast decay components of the 5D_1 fluorescence were calculated as a function of temperature by fitting exponential decays to individual intensity versus time data obtained for each of the fast and slow decay components. Detector response times of ~ 300 ns and ~ 25 μ s were used during the fast and slow decay component measurements respectively. At higher temperatures dual exponential decays, with a slow decay component of ~ 1 ms, were required for a more accurate fit of the fast decay component.

The lifetime of the fast decay component from the 5D_1 level is plotted as a function of temperature in figure 7.6.

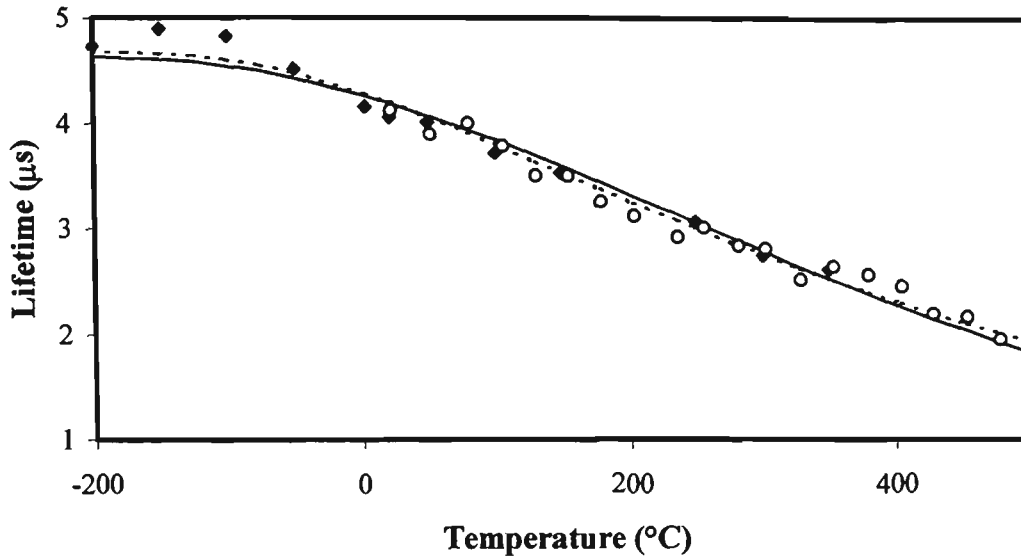


Figure 7.6: Fluorescence lifetime versus temperature of fast decay component of 5D_1 level (535 nm) with multiphonon decay fits, 0.75 m fibre length data (o), 1.84 m data (◆), solid line – 4 phonon fit, dashed line – 3 phonon fit.

In addition to the data obtained for a 0.75 m length of Eu^{3+} -doped fibre the results shown in figure 7.6 include measurements obtained between $-200\text{ }^\circ\text{C}$ and $350\text{ }^\circ\text{C}$ using a 1.84 m length of Eu^{3+} -doped fibre. The later data was included to assist in the fitting. The configuration coordinate lifetime model used previously for Yb^{3+} -doped fibre data applies to thermally coupled levels. The fast decay component however appears to occur prior to thermalisation and therefore another theory is required. The technique adopted uses the well known expression for the lifetime, τ , of an energy level:

$$\tau = \frac{1}{A + W_{\text{nr}}} \quad (7.2)$$

where A and W_{nr} are the radiative and non-radiative decay rates from the energy level respectively [56, 57, 141]. The temperature dependence of the lifetime of an energy level has been found to depend upon the non-radiative decay, W_{nr} , from the level. In materials where ion-ion interactions can be neglected (e.g. low doping concentrations) the non-radiative decay from a level is primarily due to multiphonon decay. Reasonable success in the modeling of multiphonon rates has been made through the development of a phenomenological model using intuitive arguments [56, 57, 141]. In this model the time dependence of the multiphonon rate arises due to the stimulated emission of phonons as the phonon modes become populated. In its general form the multiphonon rate, W_{nr} , is given by,

$$W_{\text{nr}} = W_{\text{nr}}(0)[n(T) + 1]^p \quad (7.3)$$

where $W_{nr}(0)$ is the multiphonon rate at a temperature of 0 K, p is the number of phonons required to bridge the gap, and $n(T)$ is the Bose-Einstein distribution given by:

$$n(T) = \frac{1}{\exp[\hbar\omega/kT] - 1} \quad (7.4)$$

where $\hbar\omega$ is the phonon energy, k is the Boltzmann constant and T is the absolute temperature [56, 57, 141]. The data in figure 7.6 were fitted using the multiphonon theory outlined above, assuming an energy gap of approximately 1750 cm^{-1} between the 5D_1 and 5D_0 levels [95]. Table 7.3 contains the results of the best fits to data.

Fit	$\hbar\omega \text{ (cm}^{-1}\text{)}$	$W_{nr}(0) \text{ (s}^{-1}\text{)}$	$A \text{ (s}^{-1}\text{)}$	$\sigma \text{ (\%)}$
3 phonon	584	1.24×10^5	8.9×10^4	3.35
4 phonon	440	3.5×10^4	1.8×10^5	4.36

Table 7.3: Data used in multiphonon fits to fast decay component of 5D_1 fluorescence from Eu^{3+} -doped silica fibre.

The fluorescence decay of the 5D_0 level was measured at temperatures between $21 \text{ }^\circ\text{C}$ and $500 \text{ }^\circ\text{C}$ using a detector response time of $\sim 25 \text{ }\mu\text{s}$ and a 0.75 m length of Eu^{3+} -doped fibre. Unlike the 5D_1 fluorescence only a slow decay component was observed for the 5D_0 fluorescence. The lifetime of the 5D_0 level calculated from exponential decay fits to the data is plotted in figure 7.7 for the range of temperatures measured. Also shown in this figure are the lifetimes of the slow decay component of the 5D_1 fluorescence which agree reasonably well with the 5D_0 lifetimes.

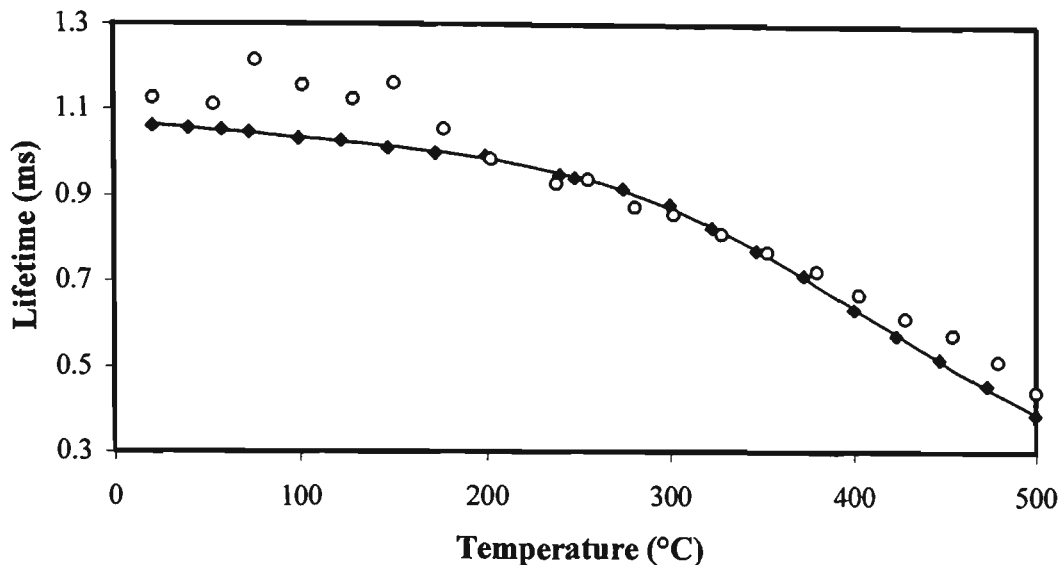


Figure 7.7: Fluorescence lifetime versus temperature of 5D_0 transition (\blacklozenge) and the slow decay component of the 5D_1 fluorescence (\circ) of Eu^{3+} -doped silica fibre. Solid line is the theoretical fit (see table 7.4).

The 5D_0 fluorescence lifetime versus temperature data were fitted using a configurational coordinate model as discussed previously for Yb^{3+} -doped fibre. The results of the fits to the data are given in table 7.4 together with energy gap values from reference 16. The two main differences between the fitted and predicted values are that:

(a) the fitted value of τ_2 (790 μs) is much larger than the fast decay component of the 5D_1 fluorescence (4 μs), and,

(b) there is a substantial difference between the expected and fitted energy gap values.

Both of these differences may possibly be due to the partial thermalisation of the 5D_0 and 5D_1 at lower temperatures. The standard deviation between the measurement temperature, as recorded by the thermocouple, and the temperature implied from the fluorescence lifetime data using the fit as a look-up table was 4.2 °C.

	τ_1 (msec)	τ_2 (msec)	τ_q (μs)	ΔE (cm^{-1})	ΔE_q (cm^{-1})	σ_n (%)
Dejneka <i>et al.</i> [85]				1750	2500	
Fit	1.095	0.79	0.8	728	3424	0.500

Table 7.4: Fitting parameters for 5D_0 level of Eu^{3+} -doped silica fibre lifetime versus temperature using configurational coordinate model.

The sensitivity of the fluorescence lifetime of the 5D_0 level was calculated using data obtained from the best configurational coordinate model fit and is given for a number of temperatures in table 7.5. At lower temperatures the sensitivity of the fluorescence lifetime of the 5D_0 level is comparable to the sensitivities obtained for

Yb³⁺-doped silica fibre. For temperatures above 100 °C however the ⁵D₀ level of Eu³⁺-doped fibre has significantly better sensitivity.

	Sensitivity (%/°C)			
	@ 22 °C	@ 100 °C	@ 300 °C	@ 500 °C
Lifetime of ⁵ D ₀	0.03	0.04	0.20	0.55
FIR	0.15	0.45	0.60	0.39

Table 7.5: Sensitivity of the ⁵D₀ fluorescence lifetime from Eu³⁺-doped silica fibre at various temperatures. Also given for comparison is the calculated sensitivity of the fluorescence intensity ratio for Eu³⁺-doped fibre using the ⁷F₁ transition.

The results obtained indicate “partial” thermalisation of the ⁵D₀ and ⁵D₁ levels of Eu³⁺-doped silica fibre for the temperature ranges investigated. This agrees with the results obtained for the fluorescence intensity ratio of these levels. The sensitivity of the fluorescence lifetime of the ⁵D₀ level is inferior to the sensitivity of the fluorescence intensity ratio of the ⁵D₀ and ⁵D₁ levels at temperatures below approximately 400 °C. For higher temperature however the fluorescence lifetime has a superior sensitivity. Information regarding the modelling of the lifetime of the ⁵D₀ and ⁵D₁ levels of Eu³⁺-doped fibre has been presented in reference 142.

7.4 COMPARISON OF THE FLUORESCENCE INTENSITY RATIO AND FLUORESCENCE LIFETIME TECHNIQUES

The sensitivity of several materials which have been tested for the fluorescence intensity ratio and fluorescence lifetime temperature sensing techniques are listed in table 7.6. This data shows that the sensitivity of both techniques depend strongly upon sensor material and temperature. Therefore the temperature range over which measurements are required for a particular application should be known before an informed choice of sensing material and technique can be made. When the sensitivities for the two techniques are compared for specific sensor materials (i.e. Pr³⁺:ZBLAN, Eu³⁺ silica fibre and Yb³⁺ silica fibre) the fluorescence intensity ratio technique appears to have better temperature sensitivity over the range of temperatures listed. This however should not be taken as a general rule as the temperature sensitivity of the lifetime of some of the materials listed (e.g. ruby, alexandrite and Cr³⁺:YAG) is of the same order of magnitude and in some cases even better than the values obtained for some materials with the fluorescence intensity ratio technique.

Sensor material	Sensitivity (%/°C)		Technique [Ref.]
	@ 20 °C	@ 200 °C	
Pr ³⁺ :ZBLANP	1.15	0.44	FIR [this work]
Nd ³⁺ silica fibre	1.64	0.63	FIR [this work]
Sm ³⁺ silica fibre	1.85	0.71	FIR [this work]
Eu ³⁺ silica fibre	0.14	0.65	FIR [this work]
Dy ³⁺ silica fibre	1.30	0.66	FIR [this work]
Yb ³⁺ silica fibre	0.94	0.61	FIR [this work]
Pr ³⁺ :ZBLANP	0.12	0.08	FLT [*]
Eu ³⁺ silica fibre	0.03	0.07	FLT [this work]
Yb ³⁺ silica fibre	0.031	0.033	FLT [34]
Ruby	0.24	0.96	FLT [*]
Alexandrite	1.15	0.46	FLT [*]
Cr ³⁺ :YAG	1.3	0.7	FLT [*]

*Table 7.6: Comparison between the sensitivity of materials used in the fluorescence intensity ratio technique and those used in fluorescence lifetime based temperature sensing, FIR - fluorescence intensity ratio, FLT - fluorescence lifetime, * - calculated using data from reference 36.*

7.5 CONCLUSION

The fluorescence lifetime characteristics of Yb³⁺ and Eu³⁺-doped silica fibres have been investigated over a wide range of temperatures. For both of the rare earth ions studied the lifetimes measured showed significant and useful changes with temperature and potentially can be used as a means of measuring temperature.

Chapter 8: Discussion and Conclusion

- 8.1 INTRODUCTION
- 8.2 SUMMARY OF FLUORESCENCE INTENSITY RATIO STUDIES
- 8.3 COMPARISON OF THE FLUORESCENCE INTENSITY RATIO METHOD WITH
COMMERCIALLY AVAILABLE FIBRE OPTIC TEMPERATURE SENSORS
- 8.4 OTHER RECENT WORK ON FLUORESCENCE INTENSITY BASED TEMPERATURE
SENSING
- 8.5 FUTURE WORK
- 8.6 CONCLUSION

Overview of Chapter

The following chapter provides a summary of the work presented in this thesis, a comparison between commercially successful optical fibre temperature sensors and the fluorescence intensity ratio technique and a discussion on possible future work which could be undertaken in the area of fluorescence intensity ratio temperature sensing.

8.1 INTRODUCTION

The final chapter of this thesis begins with a summary of the main results obtained in studies of the fluorescence intensity ratio technique of temperature sensing. To put the work in context these results are then compared to the performance characteristics of commercially available fibre optic temperature sensors. Finally areas of future research in the fluorescence intensity ratio method of temperature sensing are given.

8.2 SUMMARY OF FLUORESCENCE INTENSITY RATIO STUDIES

The aim of the work presented in this thesis was to investigate the feasibility of developing a relatively low cost optical fibre based temperature sensor using the fluorescence intensity ratio technique, with similar or better performance characteristics to commercially available devices. To achieve this goal the fluorescence intensity ratio method of temperature sensing was studied for pairs of closely spaced energy levels in six different rare earth ions. Three of the rare earth ions investigated were subsequently used in studies of the stability of the fluorescence intensity ratio and in the development of working sensor prototypes. The main conclusions of the work undertaken are given in more detail below.

In chapter 3 the basic theory of the fluorescence intensity ratio technique of temperature sensing, the Boltzmann distribution, was introduced. This theory was also expanded to show how overlap of fluorescence from the two thermalised energy levels and stray light can reduce the sensitivity and hence accuracy of the fluorescence intensity ratio method.

Prior to the commencement of this thesis the only materials to have been studied for use with the fluorescence intensity ratio technique of temperature sensing were Eu^{3+} -doped phosphors, ruby and the Er^{3+} ion doped in silica and fluoride fibre. In chapter 4 the fluorescence intensity ratio versus temperature characteristics of the Pr^{3+} , Nd^{3+} , Sm^{3+} , Eu^{3+} , Dy^{3+} and Yb^{3+} rare earth ions were presented. The fluorescence transitions originating from thermally coupled energy levels in these rare earth ions were studied using a variety of host materials and excitation schemes. Details of the materials and the transitions investigated are given in table 8.1. Several of the rare earth ions studied in this work offer significant improvements, with respect to their use in temperature sensing, over the materials studied previously. These improvements include lower

excitation power, which should help to reduce sensor cost, and increased measurement sensitivity. The fluorescence intensity ratio of the majority of rare earth ions investigated followed the predicted Boltzmann distribution behaviour with temperature. A notable exception to this however was the Eu^{3+} ion. For this material the results obtained suggest that for the relatively large energy gap between the thermalising energy levels ($\sim 1750 \text{ cm}^{-1}$), and at temperatures less than approximately $80 \text{ }^\circ\text{C}$, other processes may predominate over the Boltzmann distribution.

Rare earth ion	Thermalising levels	Energy gap	Transitions investigated	Host materials
Pr^{3+}	$^3\text{P}_0, ^3\text{P}_1+^1\text{I}_6$	580 cm^{-1}	$^3\text{H}_5, ^1\text{G}_4$	ZBLANP, silica fibre, aluminosilica fibre
Nd^{3+}	$^4\text{F}_{3/2}, ^4\text{F}_{5/2}$	1000 cm^{-1}	$^4\text{I}_{13/2}, ^4\text{I}_{11/2}, ^4\text{I}_{9/2}$	YAG, YVO_4 , ZBLANP, silica fibre
Sm^{3+}	$^4\text{F}_{3/2}, ^4\text{G}_{5/2}$	1000 cm^{-1}	$^6\text{H}_{5/2}$	silica fibre
Eu^{3+}	$^5\text{D}_0, ^5\text{D}_1$	1750 cm^{-1}	$^7\text{F}_1, ^7\text{F}_2$	silica fibre
Dy^{3+}	$^4\text{I}_{15/2}, ^4\text{F}_{9/2}$	1000 cm^{-1}	$^6\text{H}_{13/2}$	silica fibre
Yb^{3+}	$^2\text{F}_{5/2(a)}, ^2\text{F}_{5/2(b)}$	680 cm^{-1}	$^2\text{F}_{7/2}$	silica fibre

Table 8.1: Summary of the rare earth ions, thermalising levels, energy gaps, transitions and host materials used in the fluorescence intensity ratio versus temperature studies presented in chapter 4.

The stability of the fluorescence intensity ratio with excitation wavelength, excitation power, doped fibre length and applied strain was investigated in chapter 5. Measurements of the effect of variations in the excitation wavelength and intensity indicated that amplified spontaneous emission and site-selective effects can introduce changes in the fluorescence intensity ratio. The errors caused by such changes however can be minimised (i.e. $< 0.1 \text{ }^\circ\text{C}$) through sensible design rather than requiring costly stabilised excitation. The effect of changes in doped fibre length on the fluorescence intensity ratio suggest that for transitions which terminate at the ground state the errors introduced by wavelength dependent re-absorption may require individual sensor calibration. Results for fluorescence lifetime based temperature sensors [142] indicate that individual sensor calibration is also required and therefore this is not a major disadvantage for fluorescence intensity ratio based sensors.

Another significant finding reported in chapter 5 is the near zero temperature-strain cross-sensitivity of Yb^{3+} -doped silica fibre. In many of the environments in which such sensors are used the sensor may be subject to varying strains. Many optical fibre based temperature sensing techniques however are strain-temperature cross-sensitive and therefore compensation for strain induced errors is required for accurate

temperature measurement. A sensor that does not require such compensation should simplify the measurement process and as a consequence provide cost benefits.

The details of the development of sensor prototypes using Pr^{3+} :ZBLANP, Yb^{3+} -doped silica fibre and Nd^{3+} -doped silica fibre as the sensing material have been given in chapter 6. A summary of the dimensions, excitation parameters, temperature ranges and measurement accuracy of the sensor prototypes reported is given in table 8.2. The results obtained with these preliminary sensors suggest that a temperature sensor could be constructed using the fluorescence intensity ratio technique to measure temperatures over a range of approximately $-50\text{ }^{\circ}\text{C}$ to $600\text{ }^{\circ}\text{C}$ with an accuracy of better than $1\text{ }^{\circ}\text{C}$. This measurement range covers a large portion of the temperatures measured by commercially available devices, while the measurement accuracy, which should be improved through improvements in sensor design, is comparable. The excitation source required by such a sensor would have output powers of approximately 10^3 's of milliwatts at wavelengths near 800 nm or 840 nm. These devices are widely available at relatively low cost.

Sensing material	Sensor dimensions	Excitation		Temp. range ($^{\circ}\text{C}$)	σ_T ($^{\circ}\text{C}$)
		λ (nm)	P (mW)		
Pr^{3+} :ZBLANP	Rod, diameter = 8mm, length = 40mm, 1%	450	2	$-45 \rightarrow +255$	0.38
Yb^{3+} -doped silica fibre (a) (b)	14 cm, 40 μm , 2500 ppm	810	30	$30 \rightarrow 610$	0.44
	25 cm, 5.2 μm , 2500 ppm	843	2.5	$33 \rightarrow 500$	1.3
Nd^{3+} -doped silica fibre	59 cm, 5 μm , 500 ppm	808	13	$0 \rightarrow 500$	2.3

Table 8.2: Details of fluorescence intensity ratio prototype sensors reported in this thesis. λ - wavelength, P – power, σ_T – measurement accuracy.

To compare the results obtained using the fluorescence intensity ratio technique with a well known optical fibre based temperature sensing technique, the fluorescence lifetime behaviour of Yb^{3+} and Eu^{3+} -doped fibre was investigated in chapter 7. For both the materials studied the lifetime showed useful variations with temperature. Using this data, together with data presented in chapter 4 and previously published on the lifetime technique, the sensitivity of the two techniques were compared. In general the fluorescence intensity ratio technique has superior sensitivity at temperatures close to and below ambient in comparison to the fluorescence lifetime technique. At higher

temperatures however it is difficult to draw any definite conclusions as the sensitivity is largely dependent upon the dopant ion used to determine temperature.

8.3 COMPARISON OF THE FLUORESCENCE INTENSITY RATIO METHOD WITH COMMERCIALY AVAILABLE FIBRE OPTIC TEMPERATURE SENSORS

A recent compilation of commercially available fibre optic temperature sensors [7] shows that the majority of these devices are based on either blackbody radiation, Raman backscatter or fluorescence decay time processes. The first of these processes appears to be best suited to the measurement of temperatures well above ambient. At lower temperatures however the reduced levels of thermal radiation reduce measurement accuracy. Temperature sensors based on Raman backscatter on the other hand appear to have captured the market for distributed sensors due to their ability to measure temperature over large distances with a reasonable degree of accuracy. The relatively high price and limited spatial resolution (approximately 1 m) of the latter technique however restrict it being used for a large number of applications where temperature is to be measured at one precise location.

Of the common optical fibre based temperature sensing devices the fluorescence lifetime technique appears to most closely match the performance of the fluorescence intensity ratio method. In order to successfully compete with fluorescence lifetime based sensors, fluorescence intensity ratio sensors would need to show improvements in either measurement range, accuracy and/or cost. For both of these techniques however the measurement accuracy and measurable temperature range depend upon the sensing material. The recent reports of strain-temperature cross-sensitivity in the fluorescence lifetime method and the relative insensitivity of the fluorescence intensity ratio technique suggest that in measurement environments in which the sensing material is subject to variations in applied strain a sensor based on the fluorescence intensity ratio technique would be more appropriate. Therefore the most appropriate measurement technique will depend upon the particular application in which the sensor is to be used and the cost of the sensor, which is yet to be determined for the fluorescence intensity ratio technique.

8.4 OTHER RECENT WORK ON FLUORESCENCE INTENSITY BASED TEMPERATURE SENSING

Since the commencement of this thesis other groups [47, 48] have reported research on the fluorescence intensity ratio technique. This other work, outlined in chapter 1, has mainly investigated the effect of the host material on the fluorescence intensity ratio technique using the Er^{3+} ion. As indicated in this thesis the use of different host materials may allow lower power excitation sources to be used leading to cost reductions.

Aside from fluorescence intensity ratio based work, other research on fluorescence based temperature sensing appears to be focussed on the fluorescence lifetime technique and the use of changes in the amplified spontaneous emission spectra of Er^{3+} -doped fibre to measure temperature. Both of these techniques make use of the same physical principle that is used in the fluorescence intensity ratio technique of temperature sensing, i.e. the thermal coupling of closely spaced energy levels. The work presented in this thesis therefore may provide information which is useful to the further development of not only fluorescence intensity ratio based temperature sensors but fluorescence lifetime and amplified spontaneous emission based temperature sensors.

8.5 FUTURE WORK

The fluorescence intensity ratio technique appears to be roughly at the mid-point in the development of a commercial sensor with further work possible on both the fundamental aspects of the fluorescence intensity ratio technique and on the development of a practical sensor.

In terms of further work on the fundamental aspects of the technique there are still a large number of combinations of host materials and rare earth ions that could be investigated. Such combinations offer potential improvements in:

- measurement range - as introduced in chapter 2 one of the main limitations on the range of temperatures which can be measured using the fluorescence intensity ratio technique is the host material. The use of crystalline host materials, such as YAG which was studied with the Nd^{3+} rare earth ion in this work, may offer increased measurement range compared to the materials tested to date. For these host materials to be useful however the issue of connection with the doped fibres used for excitation and fluorescence capture need to be addressed.

- accuracy - the accuracy of temperature measurement with the fluorescence intensity ratio technique depends upon how accurately the fluorescence from each of the thermalising energy levels can be measured and the sensitivity of the fluorescence intensity ratio to changes in temperature. Increases in the fluorescence intensity from the thermalising levels may be possible through the use of different host materials. As for the sensitivity, the imminent availability of blue laser diodes may open the possibility of using thermally coupled levels which are yet to be investigated.
- excitation wavelength and power - the absorption spectrum of a specific rare earth ion depends upon the host material, and therefore the wavelength ranges and magnitude of absorption at a specific wavelength can be altered via changes in the host material. This may present cost savings through the use of lower power laser diodes at commonly available wavelengths.

Some of the other areas in which additional fundamental research could be performed include further measurements on the effect of strain on the fluorescence intensity ratio for other rare earth doped materials, investigating the possibility of using the fluorescence intensity ratio in remote measurements which has already achieved using the lifetime technique [136], and studying the effect of annealing on the fluorescence intensity ratio.

There are many issues which still need to be addressed in the area of sensor development, foremost of which is probably the issue of the accuracy of measurement. As outlined in chapter 3 the accuracy depends upon the combination of how precisely the fluorescence from each of the thermalising energy levels can be measured and the sensitivity of the fluorescence intensity ratio to changes in temperature. Improvements in the accuracy to which the fluorescence of each of the levels is measured should be achievable through increases in the intensity of fluorescence and the measurement/signal-processing technique used. As for the sensitivity the energy gap between the thermalising levels, the extent of overlap of fluorescence from the thermalising levels and the amount of stray light all have an effect. Other areas of sensor development which require further investigation include reduction of the dimensions of the sensing element, and testing of the long term stability and the repeatability of measurement.

8.6 CONCLUSION

The fluorescence intensity ratio technique has been studied for potential use in optical fibre based temperature sensing. This included a study of the thermal characteristics of suitable pairs of energy levels in six different rare earth ions (Pr^{3+} , Nd^{3+} , Sm^{3+} , Eu^{3+} , Dy^{3+} and Yb^{3+}) doped in a variety of host materials. The results of these tests indicated that the fluorescence intensity ratio technique can be used to measure temperature over a broad range, temperatures between $-186\text{ }^{\circ}\text{C}$ and $+500\text{ }^{\circ}\text{C}$ were tested. Several of the rare earth doped materials were subsequently used to measure the stability of the fluorescence intensity with variations in excitation power, excitation wavelength, doped fibre length and applied strain. The results of these tests indicate that the fluorescence intensity ratio is relatively stable against changes in these parameters, indicating that expensive excitation stabilisation and strain compensation should not be required, thus reducing the potential cost of such a sensor. Finally, prototype fluorescence intensity ratio based sensors were developed using three of the sensing materials tested. Measurements with these prototypes show that the fluorescence intensity ratio technique can be used to measure temperature over a wide range (the prototypes were tested between $-50\text{ }^{\circ}\text{C}$ and $+610\text{ }^{\circ}\text{C}$) with measurement accuracies in the order of $1\text{ }^{\circ}\text{C}$.

I believe that the work presented in this thesis demonstrates that the fluorescence intensity ratio technique has a high probability of being successfully developed to provide a temperature sensor which will compete with currently available commercial systems.

References

- [1] T.D. McGee, *Principles and Methods of Temperature Measurement*, (John Wiley and Sons, New York), 1988.
- [2] R.P. Benedict, *Fundamentals of Temperature, Pressure, and Flow Measurements*, (John Wiley and Sons, New York), 1977.
- [3] The New Encyclopædia Britannica, (Encyclopædia Britannica Inc., Chicago), Vol. 23, pp. 734-741, 1990.
- [4] J. Dakin and B. Culshaw, *Optical Fiber Sensors: principles and components*, (Artech House, Boston), Vol. 1, 1988.
- [5] B. Culshaw and J. Dakin, *Optical Fiber Sensors: systems and applications*, (Artech House, Boston), Vol. 2, 1989.
- [6] J. Dakin and B. Culshaw, *Optical Fiber Sensors: components and subsystems*, (Artech House, Boston), Vol. 3, 1996.
- [7] J. Dakin and B. Culshaw, *Optical Fiber Sensors: applications, analysis and future trends*, (Artech House, Boston), Vol. 4, 1997.
- [8] K.T.V. Grattan and B.T. Meggitt, *Optical Fiber Sensor Technology*, Chapman and Hall, London, 1995.
- [9] K.T.V. Grattan and Z.Y. Zhang, *Fiber Optic Fluorescence Thermometry*, Chapman and Hall, London, p. 138, 1995.
- [10] J.P. Dakin and D.A. Kahn, "A novel fiber optic temperature probe", *Opt. Quant. Electron.*, **9**, p. 540, 1977.
- [11] M. Gottlieb and G.B. Brandt, "Fiber-optic temperature sensor based on internally generated thermal radiation", *Appl. Opt.*, **20**, pp. 3408-3414, 1981.
- [12] R.R. Dils, "High-temperature optical fiber thermometer", *J. Appl. Phys.*, **54**, pp. 1198-1201, 1983.
- [13] S.R. Mordon, B. Buys and Y. Moschetto, "Zirconium fluoride glass fiber radiometer for low temperature measurements", *J. Lightwave Tech.*, **7**, pp. 1097-1100, 1989.
- [14] T.D. McGee, *Principles and Methods of Temperature Measurement*, (John Wiley and Sons, New York), pp. 58-98, 1988.
- [15] Luxtron Corp., Accufiber models 10 and 100 - optical fiber thermometers, Publicity data, Luxtron Corp., Santa Clara, California, USA.
- [16] K. Kyuma, S. Tai, T. Sawada and M. Nunoshita, "Fiber-optic instrument for temperature measurement", *IEEE J. Quantum Electron.*, **QE-18**, pp. 676-679, 1982.
- [17] A.P. Appleyard, P.L. Scrivener and P.D. Maton, "Intrinsic optical fiber temperature sensor based on the differential absorption technique", *Rev. Sci. Instrum.*, **10**, pp. 2650-2654, 1990.
- [18] M.C. Farries, M.E. Fermann, R.I. Laming, S.B. Poole, D.N. Payne and A.P. Leach, "Distributed temperature sensor using Nd³⁺-doped optical fibre", *Electron. Lett.*, **22**, pp. 418-419, 1986.
- [19] A. H. Hartog, "A distributed temperature sensor based on liquid-core optical fibers", *J. Lightwave Tech.*, **LT-1**, pp. 498-509, 1983.
- [20] K.T.V. Grattan and B.T. Meggitt, *Optical Fiber Sensor Technology*, Chapman and Hall, London, p. 332, 1995.

- [21] J.P. Dakin, D.J. Pratt, G.W. Bibby and J.N. Ross, "Distributed optical fibre Raman temperature sensor using a semiconductor light source and detector", *Electron. Lett.*, **21**, pp. 569-570, 1985.
- [22] York Sensors Ltd., DTS-800 distributed temperature sensor, Publicity data, York Sensors Ltd., Romsey, Hampshire, UK, 1998.
- [23] G.P. Lees, P.C. Wait, M.J. Cole and T.P. Newson, "Advances in optical fiber distributed temperature sensing using the Landau-Placzek ratio", *IEEE Photon. Technol. Lett.*, **10**, pp. 126-128, 1998.
- [24] G.B. Hocker, "Fiber-optic sensing of pressure and temperature", *Appl. Opt.*, **18**, pp. 1445-1448, 1979.
- [25] M. Corke, A.D. Kersey, D.A. Jackson and J.D.C. Jones, "All-fibre 'Michelson' thermometer", *Electron. Lett.*, **19**, pp.471-473, 1983.
- [26] S.C. Kaddu, S.F. Collins and D.J. Booth, "Multiplexed intrinsic optical fibre Fabry-Perot temperature and strain sensors addressed using white-light interferometry", *Meas. Sci. Technol.*, **10**, pp. 416-420, 1999.
- [27] K.O. Hill, F. Fujii, D.C. Johnson and B.S. Kawaski, "Photosensitivity of optical fibre waveguides: application to reflection filter fabrication", *Appl. Phys. Lett.*, **32**, pp. 647-649, 1978.
- [28] Y.J. Rao, "In-fibre Bragg gratings", *Meas. Sci. Technol.*, **8**, pp. 355-375, 1997.
- [29] S. Gupta, T. Mizunami, T. Yamao and T. Shimomura, "Fiber Bragg grating cryogenic temperature sensors", *Appl. Opt.*, **35**, pp. 5202-5205, 1996.
- [30] K.T.V. Grattan and Z.Y. Zhang, *Fiber Optic Fluorescence Thermometry*, (Chapman and Hall, London), 1995.
- [31] Z.Y. Zhang, K.T.V. Grattan, A.W. Palmer, V. Fericola and L. Crovini, "Temperature dependence of the YAG:Cr³⁺ fluorescence lifetime over the range 77 to 900 K", *Phys. Rev. B*, **51**, pp. 2656-2660, 1995.
- [32] T. Sun, Z.Y. Zhang, K.T.V. Grattan, A.W. Palmer and S.F. Collins, "Temperature dependence of the fluorescence lifetime of Pr³⁺:ZBLAN glass for fiber optic thermometry", *Rev. Sci. Instrum.*, **68**, pp. 3447-3451, 1997.
- [33] Z.Y. Zhang, K.T.V. Grattan, A.W. Palmer, B.T. Meggitt and T. Sun, "Characterisation of erbium-doped intrinsic optical fiber sensor probes at high temperatures", *Rev. Sci. Instrum.*, **69**, pp. 2924-2929, 1998.
- [34] T. Sun, Z.Y. Zhang, K.T.V. Grattan and A.W. Palmer, "Ytterbium-based fluorescence decay time fiber optic temperature sensor systems", *Rev. Sci. Instrum.*, **69**, pp. 4179-4185.
- [35] Z.Y. Zhang, K.T.V. Grattan, A.W. Palmer and B.T. Meggitt, "Spectral characteristics and effects of heat treatment on intrinsic Nd-doped fibre thermometer probes", *Rev. Sci. Instrum.*, **69**, pp. 139-145, 1998.
- [36] S.F. Collins, G.W. Baxter, S.A. Wade, T. Sun, K.T.V. Grattan, Z.Y. Zhang and A.W. Palmer, "Comparison of fluorescence-based temperature sensor schemes: theoretical analysis and experimental validation", *J. Appl. Phys.*, **84**, pp. 4649-4654, 1998.
- [37] K.A. Wickersheim and M.H. Sun, "Fiberoptic thermometry and its applications", *J. Microwave Power*, **22**, pp. 85-94, 1987.
- [38] Fiberoptic probes and accessories for Model 790 systems, Luxtron Corp., Santa Clara, California, USA.
- [39] O. Svelto, *Principles of Lasers*, (Plenum Press, New York), 3rd ed., pp. 70-71, 1989.

- [40] W. Koechner, *Solid-State Laser Engineering*, (Springer-Verlag, Berlin), pp. 3-4, 1992.
- [41] H. Kusama, O.J. Sovers and T. Yoshioka, "Line shift method for phosphor temperature measurements", *Japanese J. Appl. Phys.*, **15**, pp. 2349-2358, 1976.
- [42] R.V. Alves, J. Christol, M. Sun and K.A. Wickersheim, "Fluoroptic thermometry: temperature sensing using optical fibers", *Advances in Instrumentation*, **38**, pp. 925-932, 1983.
- [43] K.A. Wickersheim and R.B. Alves, "Recent advances in optical temperature measurement", *Ind. Res. Dev.*, **21**, pp. 84-89, 1979.
- [44] B.A. Weinstein, "Ruby thermometer for cryobaric diamond-anvil cell", *Rev. Sci. Instrum.*, **57**, pp. 910-913, 1986.
- [45] H. Berthou and C.K. Jörgensen, "Optical-fiber temperature sensor based on upconversion-excited fluorescence", *Opt. Lett.*, **15**, pp. 1100-1102, 1990.
- [46] E. Maurice, G. Monnom, B. Dussardier, A. Saïssy, D.B. Ostrowsky and G.W. Baxter, "Erbium-doped silica fibers for intrinsic fiber-optic temperature sensors", *Appl. Opt.*, **34**, pp. 8019-8025, 1995.
- [47] E. Maurice, G. Monnom, D.B. Ostrowsky and G.W. Baxter, "1.2- μm transitions in erbium-doped fibers: the possibility of quasi-distributed temperature sensors", *Appl. Opt.*, **34**, pp. 4196-4199, 1995.
- [48] E. Maurice, *Phénomènes multiphotoniques dans les fibres optiques de silice dopée terres rare a application à un capteur de température*, PhD thesis, University of Nice-Sophia Antipolis, 1994.
- [49] G.S. Maciel, L. De S. Menezes, A.S.L. Gomes, Cid B. De Araújo, Y. Messaddeq, A. Florez and M.A. Aegerter, "Temperature sensor based on frequency upconversion in Er^{3+} -doped fluorindate glass", *IEEE Photon. Technol. Lett.*, **7**, pp. 1474-1476, 1995.
- [50] P.V. dos Santos, M.T. De-Araujo, A.S. Gouveia, J.A.M. Neto and A.S.B. Sombra, "Optical thermometry through infrared excited upconversion fluorescence emission in Er^{3+} - and $\text{Er}^{3+}/\text{Yb}^{3+}$ -doped chalcogenide glasses", *IEEE J. Quantum Electron.*, **35**, pp. 395-399, 1999.
- [51] C. Ovrén, M. Adolfsson and B. Hök, "Fiber-optic systems for temperature and vibration measurements in industrial applications", *Optics and Lasers in Engineering*, **5**, pp. 155-172, 1984.
- [52] Y. Imai, T. Hokazono and T. Yoshida, "Temperature sensing using 1.54 μm fluorescence in erbium-doped optical fibers", 11th Optical Fiber Sensors Conf. Sapporo, Japan, pp. 268-271, 1996.
- [53] J. Jung and B. Lee, "Erbium-doped fiber temperature sensor with high resolution using 1480 nm pump source", 13th Optical Fiber Sensors Conf., Kyongju, Korea, pp. 538-541, 1999.
- [54] J. Jung, H. Nam, J.H. Lee, N. Park and B. Lee, "Simultaneous measurement of strain and temperature by use of a single-fiber Bragg grating and an erbium-doped fiber amplifier", *Appl. Opt.*, **38**, pp. 2749-2751, 1999.
- [55] W. Koechner, *Solid-State Laser Engineering*, (Springer-Verlag, Berlin), pp. 35-36, 1992.
- [56] L.A. Riseberg and M.J. Weber, "Relaxation phenomenon in rare earth luminescence", in *Progress in Optics Vol. XIV*, ed. E. Wolf (North-Holland, Amsterdam), pp. 89-159, 1976.

- [57] W.J. Miniscalco, "Optical and electronic properties of rare earth ions in glasses", in *Rare Earth Doped Fiber Lasers and Amplifiers*, ed. M.J.F. Digonnet, (Marcel Dekker, New York), pp. 19-133, 1993.
- [58] E. Desurvire, *Erbium Doped Fiber Amplifiers*, (John Wiley and Sons, New York), pp. 210-226, 1994.
- [59] W. Koechner, *Solid-State Laser Engineering*, (Springer-Verlag, Berlin), pp. 11-12, 1992.
- [60] W.S. Brocklesby, "High-resolution spectroscopy of ions in optical fibers", *Annu. Rev. Mater. Sci.*, **23**, pp. 193-221, 1993.
- [61] M.J. Weber, "Laser excited fluorescence spectroscopy in glass", in *Laser Spectroscopy of Solids*, ed. W.M. Yen and P.M. Selzer, (Springer-Verlag, Berlin), pp. 189-240, 1981.
- [62] J.R. Simpson, "Rare earth doped fiber fabrication: techniques and physical properties", in *Rare Earth Doped Fiber Lasers and Amplifiers*, ed. M.J.F. Digonnet, (Marcel Dekker, New York), pp. 1-18, 1993.
- [63] K. Arai, H. Namikawa, K. Kumata, T. Honda, Y. Ishii and T. Handa, "Aluminium or phosphorus co-doping effects on the fluorescence and structural properties of neodymium-doped silica glass", *J. Appl. Phys.*, **59**, pp. 3430-3436, 1986.
- [64] B.J. Ainsley, S.P. Craig and S.T. Davey, "The fabrication and optical properties of Nd³⁺ in silica-based optical fibres", *Mater. Lett.*, **5**, pp. 143-146, 1987.
- [65] C.J. Koester and E. Snitzer, "Amplification in a fiber laser", *Appl. Opt.*, **3**, pp. 1182-1186, 1964.
- [66] S.B. Poole, D.N. Payne and M.E. Fermann, "Fabrication of low-loss optical fibres containing rare-earth ions", *Electron. Lett.*, **21**, pp. 737-738, 1985.
- [67] S.B. Poole, D.N. Payne, R.J. Mears, M.E. Fermann and R.I. Laming, "Fabrication and characterisation of low-loss optical fibers containing rare-earth ions", *J. Lightwave Tech.*, **4**, pp. 870-876, 1986.
- [68] J.E. Townsend, S.B. Poole and D.N. Payne, "Solution-doping technique for fabrication of rare-earth-doped optical fibres", *Electron. Lett.*, **23**, pp. 329-331, 1987.
- [69] J.S. Sanghera and I.D. Aggarwal, "Rare earth doped heavy-metal fluoride glass fibers", in *Rare Earth Doped Fiber Lasers and Amplifiers*, ed. M.J.F. Digonnet, (Marcel Dekker, New York), pp. 423-495, 1993.
- [70] S. Takahashi and H. Iwasaki, "Preform and fibre fabrication", in *Fluoride Glass Fiber Optics*, eds. I.D. Aggarwal and G. Lu, (Academic Press, Boston), pp. 213-233, 1991.
- [71] *Handbook of Optics*, Ed. M. Bass (McGraw-Hill, New York), Vol. II, pp. 33.34-33.55, 1995.
- [72] T.S. Izumitani, *Optical Glass*, (American Institute of Physics, New York), 1986.
- [73] VLOC catalog, VLOC - subsidiary of II-VI Inc., New Port Richey, Florida, USA.
- [74] *The Properties of Optical Glass*, eds. H. Bach and N. Neuroth, (Springer, Berlin), pp. 308-309, 1995.
- [75] *Glass - an Engineering Material*, ed. W.F. Waller (Morgan-Grampian, Kent), p. 10, 1969.
- [76] Schott glass catalog, Schott Glass Technologies Inc., Duryea, Pennsylvania, USA.

- [77] M Poulain, "Fluoride glass composition and processing", in *Fluoride Glass Fiber Optics*, eds. I.D. Aggarwal and G. Lu, (Academic Press, Boston), pp. 1-35, 1991.
- [78] C.F. Rapp, "Laser glasses", in *CRC Handbook of Laser Science and Technology, Supplement 2: Optical Materials*, ed. M.J. Weber, (CRC Press, Boca Raton, USA), pp. 619-634, 1995.
- [79] W. Koechner, *Solid-State Laser Engineering*, (Springer-Verlag, Berlin), p. 71, 1992.
- [80] H.E. Hagy, W.H. Barney, J.S. McCartney, C.J. Parker, W.A. Plummer and F.V. Tooley, "Physical properties of glass", in *The Handbook of Glass Manufacture – Vol. II*, ed. F.V. Tooley, (Ashlee Publishing Co., New York, 3rd ed.), pp. 893-956, 1984.
- [81] E. Milcent, G. Olalde, J.F. Robert, D. Hernandez and M. Clement, "Influence of high temperatures on a fiber-optic probe for temperature measurement", *Appl. Opt.*, **33**, pp. 5882-5887, 1994.
- [82] T.D. McGee, *Principles and Methods of Temperature Measurement*, (John Wiley and Sons, New York), pp. 319-341, 1988.
- [83] H. Nagata, "Thermal analysis of jacketing materials for commercial optical fibers", *Optical Fiber Technol.*, **3**, pp. 87-89, 1997.
- [84] Private communications, J. D'Andrea, Fiberguide Industries Inc., Stirling, New Jersey, USA.
- [85] P.W. France, "Extrinsic absorption", in *Fluoride Glass Optical Fibers*, ed. P.W. France, (Blackie, Florida), pp. 165-167, 1990.
- [86] G.W. Baxter, G. Monnom and E. Maurice, "Thermal variation of absorption in Yb³⁺-doped silica fibre for high-temperature sensor applications", *Fibre Optic and Laser Sensors*, ed. R.P. DePaula and J.W. Berthold III, *Proc. SPIE* **2510**, pp. 293-296, 1995
- [87] P. Cross, Database LASERS – energy level tables, NASA Langley Research Centre, <http://aesd.larc.nasa.gov:8010/laserdbmain.htm>.
- [88] S.A. Wade, J.C. Muscat, S.F. Collins and G.W. Baxter, "Nd³⁺-doped optical fiber temperature sensor using the fluorescence intensity ratio technique", *Rev. Sci. Instrum.*, **70**, pp. 4279-4282, 1999.
- [89] E. Maurice, G. Monnom, G.W. Baxter, S.A. Wade, B.P. Petreski and S.F. Collins, "Blue LED-pumped point temperature sensor based on a fluorescence intensity ratio in Pr³⁺:ZBLAN glass", *Opt. Rev.*, **4**, pp. 89-91, 1997.
- [90] E. Maurice, S.A. Wade, S.F. Collins, G. Monnom and G.W. Baxter, "Self-referenced point temperature sensor based on a fluorescence intensity ratio in Yb³⁺-doped silica fiber", *Appl. Opt.*, **36**, pp. 8264-8269, 1997.
- [91] B.J. Ainslie, S.P. Craig and S.T. Davey, "The absorption and fluorescence spectra of rare earth ions in silica-based monomode fiber", *J. Lightwave Technol.*, **6**, pp. 287-293, 1988.
- [92] A.A. Kaminskii, *Laser Crystals: Their Physics and Applications*, (Springer-Verlag, Berlin), pp. 121-147, 1981.
- [93] M.M. Mann and L.G. DeShazer, "Energy levels and spectral broadening of neodymium ions in laser glass", *J. Appl. Phys.*, **41**, pp. 2951-2957, 1970.
- [94] W.F. Krupke, "Assessment of a promethium YAG laser", *IEEE J. Quantum Electron.*, **QE-8**, pp. 725-726, 1972.
- [95] M. Dejneka, E. Snitzer, and R.E. Riman, "Blue, green and red fluorescence and energy transfer of Eu³⁺ in fluoride glass", *J. Lumines.*, **65**, pp. 227-245, 1995.

- [96] J.L. Adam, A.D. Docq and J. Lucas, "Optical transitions of Dy³⁺ ions in fluorozirconate glass", *J. Solid State Chem.*, **75**, pp. 403-412, 1988.
- [97] J.Y. Allain, M. Monerie and H. Poignant, "Ytterbium-doped fluoride fibre laser operating at 1.02 μm", *Electron. Lett.*, **28**, pp. 988-989, 1992
- [98] Fluke 52 K/J thermometer – operators manual, Fluke Corp., Everett, Washington, USA, 1996.
- [99] M. Yamada and M. Shimizu, "Amplification characteristics of a fiber amplifier: components, design, and amplification characteristics of a fiber amplifier module", in *Optical Fiber Amplifiers: Materials, Devices, and Applications*, ed. S. Sudo, (Artech House, Boston), pp. 534-571, 1997.
- [100] J.Y. Allain, M. Monerie and H. Poignant, "Tunable cw lasing around 610, 635, 695, 715, 885 and 910 nm in praseodymium-doped fluorozirconate fibre", *Electron. Lett.*, **27**, pp. 189-191, 1991.
- [101] R.M. Percival, M.W. Phillips, D.C. Hanna and A.C. Tropper, "Characterisation of spontaneous and stimulated emission from praseodymium (Pr³⁺) ions doped into a silica-based monomode optical fiber", *IEEE J. Quantum Electron.*, **25**, pp. 2119-2123, 1989.
- [102] J.M. Senior, *Optical Fiber Communications*, (Prentice Hall, Hertfordshire), pp. 119-121, 1992.
- [103] S.A. Wade, E. Maurice, B.P. Petreski, S.F. Collins and G.W. Baxter, "Temperature sensing using the thermalisation of the ³P₀ and ³P₁ levels of praseodymium", *Proc. 20th Australian Conference on Optical Fibre Technology*, Coolum Beach, pp. 331-334, 1995.
- [104] Melles Griot, *Optics Guide 5 catalog '97-'98*, Melles Griot, Irvine, California, USA, pp. 202-205.
- [105] Newport catalog '93, Newport Corp., Irvine, California, USA, p. B-49.
- [106] Edmund Scientific, *1998 Optical and Optical Instruments Catalog*, Edmund Scientific Co., Barrington, New Jersey, USA, pp. 58-59.
- [107] Oriel instruments catalog, *New products for light research*, Oriel Instruments, Stratford, Connecticut, USA, pp. 2-35.
- [108] S.A. Wade, S.F. Collins and G.W. Baxter, "Comparison of host materials for Nd³⁺ fluorescence intensity ratio based temperature sensing", *Eurosensors XII*, *Proc. 12th European Conf. on Solid State Transducers and the 9th UK Conf. on Sensors and their Applications*, Southampton, UK, 13-16 Sept., 1998, (ed. N.M. White), pp. 311-314.
- [109] S.A. Wade, S.F. Collins and G.W. Baxter, "Fluorescence intensity-ratio-based optical fibre temperature sensing using neodymium-doped materials", *Proc. 23rd Australian Conf. on Optical Fibre Technology*, Melbourne, pp. 189-192, 1998.
- [110] S.A. Wade, V.K. Bogdanov, S.F. Collins and G.W. Baxter, "Thermalisation of the ⁵D₀ and ⁵D₁ excited states in europium-doped optical fibre", *Proc. 13th Australian Institute of Physics National Congress*, Fremantle, pp. 327, 1998.
- [111] S. Wade, G. Monnom, S. Collins and G. Baxter, "Thermalisation of the ⁴F_{9/2} and ⁴I_{15/2} levels of Dy³⁺-doped silica fibre", *11th Australian Optical Society Conf.*, Adelaide, p. WP41, 1997.
- [112] S.A. Wade, S.F. Collins, G.W. Baxter, G. Monnom and E. Maurice, "Rare-earth doped fibres for fluorescence-based temperature sensing", *Proc. 24th Australian Conf. on Optical Fibre Technology*, Sydney, pp. 195-198, 1999.
- [113] J.M. Senior, *Optical Fiber Communications*, (Prentice Hall, Hertfordshire), 1992.

- [114] J.C. Palais, *Fiber Optic Communications*, (Prentice Hall, New Jersey), pp. 152-161, 1992.
- [115] Melles Griot, *Lasers and Instruments Guide*, Melles Griot, Irvine, California, USA, pp. D3-1 - D3-20.
- [116] Photonics 1996 catalog, Newport Corp., Irvine, California, USA, pp. 1-7 - 1-15.
- [117] M.J.F. Digonnet and E. Snitzer, "Nd³⁺ - and Er³⁺ -doped silica fiber lasers", in *Rare Earth Doped Fiber Lasers and Amplifiers*, ed. M.J.F. Digonnet, (Marcel Dekker, New York), pp. 245-247, 1993.
- [118] P.F. Wysocki, "Broadband operation of erbium- and neodymium-doped fiber sources", in *Rare Earth Doped Fiber Lasers and Amplifiers*, ed. M.J.F. Digonnet, (Marcel Dekker, New York), pp. 319-373, 1993.
- [119] P.R. Morkel, E.M. Taylor, J.E. Townsend and D.N. Payne, "Wavelength stability of Nd³⁺-doped fibre fluorescence sources", *Electron. Lett.*, **26**, pp. 873-875, 1990.
- [120] D.C. Hall, W.K. Burns and R.P. Moeller, "High-stability Er³⁺-doped superfluorescent fiber sources", *J. Lightwave Tech.*, **13**, pp. 1452-1460, 1995.
- [121] D.C. Hanna, I.R. Perry, R.G. Smart, P.J. Suni, J.E. Townsend and A.C. Tropper, "Efficient superfluorescent emission at 974 nm and 1040 nm from an Yb-doped fiber", *Optics Comm.*, **72**, pp. 230-234, 1989.
- [122] S.A. Wade, S.F. Collins, K.T.V. Grattan and G.W. Baxter, "Strain-independent temperature measurement using a fluorescence intensity ratio technique in optical fibre", *Appl. Opt.*, **39**, pp. 3050-3052, 1999.
- [123] S.A. Wade, G.W. Baxter, S.F. Collins, K.T.V. Grattan and T. Sun, "Simultaneous strain-temperature measurement using Yb-doped silica fiber", *Rev. of Sci. Instrum.*, **71**, pp. 2267-2269, 1999.
- [124] T. Sun, Z.Y. Zhang, K.T.V. Grattan and A.W. Palmer, "Intrinsic strain and temperature characteristics of Yb-doped silica-based optical fibers", *Rev. Sci. Instrum.*, **70**, pp. 1447-1451, 1999.
- [125] J.V. Nicholas and D.R. Whit, *Traceable Temperatures: An Introduction to Temperature Measurement and Calibration*, (John Wiley and Sons, Chichester, UK), p. 345, 1994.
- [126] A. Stringer, K.A. Ahmed, D.M. Burgess, G. Gitlits, J.S. Jasik, R.C. Kemp, S.A. Wade, G.W. Baxter and S.F. Collins, "Development and characterisation of a new dielectric cored OPGW", 45th Int. Wire and Cable Symp., Reno USA, pp. 68-76, 1996.
- [127] S.A. Wade, E. Maurice, G.W. Baxter, K.A. Ahmed, G. Monnom, S.F. Collins and A. Stringer, "Industrial application of fluorescence intensity ratio point temperature sensor", Proc. 21st Australian Conf. on Optical Fibre Technology, Surfers Paradise, pp. 290-293, 1996.
- [128] J.C. Muscat, S.A. Wade and G.W. Baxter, "Optical fibre temperature sensing based on the fluorescence intensity ratio from neodymium Nd³⁺ doped silica fibre", 11th Australian Optical Society Conf., Adelaide, p. FP43, 1997.
- [129] W.R. Philp, D.J. Booth, A. Shelamoff and M.J. Linthwaite, "A simple fibre optic sensor for measurement of vibrational frequencies", *Meas. Sci. Technol.*, **3**, pp. 603-606, 1992.
- [130] M.C. Vergara, S.A. Wade, G.W. Baxter, Y. He and S.F. Collins, "The application of an optical fibre temperature sensor in the investigation of window glass breakage in fires", Proc. of Interflam – Fire Science and Engineering Conf.,

Interscience Communications Ltd., Edinburgh, Scotland, 29 June – 1 July, pp. 1417-1422, 1999.

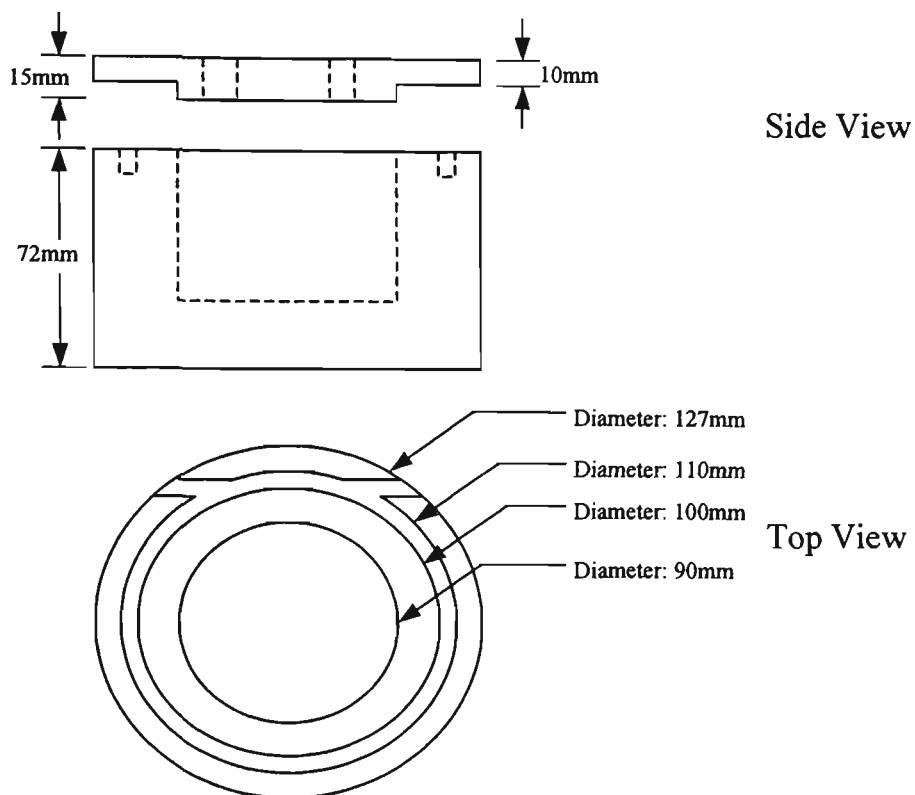
- [131] M.C. Vergara, S.A. Wade, Y. He, G.W. Baxter and S.F. Collins, “Optical fibre temperature sensing of the breakage of window glass during fires”, 12th Australian Optical Society Conf., Sydney, p. 36, 1999.
- [132] M.L. Janssens and H.C. Tran, “Data reduction of room tests for zone model validation”, *J. of Fire Sciences*, **10**, pp. 528-555, 1992.
- [133] T.S. Izumitani, *Optical Glass*, (American Institute of Physics, New York), pp. 74-83, 1986.
- [134] *The Handbook of Glass Manufacture – Vol. II*, ed. F.V. Tooley, (Ashlee Publishing Co., New York, 3rd ed.), pp. 801-805, 1984.
- [135] S.A. Wade, S.F. Collins, G.W. Baxter, T. Sun, Z.Y. Zhang, K.T.V. Grattan, and G. Monnom, “Fluorescence characteristics of several Yb-doped optical fibers for temperature sensing applications”, 13th Optical Fiber Sensors Conf., Kyongju, Korea, pp. 200-203, 1999.
- [136] S.W. Allison and G.T. Gillies, “Remote thermometry with thermographic phosphors: instrumentation and applications”, *Rev. Sci. Instrum.*, **68**, pp. 2615-2650, 1997.
- [137] K.R. German and A. Kiel, “Radiative and nonradiative transitions in LaCl₃:Pr and PrCl₃”, *Phys. Rev. B*, **8**, pp. 1846-1853, 1973.
- [138] W. Low, J. Makovsky and S. Yatsiv, “Fluorescence of rare earth ions upon X-ray excitation”, in *Quantum Electronics III*, ed. P. Grivet and N. Bloembergen, (Columbia U.P., New York), pp. 655-671, 1964.
- [139] W.D. Partlow and H.W. Moos, “Multiphonon relaxation in LaCl₃:Nd³⁺”, *Phys. Rev.*, **157**, pp. 252-256, 1967.
- [140] R. Reisfeld and C.K. Jørgensen, “Excited state phenomena in vitreous materials”, in *Handbook on the Physics and Chemistry of Rare Earths*, ed. K.A. Gshneidner Jr. and L. Eyring, (Elsevier Science), pp. 41-51, 1987.
- [141] S.A. Wade, P.M. Farrell, V.K. Bogdanov, S.F. Collins and G.W. Baxter, “Modelling of the temperature dependent lifetimes of thermally coupled levels in Eu³⁺-doped silica fibre”, Australasian Conf. on Optics, Lasers and Spectroscopy, Christchurch, NZ, pp. 204, 1998.
- [142] V.C. Fericola and R. Galleano, “Accuracy and calibration considerations for fiber optic temperature sensors”, *Fiber Optic and Laser Sensors XIV*, ed. R.P. DePaula and J.W. Berthold III, *Proc. SPIE* **2839**, pp. 248-252, 1996.

Appendix A: Sample holders for rare earth doped materials

- A.1 RARE EARTH DOPED FIBRE HOLDER
- A.2 Pr³⁺:ZBLANP SAMPLE HOLDER
- A.3 Nd³⁺:YAG SAMPLE HOLDER
- A.4 Nd³⁺:YVO₄ SAMPLE HOLDER
- A.5 Nd³⁺:ZBLANP SAMPLE HOLDER

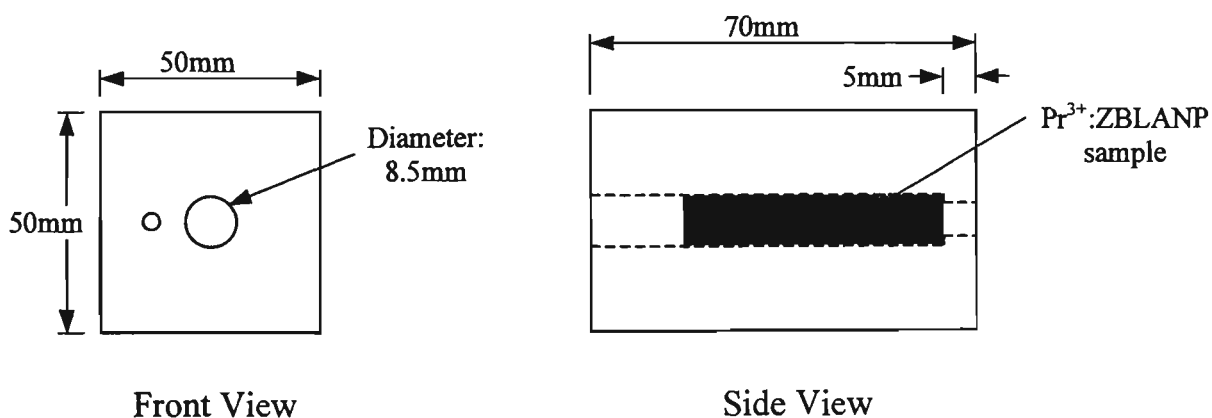
A.1 RARE EARTH DOPED FIBRE HOLDER

Mass: 1.771 kg



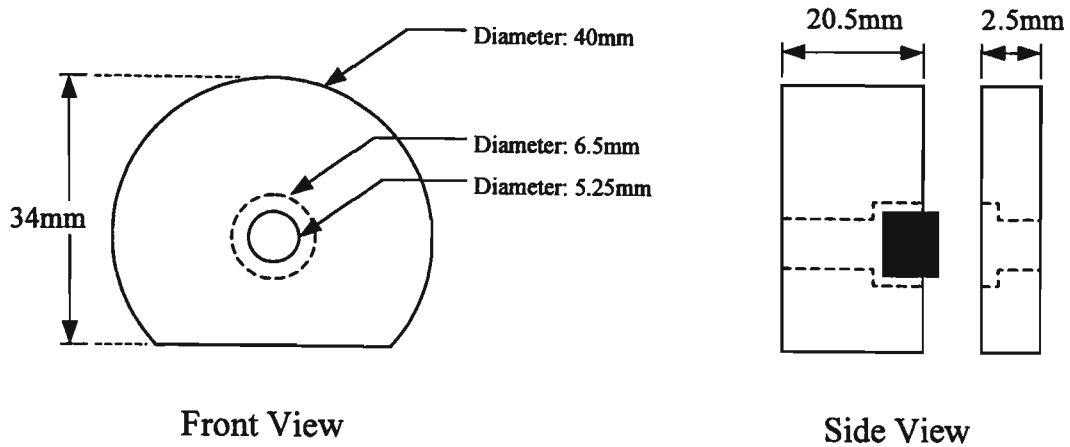
A.2 Pr³⁺:ZBLANP SAMPLE HOLDER

Mass: 460.8g



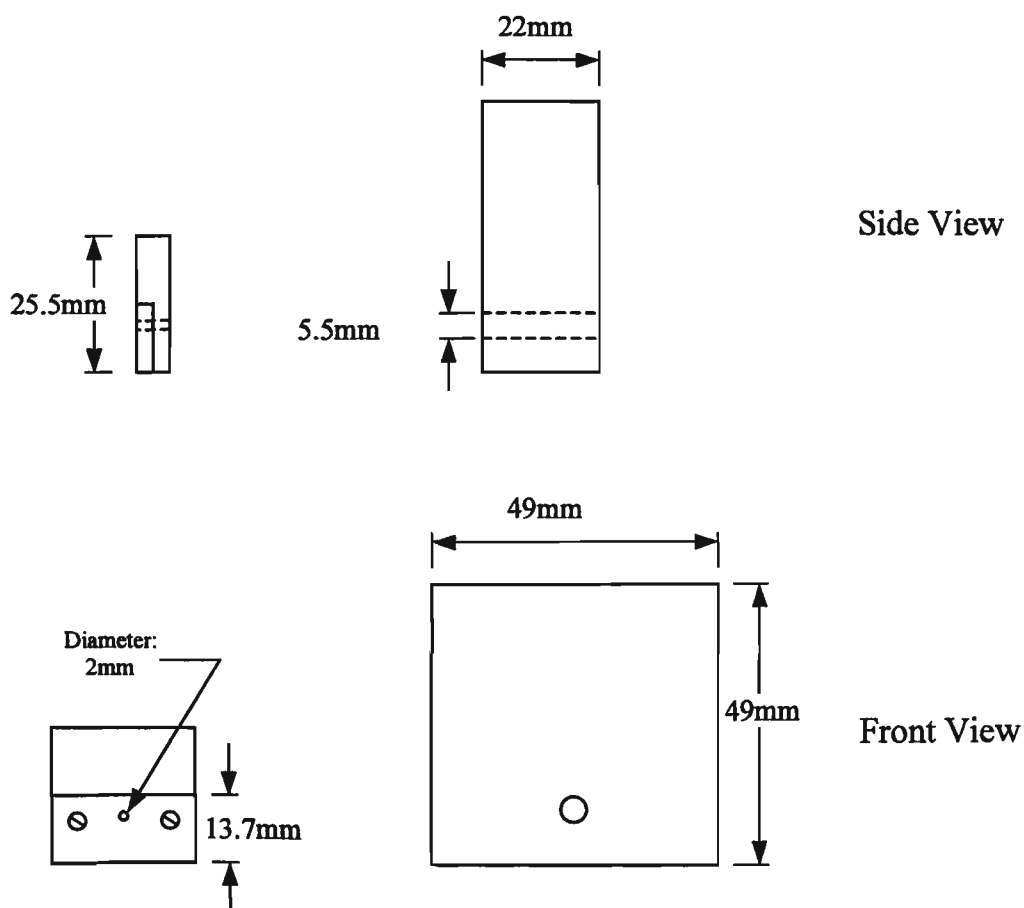
A.3 Nd³⁺:YAG SAMPLE HOLDER

Mass: 92.3 g



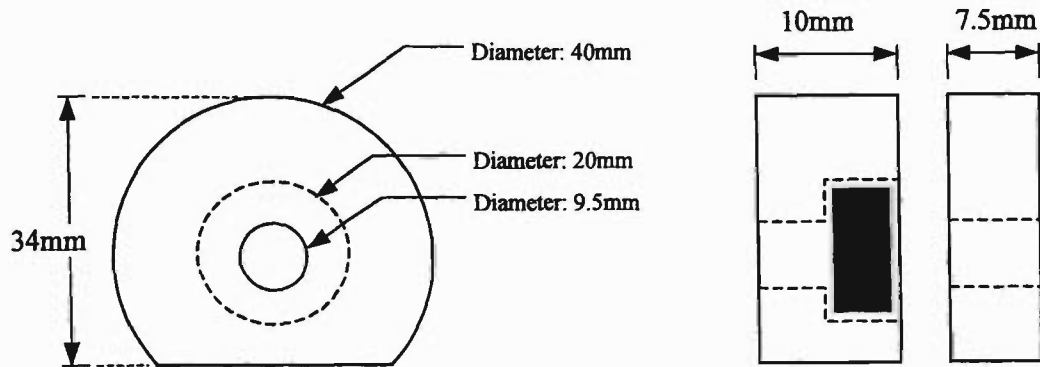
A.4 Nd³⁺:YVO₄ SAMPLE HOLDER

Mass: 153.9g



A.5 Nd³⁺:ZBLANP SAMPLE HOLDER

Mass: 75.2g



Publications

Journals

S.A. Wade, S.F. Collins, K.T.V. Grattan and G.W. Baxter, "Strain-independent temperature measurement using a fluorescence intensity ratio technique in optical fiber", *Appl. Opt.*, **39**, pp. 3050-3052, 1999.

S.A. Wade, G.W. Baxter, S.F. Collins, K.T.V. Grattan and T. Sun, "Simultaneous strain-temperature measurement using fluorescence from Yb-doped silica fiber", *Rev. Sci. Instrum.*, **71**, pp. 2267-2269, 1999.

S.A. Wade, J.C. Muscat, S.F. Collins and G.W. Baxter, " Nd^{3+} -doped optical fiber temperature sensor using the fluorescence intensity ratio technique", *Rev. Sci. Instrum.*, **70**, p. 4279-4282, 1999.

S.F. Collins, G.W. Baxter, **S.A. Wade**, T. Sun, Z.Y. Zhang and K.T.V. Grattan, "Comparison of fluorescence-based temperature sensor schemes: theoretical analysis and experimental validation", *J. Appl. Phys.*, **84**, p. 4649-4654, 1998.

E. Maurice, G. Monnom, G.W. Baxter, **S.A. Wade**, B.P. Petreski and S.F. Collins, "Blue LED-pumped point temperature sensor based on a fluorescence intensity ratio in Pr^{3+} :ZBLAN glass", *Opt. Rev.*, **4**, p. 89-91, 1997.

E. Maurice, **S.A. Wade**, S.F. Collins, G. Monnom and G.W. Baxter, "Self-referenced point temperature sensor based on a fluorescence intensity ratio in Yb^{3+} -doped silica fiber", *Appl. Opt.*, **36**, p. 8264-8269, 1997.

International Conferences

S.A. Wade, S.F. Collins, G.W. Baxter, T. Sun, Z.Y. Zhang, K.T.V. Grattan, and G. Monnom, "Fluorescence characteristics of several Yb-doped optical fibers for temperature sensing applications", 13th Optical Fiber Sensors Conf., Kyongju, Korea, p. 200-203, 1999.

M.C. Vergara, **S.A. Wade**, G.W. Baxter, Y. He and S.F. Collins, "The application of an optical fibre temperature sensor in the investigation of window glass breakage in fires", Proc. of Interflam – Fire Science and Engineering Conf., Interscience Communications Ltd., Edinburgh, Scotland, 29 June – 1 July, p. 1417-1422, 1999.

T. Sun, K.T.V. Grattan, Z.Y. Zhang, A.W. Palmer, S.F. Collins, G.W. Baxter and **S.A. Wade**, "Fluorescence-based measurement schemes using doped fiber: theoretical analysis and experimental validation", Nonlinear Optics '98, Kauai, Hawaii, p. 107-109, 1998.

International Conferences cont.

S.A. Wade, S.F. Collins and G.W. Baxter, "Comparison of host materials for Nd³⁺ fluorescence intensity ratio based temperature sensor", Eurosensors XII, Proc. 12th European Conf. on Solid State Transducers and the 9th UK Conf. on Sensors and their Applications, Southampton, UK, 13-16 Sept., 1998, (ed. N.M. White), p. 311-314.

E. Maurice, G. Monnom, G.W. Baxter, **S.A. Wade**, B.P. Petreski and S.F. Collins, "Blue LED-pumped point temperature sensor based on a fluorescence intensity ratio in Pr³⁺:ZBLAN glass", 11th Optical Fiber Sensors Conf., Sapporo (JSAP, Tokyo), p. 188-191, 1996.

G.W. Baxter, **S.A. Wade**, S.F. Collins, G. Monnom and E. Maurice, "Rare-earth doped optical fibres for point temperature sensing", In-situ Optical Sensors Conf., Denver (SPIE Vol. 2841), p. 249-256, 1996.

A. Stringer, K.A. Ahmed, D.M. Burgess, G. Gitlits, J.S. Jasik, R.C. Kemp, **S.A. Wade**, G.W. Baxter, and S.F. Collins, "Development and characterisation of a new dielectric cored OPGW", 45th International Wire and Cable Symposium, Reno USA, p. 68-76, 1996.

National Conferences

S.A. Wade, S.F. Collins, G.W. Baxter, G. Monnom and E. Maurice, "Rare-earth doped fibres for fluorescence-based temperature sensing", Proc. 24th Australian Conf. on Optical Fibre Technology, Sydney, p. 195-198, 1999.

M.C. Vergara, **S.A. Wade**, Y. He, G.W. Baxter and S.F. Collins, "Optical fibre temperature sensing of the breakage of window glass during fires", 12th Australian Optical Society Conf., Sydney, p. 36, 1999.

S.A. Wade, S.F. Collins and G.W. Baxter, "Fluorescence intensity-ratio-based optical fibre temperature sensing using neodymium-doped materials", Proc. 23rd Australian Conf. on Optical Fibre Technology, Melbourne, p. 189-192, 1998.

S.A. Wade, P.M. Farrell, V.K. Bogdanov, S.F. Collins and G.W. Baxter, "Modelling of the temperature dependent lifetimes of thermally coupled levels in Eu³⁺-doped silica fibre", Australasian Conf. on Optics Lasers and Spectroscopy '98, Christchurch, NZ, p. 204, 1998.

S.A. Wade, V.K. Bogdanov, S.F. Collins G.W. Baxter and G. Monnom, "Thermalisation of the ⁵D₀ and ⁵D₁ excited state levels in europium-doped optical fiber", Proc. 13th Australian Institute of Physics National Congress, Fremantle, p. 327, 1998.

Scott Wade, Gerard Monnom, Stephen Collins and Gregory Baxter, "Thermalisation of the ⁴F_{9/2} and ⁴I_{15/2} levels of Dy³⁺-doped silica fibre", 11th Australian Optical Society Conf., Adelaide, p. WP41, 1997.

National Conferences cont.

M.C. Vegara, **S.A. Wade**, G.W. Baxter and S.F. Collins, "Absorption by Nd³⁺ ions in YVO₄, ZBLAN and bulk silica samples in the wavelength range 540-640nm", 11th Australian Optical Society Conf., Adelaide, p. WP40, 1997.

J.C. Muscat, **S.A. Wade** and G.W. Baxter, "Optical fibre temperature sensing based on the fluorescence intensity ratio from neodymium Nd³⁺ doped silica fibre", 11th Australian Optical Society Conf., Adelaide, p. FP43, 1997.

S.A. Wade, E. Maurice, G.W. Baxter, K.A. Ahmed, G. Monnom, S.F. Collins and A. Stringer, "Industrial application of fluorescence intensity ratio point temperature sensor", Proc. 21st Australian Conf. on Optical Fibre Technology, Surfers Paradise, p. 290-293, 1996.

G. Baxter, E. Maurice, G. Monnom, **S. Wade** and D.B. Ostrowsky, "Dynamic range considerations for fibre optic temperature sensors using the green intensity ratio in erbium doped silica fibre", Australian Optical Society Conf. '95, Brisbane, 1995.

S.A. Wade, E. Maurice, B.P. Petreski, S.F. Collins and G.W. Baxter, "Temperature sensing using the thermalisation of the ³P₀ and ³P₁ levels of praseodymium", Proc. 20th Australian Conf. on Optical Fibre Technology, Coolum Beach, p. 331-334, 1995.

Others

S.A. Wade and G.W. Baxter, "Report on optical fibre temperature monitoring during fault current tests on OPGW cable", report to Olex Cables, FE207, 1996.

S.A. Wade, "Fluorescence-based temperature sensing using rare-earth doped fibres", Proc. SCIRF '99, Victoria University, Melbourne, ed. J. Singh, p. 77-78, 1999.